STUDIES ON THE STRUCTURAL, MAGNETIC, AND ELECTRICAL PROPERTIES OF NON-STOICHIOMETRIC AND RELATED RARE EARTH MANGANITES

THESIS

SUBMITTED TO THE

UNIVERSITY OF PUNE

FOR THE DEGREE OF

DOCTOR OF PHILOSOPHY

IN CHEMISTRY

By

RAJ SANKAR C.

Physical and Materials Chemistry Division

National Chemical Laboratory

Pune 411008

India

March 2006

CERTIFICATE

Certified that the work incorporated in the thesis

Studies on the Structural, Magnetic, and Electrical Properties of Non-stoichiometric and Related Rare Earth Manganites

submitted by Mr. RAJ SANKAR C. was carried out by the candidate under my supervision. Such material as has been obtained from other sources has been duly acknowledged in the thesis.

Dr. P. A. Joy
(Research Guide)

to my parents...

The secret of magnets; explain that to me!

There is no greater secret, except love and hate.

-Johann Wolfgang von Goethe

Acknowledgement

To my extreme delight, I would like to evince my whole-hearted gratitude to my research supervisor Dr. P. A. Joy, for providing me an incredible opportunity to pursue my career as a Ph.D. student, for his invaluable advice, for his benign attention, for his meticulous review and comments on the final draft of my thesis, for helping me out in most stressful times, for giving me the edge to meet future challenges... He has been an excellent guide and a great source of inspiration for me. I thank him for directing me to the wonderful area of magnetism, for extensive scientific discussions and for giving me complete freedom in research during my stay at NCL. My sincere thanks to him for his timely helps and for being a strong support, both scientific and personal, on all difficult occasions during my Ph. D research period.

My sincere thanks to Prof. S. K. Date, for his tremendous support and valuable advices. I gratefully acknowledge the past and present directors of NCL, and the head of the Physical and Materials Chemistry Division of NCL, Dr. Pal for allowing me to carry out the research work in a prestigious and well equipped laboratory. I am thankful to Dr. Vijayamohanan, Dr. Prasad, Dr. Ravi, Dr. Kulkarni and other scientists of the Physical Chemistry Division and Center for Materials Characterization, who have helped me in many ways to keep my research work smooth and steady.

With much appreciation, I would like to mention the crucial role of my colleagues and friends in my research career and providing me with an excellent working ambience. They have always been supportive, helping, and caring. I sincerely thank all of them for being with me, always, during my research period. Joly deserves a special mention, for his concern and support, helping me to learn several concepts in physics

and guiding me as an elder brother. I specially thank Vijay and Sreeja for helping me during my thesis work.

My sincere thanks to Indira teacher for guiding me to this wonderful research laboratory and for her affection. I thank all my teachers who have directly or indirectly helped me during my school and university education.

CSIR, India is acknowledged for the financial support.

I am forever indebted to my parents for their love, understanding, endless patience and encouragement throughout my life. They have been the greatest source of inspiration for me and I dedicate this thesis to them. I am thankful to my sisters for their constant encouragement. Finally, I express my special thanks to Maya, for her love, trust, and support.

Raj Sankar C

Contents

List of Tables

List of Figures

Abstract

The applications of magnetic materials are widespread and their importance especially in information storage devices is quite high after the discovery of Giant Magnetoresistance (GMR) in magnetic multilayers. A potential candidate that could replace the existing GMR read heads are the oxide based magnetoresistive materials such as the substituted perovskite type manganese oxides of the general formula $R_{1-x}D_xMnO_3$ (R = rare earth ion and D = divalent alkaline earth ion). These magnetic oxides show huge changes in their electrical resistance at the respective Curie temperatures, under a magnetic field, which is known as Colossal Magnetoresistance (CMR). These materials gained much attention by the research community in the recent past owing to a plethora of physical properties they exhibit and are usually considered as strongly correlated electron systems.

Substitution of La by divalent ions introduces ferromagnetism as well as a transition from insulator to metallic behavior in an otherwise antiferromagnetic insulator $LaMnO_3$. In $La_{1-x}D_xMnO_3$, the origin of the evolution of the interesting magnetic and electrical properties has been explained on the basis of the formation of Mn^{4+} ions in equal amounts with that of the substituted divalent ions, which results in a ferromagnetic exchange between Mn^{4+} and Mn^{3+} ions, usually known as the double exchange. Self-doped compositions of the general formula $La_{1-x}MnO_3$ and those with excess oxygen non-stoichiometry, $LaMnO_{3+\delta}$, also show physical properties similar to the divalent ion substituted manganites. The highly susceptible nature of these oxides to the changes in processing conditions result in many complex magnetic and electrical transport characteristics. Non-stoichiometry at the cationic and/or anionic sites in lanthanum manganites also affects the Mn^{3+}/Mn^{4+} ratio and plays a crucial role in deciding their electronic properties. These are not understood clearly and

many properties of these materials remain unexplained and less understood.

This thesis is divided into seven chapters with proper references at the end under the section of bibliography.

Chapter 1: General introduction to the perovskite-type manganese oxides and their structural and electronic properties are reviewed in this chapter. Previous studies on the various issues dealt with the non-stoichiometry and related problems such as effect of non-stoichiometry on structure, low-temperature magnetic properties, phase separation, spin glass-type behavior, etc. are discussed.

Chapter 2: The methods employed for the synthesis of the mixed-valent manganese oxides under the current investigation, are explained in this chapter. The theory and experimental details of the characterization techniques such as powder X-ray diffraction, estimation of the concentration of tetravalent manganese ions, various types of magnetic measurements using vibrating sample magnetometer and *ac* susceptometer, electron paramagnetic resonance (EPR), and four-probe resistivity method used in this work to study the electronic properties of the compounds are described briefly.

Chapter 3: This chapter involves the studies on the magnetic properties of the self-doped lanthanum manganites, $La_{1-x}MnO_3$. Careful studies on the structural, magnetic, and EPR properties of these compositions revealed that the limiting value of x as 0.125. This corresponds to a vacancy ordered structure (1/8 ordering). Any values larger than this resulted in the formation of a second phase which is identified as Mn_3O_4, from careful XRD analysis. The magnetic properties of different compositions in $La_{1-x}MnO_3$ have been studied by ac susceptibility and *dc* magnetization measurements in the temperature range 10-300 K. All compositions show an anomalous decrease in the *ac* susceptibility and zero field cooled ZFC *dc* magnetization at low temperatures, below the ferromagnetic ordering temperature. The temperature below which this anomalous behavior is observed, T_a, varies with the degree of La

vacancy in the series and varies with the Mn^{4+} content for a particular composition with a given value of x. Various magnetic measurements, under different conditions, have been carried out and the domain wall pinning effects are shown to be responsible for the observed low temperature magnetic anomalies. The effect of self-doping on the magnetic properties of certain Ca-substituted compositions is also discussed in this chapter.

Chapter 4: The studies on the non-stoichiometric lanthanum manganites (represented as $LaMnO_{3+\delta}$) are discussed in this chapter. Comparing with some previous reports, it is found that there is no correlation between the amount of Mn^{4+} or δ and the magnetic transition temperature for the samples of $LaMnO_{3+\delta}$ synthesized by various methods. The dependence of oxygen non-stoichiometry, structure, and magnetic properties on the processing methods used for the synthesis of $LaMnO_{3+\delta}$ is discussed in this chapter. From powder X-ray diffraction studies, it was found that those $LaMnO_{3+\delta}$ samples showing well-defined ferromagnetic transitions are of mixed phase character; a self-doped phase ($La_{1-x}MnO_3$) and minor amounts of an La-rich phase. The results give evidence to conclude that the self-doped, La-deficient, phases formed are responsible for ferromagnetism in $LaMnO_{3+\delta}$. The complex magnetic properties are explained on the basis of the formation of unequal concentration of cation vacancies.

Chapter 5: This chapter deals with the study of the origin of spin glass-type features observed in some $LaMnO_{3+\delta}$ compositions. Non-stoichiometry of oxygen in lanthanum manganite, $LaMnO_{3+\delta}$, gives rise to vacancies at both the cationic sites of the perovskite lattice. Accordingly, since the magnetic properties are very much susceptible to small changes in the Mn^{4+} concentration, a variety of features can be observed in manganite magnetism. Superparamagnetism is generally observed in nanosized materials due to their single domain (superspin) nature. The magnetic properties of certain $LaMnO_{3+\delta}$ compositions with high values of δ were found to be

similar to those of typical nanomagnets. The non-stoichiometry of oxygen creates vacancies at Mn-site thus causing a breakage of long range magnetic order and forming tiny clusters that show single domain characteristics. The present work on the time-dependent *dc* magnetic measurements by employing various cooling protocols reveals the interacting superspin behavior (superspin glass) in an oxygen non-stoichiometric lanthanum manganite as observed in certain interacting magnetic nanoparticle systems.

Chapter 6: Low temperature magnetic characteristics of some rare-earth substituted lanthanum manganites have been correlated in this chapter. $La_{0.67}Ca_{0.33}MnO_3$ is a well characterized composition with a fairly high value of T_c of 260 K with a perfect ferromagnetic character. The effect of partial substitution of La ions by other rare earth ions is studied in detail. A magnetic anomaly observed at low temperatures in certain rare-earth substituted manganite compositions is explained as the domain wall pinning effects where the pinning center is most probably the distorted Mn-O-Mn bond angle due to the difference in rare-earth ionic radii. The superspin glass and superparamagnetic nature of some Tb-doped manganites caused due to the superspin clustering are also studied in detail.

Chapter 7: In this chapter, results on the studies of the electrical properties of lanthanum manganites have been discussed. A *second peak* in the temperature variation of resistivity of certain manganite compositions, in self-doped and $La_{1-x}Ca_xMnO_3$, has been observed at temperatures below the peak corresponding to the Metal-Insulator transition. Based on the comparative studies on the transport, structural and magnetic properties of a large number of compositions, it has been concluded that small scale phase separation is the origin of the double peak-type resistivity characteristics.

Chapter 1

Introduction

The fascination of magnets dates back at least three thousand years. Perhaps, the first observations of magnetic phenomena were made by ancient Greeks. However, the fact that the magnets align in a unique way together with the fact that the earth itself is a magnet led to the discovery of the *compass*, an instrument used quite effectively for navigation purposes, and this has aided the faster development of civilization. Magnetism is one of the most interesting phenomena of materials and a major breakthrough for understanding the principles of magnetism was made through the discovery of the relation between electricity and magnetism in the 19th century. The development of quantum mechanics gave more insights to the microscopic principles of magnetism which has been able to explain various magnetic properties quite successfully. The numerous applications of magnetism and magnetic materials (ranging from *Compass* to *Spintronics*) make them one of the most important and extremely interesting areas of modern materials research.

1.1 Magnetism in Materials

Magnetism is a universal phenomenon associated with any materials that are composed of charged particles. Commonly, the origin of magnetic moment in the atoms of a material is the motion of electrons. A material may respond to an applied mag-

netic field in two ways, it may get attracted or repelled; accordingly, the magnetic materials are said to be either paramagnetic or diamagnetic, respectively. Paramagnetism is observed in materials that contain atoms with unpaired electrons whereas paired electronic systems behave as diamagnetic. Diamagnetism can be regarded as originating from the shielding currents induced by an applied magnetic field in the filled electron shells. These currents are equivalent to an induced moment present on each of the atoms. This could be better described by stating the Lenz's law for orbital motion of electrons. Lenz's law states that if the magnetic flux enclosed by a current loop is changed by the application of a magnetic field, a current is induced in such a direction that the corresponding magnetic field opposes the applied field. The magnitude of the diamagnetic response is very small in most of the materials except for superconductors which are perfect diamagnets.

1.1.1 Paramagnetism

A paramagnetic substance consists of atoms or molecules each of which has a net magnetic moment. In the absence of an applied field these atomic moments point at random directions and cancel one another, so that the net magnetization of the specimen is zero. When a magnetic field is applied, there is a tendency for each atomic moment to turn towards the direction of the field. But the thermal agitation of the moments opposes this tendency and tends to keep the atomic moments remained at random orientations. The result is only a partial alignment of the moments in the field direction. The atoms with incomplete inner electronic shells (transition metal ions and rare earth ions) can have a large net moment and compounds of these elements are strongly paramagnetic.

The magnetic moment due to the unpaired electrons is regarded as arising from spin and orbital motion of electrons. So, the atoms or ions containing unpaired electrons have an overall magnetic moment given by

$$\mu_J = [4S(S+1) + L(L+1)]^{1/2}$$

where S and L are the spin and L angular momentum quantum numbers, respectively and J is the total quantum number resulting from the coupling of the spin and orbital angular momentum. In most cases, especially in the case of the transition metal ions, L is negligible and the spin only moment alone can be calculated as:

$$\mu_S = g[S(S+1)]^{1/2}$$

where g is the gyromagnetic ratio $\sim$2. For a single electron, $\mu_S = 1.73$ Bohr Magneton (BM), which is given by

$$1BM = \frac{eh}{4\pi mc} = 0.927 \times 10^{20} ergOe^{-1}$$

where e and m are charge and mass of electron, respectively, h is the Planck's constant and c is the velocity of light. 1 BM is equal to the magnetic moment of an electron in the first Bohr orbit.

If a substance is placed in a magnetic field H (expressed in Oe or A/m), then the density of lines of force in the sample is known as the magnetic induction B (expressed in Tesla), and is given as

$$B = H + 4\pi M$$

where M is the magnetic moment of the sample per unit volume, often called as magnetization (expressed in emu cm^{-3}). The magnetic susceptibility χ can be defined as

$$\chi = M/H$$

For diamagnetic substances χ is small and negative. In the case of paramagnetic substances χ is small but positive.

1.1.2 Temperature Dependence of the Magnetic Susceptibility

According to the first systematic measurements of the susceptibility (χ) of a large number of substances over a wide range of temperature made by the French physicist Pierre Curie, χ was independent of temperature for diamagnetic substances but it varied inversely with the absolute temperature for paramagnetic substances. The magnetic susceptibility as a function of temperature can be expressed as,

$$\chi = N\frac{\mu_{eff}^2}{3kT}$$

where, N is the Avagadro number, k is the Boltzmann constant and μ_{eff} is the effective magnetic moment and is given as

$$\mu_{eff} = g[J(J+1)]^{1/2}$$

g is the gyromagnetic ratio and J is the total angular momentum quantum number. When the orbital contribution is neglected, this reduces to the spin-only value,

$$\mu_{s.o} = g[S(S+1)]^{1/2}$$

$N\frac{\mu_{eff}^2}{3k}$ is a constant and therefore the magnetic susceptibility equation can be written as

$$\chi = \frac{C}{T}$$

where, $C = N\frac{\mu_{eff}^2}{3k}$. This relation is called the Curie law and C is the Curie constant. It was later shown that Curie law is a special case of a more general Curie-Weiss law;

$$\chi = \frac{C}{T - \Theta}$$

Here, Θ is a constant with the dimensions of temperature and equal to zero for those substances which obey Curie law. The paramagnetic substances obey the simple Curie law usually at high temperatures.

1.1.3 Ordered Phenomena

Ordering of magnetic moments in most magnetic systems is controlled by the magnetic exchange interactions [Cul72, Oha00, Bus03, Dut03]. However, magnetic ordering due to dipole-dipole interactions have also been found in some materials such as in organometallic magnets. Magnetic ordering in materials is observed only below a critical temperature; above this, the materials show paramagnetic behavior.

Based on the type of ordering or exchange, magnetic materials are classified into four; *ferromagnetic, antiferromagnetic, ferrimagnetic* and *helimagnetic*. If all the net magnetic moments in atoms or molecules in a solid are spontaneously aligned in a parallel direction and the material possesses an overall magnetic moment, it is said to be *ferromagnetic*. On the other hand, an antiparallel arrangement of the magnetic moment vectors causes *antiferromagnetism*, which results in net magnetic moment of zero. A simple antiferromagnet can be considered as consisting of two magnetic sub-lattices each of which being ferromagnetically ordered but coupled antiferromagnetically (moments in opposite direction) in the unit cell of a solid. *Ferrimagnetic* substances are those with unequal adjacent moments, directions of which are opposite to each other. This is because magnetic ions occupy different types of lattice sites, which gives rise to a net magnetic moment. When the arrangement of individual atomic moments deviate from either parallel or antiparallel configurations, the angle between the magnetic moment vectors, θ_{ij} becomes $0 < \theta_{ij} < 180^{\circ}$ which results in a net small magnetization in the material and such materials are classified under *helimagnetic* materials.

Ferromagnetic substances show very large susceptibility. Above a certain temperature called the Curie temperature, T_C, (or often used as the critical temperature, T_c) the material will no longer be ferromagnetic and converts to paramagnetic. The Curie-Weiss behavior is usually obeyed at higher temperatures in the paramagnetic region. For antiferromagnetic materials the value of χ increases with rising tempera-

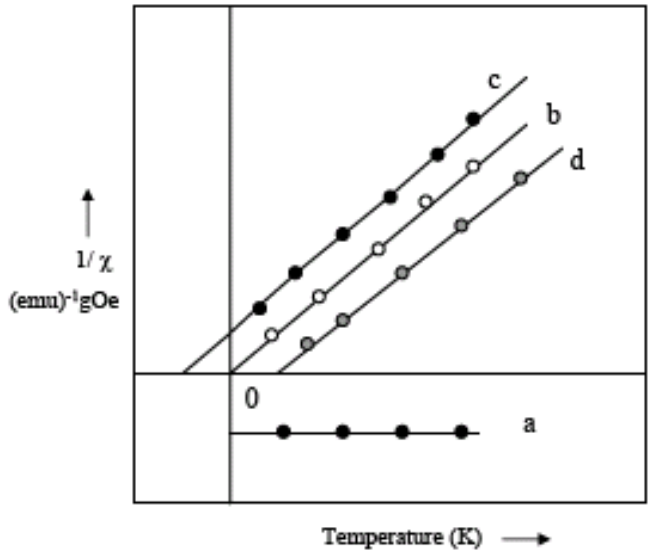

Figure 1.1: χ^{-1}-T plot of various magnetic materials.

ture up to a critical temperature known as the Neel temperature, T_N, above which the material shows paramagnetic behavior.

The temperature dependence of various types of magnetic materials can be explained on the basis of the molecular field theory proposed by Weiss in 1907. According to him, in paramagnetic substances, the elementary moments will interact with each other. This interaction can be expressed in terms of a fictitious internal field, called as the molecular field H_m that acts in addition to the applied field, H. The strength of this field depends on the extent of alignment already attained. Since the molecular field is proportional to the magnetization M,

$$H_m = \gamma M$$

where γ is called the molecular field constant and it is proportional to Weiss constant

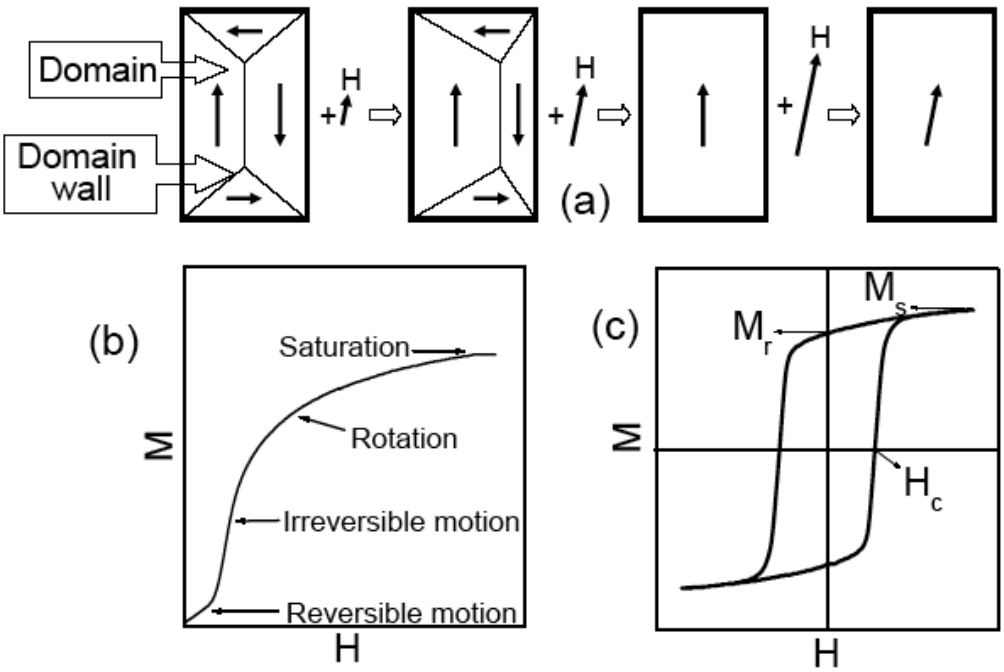

Figure 1.2: Basic magnetization processes in ferromagnetic materials.

Θ. The inverse paramagnetic susceptibility varies linearly with temperature and intercepts the temperature axis at the origin (Curie behavior) or at $T = \Theta$ (Curie-Weiss behavior) as shown in Fig. 1.1. The positive and negative values of Θ indicate that the molecular field is either aiding or opposing the applied field, respectively. For a ferromagnet, the value of Θ is approximately equal to T_c, which is large and positive on the basis of which Weiss made an assumption of the existence of a molecular field above and below the Curie temperature of the substance. The field is so strong that it can magnetize the substance to saturation even in the absence of an applied field. The substance is then said to be spontaneously magnetized. On the basis of his second assumption a ferromagnet in the demagnetized state is divided into a number of small

regions called domains. Each domain is spontaneously magnetized to its saturation value of magnetization. But the directions of magnetization of the various domains are such that the specimen as a whole has no net magnetization. The process of magnetization is then one of converting the specimen from a multi-domain state into a single domain state (Fig. 1.2a).

For a ferromagnetic material, the field dependence of magnetization is nonlinear and at large values of H, the magnetization, M becomes constant at its saturation value M_s, as shown in Fig. 1.2b. But once saturated, a decrease in H to zero does not reduce M to zero. Hence it possesses some magnetization called remnant magnetization (M_R). In order to demagnetize the substance after saturation, a reverse field is required. The magnitude of this field is called coercivity (H_c). The M-H curve in the case of ferro- and ferrimagnets is called the magnetic hysteresis loop (Fig. 1.2c). It represents an energy loss because during the process of magnetization and demagnetization in an alternating magnetic field some amount of energy is dissipated usually as heat. During one complete cycle, this amount of energy (the hysteresis loss) is proportional to the area inside the loop. In a typical M-H curve of a ferromagnet, at low field region, magnetization increases due to domain wall motion, as a result, domains which are favorably oriented to the direction of applied field grows at the expense of others and beyond that magnetization occurs only by domain wall rotation which occurs at higher field strengths (Fig. 1.2a). But when the temperature increases the saturation magnetization of a ferromagnetic substance decreases and at T_c the domain structure is collapsed, so it will act as a paramagnetic substance above T_c.

1.1.4 Magnetic Exchange Interactions

The Heisenberg exchange interaction,

$$H = -2J_{ij} \sum S_i.S_j$$

is used to describe the tendency of the adjacent, localized spin moments (S_i and S_j) to align parallel (J_{ij} is positive, ferromagnetic) or antiparallel (J_{ij} is negative, antiferromagnetic) to each other in a material consisting of magnetic atoms/ions. The strength of the exchange interaction depends on the overlap of the wave functions. The Heisenberg type of exchange (direct exchange) applies only to some localized systems, and for oxides, one needs to consider indirect forms of magnetic exchange [Oha00, Bus03, Dut03]. In oxides, the magnetic interaction between two ions should be such a way that their spin moments have either parallel or antiparallel alignment. In oxides, the distance between two magnetic ions are sometimes, two lattice constants apart and no direct exchange or orbital overlap becomes possible. In such cases, there may be an indirect exchange mechanism operating between the two magnetic ions. A possible mechanism in oxides is the superexchange which explains the magnetic interaction between two neighboring transition metal ions separated by an oxide ion, based on the symmetry of p and d states and their occupancy [Goo70]. Another type of indirect exchange interaction is Dzyaloshinskii-Moriya interaction, and its hamiltonian is,

$$H_{ij}^{DM} = -D_{ij} \cdot (S_i \times S_j)$$

where D_{ij} is a constant vector. This coupling acts to cant the spins because the coupling energy is minimized when the two spins are perpendicular to each other [Mor60].

1.1.5 Spin Glasses

Spin glasses are magnetic systems exhibiting both quenched disorder and frustration [Myd93]. Such a behavior is observed below a temperature called spin-glass transi-

tion temperature (T_g) or freezing temperature (T_f). The spin glass phenomenon was first discovered in the magnetism of dilute alloys such as AuFe [Can71] where RKKY (Ruderman-Kittel-Kasuya-Yoshida) interactions between the spins of magnetic atoms and conducting electrons play a major role. Also, such behavior is observed in certain insulators such as $Eu_xSr_{1-x}S$ with exchange interactions between first and second neighbors [Mal79, Hua85, Myd93]. It is believed that in spin glasses, a localized pair of moments (spins) have equal probability of having a ferromagnetic or an antiferromagnetic interaction which results in frustration. The experimental and theoretical features of spin glasses have been discussed in detail by Huang [Hua85] and Mydosh [Myd93], and some important physical concepts about spin glasses are briefly explained as follows.

The spin glasses are characterized by a remarkable thermomagnetic irreversibility and relaxation properties. Several theoretical models have been developed in order to explain the unusual behavior of these materials. The Sherrington-Kirckpatrick model suggests a mean field approach and considers an infinite range of coupling between the Ising spins to form infinite energy states [Myd93]. Whereas, the droplet model by Fisher and Huse claims that the real, short-range systems, behave quite differently and the glassy phase being described by only two pure states, related by a global inversion of the spins, and no phase transition occurring in a magnetic field [Fis88a, Fis88b]. Here, the important physical concepts being the domain growth or the growth of the coherence length for equilibrium spin glass order and temperature chaos [Vin00, Bou01, Jon04].

Aging, Rejuvenation and Memory Effects in Spin Glasses

The dynamic properties of a spin glass system is often experimentally studied by the aging, memory and chaos effects [Vin95, Jon98a, Jon00, Bou01, Mat01b, Zot03]. The relaxation of a spin glass material is logarithmically slow, and it depends on

the time spent at low temperature which is otherwise known as *aging*. Aging at a temperature, T, is fully reinitialized by heating the sample above the T_g. It corresponds to the slow evolution of the system towards equilibrium, starting at the time of the quench below T_g. The peculiarities of aging and related magnetic effects in spin glasses are observed during the small temperature cycles within the temperature range of existence of spin glass features. It is important to note that aging at a higher temperature barely contributes to aging at a lower temperature. Or in other words, the state formed at a higher temperature does not normally affect the aging at a lower temperature. This is explained by the *chaotic* aspect of the spin glass phase. Also, interesting memory effects are observed during a reverse thermal cycle. Or in other words, when the sample is heated back to the temperatures at which it has been previously aged, it *remembers* the state formed during aging. There have been various approaches derived from Parisi's solution of Sherrington-Kirckpatrick model [Myd93, Vin95, Jon98a, Jon00]. Here, the aging is described in terms of a random walk in the space of metastable states, and the memory and chaos (rejuvenation) effects in terms of a hierarchical organization of these metastable states, as a function of temperature. The physical picture is of the existence of a large number of nearly degenerate states at lower temperatures, these states merge again when the temperature is raised back [Vin95, Jon98a]. A droplet picture as mentioned previously, is also used to explain the aging, chaos and memory effects found in spin glasses in which at each temperature, the equilibrium spin glass state is considered to consist of a thermally activated droplet excitation of various sizes.

The existence of glassy dynamics and memory effects are also observed in some ferroelectric materials, magnetic nanoparticles and dense, frozen ferrofluids [Kit02, Pod02, Sun03, Cor04, Jon04, Par05, Sas05, Tso05, Zhe05]. They also show aging, chaos and memory effects similar to the spin glasses, but the effects are weaker in nanoparticles. The glassy nature is thought to be due to the interacting nature of

magnetic nanoparticles.

1.1.6 Superparamagnetism

Magnetic nanoparticles are in the main theme of the research for the last few years [Kod99]. The importance of such nanosized materials is for their fundamental nature and varieties of applications such as high density magnetic storage media, ferrofluids, biological applications, etc. The size confinement of the particles at the nano-regime could be easily achieved by simple chemical methods. The intrinsic magnetic properties of a material, such as spontaneous magnetization, magnetocrystalline anisotropy etc., are strongly influenced by the particle size. Thus, the particle size-property correlation becomes important when it comes to the nano-regime.

A magnetic body, generally has a multidomain structure, i.e., it is divided into uniformly magnetized regions called domains separated by domain walls or Bloch walls in order to minimize its magnetostatic energy. By reducing the size of the crystal, the size of the domains is also reduced. Consequently, the domain structure and the domain wall width would undergo changes. This results in single domain formation in magnetic nanoparticles.

The anisotropy energy in a single domain particle is proportional to the volume V. For uniaxial anisotropy, the associated energy barrier, separating the easy magnetization direction is

$$E_B = KV$$

Thus, as V decreases or particle size decreases, E_B decreases and it becomes comparable to the thermal energy kT. This implies that the energy barrier for magnetization reversal may overcome and the magnetic moment of the particle could be thermally fluctuated like a single spin in a paramagnetic material. Thus the total magnetic moment associated with the single domain particle may be as a whole rotated, whereas

the spins within the single domain particles remain magnetically coupled. The magnetic behavior of such single domain particles is called superparamagnetism. For superparamagnetic particles, the susceptibility increases as the temperature is decreased and then decreases after reaching a maximum value, below a certain temperature called the blocking temperature, T_B. The blocking temperature is related to the anisotropy energy as $KV \approx 25k_BT_B$. Below T_B, a magnetic hysteresis loop is observed, whereas no such loop is observed above T_B.

For superparamagnetic particles, no magnetic hysteresis is observed and a reasonable approximation is to regard these as individual spins and the Langevin equation may be applied, which is given by,

$$\frac{M}{M_s} = L(\alpha) = Coth\alpha - \frac{1}{\alpha}$$

where, $\alpha = \frac{\mu H}{kT}$ and μ is the magnetic moment of the particle and H, the applied magnetic field [Cul72].

Magnetism and Dipolar Interactions in Nanoparticles

Magnetic nanoparticles interact with each other, and this interaction is often of dipolar nature [Dor88, Dor97]. Thus, the interactive nature of these particles can be tuned by varying the particle concentration or by isolating the particles by using nonmagnetic matrices [Dor97]. Depending on the strength of the interaction between the particles, such magnetic nanoparticles are known to change their superparamagnetic nature to spin glass-like nature [Dor92, Sas05]. Since these nanoparticles behave as if they are single domains, each particle can be considered to posses a huge, single spin called superspin [Dor92, Sah02, Sas05]. The strongly interacting superspins are often known as superspin glasses whereas weak interaction of superspins results in superparamagnetism [Sas05]. It is important in the applications of these materials that these superspins are noninteracting or only weakly interacting. There are many

recent reports available in the literature which deals with the studies on interaction behavior of magnetic nanoparticles [Luo91, Jon95, Dju97, Jon98b, Pod02, Sun03, Jon04, Sas05, Var05, Tso05, Zhe05]. Similar to the dispersed magnetic nanoparticles, are the magnetic nanoclusters, which also behave individually like single domains or superspins. These superspins may again interact with one another and the interaction may be of dipolar nature or any other magnetic exchange types such as superexchange or antisymmetric Dzyaloshinskii-Moriya interaction. Besides, the interaction between superspins depend on the size, density and nature of the cluster. The physical concepts used for explaining the conventional spin glasses can be extended in the case of superspin glasses, due to the similarity of their response to magnetic field and relaxation behavior.

1.2 Magnetism in the Perovskite Manganites

1.2.1 Perovskites

Perovskites are the large family of crystalline ceramics (metallic elements combining with non metals, usually oxygen), which derive their name from a specific mineral known as perovskite ($CaTiO_3$). It was first described in the 1830's by the geologist Gustav Rose, who named it after the famous Russian mineralogist Count Lev Alekseevich Von Perovski. The general formula of perovskites is ABX_3, and in the perovskite structure the A-site is generally occupied by large cations such as rare earth ions or alkaline earth metal ions, B-site by smaller cations such as transition metal ions and X is an anion, usually oxide or halide. The basic structural unit of a perovskite is a cube and this can be represented by a polyhedral one in which the six X anions surround each B cation octahedrally. In such a model, the basic structural unit becomes a group of eight corner-shared octahedrons around the A-cation. The cubic perovskite structure (both A-type and B-type) is illustrated in the Fig. 1.3. The structure of

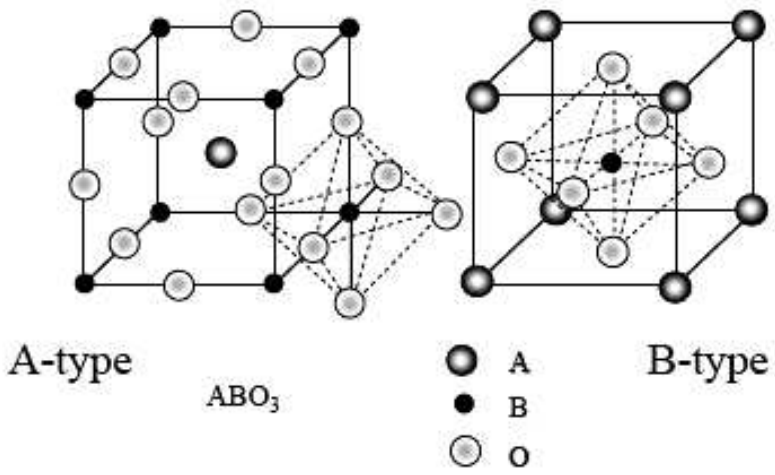

Figure 1.3: Structural features of an ideal perovskite

the perovskite oxides, ABO_3, can be considered as a cubic close packed array of O^{2-} anions and A^{2+} or A^{3+} cations (with radius r_A), with small B cations (with radius r_B) in octahedral interstitial sites where, r_A must be same as the radii of the oxide ions, $r_O = r_A = 0.14$ nm and r_B is $(2^{1/2} - 1)r_O = 0.058$ nm. Goldschmidt defined a tolerance factor [Gol26],

$$t = \frac{r_A + r_O}{\sqrt{2}(r_B + r_O)}$$

which is unity for ideally sized ions. The ideal perovskite structure is cubic, for which $t = 1$. Generally, most of the perovskite oxides show a structural distortion due to the ionic size mismatch and other factors, so that the crystal symmetry is reduced to rhombohedral, orthorhombic, monoclinic and tetragonal. Also, the structures are temperature dependent and reversibly or irreversibly converted to different structures at different temperatures. Unit cells with low symmetries are possible within the range $0.75 < t < 1$ [Goo70]. There are two possible characteristic distortions, which

influence the perovskite structure; one arises from the A-site size mismatch and the other due to the Jahn-Teller effect of B-site ions (such as Mn^{3+}). The B-O-B bond angle is also sensitive to the size of the A-site ion and is reduced from 180°. The distortion of structure due to the A-site cation size mismatch is shown in Fig. 1.4(a). Thus, if the tolerance factor is in the range $0.75 < t < 0.9$, a cooperative buckling of the corner shared octahedra to optimize the A-O bond lengths, enlarges the unit cell which results in orthorhombic distortion of the ideal cubic perovskite structure. When $0.9 < t < 1$, such buckling may not be found, although small distortions to rhombohedral symmetry occur. When $t > 1$, i.e., if the A-site ion is too large, perovskite structure will be destroyed and a hexagonal close packing results.

The structural changes by collective electrons, is commonly observed in certain ferroelectric materials, such as $BaTiO_3$. The material undergoes a structural transition from orthorhombic to rhombohedral, due to the displacement of Ti ions along the [111] direction of the crystal. Also, in multiferroics such as $TbMnO_3$, a lattice modulation is observed at low temperatures which results in ferroelectric properties.

1.2.2 Structural Distortions in Lanthanum Manganites

Lanthanum manganite is a perovskite type oxide where A = La and B = Mn. In $LaMnO_3$, the Mn^{3+} ions show Jahn-Teller effect (J-T effect) which distorts the MnO_6 octahedra in such a way that there are long and short Mn-O bonds. A distortion of this type is favored by certain conditions described by the Jahn-Teller theorem. The theorem states that for a non-linear molecule, in an electronically degenerate state, distortion must occur to lower the symmetry, to remove the degeneracy and lower the energy. Consider a manganese ion surrounded by six oxygen atoms forming MnO_6 octahedron, as in $LaMnO_3$. This causes the 3d orbitals to split into a lower t_{2g} and an upper e_g orbital. In the Mn^{3+} ion ($3d^4$) three electrons occupy each of the t_{2g} orbitals and the fourth one occupies the upper e_g orbital. The singly occupied e_g orbital can

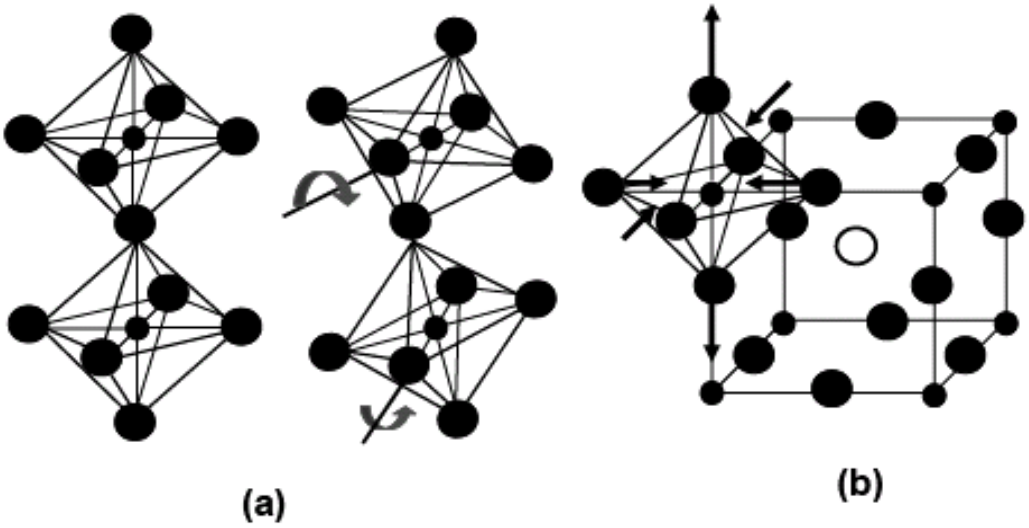

Figure 1.4: Structural distortion in manganites (a) due to cation size mismatch and (b) due to Jahn-Teller distortion of MnO_6 octahedra.

be either $d(z^2)$ or $d(x^2\text{-}y^2)$ and accordingly, in an octahedral ligand field, the e_g levels become non-degenerate. The J-T effect of Mn^{3+} ion in an octahedral oxygen ligand field is shown in Fig. 1.5. A typical J-T distortion occurring in manganites is shown in the Fig. 1.4(b). One of the most effective distortion arising from the J-T effect is a basal plane distortion with diagonally opposite oxygen pair displaced outward and the other pair distorts inward is called as orthorhombic distortion. It has been shown that a J-T distortion involving a displacement of oxygen ions > 0.01 Å can split the e_g band of the manganites.

In the parent compound, $LaMnO_3$ which contains 100% Mn^{3+} ions, the MnO_6 octahedra in Jahn-Teller distorted in such a way that the long and short Mn-O bonds lie in the *ab* plane, giving rise to orbital ordering. Due to this J-T distortion, $LaMnO_3$ has the O′-orthorhombic structure. Below 900 K, the rhombohedral structure of $LaMnO_3$ changes to O′-orthorhombic, associated with the freezing of dynamic dis-

tortion. This can be regarded as an order-disorder transition, where the static Jahn-Teller effect becomes dynamic [Goo98, Coe99]. Here, the O′-orthorhombic structure with $c/a < \sqrt{2}$ indicates that the Jahn-Teller distortions are superimposed on an O-orthorhombic crystal with $c/a > \sqrt{2}$, which is already distorted due to ionic-size mismatches [Goo61]. Nevertheless, the impact of these localized electronic effects on the structure is of ten times less, when compared to that from the ionic size/charge effects. The Mn-O-Mn bond angles are about 155° in $LaMnO_3$ [Ele71].

1.2.3 Magnetic Properties

Due to the Jahn-Teller distortion of MnO_6 octahedra in $LaMnO_3$, e_g orbitals loose their degeneracy. Also, two new e_g orbitals namely, $3x^2 - r^2$ and $3y^2 - r^2$ are formed by the linear combination of $x^2 - y^2$ and $3z^2 - r^2$ with the help of Q_2 mode of Jahn-Teller active lattice vibration [Cus01]. Now, hybridization with the oxygen $2p$ orbitals gives antibonding nature to these new orbitals. Thus, e_g orbital extending along the longer Mn–O bond has lower energy and results in the ordering of $3x^2 - r^2$ and $3y^2 - r^2$ orbitals in the *ab*-planes [Tok00]. In short, Mn^{+3}-O-Mn^{+3} exchange interactions become anisotropic and results in A-type antiferromagnetic spin ordering below 135 K, but with a positive Θ. In the A-type AFM ordering, where ferromagnetically ordered adjacent Mn-planes are coupled antiferromagnetically resulting in no net magnetic moment.

The substituted lanthanum manganites of the general formula $La_{1-x}D_xMnO_{3\pm\delta}$ (D = Ca, Sr, etc.), have been extensively studied in the recent past. In $LaMnO_3$, the substitution of La^{3+} ions by divalent ions of suitable size is possible, which introduces Mn^{4+} ions in the lattice for charge neutrality thereby reducing the J-T distortion. This kind of substitution, due to the associated changes in the valency of Mn and structural distortions, greatly modify the electrical transport and the magnetic properties of the parent compound $LaMnO_3$. Progressive substitution of rare earth ions by divalent

ions like alkaline earths introduces Mn^{4+} in the structure corresponding to the doping amount and the resulting composition shows ferromagnetism. The ferromagnetic transition temperatures (T_c) of the divalent substituted compositions are found to be highly susceptible to the amount of substitution and a *fine-tuning* of T_c is possible by varying the degree of substitution. Apart from the divalent ion substitution, self-doping and substitution at Mn-site by other transition metal ions are also known to cause rich variety of magnetic and transport properties in the lanthanum manganite family [Rao98, Coe99, Tok00, Sal01]. These effects can be either due to the amount of Mn^{4+} in the structure or variation in the Mn-O-Mn bond angle or both. The magnetic interactions and resulting nature are thus related to the crystal structures and Jahn-Teller distortion around Mn^{3+} (t_{2g}^3, e_g^1) ions.

Another way of introducing ferromagnetism in $LaMnO_3$ is by making the compound non-stoichiometric by introducing vacancies at the La-site or by varying the oxygen stoichiometry. Vacancies at the La-site or excess oxygen stoichiometry introduces Mn^{4+} in the lattice and the resulting compositions become ferromagnetic and show properties similar to that of the divalent ion substituted compositions.

An O′ →O orthorhombic →R (rhombohedral)→C (cubic)change in crystal structure has been suggested as the value of δ or Mn^{4+} is progressively varied [Mah96, Rao98, Coe99] from nearly stoichiometric to large nonstoichiometric compounds. The structural change of O′ →O→R,C, can also be observed with divalent ion substituted lanthanum manganites. The increase in Mn^{4+} content, decreases the Jahn-Teller distortion of the MnO_6 octahedra which results in a more symmetric crystal structure. As a consequence of this structural change, a large change in Mn-O-Mn bond angle from ∼155 to ∼168° results. This change considerably affects the magnetic interactions in the manganites.

In manganites, which consist of MnO_6 Octahedra, an important type of magnetic exchange is the superexchange, where the oxygen p orbitals mediate the exchange

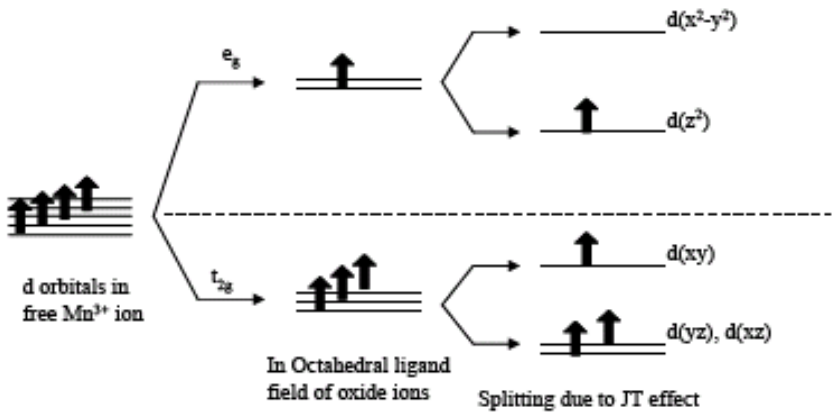

Figure 1.5: Jahn-Teller effect of Mn^{3+} ions in an octahedral ligand field of oxygen anions.

through the Mn-O-Mn linkage whose ideal bond angle is 180° [Goo55]. Depending upon the nature, symmetry, and occupancy of the e_g orbitals, the coupling results in various types of magnetic ordering; the governing factors being the Pauli antisymmetric principle and Hund's rule of spin multiplicity. If the e_g orbitals on both the Mn ions are half-filled, an antiferromagnetic type of exchange results and if e_g orbital of one Mn ion is vacant, with the other half-filled, a ferromagnetic type of exchange results.Fig. 1.6 (a) and (b) show the superexchange mechanism in manganites. However, certain correlated phenomena like co-existence of metal-insulator transition and ferromagnetic-paramagnetic transition could not be explained by the simple superexchange scenario. Hence, the concept of double exchange was suggested for explaining this behavior in certain hole-doped manganites. The double exchange between the Mn^{3+} and Mn^{4+} ions is maximum when Mn-O-Mn bond angle is 180°. Thus, any deviation of the bond angle towards 180° results in stronger magnetic exchange and

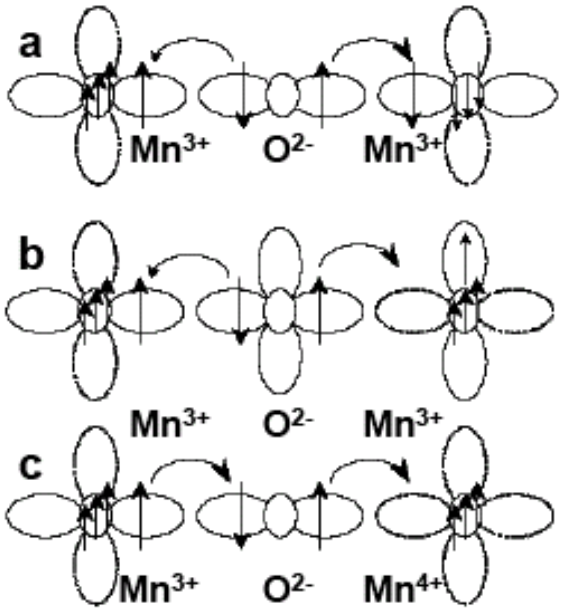

Figure 1.6: Basic magnetic exchange mechanisms

hence an increase of T_c.

1.2.4 Metal-Insulator Transition

Quite unusual about such mixed-valent manganites are that they exhibit metal-insulator transition around T_c (i.e., the compounds show insulating behavior above T_c and metallic behavior below T_c). The simultaneous itinerant electron behavior and ferromagnetism in the manganites is explained by the double-exchange mechanism as proposed by Zener and developed by various researchers [Zen51, And55, Deg60]. The double exchange involves the transfer of an electron from Mn^{3+} site to central oxide ion and simultaneous transfer of an electron from oxide ion to an Mn^{4+} site as shown in Fig. 1.6(c). The exchange energy of such a system is nonvanishing only if the spins

of the two d shells are parallel. This is the lowest energy state of the system with a parallel alignment of the spins on Mn^{4+} and Mn^{3+}. Thus the mechanism which leads to increased electrical conductivity (metallic property) requires ferromagnetic coupling. When temperature is increased the configuration of the spin is dynamically disordered and it will lead to enhancement of resistivity above T_c. The M-I transition around T_c is also explained by Millis *et al.* by considering electron-phonon interactions arising from J-T distortions [Mil98]. The J-T distortion essentially localizes the conduction electrons as polarons (often called Jahn-Teller polarons) when $T > T_c$ and the delocalization of polarons occurs at around T_c below which metallic behavior is observed.

Above T_c, it is generally accepted that [Mot90], the resistivity follows an exponential relation

$$\rho \propto exp\ (\frac{E_0}{kT})$$

where the gap E_0 is typically 0.1 eV. Other models suggested include small polaron formation, which is often explained by fitting the resistivity curve above T_c and is given by the relation,

$$\frac{\rho}{T} \propto exp\ (\frac{E_0}{kT})$$

Another possibility is the model of Mott's variable range hopping conduction, which has the following relation,

$$\rho \propto exp\ (\frac{T_0}{T})^{1/4}$$

Beznosov *et al.* have proposed a $\Delta m\tau$ model of conductivity [Bez02]. This model includes a thermally activated mechanism of conductivity, dependence of the concentration and the effective mass (m) of the itinerant charge carriers on the magnetization, and scattering of the charge carriers with characteristic time τ.

1.2.5 Colossal Magnetoresistance - CMR

Magnetoresistance (MR) is the change in the electrical resistance of a material produced on applying a magnetic field, H. MR is given by,

$$\frac{\Delta\rho}{\rho(0)} = \frac{\rho(H)-\rho(0)}{\rho(0)}$$

Where $\rho(H)$ and $\rho(0)$ are the resistance at a given temperature in an applied and zero magnetic fields, respectively. MR can be negative or positive. All the metals show some MR, but only a few percent. Very large MR, referred to as giant magnetoresistance (GMR), was first observed on the application of magnetic fields to atomically engineered magnetic superlattices (e.g., Fe/Cr). Several bimetallic or multimetallic layers, containing ferromagnetic and antiferromagnetic or nonmagnetic metals, have been found to exhibit GMR. The phenomenon is of vital interest because of its potential technological applications in magnetic recording, actuators, and sensors. Some lanthanum manganite compositions, mostly with divalent ion doping with the general formula, $La_{1-x}D_xMnO_3$ (D = divalent ion) having a perovskite structure show very huge change in the electrical resistance when a magnetic field is applied [Jin94, Jin95]. This change in resistance is called colossal magnetoresistance (colossal means very large). The CMR effect in manganites is explained by the double exchange model as illustrated in Fig. 1.7. The colossal magnetoresistance (CMR) in these materials is about hundred percent in magnetic fields of few Teslas. CMR offers potential in a number of technologies, such as for read/write heads in magnetic recording media, sensors, and spin-polarized electronics, thus making them an important class of compounds to be studied not only in the application point view, but for the scientific understanding of the various interactions involved in these [Rao98, Coe99, Tok00, Sal01, Dag03, Gor04, Van04].

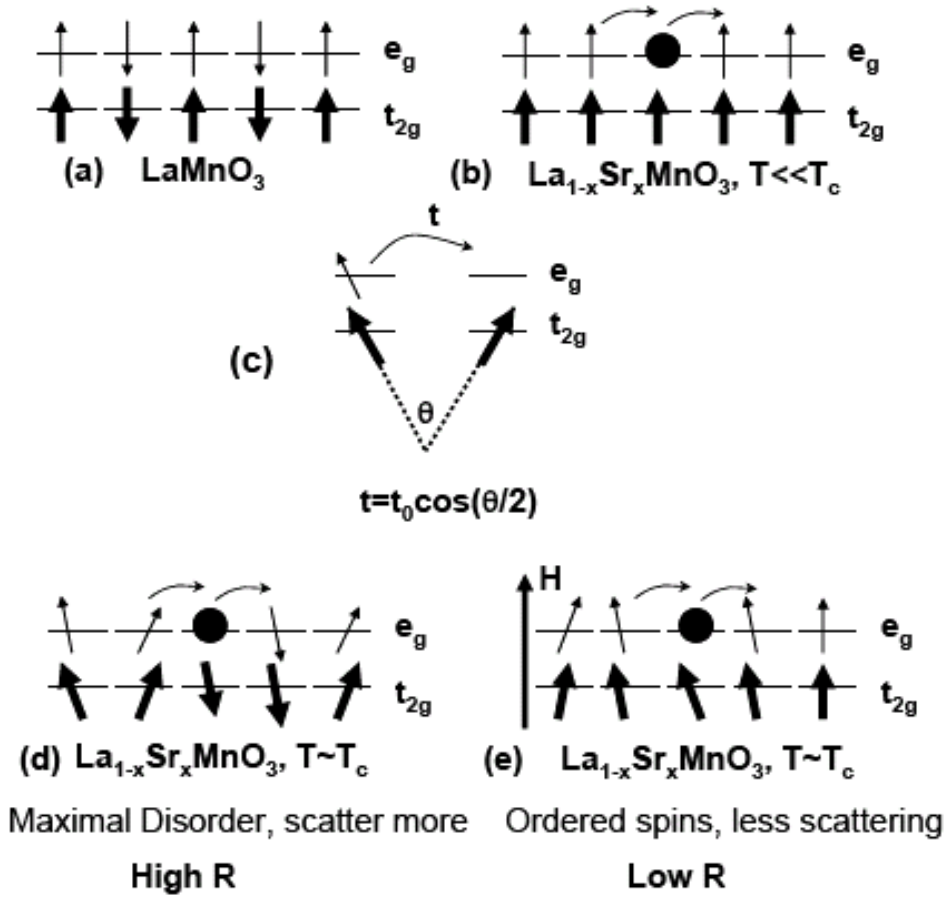

Figure 1.7: Illustration of possible double exchange mechanism in (a) $LaMnO_3$, (b) $La_{1-x}Sr_xMnO_3$, (c) the dependence of double exchange on the angle between the spin vectors is shown by the sketch . The probable mechanism of spin dependent scattering happening in CMR-type of manganites (d) in the absence of magnetic field (e) in a magnetic field

1.3 A Brief Background and Scope of the Present Work

Hole-doped perovskite-type lanthanum manganites are known for their interesting magnetic properties [Rao98, Tok00]. Divalent ion-substituted lanthanum manganites are studied in detail with special relevance to their colossal magnetoresistive properties. The stoichiometric parent compound, $LaMnO_3$, with 100% Mn^{3+} ions in its crystal lattice is an antiferromagnetically ordered compound. By doping at the La-site by divalent ions or by self-doping (creating vacancies at the La-site), Mn^{4+} ions can be introduced into the lattice of $LaMnO_3$, and this is responsible for the interesting magnetic and electrical properties of these oxides. In both cases, the observed ferromagnetic and the associated properties can be explained in terms of the double exchange interaction between manganese ions in different oxidation states through intervening oxygen ions. The possible competitions between charge, spin and orbital degrees of freedom make the perovskite La-Mn-O system one of the most complicated among the condensed matter systems.

1.3.1 La-deficient Manganites

One of the important aspects of the La-Mn-O perovskite system is the wide range of non-stoichiometry possible and the related intriguing properties. The magnetic and transport properties of the self-doped manganites, $La_{1-x}MnO_3$, resemble that of the divalent element doped CMR manganites, $La_{1-x}D_xMnO_3$ [Coe99]. This is because, self or vacancy doping in the La-site of the perovskite $LaMnO_3$ also produces Mn^{4+} in the lattice, as in the case of $La_{1-x}D_xMnO_3$, which can explain the evolution of the interesting magnetic and electrical properties, including CMR of $La_{1-x}MnO_3$ in terms of the double-exchange interactions.

Compared to the large number of studies on $La_{1-x}D_xMnO_3$, there are not many

reports in the literature on the self-doped compositions. It is reported that the limiting value of x in $La_{1-x}MnO_3$ is 0.1, based on the observation of Mn_3O_4 as an impurity phase for $x > 0.1$ [Tak91, Sak96, Dez02]. However, still there are many reports in the literature on the studies of the self-doped compositions in the doping range $0 \leq x \leq 0.33$ [Gup95, Hau96, Jim97, Che00, Kim01, Los01]. In many of these studies, minor amounts of a second phase due to Mn_3O_4 is usually observed and this is ignored while discussing the properties of the highly doped compositions. Similarly, in most cases, the ferromagnetic Curie temperature remains constant for higher values of x and this is also used to be ignored while discussing the properties of the studied compositions. The second phase Mn_3O_4 formed must be having some roles in determining the limiting value of x (a fraction y of Mn_3O_4 means the absence of three times of Mn or larger La/Mn ratio in the perovskite than expected). Recent X-ray absorption studies by Dezanneau *et al.* also suggests that the structure is no longer stable beyond a value of La/Mn = 0.9 and Mn_3O_4 is found as an impurity phase [Dez04]. Dezanneau *et al.* have also observed the similarity of the self doped compositions with the other substituted manganites and that both classes of compounds undergo a reduction in MnO_6 disortions when the temperature is lowered which in turn implies the weakening of the carrier-lattice interaction and strengthening of the double exchange between Mn^{3+} and Mn^{4+} ions [Dez04]. Bosak *et al.* [Bos04] have found the solubility limits for $La_{1-x}MnO_3$ thin films as sensitive to the oxygen partial pressure during the post-deposition annealing. They have observed different secondary phases depending on the annealing conditions. From the XRD and TEM analysis, a Mn_3O_4 phase (hausmannite) was observed as a secondary phase in the $La_{1-x}MnO_3$ film with La/Mn = 0.76, when the film was oxygen-annealed. A diminished intensity of Mn_3O_4, when La/Mn = 0.83 and absence of the impurity phase in XRD for lower values of x suggested the possible limit of x in $La_{1-x}MnO_3$ as in between 0.17-0.1. In the Ar-annealed films, an MnO phase was appeared as the impurity and the sol-

ubility limit was also changed to La/Mn ∼0.95 as compared to La/Mn ∼0.80 in the oxygen-annealed samples.

The magnetic properties of La-deficient manganites are found to be dependent on the processing conditions [Nak03]. The defect chemistry of $La_{1-x}MnO_{3+\delta}$ has been suggested as consisting of La and Mn vacancies as suggested in [Nak02a],

$$La_{1-x}\square_x MnO_{3+\delta} \rightarrow (La_{1-x}\square_x Mn_y)(Mn_{1-y}\square_y)O_{3+\delta}$$

This suggests the possibility of occupancy of La-site vacancies partially by Mn^{3+} ions. However, such a possibility is far too less because the large mismatch of the ionic radii of the La and Mn ions. The origin of the anomalous electronic transport behavior of oxygen reduced self doped compositions have been explained in the light of the above model [Nak02b]. The effect of annealing conditions on the electronic properties of self doped compositions have been studied extensively by several researchers [Pig97, Qia02, Vin02, Tro03]. The structural, magnetic and transport properties of self-doped compositions, $La_{1-x}MnO_3$ depend not only on the values of x, but a large extent to the oxygen nonstoichiometry. Vincent *et al.* have observed structural transformations of an $La_{0.8}MnO_{3-\delta}$ depending on the annealing conditions [Vin02]. The as deposited film was found to be a monoclinic phase with space group $I2/b$ which was partially changed to monoclinic $P2_1/a$ on annealing at 973 K for 3 hours.

Troyanchuk *et al.* have observed transition from an orthorhombic to a monoclinic phase when the oxygen stoichiometry is varied from 2.82 to 2.96 where orthorhombic phase is found to be stable up to a value of 2.90 and for higher values a monoclinic stricture is observed [Tro04]. A ferromagnetic nature is observed when the oxygen stoichiometry is higher than 2.86, below which an antiferromagnetic ordering is observed. In a recent report, the effect of processing conditions on the self doped compositions with values of $x = 0.9$ and 0.8 has been investigated and found that the structural features vary significantly. For the sample with $x = 0.9$ [Dha04] when the annealing

temperature was 973 K, a rhombohedral structure was observed, and correspondingly a clear magnetic transition at ∼275 K and when the annealing temperature was 1773 K, an orthorhombic structure was observed for the sample, but showed no clear magnetic transitions. A mixed magnetic phase behavior (a hole-free AFM insulating phase and hole-rich FM regions) is reported for certain single crystals of self-doped compositions [Mar03]. From the ferromagnetic resonance analysis, it was concluded that in $La_{0.87}MnO_3$ sample, variety of ferromagnetic phases are coexisting, and this is attributed to the strong inhomogeneity of the La vacancy distribution. It has been suggested that the domains with higher concentrations of Mn^{4+} show higher transition temperatures as observed from the magnetic, transport, and electron magnetic resonance studies.

Despite the numerous works reported so far, the defect chemistry, structural, magnetic and transport behavior of the compositions, $La_{1-x}MnO_{3\pm\delta}$ with various values of x have not been successfully explained so far.

1.3.2 Oxygen Nonstoichiometry in Manganites, $LaMnO_{3+\delta}$

Magnetic and electrical properties of the non-stoichiometric compound $LaMnO_{3+\delta}$ have been studied extensively for the past five decades [Rao98, Coe99, Tok00], after Jonker and Van Santen [Jon50], in 1950, first observed the effect of Mn^{4+} in determining the magnetic properties of $LaMnO_3$. In the La-Mn-O perovskite system, the stoichiometric compound $LaMnO_3$ in which Mn is present in its trivalent form, Mn^{3+}, is an antiferromagnetic material. The antiferromagnetic transition at $T_N \sim$ 100-140 K is reported in the literature [Wol55, Mat70, Pav84, Ran96], with some of the samples containing small amounts of Mn^{4+} (0-10%).

In the stoichiometric composition, the orbital degeneracy is lifted due to a cooperative Jahn-Teller distortion which leads to an anisotropic ferromagnetic ordering of Mn^{3+} ions within the *a*-*b* plane of the orthorhombic unit cell ($Pbnm$) and along

the c direction, the Mn^{3+} ions couple antiferromagnetically [Wol55]. Such a situation is often identified as A-type ordering. However, weak ferromagnetism owing to a canted spin arrangement is also reported for $LaMnO_3$, which results from the Dzyaloshinskii-Moriya type of antisymmetric exchange [Mat70]. The Curie-Weiss behavior is observed for $LaMnO_3$ with a large effective magnetic moment of 5.5 μ_B per Mn ion, which suggests the existence of local, short range ordered magnetic clusters well above the Neel temperature [Top97b]. The oxygen nonstoichiometry in $LaMnO_{3+\delta}$, however, causes ferromagnetism due to the double exchange between Mn^{3+} and adjacent Mn^{4+} ions through the oxide linkage. The structure of the compound is also strongly dependent on the oxygen nonstoichiometry. Recent studies by Laiho *et al.* on a series of compositions with values of δ in $LaMnO_{3+\delta}$, suggests an orthorhombic structure for $\delta = 0$ which varies to a rhombohedrally distorted cubic structure for $\delta = 0.065$-0.112, and then to a rhombohedral crystal symmetry for $\delta = 0.125$-0.154 [Lai03]. Pavlov *et al.* from their neutron diffraction studies concluded that an antiferromagnetic to a ferromagnetic character is induced when the oxygen nonstoichiometry is varied, and this is due to the structural O′-O orthorhombic phase transition [Pav84]. The O′-orthorhombic structure ($c/a < \sqrt{2}$) is conditioned by the cooperative, static Jahn-Teller (J-T) distortion of the MnO_6 octahedra. The decrease of Mn^{3+} concentration leads to the partial removal of such J-T distortion, which results in O-orthorhombic phase ($c/a > \sqrt{2}$). An A-type ordering as discussed above operates and O′-orthorhombic lanthanum manganites are antiferromagnetic. Whereas, in O-orthorhombic lanthanum manganite, with more than 14% Mn^{4+}, ferromagnetism is observed which is explained by the isotropic indirect interaction of Mn^{3+}-O-Mn^{3+} caused by the dynamic J-T effect or it may be the double exchange between Mn^{3+} and Mn^{4+} ions. A mixed ferromagnetic and antiferromagnetic behavior is observed for compositions with Mn^{4+} in the range of 10-14% corresponding to the mixed O′ and O-orthorhombic structural phases.

Generally, it is not possible to obtain the compound in stoichiometric form under the general preparation conditions (heating oxides of La and Mn in air), due to the tendency of Mn to form tetravalent ions, so that the formula is generally written as $LaMnO_{3+\delta}$ which takes care of the presence of Mn^{4+} ions. Jonker and Van Santen [Jon50] had commented that the tendency to take up excess oxygen might be an indication of a region of mixed crystals extending from $LaMnO_3$ to $La_{2/3}MnO_3$. As the perovskite structure cannot accommodate excess oxygen, there have been attempts to elucidate the structure and composition of the non-stoichiometric compound. Tofield and Scott [Tof74], in 1974, from neutron diffraction studies, found that the actual composition of $LaMnO_{3.12}$ is $La_{0.94}Mn_{0.98}O_3$ ($\sim La_{0.96}MnO_3$) which is an La-deficient compound. Later on, Van Roosmalen *et al.* [Van94a, Van94b], in 1994, from refinement of their neutron diffraction data on $LaMnO_{3+\delta}$, have argued that the studied composition contains equal amounts of La and Mn deficiency (La and Mn in 1:1 ratio), $La_{1-y}Mn_{1-y}O_3$, though they obtained a lower residual factor for unequal La and Mn deficiency as found by Tofield and Scott [Tof74]. Recently, Malavasi *et al.* have also explained the role of cation vacancy distribution in defining the magnetic properties of such non-stoichiometric perovskites [Mal05].

The ferromagnetism and metal-insulator transition is observed in $LaMnO_{3+\delta}$ with high Mn^{4+} content and this has been explained in terms of the double exchange interactions between Mn^{3+} and Mn^{4+} ions, as in the case of the divalent ion substituted CMR manganites. It is generally considered that the ferromagnetic Curie temperature increases with increasing Mn^{4+} content in $LaMnO_{3+\delta}$, due to the increasing strength of the double exchange interactions [Tiw97]. However, several reports are available showing a weak ferromagnetism or spin glass (or cluster glass) behavior for sufficiently high values of δ [Hau96, Alo97a, Rit97, Ghi99]. Recently, the effect of cooling rate on the magnetic properties of $LaMnO_{3+\delta}$ has been studied and the unusual effects observed in the fast cooling magnetic measurements are attributed to

the Dzyaloshinskii-Moriya interaction [Pap04].

The value of δ is found to be changing with the processing conditions and synthesis methods which in turn affects the electronic properties significantly. Commonly, high values of δ are observed when the samples are prepared by soft-chemical routes [Ver93]. Heat treatment at higher temperatures cause reduction in the value of δ. The heating conditions and availability of oxygen atmosphere drastically change the situation [Pra99, Lai05]. Thus, the δ factor plays an important role in determining the magnetic properties of these mixed oxides. The extent of vacancies both at La-site and/or Mn-site produced due to the oxygen nonstoichiometry and its effects on structural and magnetic properties are yet to be understood clearly.

1.3.3 Low-Temperature Magnetic Anomaly and Spin Glass Behavior in Lanthanum Manganites

Some anomalous magnetic behavior at low temperatures is observed in the ferromagnetic regime of the CMR oxides $La_{1-x}A_xMnO_3$ (A = Ca, Sr, Ba), for low-concentrations of the substituted ions. This is observed in the form of a decrease in the *ac* susceptibility or zero field cooled *dc* magnetization measured using very low magnetic fields, at temperatures much below the paramagnetic to ferromagnetic ordering temperature of the specific compositions [Mit96, Kaw96, Bar98, Dho99, Lob00, Gec01, Has04]. This is generally explicated as due to the glassy-spin configuration or spin frustration, presence of a mixed state of ferromagnetic and antiferromagnetic phases in the sample, ferromagnetic to antiferromagnetic transition, and sometimes attributed to the effect of charge ordering. However, sufficient evidences for the existence of long-range magnetic order in such samples have been obtained from the neutron diffraction studies even at temperatures below the magnetic anomaly is observed.[Hau96, Rit97, Bra03]

From ^{139}La NMR studies, Dho *et al.* have attributed the origin of this low-

temperature anomaly in $La_{1-x}Ca_xMnO_3$ ($0.1 \leq x \leq 0.2$) to mixed state of ferromagnetic and antiferromagnetic phases in the sample [Dho99]. On the other hand, Castro *et al.* [Cas99] have concluded that the decrease in the *ac* susceptibility of $La_{7/8}Ca_{1/8}MnO_3$ at low temperatures is due to a magnetic transition from ferromagnetic to antiferromagnetic phase with a possible charge ordering process. However, Lobanov *et al.*, from neutron diffraction studies [Lob00], have reported that their $La_{0.85}Ca_{0.15}MnO_3$ sample remains ferromagnetic down to low temperatures though a decrease in the susceptibility is observed below ∼100 K. A similar magnetic behavior has also been reported for $La_{0.83}Sr_{0.17}MnO_3$ by Kawano *et al.* [Kaw96]. This compound exhibits only a ferromagnetic component down to low temperatures in neutron diffraction measurements and the decrease in the ZFC magnetization of the compound from the ferromagnetically ordered phase is attributed to a structural phase transition. Based on the observation of frequency dependence of the ac-susceptibility and the thermomagnetic irreversibility in $La_{0.82}Ca_{0.18}MnO_3$ single crystal Markovich *et al.* have concluded that the composition shows cluster-glass properties [Mar02]. The models based on mixed ferro- and antiferromagnetic phases, two different ferromagnetic phases, charge ordering, etc., as in the case of $La_{1-x}Ca_xMnO_3$ have also been used to explain the similar properties observed in $La_{1-x}Sr_xMnO_3$ [Yam96, Det96, Yun98, Sen98, Noj99].

A similar effect is also observed when the rare-earth (R) ion concentration in certain $La_{0.7-x}R_xCa_{0.3}MnO_3$ (where R = Pr,Y, and Dy) compositions is increased [Hwa95, Ter98]. De Teresa *et al.* suggests that the substitution by Tb ions at La-site in $La_{0.67}Ca_{0.33}MnO_3$, results in a spin-glass insulator state and is thought to be due to the competition due to the ferromagnetic double exchange and antiferromagnetic superexchange interaction, which prevents the occurence of a long range magnetic order [Det96]. The evolution of a conventional spin glass state is suggested by Mathieu *et al.* for $Y_{0.7}Ca_{0.3}MnO_3$, based on their magnetic relaxation studies [Mat01a]. A

reentrant spin glass behavior is suggested for certain Cr-doped manganites, which exhibit similar low tempearture magnetic features [Dho02]. Magnetic anomalies below the Curie temperature is also observed when Mn ions are partially substituted by Ni and Cu ions [Sun00, Bla02].

Alternatively, a cluster glass behavior of manganites has been suggested [Rit97, Wat01]. In the cluster-glass picture, magnetic clusters are formed as a result of concentration fluctuations and at sufficiently low temperature, these clusters would freeze with random orientation in a manner analogous to the spin-glass freezing. Such isolated magnetic clusters have been observed in certain manganites from the low temperature Neutron Scattering measurements [Det97]. It is also suggested that at larger fields, such tiny clusters merge into one to form a single ferromagnetic domain [Wat01].

Thus, several similarities in the magnetic behavior of conventional spin glasses and some manganite compositions have been observed. However, it is not obvious that they follow the typical conventional spin glass dynamics. The complicated nature of manganites make them difficult to be categorised as canonical spin glasses or a totally new kind of spin glass.

1.3.4 Phase Separation in Manganites

Lanthanum manganite compositions, even in the single crystalline form, exhibit compositional and electronic inhomogeneities arising from the existence of more than one phase and this phenomenon is referred to as phase separation [Mor99, Rao03, Bel04]. The phase separation in manganites may be compositional or electronic type. This depends on the size of the cations at the La-site in the lanthanum manganites, carrier concentration (in case of hole doping), temperature, magnetic field etc. It is believed that such a phase separation scenario has several important implications in defining various magnetic and conducting features of manganites. The small scale phase sep-

aration in manganites is sometimes explained in terms of droplets, domains, clusters and polarons [Ueh99, Dag03].

In a substituted manganite, if the carrier concentration is less, ferromagnetic ordering would occur at one portion of the crystal forming *droplets* or *domains*, the rest of the portions remains antiferromagnetic and insulating. Thus, depending on the concentration of charge carriers, such an electronic phase separation may be ensued. A similar feature would be envisaged when the carrier concentration is very high, in which case, antiferromagnetic *droplets* or *domains* will be formed in a ferromagnetic matrix. Another way of different phases getting separated in a crystal is due to the impurity or disorder effects. The disorder would arise from the cation-size mismatch in perovskite-type manganites. The size of the clusters depends on the magnitude of disorder, and large clusters may be formed for smaller disorder.

In substituted lanthanum manganites, when the concentrations of Mn^{3+} and Mn^{4+} become almost equal, signatures of charge ordering is commonly seen at low temperature magnetization studies, where a CE-type of antiferromagnetic ordering sets in [Rao98, Tok00, Fre02, Dag03]. Thus, a competition between a charge ordered antiferromagnetic state and a double exchange ferromagnetic state becomes possible in the crystal. Consequently, a ferromagnetic-charge ordered transition is observed in many $R_{1-x}D_xMnO_3$ compositions (R = rare earth ions and D = divalent ions), especially in the concentration regime of $x \sim 0.5$ [Rao98, Tok00, Par01, Fre02, Dag03]. At low substitution levels of divalent ions, ferromagnetic clusters are formed in an antiferromagnetic matrix, and such compositions are known to behave like spin glasses [Rao98, Dag03]. A disorder effect may also result in the formation of ferromagnetic clusters due to the restriction of double exchange mechanism. Such a phase separation scenario, thus, has a great significance in the manganite compositions and has been used to explain various magnetic and transport characteristics including colossal magnetoresistive behavior. Another closely related topic is the compositional

inhomogeneity [Bel04]. Since the substituted manganites can form a wide range of compositions and the method of synthesis and processing conditions are the same to get different compositions, it is possible that all possible compositions will be formed initially and the final composition depends on the processing conditions. If the processing is insufficient, several compositions in the solid solution may co-exist in a sample giving rise to compositional inhomogeneity. This also will give rise to unusual and anomalous properties for the manganites [Kum98b, Bel04].

1.3.5 Quantum Critical Point in Manganites

It is very essential to understand the role of the La and the Mn-site ions (for fixed concentrations of Mn^{3+} and Mn^{4+}) in determining the magnetic properties of compositions of the class $La_{1-x}Ca_xMnO_3$. One of the ways to study this problem is by partially replacing the Mn ions by other transition metal ions and the other by varying the Mn-O-Mn bond angle which is crucial in deciding the long range exchange between the magnetic manganese ions. The Mn-site substitution of perovskite-type manganite compositions, $La_{1-x}Ca_xMn_{1-y}(T)_yO_3$, by transition metal ions (T), like Ti^{3+}, Cr^{3+}, Fe^{3+}, Co^{3+} etc. has been studied in detail in the recent past. Substitution with these ions is found to weaken the ferromagnetic exchange there by affecting the magnetic long range to a considerable extent, which ultimately results in the lowering of T_c. Also, substitution by other magnetic ions give rise to different kind of exchange interactions involving two types of ions with different spin states (due to variable oxidation state of the transition metal ions) which result in complex magnetic behavior of the material [Veg05]. A rather straightforward approach to study the weakening of magnetic exchange interactions associated with the magnetism in manganites would be substitution of the Mn ions by a nonmagnetic ion like, Ga^{3+}, Al^{3+} etc. The substitution of Mn ions with Ga ions has recently been studied in detail and predicted the possible existence of a quantum critical point (QCP) which is in fact, a second

order phase transition, occurring at zero temperature when non-thermal parameters such as pressure, magnetic field, or chemical composition is changed. Such a QCP is observed when the concentration of the substituent ions (Ga ions) is increased. At some concentrations of the substituted ions, the magnetic and transport properties of the compounds are found to undergo sudden changes. The magnetic moments of the compositions are found to decrease with the Ga concentration and a sudden drop is observed at around 12%. Also coexistence of ferromagnetic and short range clusters are observed for an intermediate range of Ga-substitution and above which only short range clusters are observed. Similarly, when the concentration of Ga exceeds 11%, the metal-insulator transition is found to be vanished and further increase in Ga concentration results in perfect insulator behavior regardless of the same Mn^{3+}/Mn^{4+} ratio maintained through out the whole concentration range of Ga ions in the compositions (5% to 30%). The effects of Mn-O-Mn bond angle on such short range ordering is interesting and may be observed in heavier rare-earth substituted manganites and are studied in the present work.

1.3.6 Anomalous Electrical Resistivity Behavior in Manganites

The low temperature transport properties of poly crystalline manganites are sensitive to the extrinsic effects such as grain boundaries and magnetic domain boundaries [Mat99, Sal01, Ver01]. These effects are related to grain boundary tunneling. The giant magnetoresistance observed in manganites are suggested to be due to spin dependent tunneling of conduction electrons across grain boundaries [Zha97]. The spin dependent tunneling, thus, depends on the grain size and the properties of intergranular material which constructs the intergrain barrier. It is suggested that these materials show interfacial tunneling between adjacent grains due to the difference in magnetic order between surface and core [Zha97].

However, in some cases, a double peak behavior is observed in the temperature dependence of resistivity, the first one commensurate with T_c and the second normally below T_c [Man97, Sun98, Abr99, See04, Bel05]. An important feature is the processing dependence of the double peak resistivity. From a large number of available literature on the resistivity behavior of manganites, it is concluded that the double peak character is not always observed for the same composition prepared by same or different methods [Zha97, Bar98, Rao98, Tok00, Ver01, Bel05]. Various reasons for the observation of the double peak resistivity, those have been suggested include inhomogeneous oxygen content, phase separation, grain and grain boundary effects, intergrain tunneling, etc. as discussed in the section 7.1. The origin of this behavior still remain unclear and an attempt to study the origin of such behavior has been done in the present work.

Chapter 2

Experimental Methods

Various synthetic as well as materials characterization techniques have been used in the present study on the rare-earth manganites. To study the processing dependence of the physical properties changes in either the preparative methods or the processing conditions are required. For the determination of the physical properties, mostly non-destructive techniques are utilized. The characterizations have been made mostly at or below the room temperature.

2.1 Synthesis Methods

The common methods of synthesis of oxide materials are the ceramic (also known as solid state method and high-temperature method), sol-gel, combustion, coprecipitation, etc [Rao94]. Except the first one, all the other methods belong to the class of soft-chemical routes of synthesis. Both the ceramic and some soft-chemical methods have been utilized in the present study. The sample purity is very important, and hence the starting chemicals used for the synthesis in the present study were of the purity $\geq 99.9\%$. Sensitive oxides such as La_2O_3 absorbs moisture and CO_2 under normal atmospheric conditions to form $La(OH)_3$ and $La_2O_2CO_3$, respectively. Hence, such oxides were preheated at 1273 K for 6 h and kept in a suitable desiccator, prior to the synthesis of every batch of compounds. A furnace with controlled

heating and cooling arrangements was used for heating the samples from 1273 K to 1723 K (Nabertherm, Germany) and the samples were heated in high purity alumina crucibles or boats. A tubular furnace was used for heating the sample under dynamic gas atmosphere.

2.1.1 Ceramic Method

Ceramic method involves heating the mixed starting solid chemicals at high temperatures so that the ionic diffusion results in the formation of a stable compound. The solid state ionic diffusion requires high thermal energy and is generally a slow process. Hence, high temperatures and longer heating durations are required for the movement of ions and reorganization of the structures. In a typical ceramic method, the components in the form of metal oxides, carbonates, or other easily decomposable salts of organic acids, etc., were taken in the required stoichiometric proportions. For example, $LaMnO_3$ can be prepared from a 1:2 stoichiometric mixture of La_2O_3 and MnO_2 or $MnCO_3$, so that a 1:1 stoichiometric ratio of La:Mn is maintained. The weighed components were mixed thoroughly in an agate mortar using a pestle. The well-ground mixtures were then initially heated at 1273 K and further at various temperatures with many intermediate grindings in order to ensure the sample homogeneity. In some cases, the powder samples were made in to the form of pellets by cold pressing at a pressure of 10,000 psi and heated at high temperatures and these pellets where then used for some of the measurements. All the samples were characterized for their phase purity, after each heating cycle, using powder X-ray diffraction method and accordingly, the processing conditions were modified to obtain single phase materials.

2.1.2 Low-Temperature Methods - Soft Chemical Routes

Several soft-chemical routes were employed in the present study. They are

Coprecipitation Method

Coprecipitation method is a precursor method for the solid state reaction. Here, the components were taken in solution (commonly nitrates of the corresponding metals as aqueous solutions) and precipitated together as easily decomposable salts (commonly carbonates) by adding excess of precipitating reagent. This method ensures molecular level mixing of the starting components in solution and small size of the particles of the precipitate mixed homogeneously, and requires rather low temperature for the diffusion of ions during the solid state reaction. In the present work, the reported method using ammonium carbonate as the precipitation agent was used [Hau96]. The component metal nitrates taken in the required stoichiometric ratio were individually dissolved in water and mixed together. Ammonium carbonate was added to the mixed nitrate solution with continuous stirring. A precipitate obtained was filtered, washed several times and dried in an oven. The dried precipitate was then heated above the decomposition temperature of the salts. The firing temperature was determined by verifying the XRD patterns for any impurities present.

Combustion Method

The combustion method involves the spontaneous burning of the mixture of reacting ions which are in close proximity, in a very short time duration. In a typical combustion reaction, a fuel and an oxidizer are required. The combustion reaction ensures a better homogeneity for the products than those obtained by the ceramic or the coprecipitation method. In the present study, metal nitrates were used as the oxidizer and different glycine was used as the fuel. This method is known as the

glycine nitrate process (GNP) [Chi90]. A well mixed aqueous solution of the metal nitrates taken in the required stoichiometry is mixed with a water solution of glycine ensures a molecular level mixing of the components. Glycine not only acts as a fuel but act as a bidentate ligand and coordinates to the metal ions through its amino and/or carboxylic groups.

Initially, the metal nitrates were dissolved in minimum amount of water and then mixed together. Glycine, dissolved in minimum amount of water (2 moles of the fuel for each mole of metal ions), is then added into this solution to form a water soluble complex of individual metal ions. The final solution was taken in a 5000 ml beaker which was then covered with a stainless steel wire-gauze, and heated at 473 K on a laboratory hot plate. Auto-ignition starts as soon as the evaporation of water is completed and a solid mass is obtained within 5 minutes. The resulting mass contains the oxide phase, is then analyzed using various techniques and heated further at higher temperatures in a furnace to form the desired phase.

This solution-combustion method has a serious disadvantage that the oxidation of nitrogen and carbon results in toxic gases such as NO_x and CO_2. Hence this method is not employed quite frequently for the synthesis of the samples during the present study.

Citrate Method

The citrate gel method is commonly employed for the synthesis of oxides [Alo97a, Tag97]. In this method also, the soluble metal salts are used and citric acid is used as the complexating agent. For the synthesis of the oxides using this method, the metal nitrates taken in the required stoichiometric ratio were individually dissolved in water and then mixed together. To the mixed metal nitrates solution, citric acid solution in water was added by keeping the metal to citric acid ratio as 1:2. This mixed solution was then kept on a water bath for the evaporation of water and a gel

formed was calcined in a furnace at 673 K. A powder obtained after the decomposition of the metal-citrate complex is then heated at higher temperatures, as described in the previous cases.

2.2 Characterization Methods

2.2.1 X-ray Diffraction

The powder X-ray diffraction (XRD) technique is used to identify which crystalline phases are present in a solid material [Klu54, Cul56]. Each crystalline material has its own characteristic powder X-ray diffraction pattern, which serves as a fingerprint for its identification. The powder X-ray method serves to indicate the completeness of a reaction and the presence/absence of unwanted side products and impurity phases.

By analogy with the diffraction of light by an optical grating, a crystal with their regularly repeating structures should be capable of diffracting radiation that has a wavelength similar to the interatomic separation (approximately 1Å). Diffraction of X-rays from a crystal is illustrated in Figure 2.1.

Consider two X-ray beams 1 and 2 are reflected from adjacent planes A and B separated by a distance d within the crystal, which is the interlayer spacing separating the corresponding hkl planes. The rays $1'$ and $2'$ are in phase if path difference, XYZ is equal to whole number of wavelengths. If θ is the angle of incidence,

$$XY = YZ = dsin\theta$$

$$XYZ = 2dsin\theta$$

If $1'$and $2'$ are in phase,

$$XYZ = n\lambda$$

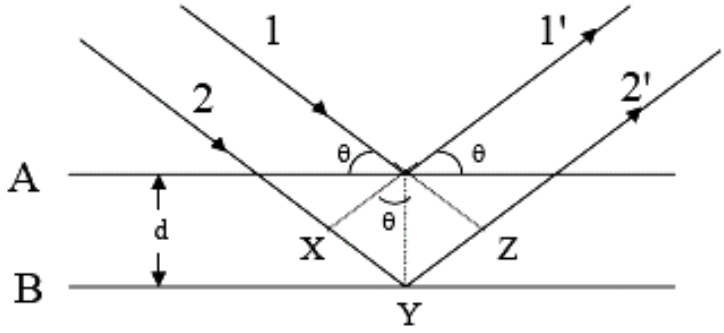

Figure 2.1: Bragg's law of diffraction.

Therefore,

$$2dsin\theta = n\lambda$$

This is called the Bragg's law.

When Bragg's law is satisfied, the diffracted beams are in phase and interfere constructively. At angles of incidence other than the Bragg angle, the diffracted beams are out of phase and destructive interference or cancelation occurs. When crystals diffract X-rays, it is the atoms or ions, which act as secondary point sources and scatter the X-rays, since X-rays have an oscillating electric field, which sets each electron of an atom into vibration. This vibrating charge emits radiation which is in phase or coherent with the incident X-ray beam. The efficiency of scattering of a given atom in a given direction is called as the atomic scattering factor f.

$$f = \frac{Amplitude\ of\ wave\ scattered\ by\ anatom}{Amplitude\ of\ wave\ scattered\ by\ an\ electron}$$

The resultant wave scattered by all the atoms of the unit cell is called the structure factor F. It is obtained by adding all the waves from individual atoms. If a unit cell

contains n (n = 1,2, 3, etc.) number of atoms with fractional coordinates (u_n, v_n, w_n) with scattering factors f_1, f_2,.....,f_n,

$$F_{hkl} = \sum_{1}^{n} f_i e^{2\pi i(hu_i + kv_i + lw_i)}$$

(hkl) is a set of three numbers used for labeling lattice planes, usually called Miller indices. F_{hkl} is an expression for any scattered wave from any crystal system.

Thus an X-ray diffraction pattern is a set of lines or peaks, each of different intensity and position (usually measured as 2θ). The diffraction directions are determined solely by the shape and size of the unit cell whereas the intensities of diffracted beams are determined by the type of atom and the coordinates of the atoms within a unit cell. Thus, from the position of the peaks in a typical X-ray powder diffraction pattern, the structural information such as size and shape of the unit cell can be obtained and from the intensities, the information regarding the atomic coordinates within the unit cell can be obtained. Also, X-ray diffraction may be used to measure the average crystallite size in a powder sample (from the Scherrer formula), provided the particle has the average diameter less that 1000Å. The peaks in a powder diffraction pattern are of finite breadth, but if the crystallites are very small the peaks are broader than the usual. The Scherrer formula is given by,

$$t = \frac{0.9\lambda}{Bcos\theta_B}$$

where, t is the thickness of the crystal (in Å), λ, the X-ray wavelength and θ_B, the Bragg angle and B is the line broadening which is the full-width at half maximum. B is corrected for the instrumental line broadening using the diffraction pattern of a standard material having very large crystallite size in the range of μm.

In the present study, a Philips PW1830 powder X-ray diffractometer was employed for the structural characterization of the polycrystalline samples. Cu Kα radiation was used with a wavelength of wavelength of 1.5418 Å, using Ni filter. The calibration

of the instrument was done by using a standard (oriented Si wafer). For the usual phase analysis, a scan rate of 4°/minute was used and slow-scan measurements were done at a scan rate of 0.25°/minute, to identify the presence of small amounts of impurity phases. The least-squares method was used to fit the powder diffraction data in order to calculate the unit cell parameters. The computer programs used for the powder XRD analysis were Lazy-Pulverix [Yvo77] (Yvon, K., Jeitschko, W., and Parthe, E.), Powder Diffraction Package 1.1 (Calligaris, M. and Geremia, S.), and PowderCell 2.3 (Kraus, W. and Nolze, G., downloaded from web www.ccp14.ac.uk).

2.2.2 Determination of Mn^{4+} Concentration by Iodometric Titration

The concentration of Mn^{4+} in the perovskite manganites can be determined by redox methods such as the iodometric method,by the estimation of the liberated iodine in a chemical reaction by titrimetry [Lic96, Jef97]. The redox reaction involved in the acid solution of potassium iodide can be represented as,

$$M^{(n+1)+} + I^- \rightarrow M^{n+} + \tfrac{1}{2} I_2$$

The liberated iodine is then titrated against standard thiosulphate solution.

$$2\ {S_2O_3}^{2-} + I_2 \rightarrow {S_4O_6}^{2}- + 2\ I^-$$

Standardization of thiosulphate solution is usually done by titrating against standard potassium dichromate solution. Cr^{6+} in dichromate solution is reduced by an acid solution of KI and iodine is set free which reacts with thiosulphate as already discussed.

$${Cr_2O_7}^{2-} + 6\ I^- + 14\ H^+ \rightarrow 2\ Cr^{3+} + 3\ I_2 + 7\ H_2O$$

Perovskite manganites contain manganese ions in mixed valence states, normally in trivalent (Mn^{3+}) and quadrivalent (Mn^{4+}) states. The amount of Mn^{4+} in the manganite compositions can be determined by dissolving a known quantity of a sample in dilute hydrochloric acid where Mn^{3+} and Mn^{4+} ions are reduced to divalent state. The chlorine gas evolved reacts with the iodide ions present in the solution and iodine is liberated. The amount of liberated iodine can be estimated by titrating against standard thiosulphate solution using starch as indicator. The endpoint of the titration is indicated by the disappearance of blue color. The concentration of Mn^{4+} can be calculated by taking the mole fraction of the manganese ions in the compound.

2.2.3 Magnetic Measurements Using a Vibrating Sample Magnetometer (VSM)

A Vibrating Sample Magnetometer (VSM) was used for the magnetic characterization of the sample. Its working is based on Faraday's law, which states that, an emf, V, will be generated in a coil when there is a change in flux with time ($\frac{dB}{dt}$) linking the coil [Fon59, Bus03]. For a coil with n turns of cross-sectional area a,

$$V = -na\frac{dB}{dt}$$

If the coil is positioned in a constant magnetic field,

$$B = \mu^0 H$$

where H is the external magnetic field applied and μ^0 is the permeability in vacuum. When a sample of magnetization M is brought into the coil,

$$B = \mu^0(H + M)$$

The corresponding flux change is

$$\Delta B = \mu^0 M$$

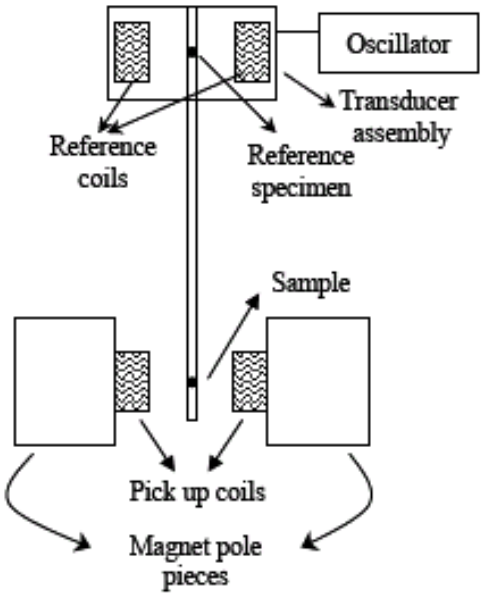

Figure 2.2: Main components of a VSM.

Thus the voltage induced in the coil is,

$$Vdt = -na\mu^0 M$$

This means that the output signal of the coil is proportional to the magnetization M, but independent of the magnetic field in which the size of M is to be determined. In the VSM, a sample is subjected to a sinusoidal motion (with frequency, ν) and the corresponding voltage is induced in suitably located stationary pickup coils. The electrical output signal of these pick up coils has the same frequency. The magnitude of the signal is proportional to the magnetic moment of the sample, the vibration amplitude, and the frequency ν. A simplified schematic representation of a VSM is as given in figure 2.2.

The sample to be measured is centered in the region between the poles of an

electromagnet, which generate the measuring field H. A thin vertical sample rod connects the sample holder with a transducer assembly located above the magnet. The transducer convert the sinusoidal *ac* drive signal, provided by an oscillator/amplifier circuit, into a sinusoidal vertical vibration of the sample rod. The sample is thus subjected to a sinusoidal motion in the uniform magnetic field H. Coils mounted on the poles of the magnet pick up the signal resulting from the motion of the sample. This *ac* signal at the vibrating frequency ν is proportional to the magnitude of the moment of the sample. However, since it is also proportional to the vibration amplitude and frequency, the moment readings taken simply by measuring the amplitude of the signal are subject to errors due to variations in the amplitude and frequency of vibration. In order to avoid this difficulty, a nulling technique is employed to obtain moment readings that are free of these sources of errors. This technique makes use of a vibrating capacitor for generating a reference signal that varies with vibration amplitude, and vibration frequency in the same manner as the signal from the pick up coils. Thus, it is possible to eliminate the effects of vibration amplitude and frequency shifts. In that case, one obtains readings that vary only with the moment of the sample.

M vs T, M vs H and M vs t Measurements

A PAR EG&G 4500 VSM was used for all the DC magnetization measurements. In addition to the magnetometer set up, the assembly consists of a closed cycle helium refrigerator (CCR) or a liquid nitrogen cryostat, a turbo vacuum pump and a temperature controller which measures and control the temperature. The temperature measurement was carried out using a Pt-100 resistance thermometer which is placed in very close proximity with the sample.

Mainly two protocols were used for the measurement of temperature (T) variation of magnetization (M)- one is the zero field cooled (ZFC) and another the field cooled

(FC) protocol. In the ZFC method, the sample was cooled to the lowest temperature (12 K by using the helium CCR and 80 K by using the liquid nitrogen cryostat) in the absence of an applied field and the measurement was carried out while heating the sample to room temperature in an applied field. On the other hand, FC method involves cooling the sample in the presence of an external magnetic field and measurements taken while cooling or heating. In most of the ZFC and FC experiments, low magnetic fields are employed in order to be useful for the studies related to domain wall motion, spin glass-type of behavior and superparamagnetic character of various manganites.

The Field dependence of magnetization (M-H behavior) was studied for various samples using an electromagnet with maximum field up to $\pm$15 kOe. The M-H curves were recorded at various temperatures with different field sweep rates. For the M-H measurements, the samples were cooled to the required temperature in zero applied field. The variation of the coercivity and saturation magnetization were studied in detail for various manganite compositions. Also, the calculation of differential susceptibility has also been made in order to study the low-field domain properties of the materials.

The relaxation studies are generally been carried out mainly by employing either the ZFC protocol or FC protocol, where the latter method is commonly known as thermoremnant magnetization. In the present work, mainly the ZFC relaxation method is used. For this, the sample was cooled under zero magnetic field to the required temperature and the magnetization was measured by applying a low magnetic field (50 Oe in most of the experiments), as a function of to time, keeping the temperature constant.

Degaussed magnetization studies were performed in certain cases, where, the sample after cooling under zero field conditions was subjected to a field for magnetic saturation and the remnant magnetization was reduced to zero by degaussing. The

method was useful to investigate the low-temperature magnetic anomalies due to domain wall pinning effects.

Aging, Rejuvenation and Memory Studies

Aging, rejuvenation and memory experiments were used for various samples which showed spin-glass type behavior and for magnetic nanoparticles. Here, two methods were employed, FC and ZFC protocols with temperature steps and cycling. The spin glass systems are known to show aging and memory effects. Recent interest in various magnetic nanoparticle systems also makes them important to study such closely resembling properties. For this, commonly multiple memory experiments are used. In the present work, single or double memory experiments are mainly employed. A typical memory experiment (by *dc* method) employed in the present work is as illustrated in figures 2.3, (a) and (b) for FC and ZFC methods, respectively. The sample was initially cooled to a lower temperature below the existence of spin glass-like phase by FC or ZFC methods. Sufficient waiting time is given at one or more temperatures during cooling. The magnetization was then recorded on heating. It is important that the heating/cooling should be in a controlled fashion and a heating/cooling rate of 2K/min has been used in the present work.

2.2.4 *ac* Susceptibility

A versatile method for studying the magnetization dynamics of materials is by *ac* susceptibility method [Van82]. This technique generally uses very low *ac* magnetic fields and are very important in probing the effects on domain wall motion and spin glass-type of compounds. The technique is based on the change of the mutual inductance of a pair of coils or the self-inductance of a single coil due to a magnetic sample. In a typical *ac* susceptibility measurement, an *ac* field is applied through a primary coil, and in a secondary coil where a magnetic sample isplaced, an emf is generated

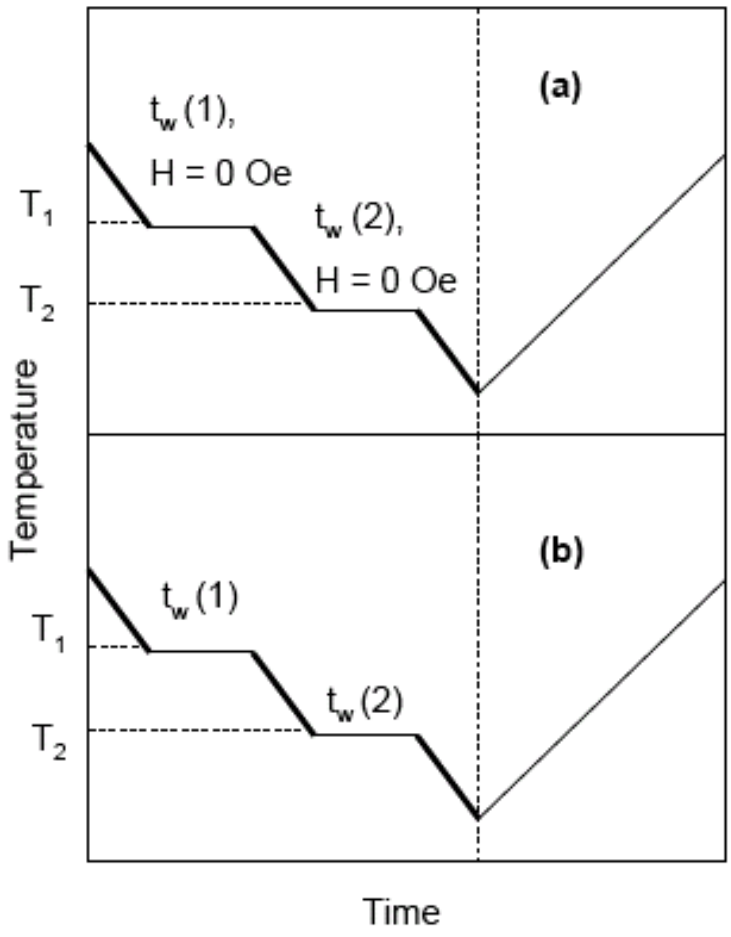

Figure 2.3: Typical memory experiments following (a) FC protocol and (b) ZFC protocol. T_1 and T_2 are two temperatures in the spin glass-like regime where the sample is aged or allowed for waiting times of $t_w(1)$ and $t_w(2)$, respectively. Field, H = 0 at the halts, but a finite value of H (say, 50 Oe) is maintained during cooling in the FC method. The measurement was carried out during heating by applying a low field (say, 50 Oe).

corresponding to the magnetization of the sample. A lock-in amplifier is used for the separation of the in-phase (real, χ') and the out-of-phase (imaginary, χ'') components of the resulting *ac* signal in the secondary coil. The susceptibility χ is then,

$$\chi = \sqrt{\chi'^2 + \chi''^2}$$

During the present study, an *ac* susceptometer coupled with a closed cycle helium refrigerator (APD cryogenics) assembly was extensively used for the characterization of various samples. Low field strengths of 0.5, 2, or 5 Oe has been applied and the frequency dependence was studied by varying the frequency of the applied *ac* current using an external function generator (General Radio 1310-B). A PAR EG&G 5210 lock-in-amplifier was used for the analysis of the signal from the secondary coil, and for continuous data collection through a computer.

2.2.5 Four-probe Method for Resistivity Measurement - van der Pauw Method

For semiconducting materials, a four-probe method for the resistivity measurements is often performed [Sin01]. In the four-probe method, separate pairs of wires are used for providing the current through the sample and measuring the voltage across it. The advantage of such a four-wire method over the conventional two-wire method is that the contact resistance due to electrical contacts with the material and the wire resistance can be avoided. Another effect that may arise during the resistance measurement is due to the dissimilar metal contact, which results in a thermal voltage. This can be nullified by changing the direction of the current. For a four-probe measurement, sample geometries and contacts type are important. In studying the bulk materials, measurements are usually made on rod-shaped samples. Contacts are either soldered, evaporated or glued using electrically conducting paint to the faces of the rod-shaped sample. Commonly the contacts are given *in-line*. An alternate

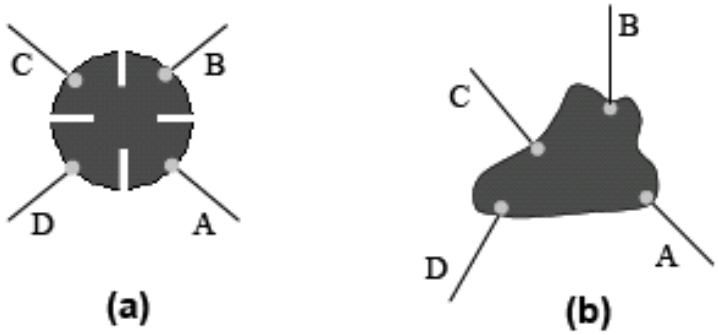

Figure 2.4: Four-probe resistance measurement using van der Pauw method.

four-probe method is van der Pauw method [Van58]. In this technique ideally the sample should be of the clover-leaf shape (Figure 2.4a). But it is successfully applied to quite arbitrarily shaped samples (Figure 2.4b).

The method for obtaining the resistivity is as follows,

1. A current I_{AB} is driven from contact A to contact B, the resulting voltage V_{CD} is measured between contacts C and D. The resistance $R_{AB,CD} = V_{CD}$ / I_{AB}.

2. A current I_{BC} is driven from contact B to contact C, the resulting voltage V_{AD} is measured between contacts A and D.The resistance $R_{BC,AD} = V_{AD}$ / I_{BC}.

3. The resistivity can be calculated using the formula,

$$\rho = \frac{\pi}{ln2} d \frac{R_{AB,CD} + R_{BC,DA}}{2} f$$

Where the function f depends on the ratio

$$\frac{R_{AB,CD}}{R_{BC,AD}}$$

or on the geometry of the contacts, often known as the van der Pauw factor and d is the sample thickness.

A Keithley model 220 *dc* current source and a Keithley model 196 digital multimeter were used for the resistivity measurements. A Keithley model 705 scanner was used for changing the contacts. The temperature dependence of the resistivity was studied using an APD cryogenics closed cycle helium cryostat (15–300 K).

2.2.6 Electron Paramagnetic Resonance (EPR)

The EPR technique is based on the following principle. In a magnetic field, different energy states arise from the interaction of the unpaired elecron spin moment (given by $m_s = \pm 1/2$ for a free electron), which is called the Zeeman effect. The difference between the two spin states, $m_s = +1/2$ and $m_s = -1/2$ corresponds to frequencies in the microwave region. Thus, for a particular applied field strength, an absorption of microwave radiation of a particular frequency results in the resonance. However, in a typical EPR spectrometer, the experiments are generally carried out at a fixed frequency of microwave radiation and varying the applied field. Two common frequencies are in the X-band frequency range ($\sim$9.5 GHz, where a field strength of approximately 3400 gauss is employed) and the so-called Q-band frequency (35 GHz, where a field strength of approximately 12,500 gauss is used). However, in the present study of the strongly exchange coupled systems [Ben90], only the X-band EPR measurements have been carried out.

In the manganites, where the interacting spins becomes very large, the extended interactions have to be considered. The interactions can occur in various dimensions, with almost infinite number of possible variations. An immediate consequence is the appearance of a broadened EPR signal in the spectrum. Thus, two important parameters are measured in the current study. The first one being the peak-to-peak line width represented by ΔH_{pp} and second is the integrated intensity (I). The present studies have been made on a Bruker ER-200D-SRC spectrometer at the X-band frequency regime at the room temperature.

Chapter 3

Studies on Self-doped Lanthanum Manganites

One of the important aspects of the La-Mn-O perovskite system is the wide range of non-stoichiometry possible and the related intriguing properties. The magnetic and transport properties of the self-doped lanthanum manganites, represented as $La_{1-x}MnO_3$, resemble that of the divalent ion doped CMR manganites, $La_{1-x}D_xMnO_3$ [Coe99]. This is because, self or vacancy doping in the La-site of the perovskite $LaMnO_3$ also produces Mn^{4+} in the lattice, as in the case of $La_{1-x}D_xMnO_3$. This can explain the evolution of the interesting magnetic and electrical properties, including CMR of $La_{1-x}MnO_3$ in terms of the double-exchange interactions.

3.1 Limiting Value of Self-doping

The self-doped lanthanum manganites, $La_{1-x}MnO_3$, must be tolerating large structural strains for high values of x. As a result, the structure may collapse and stability of the structure will be controlled by the extent of vacancy at the La-site. The theoretically possible value of x is 1/3 (based on the maximum amount of Mn^{4+} possible).

Compared to the large number of studies on $La_{1-x}D_xMnO_3$, there are not many reports in the literature on the self-doped compositions. Especially, the phase diagram of $La_{1-x}MnO_3$ is not yet established. There are many reports in the literature on the

studies of the self-doped compositions in the doping range $0 \leq x \leq 0.33$ [Gup95, Hau96, Jim97, Che00, Los01, Kim01, Qia02, Dha04]. The limiting value of x in $La_{1-x}MnO_3$ has been suggested as $\sim$0.1, based on the observation of Mn_3O_4 as an impurity phase for $x > 0.1$ [Tak91, Sak96, Dez02, Dez04]. However, such a conclusion is based on the studies on very few self-doped compositions. The observation of phase separation in self-doped compositions, $La_{1-x}MnO_3$, with high values of x has been observed recently from the XANES analysis [Dez04]. The above reports suggest the possibility of a maximum limit for the vacancy concentration which the perovskite manganite structure can withstand. Hence, a detailed analysis has been made in the present work to determine the limiting value of x in $La_{1-x}MnO_3$.

3.1.1 Synthesis

Different compositions in $La_{1-x}MnO_3$ (the values of x were taken as fractions in the range $1/32 \leq x \leq 1/3$) were synthesized by the ceramic method from the corresponding oxides La_2O_3 and MnO_2. The mixture of the two oxides, taken in the appropriate stoichiometric ratio, were initially heated at 1273 K for 48 h with an intermediate grinding. The polycrystalline materials obtained were then heated at 1473 K for 48 h with an intermediate grinding and then pressed into the form of pellets and finally heated at 1473 K for 24 h. All the compositions were prepared under identical conditions, as the properties and Mn^{4+} content are known to be sensitive to the preparation conditions [Mai97].

3.1.2 Results and Discussion

The powder X-ray diffraction (XRD) patterns of some compositions in $La_{1-x}MnO_3$ are shown in Fig. 3.1. The diffraction patterns correspond to a rhombohedral perovskite structure and all compositions in the range $1/32 \leq x \leq 1/3$ showed reflections

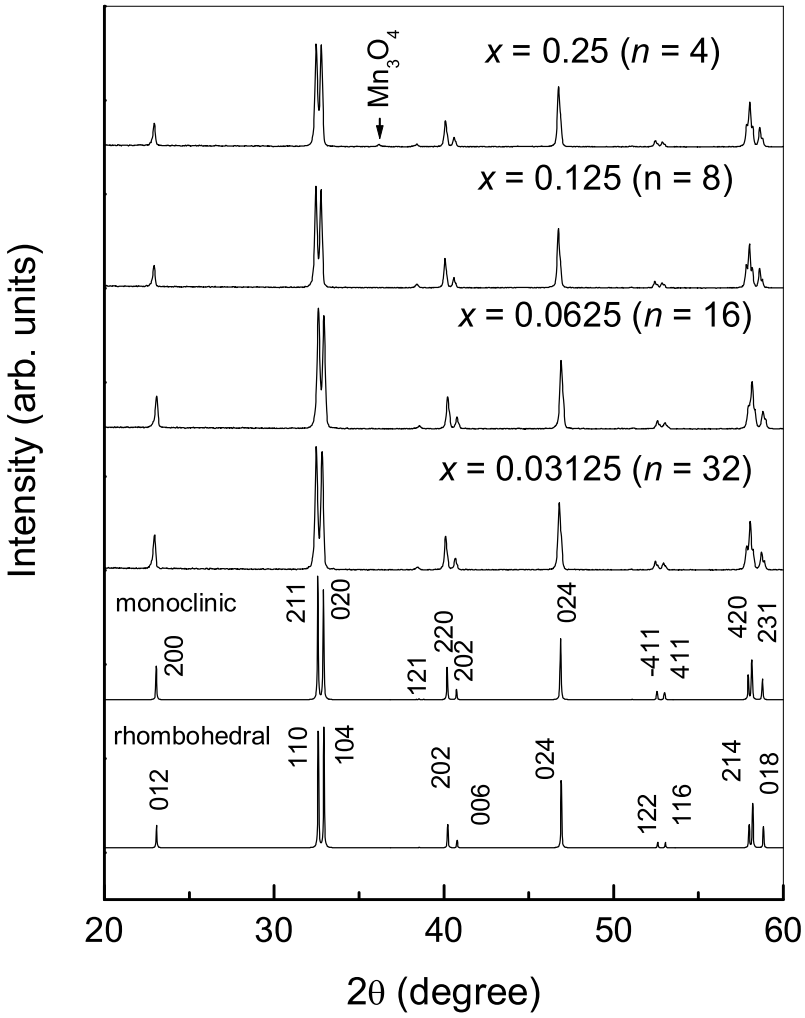

Figure 3.1: Powder X-ray diffraction patterns of some compositions in $La_{1-x}MnO_3$ ($n = 1/x$). The reflection marked by arrow is due to Mn_3O_4.

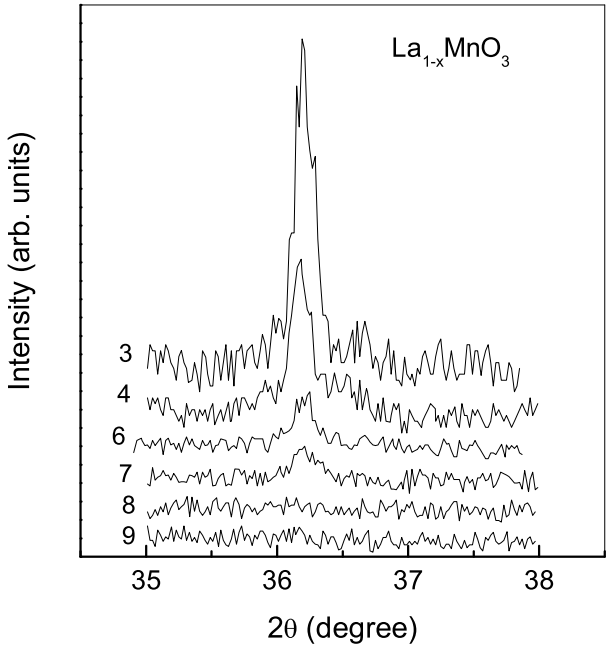

Figure 3.2: Powder X-ray diffraction patterns of some compositions in $La_{1-x}MnO_3$, recorded at a very slow scan rate, in the 2θ region where the most intense peak of Mn_3O_4 is observed. The numbers on the curves indicate the value of $n = 1/x$.

due to a rhombohedral perovskite lattice. Maignan *et al.* [Mai97] found that though the powder XRD patterns of some of their $La_{0.9}MnO_3$ samples could be indexed on the classical rhombohedral cell with the space group $R\bar{3}c$, the actual symmetry is monoclinic with space group I2/a and additional weak reflections due to this symmetry change could be observed only in the electron diffraction patterns. The XRD patterns in Fig. 3.1 are compared with the simulated patterns (using the *powder cell* software) of the rhombohedral ($R\bar{3}c$) and the monoclinic (I2/a) unit cells. Both the simulated patterns are almost identical and therefore, the rhombohedral structure is used for the analysis of the data in this work.

Presence of an additional weak reflection at $2\theta = 36.2°$, is indicated in the XRD

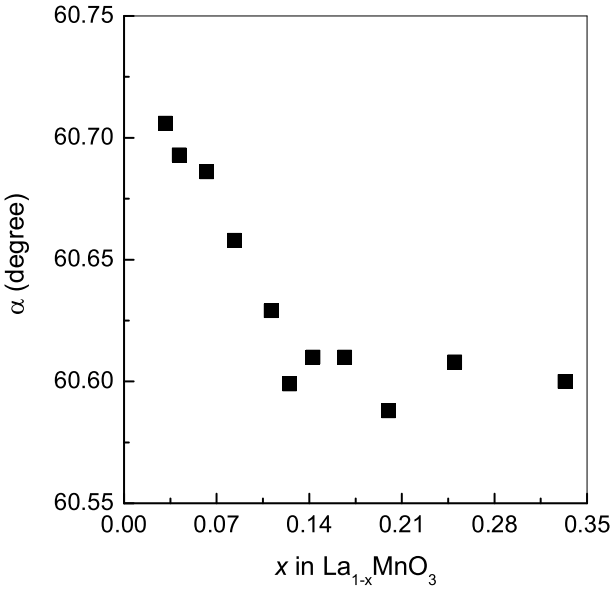

Figure 3.3: Variation of the rhombohedral angle, α, as a function of x in $La_{1-x}MnO_3$.

pattern of the $x = 1/4$ sample. This weak reflection is found to be due to Mn_3O_4 and is observed for all compositions for $x > 1/8$. The XRD patterns of some compositions, in the 2θ region where the most intense peak of Mn_3O_4 is observed, are compared in Fig. 3.2. The patterns, shown in Fig. 3.2, were recorded at a very slow scan rate, as this procedure [Tay95] is known to be highly efficient in detecting very small quantities of impurity phases. It may be seen that the peak due to Mn_3O_4 impurity is suddenly appeared when $x > 1/8$. The intensity of the additional reflection increases with increasing x, above $x > 1/7$.

The rhombohedral angle, α, decreases initially with increasing x and then becomes almost constant for $x > 1/8$, as shown in Fig. 3.3. These results point to the fact that $x = 1/8$ may be the limiting value of vacancy doping in $La_{1-x}MnO_3$ and that at larger values of x, the composition of the self-doped manganite is adjusted to this

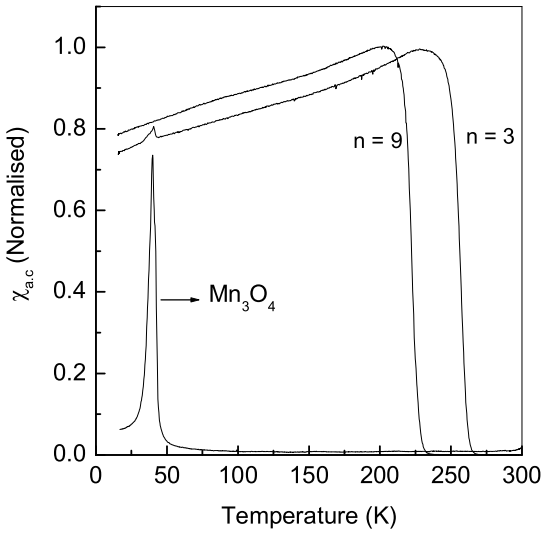

Figure 3.4: *ac* susceptibility curves of two $La_{1-x}MnO_3$ compositions with $1/x = 3$ and 9. The peak observed at 40 K in the *ac* susceptibility of $La_{0.67}MnO_3$ is shown to be due to that of Mn_3O_4, present as an impurity.

value of $x = 1/8$ and the excess Mn used is converted to Mn_3O_4. The increasing intensity of the reflection from Mn_3O_4 and the constancy of the lattice parameter, α, with increasing x above 1/8, is in agreement with this conclusion.

Mn_3O_4 is paramagnetic at room temperature and undergoes a ferrimagnetic transition below ∼43 K [Goo63]. The *ac* susceptibility measurements on Mn_3O_4 and the self-doped manganite compositions in the temperature range from 15-300 K were carried out which revealed the presence of Mn_3O_4 in heavily doped composition $La_{0.67}MnO_3$ as shown in Fig. 3.4. This clearly indicates that the impurity peak observed in slow-scan XRD patterns is due to Mn_3O_4.

Fig. 3.5 shows the zero field cooled (ZFC) magnetization curves of the different $La_{1-x}MnO_3$ compositions, measured in the temperature 80-300 K. Some of the important features observed are; a) a monotonous increase in the ferromagnetic transition

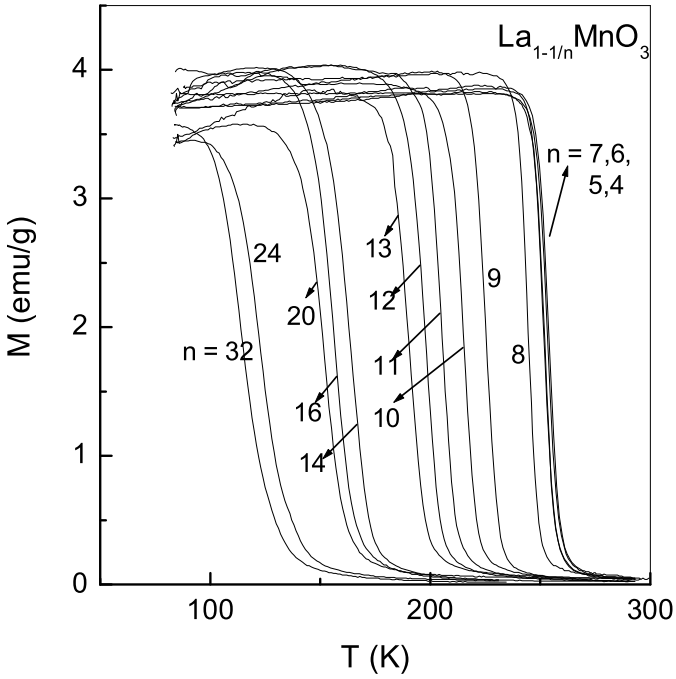

Figure 3.5: Temperature dependence of the ZFC magnetization of $La_{1-x}MnO_3$ (H = 50 Oe) for various values of x. The numbers on the curves indicate the value of $n = 1/x$.

temperature (T_c) with increasing x up to $x = 1/7$ (n = 7 in Fig. 3.5) and b) increasing sharpness of the magnetic transition as x is increased. The trend in the variation of T_c as a function of x is shown in Fig. 3.6. T_c is defined as the temperature at which dM/dT is maximum. T_c increases almost linearly with increasing value of x and a maximum $T_c = 251$ K is obtained for $x = 1/7$, after which T_c remains almost constant. Similarly, the saturation magnetization, measured at 82 K and a maximum applied field of 15 kOe, as a function of x, shows the same trend as in the case of T_c, as shown in Fig. 3.6. The magnetization increases with increasing x till $x = 1/8$ and then decreases and becomes constant. The lower values of M for $x > 1/8$ may be due

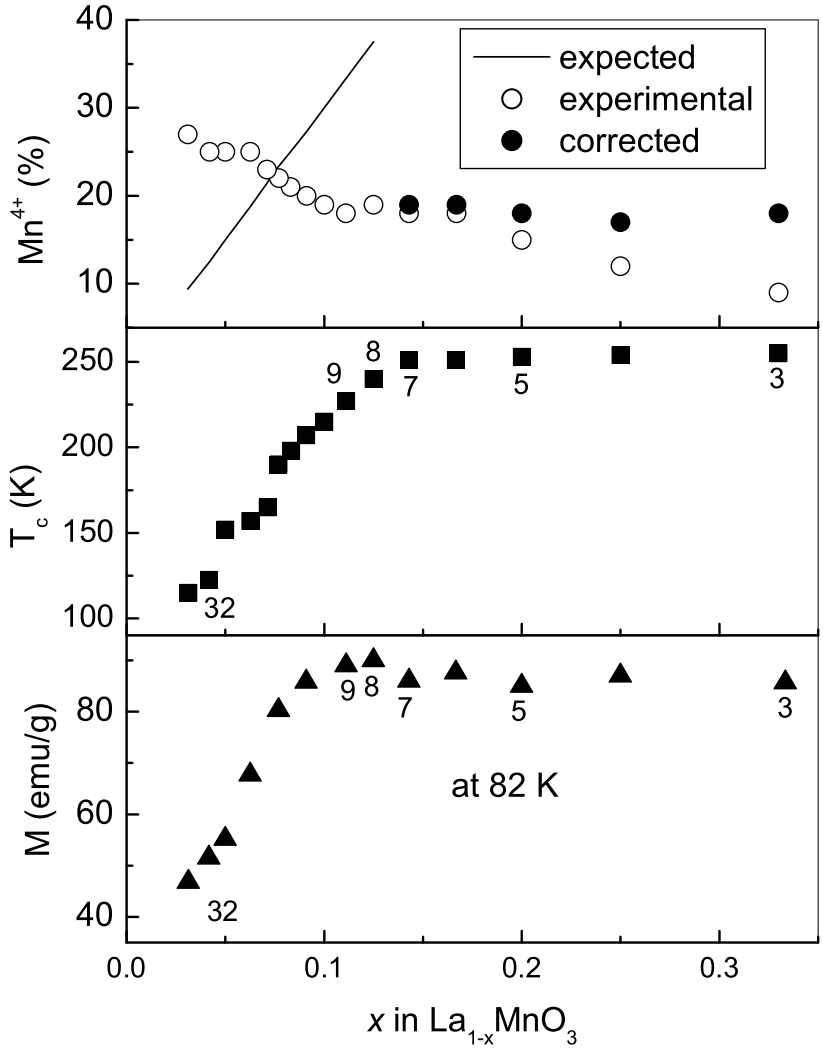

Figure 3.6: The variation of Mn^{4+} concentration (upper panel), Curie temperature (middle panel), and saturation magnetization at 82 K (lower panel), as a function of x in $La_{1-x}MnO_3$. The numbers indicate the value of $n = 1/x$.

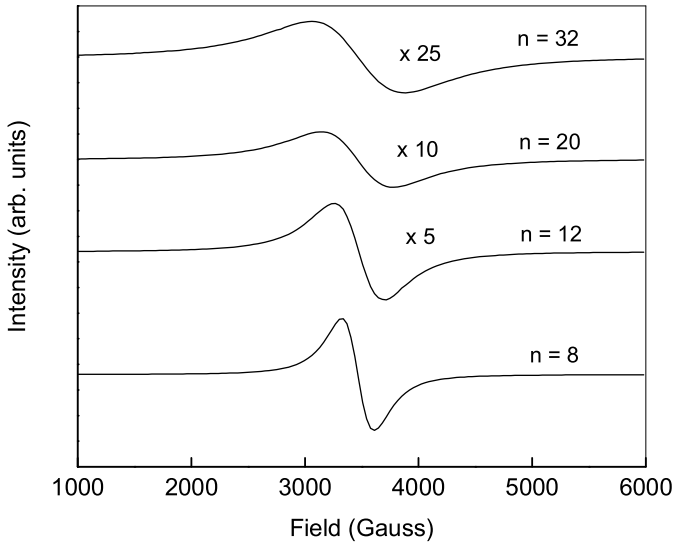

Figure 3.7: X-band EPR spectra of some $La_{1-x}MnO_3$ compositions; $n = 1/x$.

to the presence of the impurity phase Mn_3O_4 which is not ferromagnetic at 82 K.

The Mn^{4+} concentration in the different compositions, as a function of x, is also compared in Fig. 3.6 with the expected Mn^{4+} concentration assuming the formula $La_{1-x}MnO_3$. The theoretical Mn^{4+} concentration increases linearly from 0 to 100% for $x = 0$ to 1/3. On the other hand, the experimentally determined Mn^{4+} concentration, calculated neglecting the Mn_3O_4 content in the samples for $x > 1/8$, decreases continuously with increasing x and a very low value of 9% Mn^{4+} content is obtained for $x = 1/3$. However, it is known that at lower Mn^{4+} contents, the crystal structure is orthorhombic for $La_{1-x}MnO_3$ [Hau96].

Therefore, such a low Mn^{4+} concentration is not possible for $x = 1/3$, considering the rhombohedral structure observed for this compound. Assuming that $x = 1/8$ is the limiting value of x and Mn_3O_4 is formed in equivalent amounts for higher values of x, the corrected Mn^{4+} concentration in the compositions for $x \geq 1/7$ is

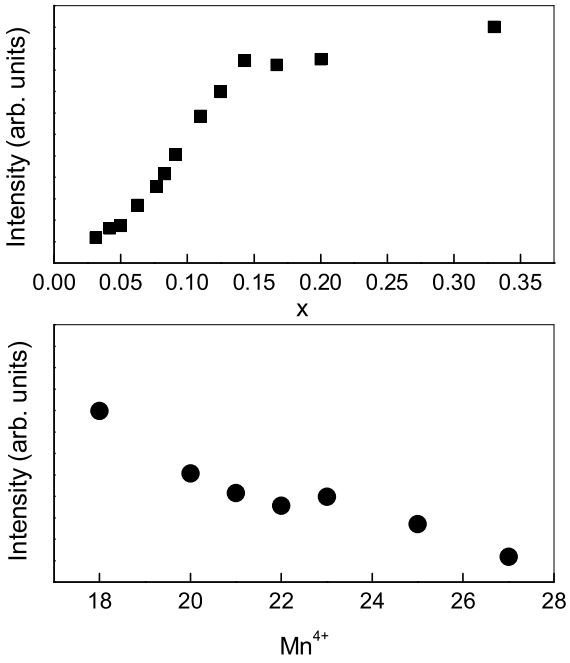

Figure 3.8: Variation of EPR integrated intensity with values of x in $La_{1-x}MnO_3$ and amount of Mn^{4+}.

found to become almost constant, approximately 18%, as shown in Fig. 3.6 as the corrected values. This high value of the Mn^{4+} content supports the rhombohedral structure of these compositions. It may be noted that for La vacancies $x < 1/14$, the experimental Mn^{4+} concentration is much larger than the theoretical values and vice versa for $x > 1/14$. The room temperature X-band EPR spectra of the self-doped lanthanum manganites show strong EPR signals as shown in Fig. 3.7, with Lorentzian line shape over the whole range of doping concentration.The parameters; the peak-to-peak line width as well as the integrated intensity, are found to have a regular deviation in the EPR spectra of these exchange coupled systems as the doping concentration is varied. It is observed in the spectra that as the doping concentration

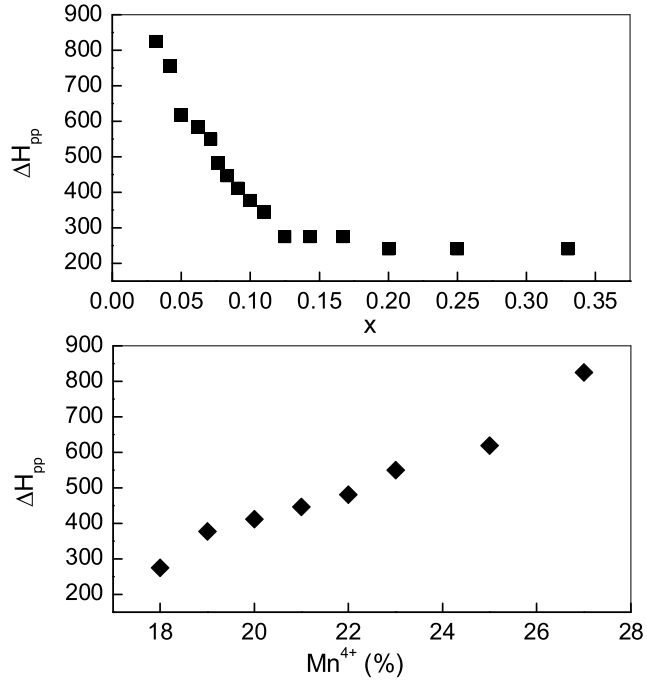

Figure 3.9: Variation of peak-to-peak linewidth with values of x in $La_{1-x}MnO_3$ and amount of Mn^{4+}.

is decreased (and the amount of Mn^{4+} is unexpectedly increased), the intensity of the EPR signal is decreased. Also, the peak-to-peak line width is decreased with decreasing x. These features are similar to that observed by Oseroff *et al.* [Ose96] for $LaMnO_{3+\delta}$ with different values of δ and for $La_{1-x}A_xMnO_3$, where $x = 0$, 0.33 and 1. The variations of the integrated EPR intensity and the peak-to-peak line width, ΔH_{pp}, with x as well as the amount of Mn^{4+} in $La_{1-x}MnO_3$ are shown in Fig. 3.8 and Fig. 3.9, respectively. The integrated intensity increases linearly with x and reaches a maximum value for $x = 1/8$ and remains almost constant for higher values of x whereas no specific trend is observed in the variation as a function of Mn^{4+} concentration. Similarly, ΔH_{pp} decreases following a linear relation with the

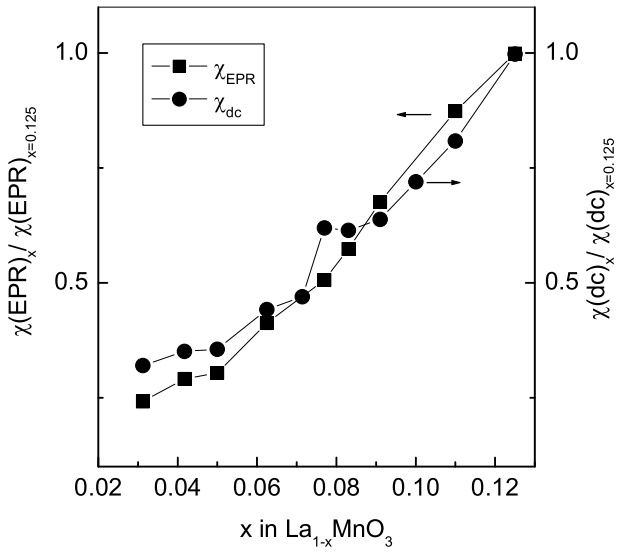

Figure 3.10: Comparison of the paramagnetic susceptibility and EPR intensity. The values are normalized with respect to those of $La_{0.875}MnO_3$.

doping concentration up to a value of $x = 0.125$ and becomes constant for larger x, as shown in Fig. 3.9.ΔH_{pp} continuously increases with increasing amount of Mn^{4+}. From these results it is clear that some limit is reached for compositions with $x \geq 0.125$.

The room temperature paramagnetic susceptibility and EPR integrated intensity follow a similar variation as shown in Fig. 3.10. These results indicate that EPR signal obtained for the $La_{1-x}MnO_3$ compositions are not solely due to the presence of Mn^{4+}, but shows a contribution from Mn^{3+} ions as well. This is in agreement with the previous reports on EPR studies on substituted manganites [She96, Cau98, Iva00]. The paramagnetic ions present in the $La_{1-x}MnO_3$ system, both Mn^{3+} and Mn^{4+}, are believed to contribute to the intensity of EPR signal by the probable formation of complex of Mn^{3+}-Mn^{4+} spin clusters [Ret97].

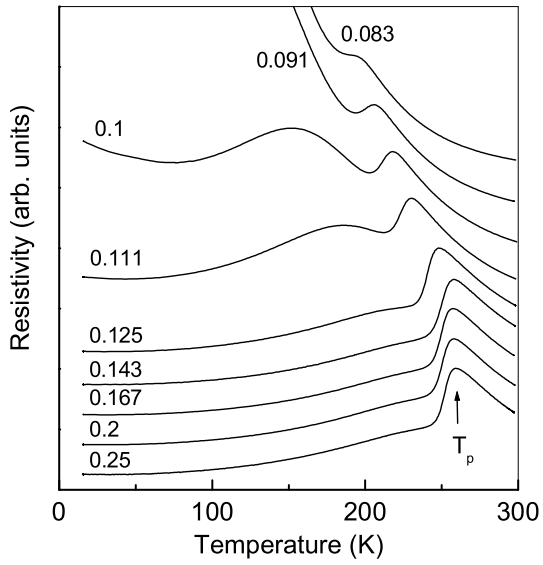

Figure 3.11: Temperature dependence of resistivity (normalised) of $La_{1-x}MnO_3$ samples; the values of x are given in the figure.

Temperature variation of the electrical resistivity of different compositions in $La_{1-x}MnO_3$ is shown in Fig. 3.11. The peak temperature, T_p, is found to become constant when $x \geq 0.125$. The shape and nature of the resistivity curves for $x \geq 0.125$ are identical, except that the magnitude of the resistivity increases with x. This is likely to be due to the increasing amount of the insulating impurity phase of Mn_3O_4. In fact, the resistivity curves of these compositions overlap when normalized with respect to the peak resistivity at T_p. The presence of a second peak in the resistivity curves of the samples with lower x values (known as double peak resistivity behavior) is discussed in detail in chapter 7. When x becomes less than 0.083, insulating behavior is observed and T_p is not defined for these compositions. Thus, i) the powder XRD studies showed the presence of unreacted Mn, in the form of Mn_3O_4 and lattice parameters independent of x, for values of $x > 1/8$, ii) the magnetic measurements

show maximum value of magnetization for $x = 1/8$ and maximum T_c for $x = 1/7$, in $La_{1-x}MnO_3$, iii) the EPR measurements show constancy of ΔH_{pp} and integrated intensity beyond $x = 0.125$, and iv) the resistivity curves of the compositions show identical features (T_p as well as nature of the curves) for $x > 1/8$. These results lead to the conclusion that $x = 1/8$ is the limiting value of x possible in $La_{1-x}MnO_3$. The value of $x = 1/8$ corresponds to an ordered structure in which one La vacancy is present at the corner of the simple cubic perovskite unit cell, which is shared by eight unit cells, as shown in Fig. 3.12 for a B-type perovskite lattice. That is, every rhombohedral perovskite unit cell in the lattice contains one La vacancy. Increasing the La vacancy beyond this limit may collapse the perovskite structure and therefore, $La_{1-x}MnO_3$ with a limiting value of $x = 1/8$ is formed if the initial La/Mn ratio is kept below 0.875 and excess MnO_2 remains unreacted, which is converted to and observed as Mn_3O_4 in the XRD patterns. $x = 1/8$ corresponds to a maximum possible concentration of 37.5% Mn^{4+} in $La_{1-x}MnO_3$. Interestingly, the maximum T_c in the divalent ion substituted manganites is observed for the composition $La_{5/8}D_{3/8}MnO_3$ [Tok00], with a possible amount of Mn^{4+} as 37.5%.

The larger values of experimental Mn^{4+} concentration for $x < 1/14$ when compared to the expected values, considering the formula $La_{1-x}MnO_3$, needs further consideration. Such large value of Mn^{4+} content, than expected, is possible only if there are excess oxygen in the structure, expressed by the formula $La_{1-x}MnO_{3+\delta}$.

However, it is known that the perovskite structure cannot accommodate excess oxygen [Mit02]. Therefore, to accommodate excess Mn^{4+}, the only way is to have Mn deficiency in the compounds, as given by the formula, $La_{1-x}Mn_{1-y}O_3$. The actual compositions, as calculated based on the values of x and the observed Mn^{4+} concentrations are shown in Table 3.1. For $x = 1/16$, the composition obtained, $La_{0.937}Mn_{0.981}O_3$, is comparable to that of the single crystal composition $La_{0.936}Mn_{0.982}O_3$, reported by McCarroll *et al.* [Mcc98], except that the T_c of the

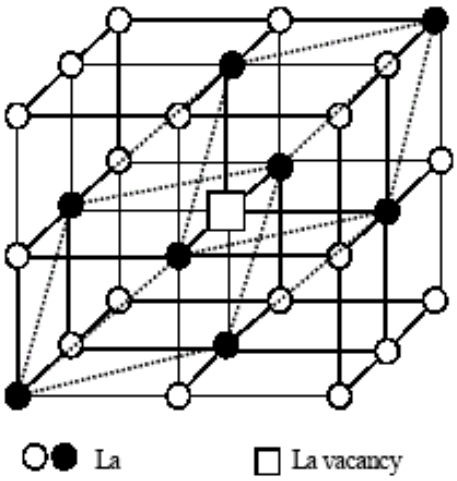

Figure 3.12: The structure of $La_{7/8}MnO_3$ showing one La vacancy for eight B-type basic perovskite unit cells. The actual rhombohedral unit cell is also shown for comparison.

Table 3.1: Actual compositions for different values of x in $La_{1-x}MnO_3$, based on the experimental Mn^{4+} concentrations.

x	$Mn^{4+}(\pm 1\%)$	composition	La/Mn
0.031	27	$La_{0.969}Mn_{0.946}O_3$	1.024
0.042	25	$La_{0.958}Mn_{0.964}O_3$	0.994
0.05	25	$La_{0.950}Mn_{0.969}O_3$	0.980
0.062	25	$La_{0.937}Mn_{0.981}O_3$	0.955
0.071	23	$La_{0.929}Mn_{0.996}O_3$	0.933
0.077	22	$La_{0.923}MnO_{2.99}$	0.923
0.083	21	$La_{0.917}MnO_{2.98}$	0.917
0.091	20	$La_{0.909}MnO_{2.96}$	0.909
0.10	19	$La_{0.900}MnO_{2.94}$	0.900
0.111	18	$La_{0.889}MnO_{2.92}$	0.889
0.125	18	$La_{0.875}MnO_{2.90}$	0.875

single crystal sample is larger than that in the present study on polycrystalline samples. The higher T_c of single crystals may be due to the ordering of La and Mn vacancies in the lattice for $x = 1/16$ (1/8x2).

On the other hand, for values of $x > 1/14$, Mn^{4+} concentrations are less than that expected and therefore the formula of the compound can be represented as $La_{1-x}MnO_{3-\delta}$. This indicates that Mn deficiency is most favored to stabilize the perovskite structure of $La_{1-x}MnO_3$ at lower values of x and oxygen deficiency is favored at higher values of x. Similar Mn deficiencies at low values of x have been observed by earlier researchers [Jim97, Kim01, Dez02]. Ferris *et al.* [Fer97], from Rietveld refinement analysis, have shown that the Mn occupancy is less than 1 in the few $x < 0.1$ compositions studied.

It may be seen that the Mn deficiency is larger than the La vacancy at very low values of x. The concept of Mn deficiency, at low values of x, can explain the broadness of the ferromagnetic transitions. The deficiency of Mn will create ferromagnetic clusters. Larger the Mn deficiency, the size distribution of such clusters will be larger and the broad magnetic transition may be considered as a sum of the magnetic transition of individual ferromagnetic clusters of varying size. This also can explain the increasing sharpness of the magnetic transition as x is increased, due to decreasing Mn deficiency.

3.2 Low-temperature Magnetic Properties of Self-doped Compositions

It is known that doping at the La-site by divalent ions or by self-doping (creating vacancies at the La-site), Mn^{4+} ions can be introduced into the lattice of $LaMnO_3$, and this is responsible for the interesting magnetic and electrical properties of these oxides. In both cases, the observed ferromagnetic and the associated properties can

be explained in terms of the double exchange interaction between manganese ions in different oxidation states through intervening oxygen ions. The possible competitions between charge, spin and orbital degrees of freedom make the perovskite La-Mn-O system one of the most complicated among the condensed matter systems. One of the unusual properties of the divalent ion doped $LaMnO_3$ is their magnetic behavior at low temperatures when the concentration of doping is very low. An anomalous decrease in the zero field cooled or *ac* magnetic susceptibility is generally observed at very low temperatures in the ferromagnetic compositions [Hwa95, Bar98, Dho99]. The temperature at which this anomaly is observed is lower than the ferromagnetic ordering temperature. Though earlier studies attributed this phenomenon to spin glass, re-entrant spin glass, antiferromagnetic transition, mixed phase behavior, charge ordering transition, etc., recent studies have revealed that the anomaly probably originates from domain wall pinning effects [Ste02], as similar behavior is observed in many other ferromagnetic systems [Sku99, Tsu01] other than the manganites.

In $La_{1-x}MnO_3$, the magnetic interactions are depending on the Mn^{4+} content as well as on the amount of vacancy, which determines the Mn-O-Mn bond angle due to structural distortions associated with La vacancy. Earlier, De Brion *et al.* [Deb99] reported a decrease in the *ac* susceptibility of $La_{0.93}MnO_3$ at low temperatures, similar to that observed for the divalent ion substituted compositions, at low-doping levels. However, no systematic or detailed study is reported in the literature on this anomalous low-temperature behavior of the self-doped manganites. In this section, the results of detailed studies on the evolution of such a low-temperature magnetic anomaly in the self-doped compositions are discussed.

In the preceding section (Section 3.1) of this chapter, it has been shown that the limit of self-doping possible in $La_{1-x}MnO_3$ is $x = 1/8$. Therefore, detailed studies are made on the compositions with $x \leq 0.125$. Based on the Mn^{4+} concentrations, the actual compositions were identified as Mn-deficient, $La_{1-x}Mn_{1-y}O_3$, for $x < 0.07$

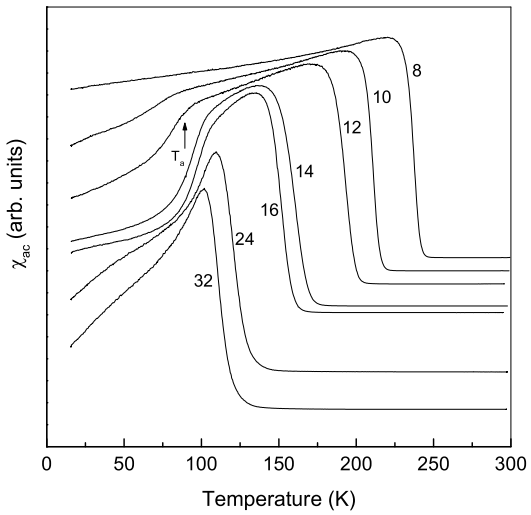

Figure 3.13: *ac* susceptibility curves for different compositions in $La_{1-x}MnO_3$. The numbers indicate $n = 1/x$. The curves are shifted along the y-axis for clarity.

and oxygen deficient, $La_{1-x}MnO_{3-\delta}$ above this value of x. For small values of x, the Mn-deficiency, y, is larger than the La vacancy, x. All the compositions were found to be having the rhombohedral perovskite structure. Though some of the compositions are Mn-deficient and others O-deficient, for convenience, the self-doped compositions are denoted as $La_{1-x}MnO_3$, where x is the degree of self-doping.

The *ac* susceptibility curves for some of the self-doped compositions are shown in Fig. 3.13. The Curie temperature decreases with decreasing amount of self-doping in $La_{1-x}MnO_3$. The variation of the Curie temperature, obtained as the temperature at which a minimum in the temperature dependence of the derivative of the susceptibility, $d\chi/dT$, is observed, as a function of x as well as Mn^{4+} concentration is shown in Fig. 3.14. In both the plots, the T_c variation show three distinct regions. In the first region, at larger values of x , T_c decreases linearly with x down to $x = 0.077$

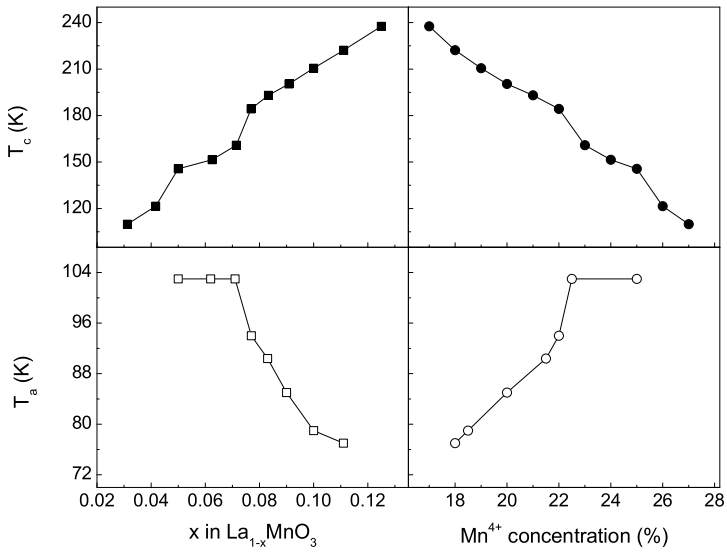

Figure 3.14: Variations of T_c and T_a as functions of x in $La_{1-x}MnO_3$ and the Mn^{4+} concentration.

and then drops drastically. Another linear region is observed between $x = 0.05$ and 0.071 and a third region is observed below $x = 0.05$. The interesting observation is that, the first linear region corresponds to oxygen deficient compositions, the second to Mn deficient compositions where the Mn vacancy is smaller than La vacancy and the third region to Mn deficient compositions where the Mn vacancy is larger than the La vacancy, as given in Table 3.1. For $x = 0.125$, the susceptibility decreases continuously, down to the lowest temperature, as the temperature is decreased. An interesting feature observed is the appearance of a drop in the susceptibility at low temperatures in the ferromagnetic regime, for compositions with $x < 0.125$. The temperature at which the anomalous drop in the susceptibility is observed, T_a, as well as the drop in the susceptibility below T_a increases with decreasing amount of doping. The variation of T_a as functions of x and Mn^{4+} concentration is shown in

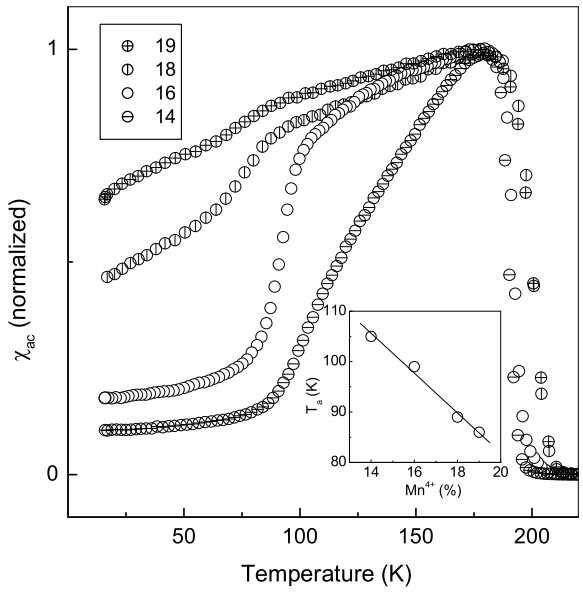

Figure 3.15: *ac* susceptibility curves of $La_{0.909}MnO_3$ for different Mn^{4+} concentrations. The numbers indicate percentage Mn^{4+} concentrations. Inset: T_a as a function of Mn^{4+} concentration.

Fig. 3.14. T_a increases almost linearly with decreasing x in the oxygen deficient compositional region and becomes constant ($\sim$105 K) for the Mn-deficient compositions. Another way of looking at the variation is with respect to the Mn^{4+} concentration. T_a remains constant when the Mn^{4+} concentration is more than 23% and decreases with decreasing Mn^{4+} content. Since the compositions for $x < 0.07$ are both La- and Mn-deficient, it is not clear whether the responsible factor for the low-temperature decrease in the susceptibility is La-deficiency, Mn-deficiency, oxygen deficiency, Mn^{4+} concentration or a combination of all these factors.

However, as shown in Fig. 3.15, for a given La-vacancy concentration in the oxygen deficient region of the compositions ($x = 0.091$), both T_a as well as the slope of the decrease in the susceptibility below T_a increases with decreasing Mn^{4+} concentration.

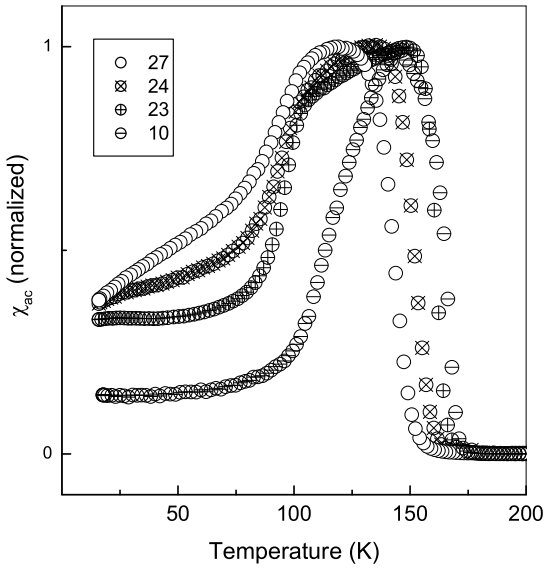

Figure 3.16: *ac* susceptibility curves of $La_{0.937}MnO_3$ for different Mn^{4+} concentrations. The numbers indicate percentage Mn^{4+} concentrations.

T_c is found to be slightly decreased with decreasing Mn^{4+} content, from 201 to 190 K, for the decrease in the Mn^{4+} concentration from 19 to 14%. This amounts to the decrease in the oxygen stoichiometry in $La_{0.91}MnO_{3-\delta}$ from 2.96 to 2.93. An interesting observation is that the value of T_a approaches towards the constant value of ∼105 K as observed for higher Mn^{4+} content or for lower vacancy concentrations in the series. Similarly, the shape of the ac susceptibility curve also approaches that of the lower La-vacancy compositions where the susceptibility drops off immediately below T_c and a sharp peak is observed. Such sharp peaks in the ac susceptibility curves are generally observed for compounds with large magnetocrystalline anisotropy [Kum98a]. When the magnetic field used for the measurements is much smaller than the anisotropy field which increases with decreasing temperature, the response of the

magnetic moments to the *ac* field decreases with temperature. Therefore, it may be assumed that there is a corresponding increase in the anisotropy field when the Mn^{4+} concentration is decreased considerably. Troyanchuk *et al.* have observed such an increase in the anisotropy field with decreasing Mn^{4+} concentration for $La_{0.88}MnO_{3-\delta}$ [Tro03]. However, similar ac susceptibility behaviour is observed for the compositions with larger Mn^{4+} compositions (smaller La-vacancies) also in the series (see Fig. 3.13) making it difficult to arrive at a particular conclusion on the specific role of Mn^{4+} concentration.

On the other hand, for the Mn-deficient compositions, where T_a is in the maximum range, there is no considerable effect on T_a on decreasing the Mn^{4+} concentration, as shown in Fig. 3.16 for $La_{0.937}MnO_3$. The samples with Mn^{4+} content of 27, 24 and 23% were obtained by repeatedly heating the sample at 1473 K in air and the one with low Mn^{4+} concentration is obtained after annealing in nitrogen atmosphere. Theoretically, the maximum possible Mn^{4+} content for this value of x in $La_{1-x}MnO_3$ is 18.9%, assuming there are no Mn vacancies. Larger than this value automatically assumes Mn vacancies. The composition $La_{0.937}Mn_{0.984}O_3$ is calculated for 24% Mn^{4+} concentration.

Based on this, the composition with 27% Mn^{4+} should have excess oxygen. Since the perovskite structure is a close packed structure with the oxygen sites fully occupied [Mit02], it will not be possible to accommodate more oxygen in the structure. Also, if the oxygen stoichiometry is maintained, then increasing the Mn^{4+} concentration implies a decrease in the overall Mn content in the compositions for a given La-deficiency, $La_{0.937}Mn_{0.975}O_3$ for 27% Mn^{4+}, which is not feasible. Hence the only possible way to accommodate excess Mn^{4+} in the otherwise oxygen stoichiometric compositions is to assume that even these compositions are oxygen deficient, initially, to some extent, so that the actual composition is $La_{1-x}Mn_{1-y}O_{3-\delta}$ for all La-deficient compositions. In this case, it is possible to further decrease or increase the oxygen

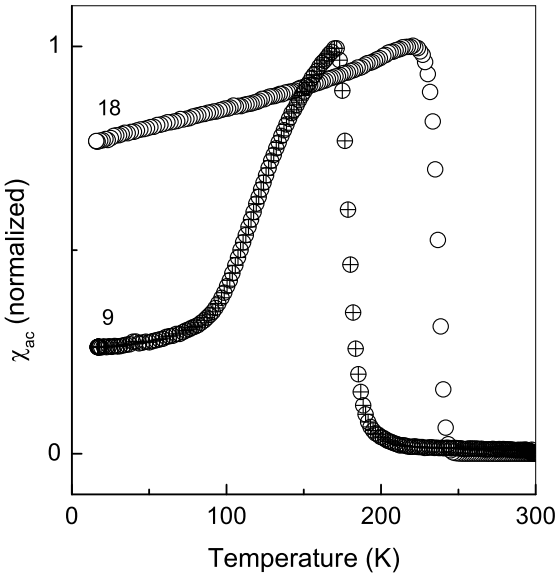

Figure 3.17: *ac* susceptibility curves of $La_{0.875}MnO_3$ for two different Mn^{4+} concentrations. The numbers indicate percentage Mn^{4+} concentrations.

stoichiometry to accommodate larger or smaller amount of Mn^{4+}. It is not possible to obtain the values of both y and δ at the same time from the Mn^{4+} content estimations. For $La_{0.875}MnO_3$, though no drop in the susceptibility is observed at low temperatures (see Fig. 3.14), based on the above observations it is expected that the anomaly can be induced on decreasing the Mn^{4+} content. Fig. 3.17 shows the ac susceptibility curve of a nitrogen annealed sample with lower Mn^{4+} concentration. A sharp magnetic transition is observed at a lower temperature for the sample with 9% Mn^{4+} content. A decrease in the susceptibility is observed after going through a maximum below T_c. Also, a slope change with a faster drop in the susceptibility is observed below ∼110 K, close to the maximum value of T_a observed for other compositions. The shape of the curve of the sample with lower Mn^{4+} concentration, at low temperatures, is

similar to that observed for the compositions with $x = 0.091$ and 0.063 having the Mn^{4+} concentrations close to 13%. Thus, the Mn^{4+} content is found to have serious effects on the magnetic properties of the self-doped manganites in the ferromagnetic region also apart from the effect on the magnetic transition temperatures. However, a large decrease in Mn^{4+} content in such manganites causes structural distortion which may probably affect the magnetic characteristics. All the compositions with the lower Mn^{4+} concentrations were found to be orthorhombic, compared to the rhombohedral perovskite structure of the other compositions.

For $La_{0.937}MnO_3$, T_a is already the limiting larger value obtained for the series ($\sim$105 K) and therefore there is no further increase in the value of T_a with decreasing Mn^{4+} content. Though T_a is unchanged on decreasing the Mn^{4+} concentration, larger drop in the susceptibility is observed when Mn^{4+} concentration is decreased. Interestingly, in this case T_c increases with decreasing the Mn^{4+} content, opposite to the trend observed for $La_{0.909}MnO_{3-\delta}$ (see Fig. 3.15 and Fig. 3.16). This is attributable to the increasing strength of the double exchange interactions with increasing the concentration of Mn^{3+} or that Mn^{3+}-O-Mn^{3+} ferromagnetic exchange interactions become more predominant when the Mn^{4+} concentration is lower. Assuming that the actual composition is $La_{0.937}Mn_{0.975}O_3$ for 27% Mn^{4+}, the oxygen stoichiometry will be decreased from 3 to 2.98 corresponding to the decrease in the Mn^{4+} concentration from 27 to 23%. When the Mn^{4+} concentration is as low as 10%, the composition becomes more oxygen deficient as $La_{0.937}Mn_{0.975}O_{2.92}$. This is equivalent to the composition having no Mn-deficiency as $La_{0.953}MnO_3$ and for this composition, the susceptibility decreases sharply below the T_c, almost similar to that observed for $La_{0.909}MnO_{2.93}$ with 14% Mn^{4+}, as shown in Fig. 3.15.

The above observations imply that there is no specific trend in the variation of the Curie temperature with Mn^{4+} concentration in the self-doped (La-deficient) manganites. The magnetic transition temperature varies in both directions with increasing

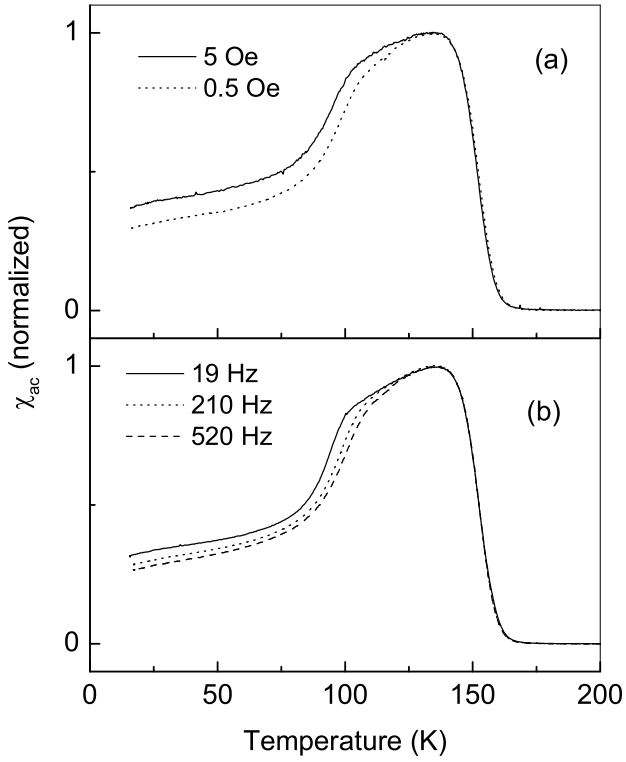

Figure 3.18: *ac* susceptibility curves of $La_{0.937}MnO_3$ recorded at (a) two different *ac* fields at a frequency of 210 Hz and (b) at different frequencies in a field of 0.5 Oe.

Mn^{4+} concentration when there is no Mn deficiency in the structure and increases with increasing Mn^{4+} concentration for Mn-deficient compositions. This is based on the assumptions of the estimated Mn^{4+} concentrations and the compositions derived from these values, assuming that the La-deficiency is same as that in the starting composition. It is possible that this discrepancy is due to the assumed compositions of the self-doped manganites, where the compositions are derived from the Mn^{4+} content. A uniform tendency for the variation of T_c with Mn^{4+} content for all com-

positions in the self-doped series might be possible assuming Mn and O deficiencies in all cases and that the general composition is $La_{1-x}Mn_{1-y}O_{3-z}$. The difficulty to obtain both y and z values hinder the calculation of the actual composition. In general, it can be concluded that the magnetic behaviour of the self-doped manganites below the magnetic transition temperature is determined by the Mn^{4+} concentration rather than the La-vacancy. A sharp decrease in the susceptibility below T_c is obtained for compositions with very low Mn^{4+} content, irrespective of the La-deficiency. There exists a limiting maximum value for T_a, which is independent of the Mn^{4+} concentration. Also, T_a varies with Mn^{4+} concentration for a given composition only when it is less than a maximum possible value.

Fig. 3.18(a) shows the *ac* susceptibility curves of the $x = 0.063$ composition recorded at two different *ac* magnetic fields, at the *ac* frequency of 210 Hz. Though the transition temperature and the broad maximum below T_c are not affected by this change in the *ac* field, large difference is observed in the region of the anomalous drop in the susceptibility. T_a is decreased from 103 K to 99 K, when the *ac* field is increased from 0.5 to 5 Oe. Similar effect is observed when the measurement frequency is varied at a constant *ac* field, as shown in Fig. 3.18b. T_a is decreased from 106 to 99 K when the *ac* frequency is decreased from 520 to 19 Hz, whereas the T_c and the broad maximum are unaffected. The *ac* field and frequency dependence of the features in the susceptibility curves are typical of spin glass (SG) systems [Myd93, Det96]. Therefore, such systems showing a ferromagnetic transition and a drop in the susceptibility at a lower temperature associated with frequency dependence are termed as reentrant spin glass (RSG) systems [Ter98, Sat01, Abi05], where the low-temperature drop in the susceptibility is ascribed to a ferromagnetic to spin glass transition.

The signatures of the *ac* susceptibility curves are usually observed in the *dc* magnetization curves also when measured under zero field cooled conditions in the presence of sufficiently low magnetic fields [Kum98a]. Zero field cooled (ZFC) and field cooled

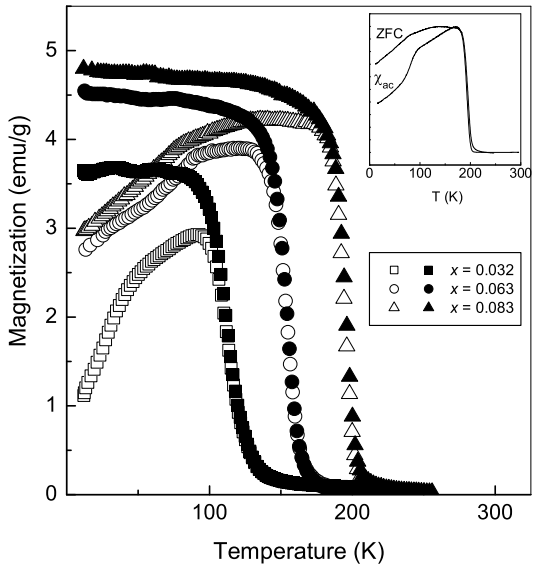

Figure 3.19: FC (closed symbols) and ZFC (open symbols) magnetization curves of three different compositions in $La_{1-x}MnO_3$. inset: normalized ZFC and *ac* susceptibility curves of $x = 0.083$.

(FC) magnetizations recorded in a *dc* magnetic field of 50 Oe, for three different self-doped compositions, are shown in Fig. 3.19. Characteristic features observed in the ac susceptibility curves are found in the ZFC magnetization curves also. However, as shown in the inset of Fig. 3.19, the anomaly is shifted to lower temperatures and the feature is broadened in the ZFC curve. This is expected because, as shown in Fig. 3.18, T_a decreases with decreasing the frequency towards the *dc* limit and moreover, a field of 50 Oe is used in the *dc* measurement which is comparatively larger than the *ac* fields used for the typical *ac* susceptibility measurements (T_a decreases with increasing ac field). Thermomagnetic irreversibility (divergence of FC and ZFC magnetizations) is observed below T_c for all three compositions. A drastic decrease

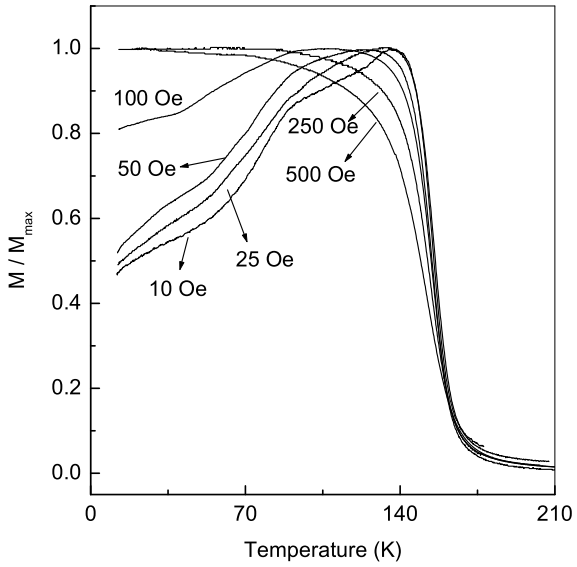

Figure 3.20: Zero field cooled magnetization curves of $La_{0.937}MnO_3$, measured in different *dc* magnetic fields.

in the magnetization observed in the ZFC magnetization curve is not observed in the FC case. Thermomagnetic irreversibility is a common feature observed for ferromagnetic and ferrimagnetic systems [Roy96, Roy97, Joy98, Cha04] which were earlier thought to be characteristic features of spin glasses. There are studies on well-defined ferromagnetic or ferrimagnetic systems showing frequency dependence of the features in the *ac* susceptibility below the ferromagnetic transition temperature. For example, neutron diffraction studies on the ferrimagnetic oxide $YFeMnO_5$ show magnetic ordering down to 2.9 K whereas a frequency dependence of the susceptibility is observed below $T_c = 165$ K [Mun04]. Similarly, in the case of $La_{0.83}Sr_{0.17}MnO_3$, where a similar feature as in the case of the self-doped manganites studied here, only a ferromagnetic component is observed down to low temperatures [Kaw96]. However a

structural transition was observed at the temperature where an anomaly is observed. $La_{0.85}Ca_{0.15}MnO_3$ was also found to exhibit similar behaviour from *ac* susceptibility and neutron diffraction studies [Cas99]. De Brion *et al.* observed a similar behaviour in the *ac* susceptibility and ZFC magnetization curves in the case of $La_{0.93}MnO_3$ [Deb99]. Magnetic saturation was observed at very low temperatures, with no time dependence of the magnetization, indicating the absence of any spin glass behaviour. Fe_3O_4, the well known ferrimagnetic oxide exhibits a frequency dependence of a low-temperature anomaly of single crystals in the *ac* susceptibility and this has been ascribed to freezing out of domain wall motion due to the rearrangements of the electron states within the domain wall [Sku99]. Similarly, studies on single crystals of ferrimagnetic $FeCr_2S_4$ suggest that domain wall pinning effects are responsible for similar features [Tsu01]. High driving fields are required to overcome the pinning forces and the origin of the relaxation processes can be due to temperature variation of the magnetocrystalline anisotropy. There are also other causes for the relaxation arising from the changes in the domain structure due to structural transformation, domain wall pinning due to non-uniform distribution of magnetic ions, presence of antiphase boundaries, etc.

It was found that in the *ac* susceptibility curve, increasing the measuring field decreases T_a, with an increase in the susceptibility. A similar behavior is observed in the ZFC magnetization also, with increasing the *dc* field, as shown in Fig. 3.20. For $La_{0.937}MnO_3$, a systematic change in the ZFC magnetization behavior is observed when the applied field strength is increased and no anomaly at low temperatures is observed when the applied field is increased from 100 to 250 Oe. The magnetization increases continuously with decreasing temperature, when measured using higher magnetic fields. The difference (or feature) between the ZFC magnetizations, measured at field strengths of 50 and 250 Oe decreases continuously with increasing temperature. This indirectly tells that, there may exist a critical field and if the ZFC

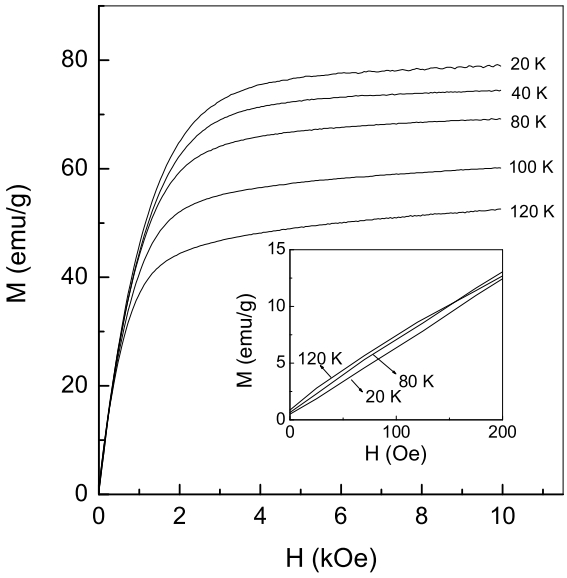

Figure 3.21: Initial magnetization curves of $La_{0.937}MnO_3$, recorded at different temperatures. Inset: Initial magnetization curves in small magnetic fields

magnetization measurements are made at or above this field no anomaly could be observed in the ZFC magnetization below T_c. That is, the anomaly appears to be originating from some feature whose effect can be canceled by sufficient activation energy in the form of larger magnetic fields at lower temperatures or by thermal activation in the presence of lower magnetic fields. This is true if domain wall pinning effect is responsible for the anomaly where higher magnetic fields can de-pin the walls at lower temperatures when magnetic fields larger than the pinning fields completely destroy the pinned state. Previous studies have shown that the features in the ZFC magnetization curves, measured at a given low magnetic field, are directly related to the initial magnetization at this field at different temperatures [Joy00c]. Since the initial magnetization behavior at low magnetic field strengths is dominated by domain

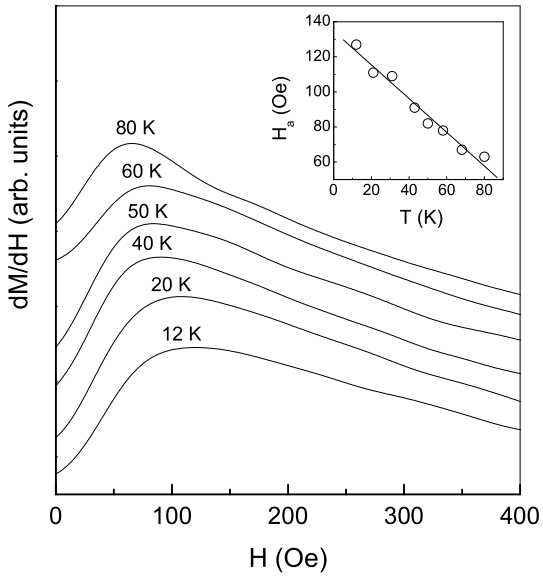

Figure 3.22: Variation of dM/dH as a function of field at different temperatures, for $La_{0.937}MnO_3$. The field at which a maximum is observed in dM/dH vs H, H_a, as a function of temperature is shown in inset.

wall motion, the characteristic features of the ZFC magnetization curves recorded at different magnetic fields are a reflection of the domain structure of the individual material. Fig. 3.21 shows the initial magnetization curves of $La_{0.937}MnO_3$ measured at different temperatures. Though the magnetization is saturated above 5 kOe and the magnetization continuously decreases with increasing temperature at larger magnetic fields, the reverse trend is observed at lower magnetic fields at temperatures below 100 K. The magnetization is lower at lower temperatures at low magnetic fields, as shown in the inset of Fig. 3.21. Such behavior in multidomain particles is known to be a characteristic feature of domain wall pinning [Dem98]. The indication for the existence of a critical field, as observed from the ZFC measurements, suggests

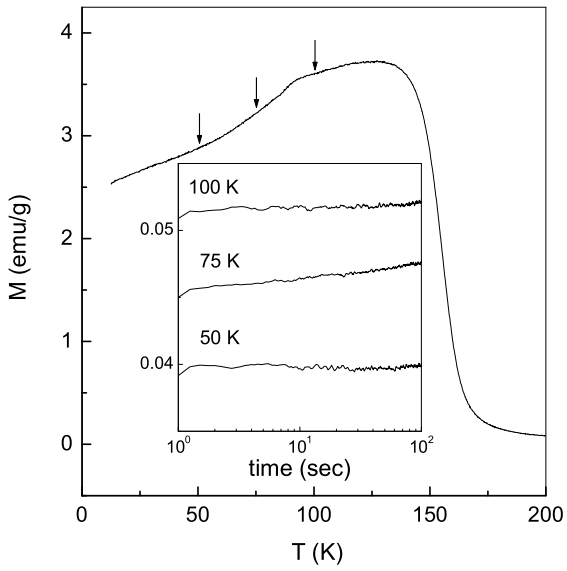

Figure 3.23: Time dependence of the ZFC magnetization of $La_{0.937}MnO_3$ recorded at three different temperatures, as indicated by arrows in the ZFC magnetization curve, H = 50 Oe.

that the pinning of domain walls is responsible for the anomalous behavior at low temperatures. Hence an attempt is made to trace the critical field by studying the isothermal magnetization processes at moderately low magnetic fields. In the initial magnetization curve of a virgin sample, the first part of the curve at low magnetic fields corresponds to reversible domain wall motion followed by irreversible movement of the walls due to unpinning and this corresponds to a steep rise in the magnetization. The domain wall unpinning field is obtained by differentiating the magnetization with respect to the magnetic field. Fig. 3.22 shows the dM/dH curves as a function of field, at different temperatures. A broad maximum is observed in each curve at a certain field, and this field decreases with increasing temperature. The maximum of the curve corresponds to the steepest part of magnetization curve in which the change

in M is mainly due to irreversible domain wall motion in a polycrystalline sample as observed in several magnetic systems [Zen93, Dem98, Liu99] and can be identified as domain wall unpinning field, H_a. It can otherwise be defined as the threshold field required in order to unpin the domain walls. Understandably, this must vary with the rate at which field is applied and the temperature [Zen93].

In the present study the rate of variation of the field was kept constant as 1.6 Oe s^{-1}. It was found that no maximum is observed in the differential magnetization curves above 100 K matching with the maximum value of T_a observed in ac susceptibility curve for $La_{0.937}MnO_3$. This is in accordance with the finding that there is no magnetic anomaly due to domain wall pinning beyond 105 K. Also, inset in Fig. 3.22 shows that H_a decreases with increasing temperature at the rate of approximately 1 Oe/K and the intercept on the y-axis is 135 Oe. This is in agreement with the observation made from ZFC magnetization curves obtained using different applied field strengths. The anomalous drop of magnetization in the ZFC magnetization curves, as shown in Fig. 3.20, is observed when applied field, $H < H_a$ and disappeared when $H > H_a$. The above results imply that the temperature above which the domain walls are de-pinned, T_{dw}, will be decreased with increasing the field used for the ZFC magnetization measurements and no anomaly is expected down to lowest temperatures when the magnetic field is larger than 135 Oe, supporting the results shown in Fig. 3.20 and Fig. 3.21. That is, there is a direct correlation between the nature of M_{ZFC} curves and the domain structure of a material.

A large magnetic relaxation effect is usually observed at a temperature where the domain walls become unpinned [Joy00c]. This argument directly supports the conclusion that the frequency dependence of the low-temperature feature observed in the ac susceptibility curve is associated with domain wall pinning effects. In fact, relaxation of the ZFC magnetization is observed in the temperature region where the anomaly is observed. Fig. 3.23 shows the time dependence of the ZFC magnetization

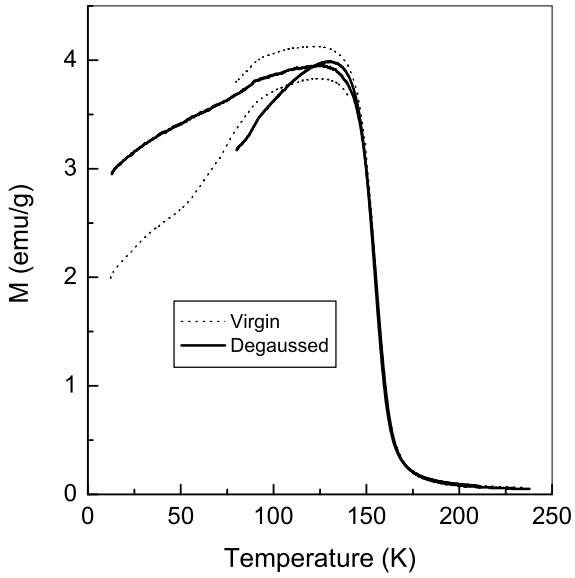

Figure 3.24: Comparison of the temperature dependence of the magnetization of $La_{0.937}MnO_3$ recorded after zero-field cooling (broken lines) and after applying a field and degaussing the ZFC sample (solid lines).

of $La_{0.937}MnO_3$, measured at three different temperatures as indicated in the figure; i) where the *ac* susceptibility becomes almost constant after the anomalous decrease below T_a, ii) where maximum slope change is observed, and iii) slightly above T_a. For each measurement, the sample was cooled through the T_c in zero field, to the required temperature, and the magnetization was recorded as a function of time immediately after applying a magnetic field of 50 Oe. It may be seen that there is no appreciable variation in the magnetization for cases (i) and (iii) whereas the magnetization continuously increases with time in the temperature region where the anomaly is observed. Another important observation supporting the conclusion that the anomalous low-temperature behaviour is not because of any antiferromagnetic transition or im-

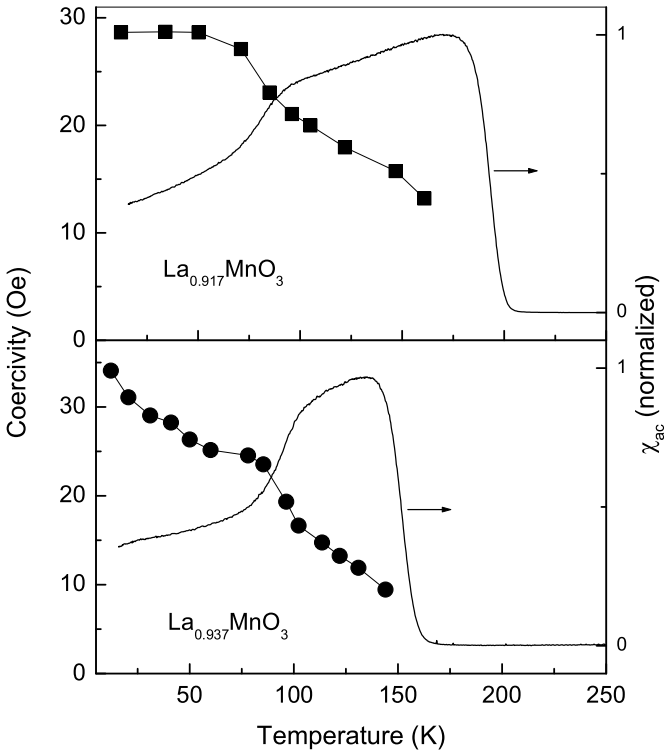

Figure 3.25: Temperature dependence of the coercivity (H_c) and *ac* susceptibility (χ_{ac}) of $La_{0.917}MnO_3$ and $La_{0.937}MnO_3$.

purity and that it is mainly due to some domain wall effects comes from degaussing experiments [Joy00c]. The sample after cooling to the lowest temperature in zero field is exposed to a field for magnetic saturation and the remnant magnetization was reduced to zero by degaussing. The magnetization was then continuously monitored on warming in a field of 50 Oe, the same way as in the case of the ZFC magnetization measurement. The virgin ZFC magnetization curve measured after cooling to 12 K and the corresponding curve obtained after degaussing are compared in Fig. 3.24.

The magnetization at low temperatures is increased considerably and the anomalous behaviour is almost vanished after degaussing the sample. On the other hand, if the sample is cooled only to the temperature region where large drop in the magnetization is observed, the virgin and degaussed ZFC magnetization curves show different behaviour. Here, though the anomalous drop in the magnetization is almost vanished, the magnetization after degaussing is lower than that when the sample is not degaussed. The behaviour of the degaussed sample is as if there is a hindrance to the alignment of the magnetic moments in the direction of the field. This is possible if the moments are locked in certain regions and directions. This implies that the anomalous drop in the magnetization below 100 K is associated with domain wall pinning effects. If this was due to any other magnetic phases present in the sample or any other magnetic transition, this would not have been destroyed on degaussing. If the low-temperature anomalous feature in the *ac* susceptibility as well as ZFC magnetization is due to domain wall motion effects, due to the pinned domain walls, this should be reflected in the coercivity of the material also [Ste02]. Figure. 3.25 shows a comparison of the *ac* susceptibility and the variation of coercivity as a function of temperature for $La_{0.917}MnO_3$ and $La_{0.937}MnO_3$. For both the samples, the coercivity initially increases almost linearly below T_c and a small jump in the coercivity is observed below T_a. This correlation between the changes in the coercivity and the *ac* susceptibility can be seen clearly in Fig. 3.26. Fig. 3.26 compares the shapes of the inverse of the coercivity and *ac* susceptibility curves, normalized at a certain temperature, for four compositions, $x = 0.031$, 0.063, 0.083, and 0.091 in $La_{1-x}MnO_3$. In all cases, there is a direct comparison of the changes in the *ac* susceptibility as well as the coercivity with temperature, especially in the temperature region where the drop in the susceptibility is observed. Moreover, as shown in Fig. 3.27 for $La_{0.909}MnO_3$ and $La_{0.937}MnO_3$, when the susceptibility drops drastically below T_a, as the Mn^{4+} concentration is decreased (see Fig. 3.15 and Fig. 3.16), a corresponding increase in

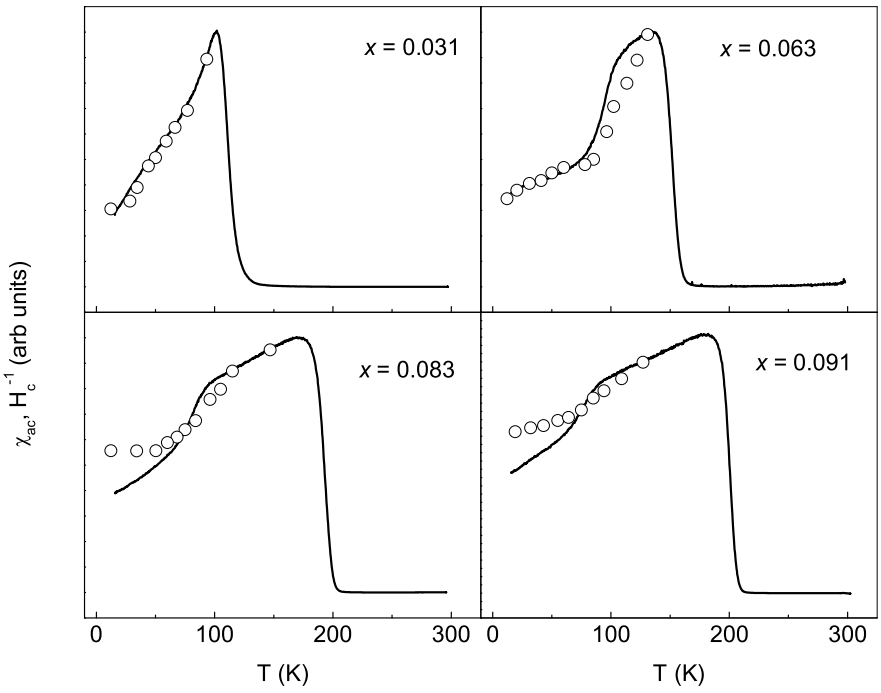

Figure 3.26: Normalized *ac* susceptibility and $H_c^{-1}(T)$ curves of four different compositions.

the coercivity at low temperatures is observed. As long as T_a is unaffected for Mn^{4+} concentration $> 22\%$, the coercivity also remains almost the same and the increase in the coercivity is observed only for a decrease in the Mn^{4+} concentration below 22%. This tells about the increasing anisotropy on decreasing the Mn^{4+} concentration, likely due to the increased domain wall pinning effects. It is possible that the distribution of Mn^{4+} ions, at lower concentrations, in the lattice, is responsible for the effect of increased anisotropy.

In fact, Troyanchuk *et al.* have reported the magnetic properties of $La_{0.88}MnO_{3-\delta}$ with different Mn^{4+} concentrations [Tro03]. The sample with 22% of Mn^{4+} shows

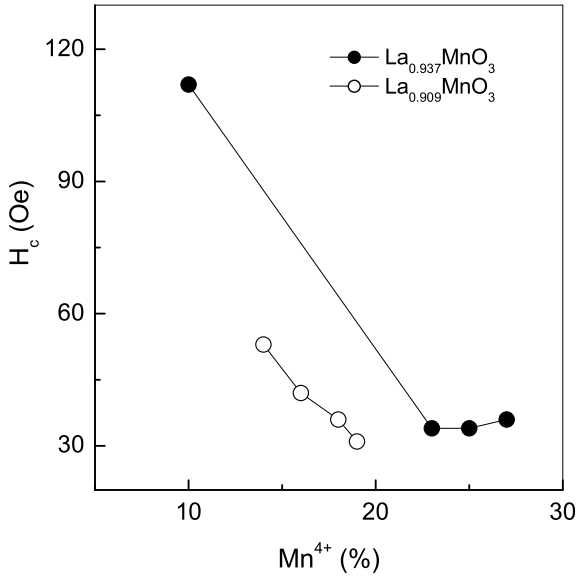

Figure 3.27: Coercivity, measured at 12 K, as a function of Mn^{4+} concentration for $La_{0.909}MnO_3$ and $La_{0.937}MnO_3$.

a similar behaviour in the zero field cooled magnetization curve measured at a field strength of 100 Oe, as in the case of the ac susceptibility curve of the $La_{0.875}MnO_{3-\delta}$ sample studied in this work. Decreasing the Mn^{4+} concentration from 22 to 18% gives rise to a small decrease in the ZFC magnetization below 100 K. This drop is enhanced and the temperature at which this drop is observed is increased to slightly above 100 K with further decreasing the Mn^{4+} concentration. Moreover, the magnetic transition temperature decreases continuously and the transition becomes broad with decreasing Mn^{4+} concentration. Thus the studies on different compositions in the self-doped lanthanum manganite series, $La_{1-x}MnO_3$, show some interesting features in the ferromagnetic regime. A drop in the ac susceptibility and ZFC magnetization observed at low temperatures is influenced by the Mn^{4+} concentration. Irrespective

of the degree of La-vacancy, the temperature below which the anomalous drop is observed never exceeds a maximum value of ∼105 K. There is a direct correlation between the magnetic anisotropy and the decrease in the susceptibility, as evidenced from the variation in the coercivity at low temperatures as a function of Mn^{4+} concentration as well as temperature for different compositions. The larger changes in the zero field cooled magnetization as a function of time in the temperature region where the anomaly is observed, the disappearance of the anomaly in the ZFC magnetization measurements at larger fields, the absence of the anomaly in the FC magnetization measurements, the dependence of the anomalous feature with *ac* field and frequency in the *ac* susceptibility measurements, etc., point to the role of domain wall pinning effects as the origin of the anomaly, rather than due to other magnetic transitions or spin glass or reentrant spin glass behaviour. As to the cause for the domain wall pinning effects, the likely contributions are the inhomogeneous distribution of Mn^{4+} ions in the lattice. However, there is a more possible chance for a structural phase transition at the temperature where the anomaly is observed, as reported by Kawano *et al.* [Kaw96]. This minor structural change affects the Mn-O-Mn bond angle which may cause a small canting of the spins so that the applied field is not sufficient to orient the moments in lower magnetic fields. The fact that the anomaly is not observed when measured in larger magnetic fields is supporting this conclusion.

Further, for the self-doped composition with Mn^{4+} content less than 15% a structural change from rhombohedral to orthorhombic symmetry is observed. This may be attributed to the large structural distortion due to strong Jahn-Teller effect prevailing in the Mn^{3+} rich lattice. The nature of the magnetization curves of these samples are almost identical, with no apparent flat region immediately below T_c but with a sharp decrease in susceptibility. The structural change which is highly susceptible to the amount of Mn^{4+} in the lattice suggests that a structural phase transition is a probable cause of the low-temperature anomalous magnetic behavior observed in $La_{1-x}MnO_3$.

Moreover, a large value of coercivity is observed at 12K for the orthorhombic perovskite with $x = 0.063$ and $Mn^{4+} = 13\%$. This is consistent with the observations made in $LaMnO_{3+\delta}$ by Pavlov *et al.* [Pav84], where coercivity of the sample is found to undergo a drastic increase when the amount of Mn^{4+} is decreased below 15% which is accompanied by a structural phase transition. Thus, a structural rearrangement involving a change from rhombohedral to orthorhombic geometry which might hinder the domain wall motion can be thought to have such a magnetic hardening effect on the manganites under investigation similar to the La-Sr-Mn-O compositions as stated by Kawano *et al.* [Kaw96].

However, this is not a definite conclusion, and another factor which is worth mentioning in this context is regarding the role of ordered and disordered local structural distortions in defining the domains and domain walls. Shibata *et al.* have observed the tendency for local structural inhomogeneity in lightly doped $La_{1-x}Sr_xMnO_3$ and they presumed this might have serious effects on the magnetic and electronic properties of manganites [Shi02]. In $La_{1-x}MnO_3$ also, due to the presence of La-site vacancies, there might be a change in local structure since the crucial parameters determining the properties such as Mn-O distance and Mn-O-Mn bond angles would undergo certain changes in the vicinity of the vacancies. When such vacancies are homogeneously distributed in the lattice as in the case of $x = 0.125$ composition, the local distortions may become globally ordered. As soon as the vacancies are inhomogeneously distributed when $x < 0.125$, the global ordering is destroyed and the local distortions may act as impurity centers for the pinning of domain walls. It can be assumed that as the vacancy ordering deviates from 1/8, distribution of vacancies become more and more inhomogeneous ultimately resulting in the formation of strong domain wall pinning centers when the values of x become sufficiently small. It may be for the similar reason that such low-temperature magnetization anomaly has been observed in the lightly doped calcium and strontium manganites

[Hwa95, Mit96, Bar98, Dho99, Nie99, Joy00c, Ste02].

Another factor to be considered as domain wall pinning centers in the manganites generally is the Mn-deficiency in the structure especially since strong pinning is observed in self-doped compositions when manganese vacancy is increased. It is known that lanthanum calcium manganites have a tendency to form compositions with excess oxygen stoichiometry [Tok00]. This may create vacancies at cationic site, probably both at La (and/or Ca) and Mn sites leading to domain wall pinning at Mn-vacancy defect centers. A detailed investigation is required to probe the exact compositional/structural features that provide centers for domain wall pinning.

Another important observation is that the magnetic transition temperatures of different compositions is not directly related to the Mn^{3+} to Mn^{4+} ratio. The magnetic transition temperature increases with Mn^{4+} content for certain compositions whereas the reverse is observed for some other compositions. These compositional regions are marked by the degree of vacancies at the cationic and anionic sites of the perovskite structure and need to be studied in detail.

3.3 Self-doping Effects in $La_{0.90}Ca_{0.10}MnO_3$

The substitution of La^{3+} by Ca^{2+} ions produces corresponding amount of Mn^{4+} in the perovskite-type manganite lattice. A double exchange mechanism involving both the Mn^{3+} and Mn^{4+} ions together with strong lattice effects control the electronic properties of these strongly correlated electron systems. Such a double exchange mechanism is sensitive to the structural and/or compositional changes induced by the type and amount of the substitutional ions, nonstoichiometry etc. A large number of reports on divalent ion substituted manganites are available but effects of nonstoichiometry both at cationic and anionic sites are not much investigated. Some of the studies have shown changes in the magnetic properties of cation deficient divalent ion doped

lanthanum manganites [Zhe01, Pha03, Alo03, Hon04, Dha05]. Interesting magnetic behaviors such as increasing as well as decreasing magnetic transition temperature, spin glass nature, etc. have been shown in these reports. Alonso *et al.* have discussed the results in terms of a hole-attractor model to explain the observed characteristics. The studies on self doped lanthanum manganite compositions reveal interesting characteristics of dependence of magnetic properties on self-doping concentration and the amount of Mn^{4+} ions formed. Also these compositions were found to have either deficiency or excess of oxygen [Rao98, Tok00]. The deviation from oxygen stoichiometry is generally observed in compositions with low amounts of Ca-doping [Tok00]. The excess oxygen nonstoichiometry may result in cationic vacancies and have serious consequences on the magnetic exchange interactions. Small amount of vacancies at La site or Ca site (A-site) in lanthanum calcium manganites may be expected to create more number of Mn^{4+} ions in the lattice, which could aid the double exchange and hence an enhancement in T_c. Similarly, slight excess of A-site ions would form manganese deficient structures. As part of the studies on self-doped manganites, we have investigated the effect of cation vacancies in a calcium doped lanthanum manganite. The effects of cationic nonstoichiometry at both La and Ca sites on the magnetic properties have been investigated on a nominal composition $La_{0.9}Ca_{0.1}MnO_3$.

3.3.1 Synthesis

The current study is restricted to the compositions of the formula $La_{0.9+x}Ca_{0.1}MnO_3$ and $La_{0.9}Ca_{0.1+y}MnO_3$, where $x = y = 0$ and ± 0.05. The samples were prepared by the solid state reaction method from stoichiometric amounts of La_2O_3, MnO_2, and $CaCO_3$. The powder samples were heated at 1273, 1473, and 1573 K for 48 h each with intermediate grinding after each 24 h heating cycle, and then at 1673 K for 12h. Pellets made from the powders were then heated at 1673 K for 12 h. All samples were made in a single batch to keep the processing conditions identical.

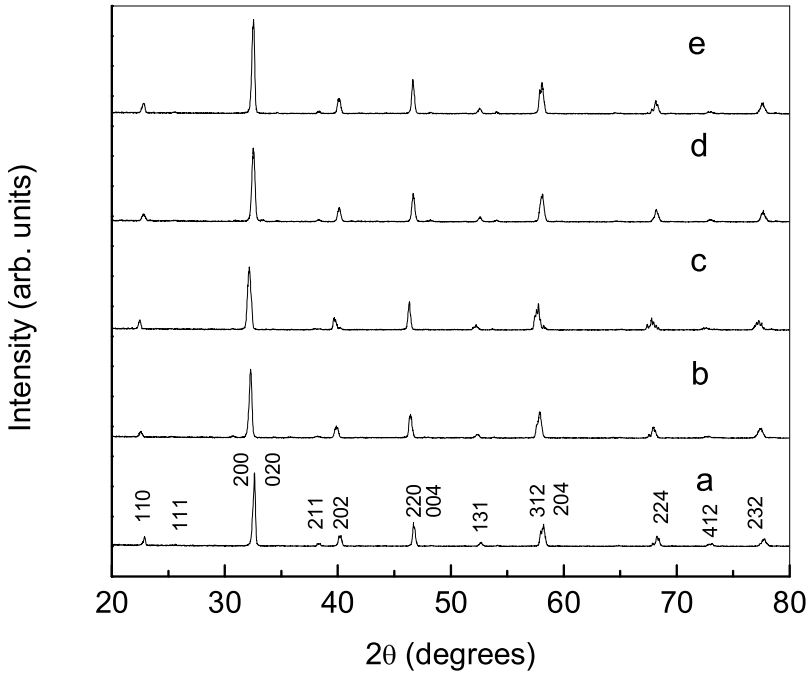

Figure 3.28: XRD patterns of $La_{0.9+x}Ca_{0.1}MnO_3$ ((a) x = 0, (b) x = -0.05, and (c) = +0.05) and $La_{0.9}Ca_{0.1+y}MnO_3$ ((d) y = -0.05 and (e) = +0.05)

3.3.2 Results and Discussion

The powder XRD patterns of the five compositions are as shown in Fig. 3.28. All the XRD patterns are identical and correspond to the orthorhombic perovskite unit cell. There are no impurity peaks observed in the XRD patterns of any of the samples indicating complete reaction of the reactants. The orthorhombic lattice parameters were found to be slightly smaller than that of $La_{0.9}Ca_{0.1}MnO_3$ and almost identical for the cation deficient compositions whereas for the cation excess compositions, the lattice prameters were found to be slightly larger and comparable. The parent composition, $La_{0.9}Ca_{0.1}MnO_3$ is found to have a well defined T_c of 170 K whereas the

Table 3.2: Mn^{4+} content and Curie temperatures of $La_{0.9\pm x}Ca_{0.1\mp y}MnO_3$.

Composition	$Mn^{4+}(\pm 1\%)$	T_c (K)
$La_{0.95}Ca_{0.1}MnO_3$	26	126
$La_{0.9}Ca_{0.15}MnO_3$	25	132
$La_{0.9}Ca_{0.1}MnO_3$	21	170
$La_{0.85}Ca_{0.1}MnO_3$	12	208
$La_{0.9}Ca_{0.05}MnO_3$	17	203

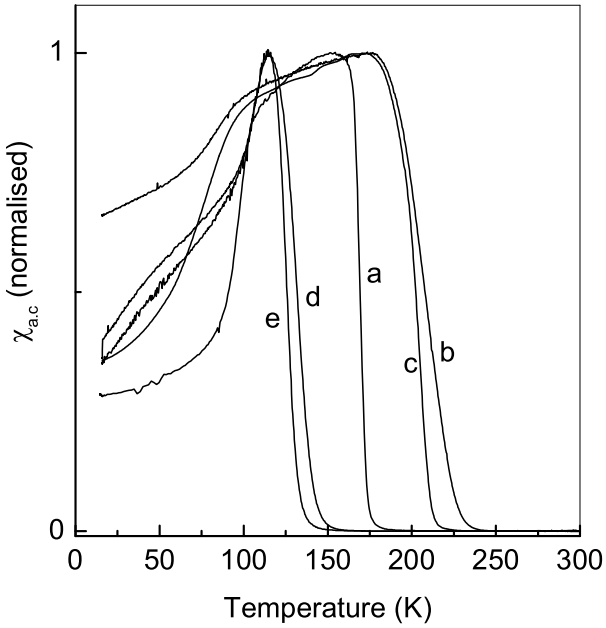

Figure 3.29: Normalized *ac* susceptibility curves of $La_{0.9+x}Ca_{0.1}MnO_3$; (a) $x = 0$, (b) x = -0.05, and (d) x = +0.05 and $La_{0.9}Ca_{0.1+y}MnO_3$; (c) y = -0.05 and (e)y = +0.05 compositions.

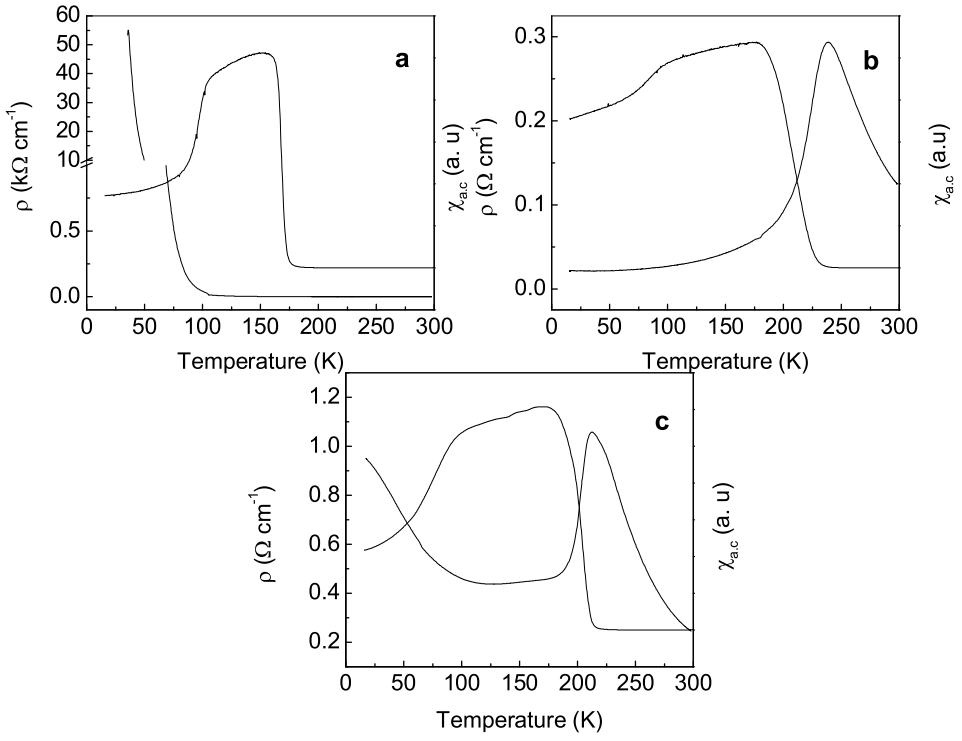

Figure 3.30: Comparison of the temperature dependence of the *ac* susceptibility and resistivity of various samples, a) $La_{0.9}Ca_{0.1}MnO_3$, b) $La_{0.85}Ca_{0.1}MnO_3$, and c) $La_{0.9}Ca_{0.05}MnO_3$.

values of T_c for both the compositions with negative values of x and y are shifted to ∼205 K as shown in Fig. 3.29. When the values of x and y are positive, the values of T_c for the compositions are found to be dropped to ∼130 K regardless of the type of A-site ion. The Mn^{4+} concentration is decreased considerably after vacancy doping, which is opposite to the expected trend. The magnetic transitions of the cation excess and deficient compositions are slightly broader than that of the stoichiometric compound. The low-temperature anomaly in the *ac* susceptibility is observed for the pristine and the cation deficient compositions. The temperature at which the

anomaly is observed is shifted to lower values for cation deficient compositions though the T_cs are enhanced on self-doping. This is also opposite to the trend observed in $La_{1-x}MnO_3$, where the T_a is found to be increased with decreasing Mn^{4+} content for a particular composition. It is observed that the compositions with negative values of x and y show M-I transition around T_c, whereas compositions with zero and positive values of x were found to be insulating. The temperature dependence of the electrical resistivity of the stoichiometric, La-deficient and Ca-deficient compositions are shown in Fig. 3.30.

The amount of Mn^{4+} estimated in the compositions with $x = y =$ -0.05, are found to be much less than what is expected whereas a large increase in Mn^{4+} was observed when $x = y =$ -0.05 against the anticipated values. The parent composition itself is having 21% Mn^{4+} which is more than the expected value of 10 %. This is often accounted in terms of excess oxygen nonstoichiometry or in other words as cationic deficiency (A-site as well as Mn site) resulting in the formation of $La_{0.9-p}Ca_{0.1-q}MnO_3$ with different possible values of p and q as in the case of $LaMnO_{3+\delta}$ (which is discussed in detail in the section 4.3). Also, an inhomogeneous distribution of Mn^{4+} ions may be expected since a deviation from the ideal composition is observed. Thus the vacancies at La, Ca and Mn-sites and distribution of Mn^{4+} in the lattice could be expected to affect the magnetic properties to a large extent. The estimated amount of Mn^{4+} in various compositions suggest either oxygen deficient or oxygen excess nonstoichiometry depending on the sign and values of x and y. An unexpectedly lower amount of Mn^{4+} in the A-site deficient structures suggest oxygen deficiency whereas larger amount of Mn^{4+} for positive values of x and y suggest oxygen excess nonstoichiometry.

The changes in the magnetic behavior clearly indicate the lattice effects on the strength of the magnetic exchange which may be by the reduction of Jahn-Teller effect in the case of oxygen deficient structures. The reduction of J-T distortion may

be thought to decrease the carrier-lattice coupling resulting in delocalization and a greater double exchange strength. At the same time, a competing effect may be the reduction in hybridization of O(2p) and Mn(3d) orbitals which narrows the band width and hence the strength of double exchange interactions. But a large increase in the T_c being a measure of stronger interaction, suggests that the reduction in J-T distortion is the predominant effect. On the other hand, excess oxygen non-stoichiometry introduces a large number of vacancies at Mn-site as in $LaMnO_{3+\delta}$, which causes abrupt breaking of long-range order along with the inhomogeneous distribution of Mn^{4+} ions. This considerably reduces the exchange strength and long range order resulting in compositions with lower T_cs. A support for the above interpretation is obtained from the *ac* susceptibility studies where a sudden drop is observed below the T_c at around T = 105 K which becomes less prominent and shifts to lower temperature in the case of compositions with $x = y$ = -0.05. Such effects are observed in closely related self doped lanthanum manganites, $La_{1-x}MnO_3$, and are found to be due to domain wall pinning effects with probable pinning centers formed from the inhomogeneous distribution of Mn^{4+} ions and/or vacancies created at Mn-sites. In the compositions with $x = y = +0.05$, the nature of the low-temperature anomaly is changed completely resulting in a cusp like behavior. Such a behavior can be expected in a strongly pinned magnet.

3.4 Conclusions

The detailed systematic studies made on the self-doped lanthanum manganites revealed many unusual characteristics. The theoretically possible self-doping limit to form a composition $La_{0.67}MnO_3$ ($x = 1/3$) is far from the experimental results which showed a maximum limit with which the above perovskite system can be self-doped is $La_{0.875}MnO_3$ ($x = 1/8$). This was concluded from the *dc* magnetic measurements,

XRD analysis, EPR and resistivity measurements. The EPR spectra of the polycrystalline samples showed a definite contribution of all Mn ions in the lattice to the total intensity. This is confirmed by comparing the integrated intensity of EPR spectra with the room temperature paramagnetic susceptibility. Formation of a complex Mn^{3+}-Mn^{4+} spin cluster may be feasible which is thought to be responsible for the observed resonance in lanthanum manganites [Ret97]. The linear variation of the parameters, intensity and ΔH_{pp} with doping concentration further confirms the contribution of Mn^{3+}-Mn^{4+} exchange interactions to the total EPR signal. Furthermore, it is evident from the data obtained from magnetic, structural and resistance measurements on $La_{1-x}MnO_3$ with different values of x, that the limiting value of x in these self-doped compositions is $x = 0.125$, which corresponds to a structure in which a vacancy is shared by eight nearby cubic perovskite unit cells or one vacancy per rhombohedral perovskite lattice.

Studies on different ferromagnetic compositions in the self-doped manganites, $La_{1-x}MnO_3$, show that there is no direct correlation between the magnetic ordering temperature and the Mn^{4+} concentration. The variation of Curie temperature with Mn^{4+} content show opposite trends in the low La-vacancy and the high La-vacancy compositional regions. Moreover, the Mn^{4+} concentration decreases with increasing the deficiency of La, which is opposite to that expected whereas Curie temperature is increased. Ac susceptibility measurements show that a decrease in the susceptibility, in the ferromagnetic region, below the Curie temperature, is directly linked with the concentration of Mn^{4+} ions. The temperature below which the decrease in the susceptibility is observed varies with the Mn^{4+} concentration for different compositions. In general, more pronounced effects are observed at lower Mn^{4+} content for each compositions. There is an associated increase in the coercivity linking the anomalous behaviour to contributions from magnetic anisotropy. The observations of relaxation of magnetization in the temperature region where the anomalous behaviour is ob-

served, disappearance of the anomalous behaviour when higher *dc* magnetic fields are used for the ZFC magnetization measurements, the absence of the feature in the FC magnetization measurements, lower initial magnetization at lower magnetic field strengths and lower temperatures though the magnetization continuously decreases with increasing temperature at higher fields, etc., point to the contribution from domain wall pinning effects in determining the low-field magnetic behaviour. The likely origin of the domain wall pinning effects is either from a non-uniform distribution of the Mn^{4+} ions which form as pinning centers or from mild structural distortions at lower temperatures so that the magnetic moments are canted at certain regions in the structure. Other possibilities such as vacancies of manganese ions, local structural distortions, etc. may also form as pinning centers. Relatively higher temperatures at lower magnetic fields or higher fields at lower temperatures are required to overcome the influence of the pinning effects.

The role of cationic nonstoichiometry in the Ca-substituted lanthanum manganite composition, $La_{0.9}Ca_{0.1}MnO_3$, with cation deficient and excess compositions has been studied. The studies indicate the sensitivity of the electronic properties on the nonstoichiometry of CMR oxides of the type $La_{1-x}Ca_xMnO_3$.

Chapter 4

Ferromagnetic Properties of $LaMnO_{3+\delta}$

Oxygen nonstoichiometry is an inherent problem in many oxide materials[Sor81]. The crystal structure as well as the physical properties are very much susceptible even to the slightest variations in oxygen stoichiometry as observed in vanadium oxides, high-T_c superconducting oxides and lanthanum manganites. The magnetic properties of lanthanum manganites change drastically with the variations in oxygen stoichiometry and will be discussed in this chapter.

4.1 Introduction

Studies on $LaMnO_{3+\delta}$ gained momentum after the discovery of CMR in $La_{1-x}A_xMnO_3$ [Rao98, Coe99, Tok00] and there are many reports, in the recent literature, on the studies of the electronic and magnetic properties of the non-stoichiometric compound. Ferromagnetism and metal-insulator transition are observed in $LaMnO_{3+\delta}$ with high Mn^{4+} content and this has been explained in terms of the double exchange interactions between Mn^{3+} and Mn^{4+} ions, as in the case of the divalent ion substituted CMR manganites. It is generally considered that the ferromagnetic Curie temperature increases with increasing Mn^{4+} content in $LaMnO_{3+\delta}$, due to the increasing strength of the double exchange interactions [Tiw97]. One of the important aspects of the La-Mn-O

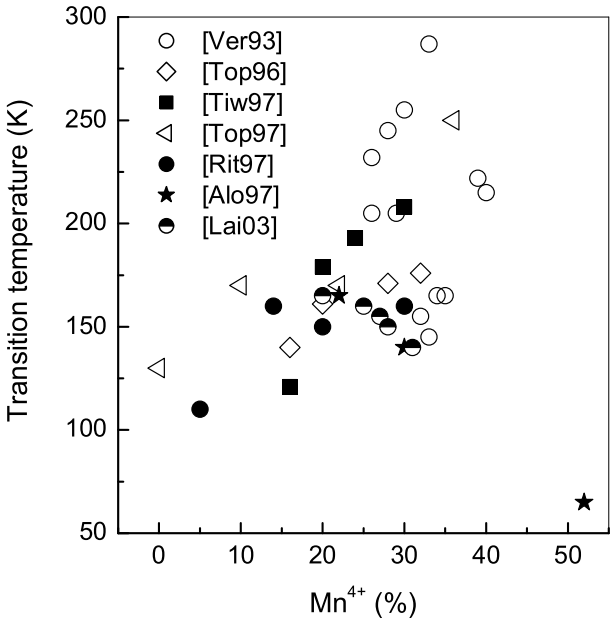

Figure 4.1: Comparison of the transition temperature of $LaMnO_{3+\delta}$ as a function of Mn^{4+} content, from different reports in the literature.

perovskite system is the wide range of non-stoichiometry possible and the related interesting properties. The self-doped, La-deficient, compositions $La_{1-x}MnO_{3+\delta}$ are ferromagnetic because of the presence of Mn^{4+} ions. Both $LaMnO_{3+\delta}$ and $La_{1-x}MnO_{3+\delta}$ are reported to be orthorhombic for lower Mn^{4+} concentrations ($< 20\%$) and rhombohedral for higher Mn^{4+} content [Top97a].

Many reports on the studies on the magnetic properties of $LaMnO_{3+\delta}$ suggest that the compositions are ferromagnetic and the magnetic transition temperature increases with increasing Mn^{4+} concentration. However, a comparison of the data reported on $LaMnO_{3+\delta}$, in the literature, suggests that the general assumption of the Curie temperature increasing with Mn^{4+} concentration is not true. The magnetic transition temperature as a function of Mn^{4+} content, observed by different

researchers [Ver93, Top96, Alo97a, Rit97, Tiw97, Top97a, Lai03], is compared in Fig. 4.1. Verelst *et al.* [Ver93] found varying transition temperatures (the metal-insulator transition temperatures are reported, the ferromagnetic T_cs are noted to be 10-15 K higher) for $LaMnO_{3+\delta}$ samples synthesized by different methods and having identical Mn^{4+} concentrations. For example, for compositions containing 33% Mn^{4+}, the transition temperatures as 145, 167 and 287 K are reported for samples synthesized by three different low-temperature methods and higher transition temperatures are found for low Mn^{4+} containing compositions. Similarly, Ritter *et al.* [Rit97] have found a non-monotonous change in the Curie temperature of $LaMnO_{3+\delta}$ with increasing Mn^{4+} content. T_c = 125 K is reported by Ranno *et al.* [Ran96] for a composition containing 31% of Mn^{4+}. Contrary to the general observations, there are also reports of continuously decreasing Curie temperature with increasing Mn^{4+} content [Alo97a]. Karavay [Kar80] found that with the decrease in the degree of crystal lattice distortions, the ferromagnetic phase content increases at the expense of the antiferromagnetic phase whereas Hauback *et al.* [Hau96] found that for $\delta = 0.08$ (16% Mn^{4+}), the structure of the compound is orthorhombic with a ferromagnetic transition at 125 K whereas when the structure is rhombohedral with 30% Mn^{4+} ions, the compound is not ferromagnetic. A report by Laiho *et al.* [Lai03] describes the low-field magnetic properties in which they found a regular decrease of T_c as the amount of Mn^{4+} is increased. These and many other results suggest that no two reports agree on the Curie temperatures of $LaMnO_{3+\delta}$ containing identical Mn^{4+} contents and the Curie temperature depends on the processing conditions. Higher transition temperatures are generally reported for samples synthesized at lower temperatures. This implies that reasons other than the Mn^{4+} concentration or crystal structure may be responsible for ferromagnetism in $LaMnO_{3+\delta}$.

To understand the origin of ferromagnetism and to investigate the absence of ferromagnetic ordering in certain compositions despite the right structure and Mn^{4+}

concentrations, we have studied the magnetic properties of $LaMnO_{3+\delta}$ in detail. The strong dependence of structural and magnetic properties on the processing methods and conditions has also been investigated by employing the ceramic and some soft-chemical synthesis procedures.

4.2 Synthesis

Different $LaMnO_{3+\delta}$ samples were prepared by the ceramic method from La_2O_3 (pre-heated at 1273 K for 12 h) and (1)MnO_2, (2)$MnCO_3$ and (3)Mn_2O_3, taking La and Mn in the 1:1 stoichiometric ratio and the samples have been given the codes LMO1, LMO2, and LMO3 series, respectively. The samples were fired at various temperatures as given in Table 4.1. Low temperature methods such as the glycine nitrate process (GNP), the citrate-gel process and a coprecipitation method were also employed for the synthesis of the samples and the samples codes are LMO4, LMO5, and LMO6, respectively. The details of the preparation methods are described in Chapter 2. The alphabets along with the sample codes are used in order to indicate the firing temperature or conditions as given in Table 4.1. The concentration of Mn^{4+} ions was estimated by iodometric method and all the samples are found to contain excess oxygen stoichiometry.

The magnetization was measured as a function of temperature under zero field cooled conditions in a field of 50 Oe.

4.3 Results and Discussion

The temperature dependence of the magnetization of $LaMnO_{3+\delta}$, synthesized from MnO_2 (LMO1), $MnCO_3$ (LMO2) and Mn_2O_3 (LMO3) and heated at 1273 K (sample A) and 1473 K (sample B) for 48 h each, is shown in Fig. 4.2. The Mn^{4+} concentrations in the two samples A and B of LMO1 were found to be 33% and 26%, respectively.

Table 4.1: Processing conditions and change in Mn^{4+} content in samples prepared during the present study

SampleCode	Method (Starting materials)	Firing temperature	Mn^{4+}(%)
LMO1A	Ceramic (La_2O_3 & MnO_2)	1273 K	33
LMO1B	(LMO1A)	1473 K	26
LMO2A	Ceramic (La_2O_3 & $MnCO_3$)	1273 K	20
LMO2B	(LMO2A)	1473 K	27
LMO3A	Ceramic (La_2O_3 & Mn_2O_3)	1273 K	26
LMO3B	(LMO3A)	1473 K	26
LMO4A	GNP	1073 K	34
LMO4B	LMO4A	1273 K	25
LMO4C	LMO4B	1473 K	27
LMO5A	Citrate process	1073 K	36
LMO5B	LMO5A	1273 K	33
LMO5C	LMO5B	1473 K	22
LMO6A	Coprecipitation	1273 K	28
LMO6B	LMO6A	1473 K	31
LMO7A	Ceramic (Excess La_2O_3 & MnO_2)	1273 K	-
LMO7B	LMO7A	1473 K	-
LMO7C	LMO7B	1573 K	-

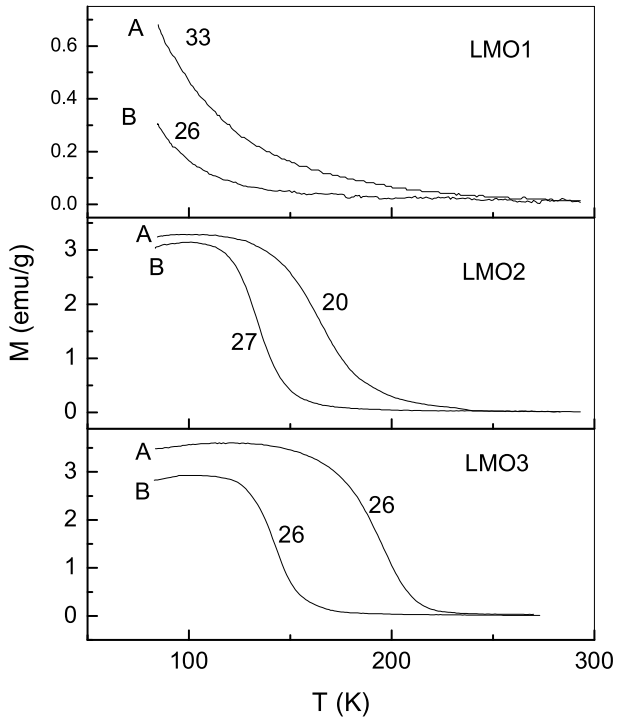

Figure 4.2: Temperature variation of the magnetization (H = 50 Oe) of LMO1, LMO2, and LMO3 heated at (A) 1273 K and (B) 1473 K. The numbers on the curves are the Mn^{4+} concentration of the particular sample.

However, there are no well-defined magnetic transitions for these two samples, as expected from the high Mn^{4+} concentrations, as shown in the magnetization (M) Vs temperature (T) curves shown in Fig. 4.2. The magnetization at low temperatures is larger for sample A compared to that of sample B. On the other hand, well-defined magnetic transitions are observed for the samples A and B of LMO2 and LMO3 series. But the magnetic transitions observed for the samples of LMO2 and LMO3 series are of broad nature and the Curie temperatures (T_c) are found to be below 200 K. The samples LMO2A and LMO2B (suffices A and B indicate the firing temperatures of 1273 K and 1473 K, respectively) are found to have Mn^{4+} concentration of 20 and

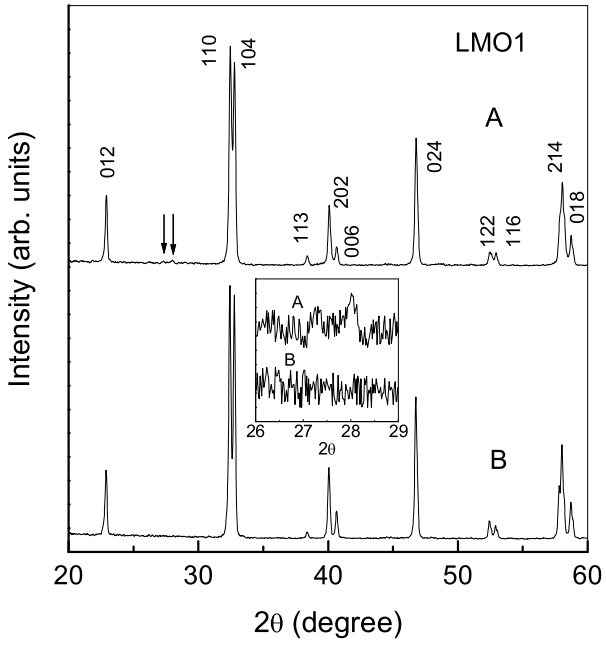

Figure 4.3: Powder X-ray diffraction patterns of LMO1, heated at (A) 1273 K and (B) 1473 K. The arrows indicate weak reflections due to $La(OH)_3$. Inset: expanded patterns clearly showing reflections due to $La(OH)_3$ in LMO1A.

27 %, with the values of T_c of 166 and 133 K, respectively. Also, for the samples LMO3A and LMO3B, the estimated amount of Mn^{4+} is 26% while the values of T_c are found to be 190 and 142 K. However, the magnitude of magnetization at the lowest temperature is almost five times larger for LMO2 and LMO3 when compared to that of LMO1. From the results on LMO1, LMO2 and LMO3, it is obvious that the amount of Mn^{4+} is not solely responsible in determining the ferromagnetic properties of $LaMnO_{3+\delta}$.

The powder X-ray diffraction patterns of the samples of LMO1, LMO2 and LMO3 series are shown in Fig. 4.3, Fig. 4.4, and Fig. 4.5, respectively. All the patterns are found to be due to a rhombohedral perovskite structure. This nature is expected

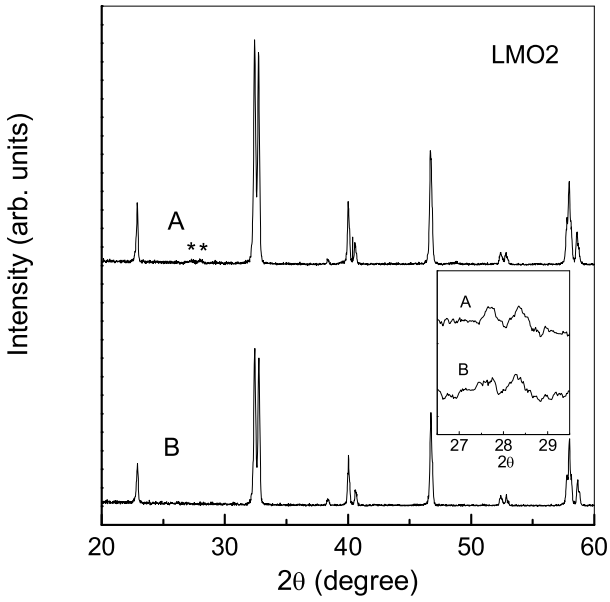

Figure 4.4: Powder X-ray diffraction patterns of LMO2, heated at (A) 1273 K and (B) 1473 K. Reflections marked by * are due to $La(OH)_3$. Inset: the XRD patterns of LMO2A and LMO2B, showing weak reflections due to $La(OH)_3$ in the slow scanned (0.25° per minute) XRD pattern of both the samples

because of the high Mn^{4+} content in the samples. Previous studies have shown that $LaMnO_{3+\delta}$ adopts a rhombohedral structure for $\delta > 0.1$ (>20% Mn^{4+}) [Pav84].

Two very weak reflections close to $2\theta = 28°$ are observed for LMO1A (indicated by arrows in Fig. 4.3) on close examination of the powder patterns of LMO1A and LMO1B (samples heated at 1273 and 1473 K). This region of the XRD pattern of the two samples is shown in the inset of Fig. 4.3, which clearly shows two weak reflections in sample LMO1A and no reflections in this 2θ region for sample LMO1B. These two reflections are not expected for the rhombohedral perovskites and have been identified as that of the two most intense reflections of $La(OH)_3$. For LMO2A, showing a clear ferromagnetic transition at 163 K, these two reflections are of relatively larger

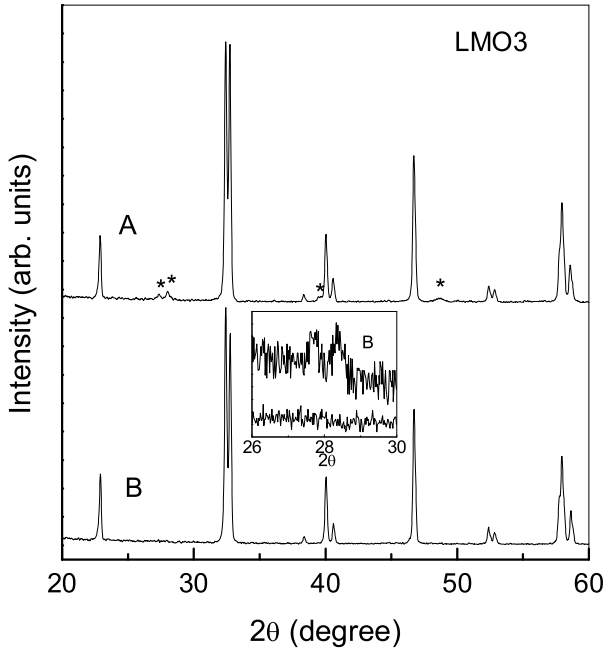

Figure 4.5: Powder X-ray diffraction patterns of LMO3, heated at (A) 1273 K and (B) 1473 K. Reflections marked by * are due to $La(OH)_3$. Inset: comparison of the pattern of LMO3B recorded at the normal and a slow scan rate (0.25° per minute), showing weak reflections due to $La(OH)_3$ in the slow scanned spectra of the sample

intensities (Fig. 4.4) with some other additional reflections also which are again due to $La(OH)_3$. Though no additional reflections are observed for LMO2B, the two weak reflections could be detected when the diffraction pattern was recorded at a very slow scan rate [Tay95]. This is shown in the inset of Fig. 4.4 for LMO2B which shows a ferromagnetic transition at 133 K. A similar feature is observed for the samples LMO3A and LMO3B, where the slow scan method is employed in order to detect the traces of impurity phase of $La(OH)_3$ in powder XRD (Fig. 4.5). The additional reflections due to $La(OH)_3$ in the XRD patterns of $LaMnO_{3+\delta}$ (in LMO1, LMO2 and LMO3) indicate that not all La is reacted to form a 1:1 composition, even if

the starting ratio of La and Mn is 1:1, and the compounds obtained are likely to be La-deficient, ie $La_{1-x}MnO_{3+\delta}$. The samples showing higher magnetic transition temperatures have larger amount of unreacted La and therefore the deficiency of La is larger in those samples. It is already known that the Curie temperature increases with increasing La-deficiency in $La_{1-x}MnO_{3\pm\delta}$ (section 3.1.2).

The above observations suggest the possibility for the formation of compositions with La/Mn < 1. This results in the formation of La-deficient compositions which are already known to show typical ferromagnetic transition tempeartures above 100 K. According to Tofield and Scott [Tof74], perfect Mn and oxygen stoichiometry can be maintained at the expense of vacancies at the La site, ie the formation of $LaMnO_{3+\delta}$ can be visualized as,

$$La(Mn^{3+}_{1-2\delta}Mn^{4+}_{2\delta})O_{3+\delta} \longrightarrow \frac{1}{3}\delta La_2O_3 + La_{1-2\delta/3}(Mn^{3+}_{1-2\delta}Mn^{4+}_{2\delta})O_3$$

but the authors could not detect any second phase in the Debye-Scherrer X-ray photograph. However, from the refinement of the structure of $LaMnO_{3.12}$ from neutron diffraction data, the authors found that the true composition is $La_{0.94}Mn_{0.98}O_3$. It was reasoned that the failure to detect the presence of La_2O_3 in the sample was either due to the small amount of this phase which is below the limit of detection of the instrument or that during exposure of the sample to the atmosphere, the moisture sensitive La_2O_3 is converted to the poorly crystalline hydroxide $La(OH)_3$ which will be difficult to detect. However, the present studies show that careful slow scan method can be used to detect the trace amounts of impurity phase of $La(OH)_3$.

To confirm whether it is La-deficiency in the samples which makes $LaMnO_{3+\delta}$ ferromagnetic and to see whether the results are reproducible, another sample of $LaMnO_3$ was again made from MnO_2 with controlled heating (2-LMO1). Powder XRD and magnetic studies were made immediately after cooling the samples in the furnace to room temperature, to look for the presence of La_2O_3 in the samples, since

it is known that La_2O_3 forms weakly crystalline $La(OH)_3$ on exposure to moisture.

The powder XRD patterns of some $LaMnO_3$ samples prepared from MnO_2 (in the 2-LMO1 series) and heated at different temperatures are shown in Fig. 4.6 and the magnetization curves of these samples are shown in Fig. 4.7. The La_2O_3-MnO_2 mixture taken in the required stoichiometric ratio (La:Mn = 1:1) was initially heated at 1273 K for 24 h and stored in a sample bottle in the atmospheric conditions for three weeks (sample A). This sample was further heated at 1273 K for 2 h (sample B), 6 h (sample C), 24 h (sample D) and then finally at 1473 K for 24 h (sample E) and 48 h (sample F). The powder XRD and magnetic measurements were made on sample A, and on other samples immediately after each heating schedule. For all samples, the powder patterns are found to be due to a rhombohedral perovskite structure, as in the case of LMO1. For both 2-LMO1A and 2-LMO1B, many weak additional reflections are observed in the XRD patterns.

A comparison with the simulated powder XRD patterns of $La(OH)_3$ and La_2O_3 indicate that all the strong reflections of $La(OH)_3$ are found in the pattern 2-LMO1A and the reflections due to La_2O_3 are found in the pattern of 2-LMO1B (XRD pattern recorded immediately after cooling the sample in a furnace). This indicates that a small portion of La_2O_3 is not reacted initially and this is converted to $La(OH)_3$ during the course of time. The amount of unreacted La_2O_3 is decreased after each heating. After heating the sample at 1473 K for a long duration (sample F), presence of La_2O_3 is still observed, in very small amounts, in the XRD pattern.

Magnetization curve of 2-LMO1A shows a broad ferromagnetic transition close to 270 K (Fig. 4.7). Such a high transition temperature is expected because part of La is not reacted and therefore the compound obtained must be an La-deficient $La_{1-x}MnO_{3\pm\delta}$ since the T_c corresponds to those of $La_{1-x}MnO_{3\pm\delta}$ samples with large values of x. Samples B, C, and D show a continuous increase in magnetization as the temperature is decreased, with no well-defined magnetic transitions. A clear magnetic

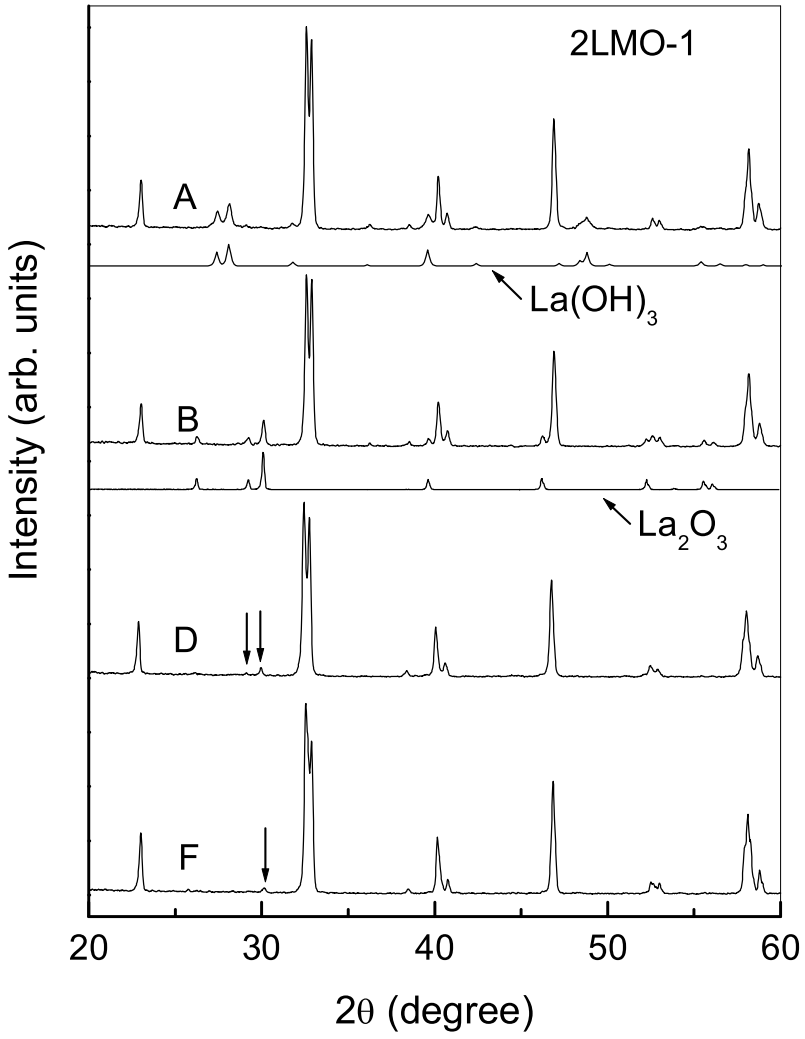

Figure 4.6: Powder XRD patterns of 2-LMO1, initially heated at (A)1273 K for 24 h and then for different durations; at (B) 1273 K 2 h, (D) 24 h and at (F) 1473 K for 48 h . The arrows indicate the reflections due to La_2O_3. The simulated XRD patterns of La_2O_3 and $La(OH)_3$ are also shown for comparison.

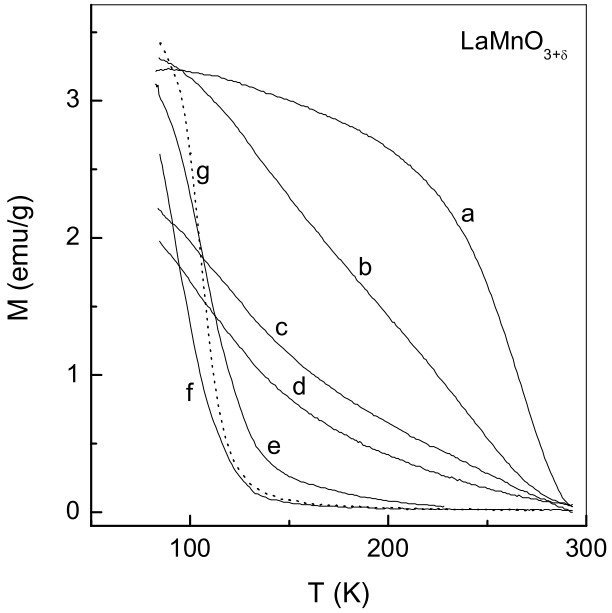

Figure 4.7: Temperature variation of the magnetization (H = 50 Oe) of LMO3, initially heated at (A)1273 K for 24 h and for different durations; at (B) 1273 K 2 h,(C) 6 h , (D) 24 h and (E) at 1473 K for 24 h and (F) at 1473 K for 48 h. The dotted line is the magnetization curve of $La_{0.97}MnO_{3+\delta}$.

transition is observed for sample F below 120 K and the Mn^{4+} concentration in this sample was estimated as 28%. This magnetic transition temperature is less than that observed for LMO3B with 26% of Mn^{4+} (150 K) and having the same rhombohedral structure. More over, the low Curie temperature of this sample is contrary to the various reports in the literature on the ferromagnetic properties of $LaMnO_{3+\delta}$ having a rhombohedral structure and high Mn^{4+} content. Estimation of the true composition of sample F, from the relative intensities of the peak due to La_2O_3 and the most intense reflection of the perovskite phase, gives the value of $x \approx 0.03$ in $La_{1-x}MnO_{3+\delta}$. The magnetization curve of a sample of $La_{0.97}MnO_{3+\delta}$ processed under identical conditions and having a comparable Mn^{4+} concentration of 29% also shows a magnetic transition

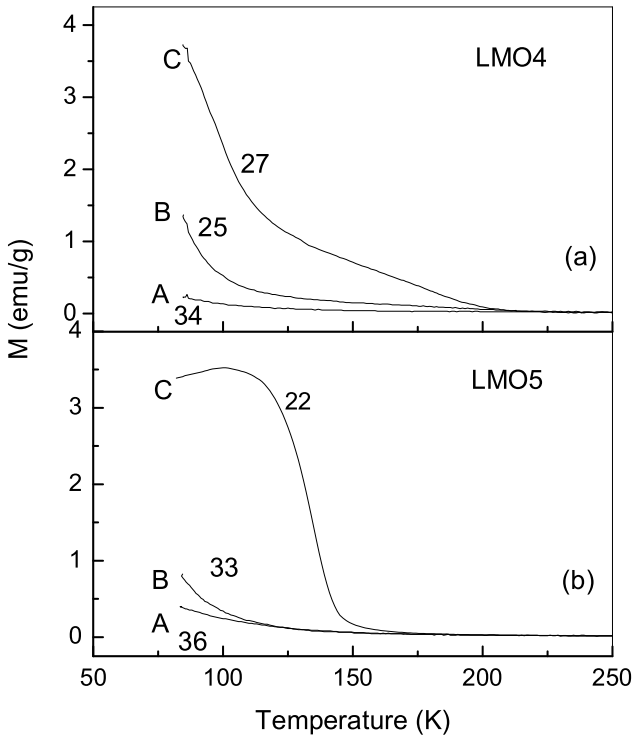

Figure 4.8: Temperature variation of the magnetization (H = 50 Oe) of the samples LMO4 and LMO5 heated at (A) 1073 K and 1273 K (C) 1473 K. The numbers on the curves are the Mn^{4+} concentration of the particular sample.

at ∼120 K similar to that of sample F. As shown in Chapter 3, large values of Mn^{4+} concentrations are known for low values of x in $La_{1-x}MnO_{3+\delta}$, further confirming that the $LaMnO_{3+\delta}$ sample is an La-deficient composition.

Generally, high Mn^{4+} concentrations and high Curie temperatures are reported for $LaMnO_{3+\delta}$ samples synthesized by low-temperature methods [Ver93, Hau96, Tiw97]. In this work, the samples prepared by the GNP method (LMO4) show high values of Mn^{4+} concentration when annealed at 1073 K (LMO4A), 1273 K (LMO4B) and 1473 K (LMO4C) as indicated in Table 4.1. However, no clear ferromagnetic transition is

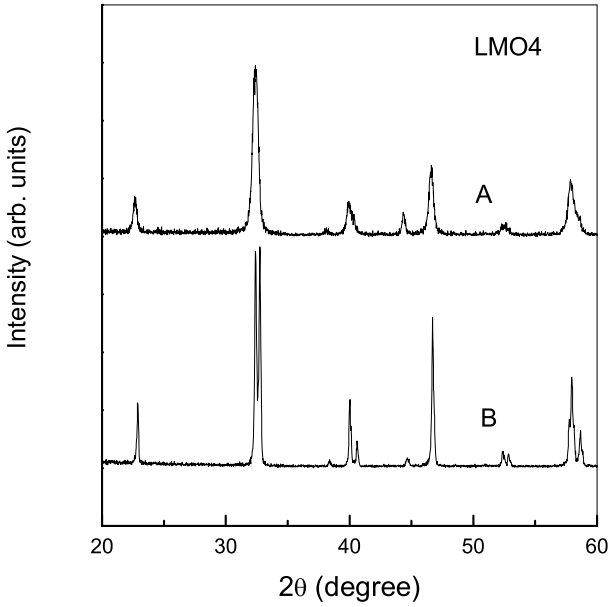

Figure 4.9: Powder X-ray diffraction patterns of LMO4, heated at (A) 1273 K and (B) 1473 K. No reflections due to impurities are observed in the XRD spectra of the sample

observed in the ZFC magnetization in the measured temperature range as shown in Fig. 4.8.

Similarly, the samples prepared by the citrate gel method also show high values of Mn^{4+} concentration when annealed at 1073 K (LMO5A) and 1273 K (LMO5B). But when fired at 1473 K for 24h, this sample (LMO5C) is found to contain 22% of Mn^{4+} ions and shows a well defined magnetic transition. However, in any of these samples, no impurity peaks corresponding to La_2O_3 or $La(OH)_3$ were observed in the XRD patterns (shown in Fig. 4.9) even when the slow scan method was followed. The presence of small amounts of $La(OH)_3$ is observed in the powder XRD pattern for the sample prepared by a coprecipitation method and heated at 1273 K (LMO6A)

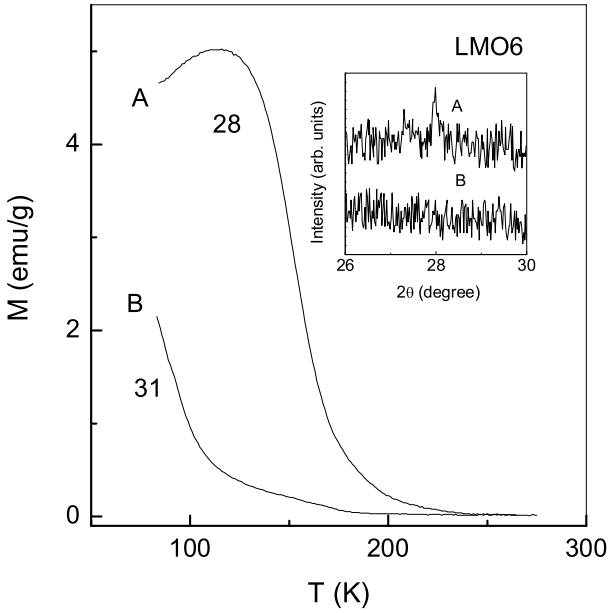

Figure 4.10: Temperature variation of the magnetization (H = 50 Oe) of the sample LMO6 heated at (A) 1273 K and (B) 1473 K The numbers on the curves are the Mn^{4+} concentration of the particular sample. Inset: the powder XRD patterns showing the impurity phase due to $La(OH)_3$ in sample A.

as shown in the inset of Fig. 4.10 and this sample shows a ferromagnetic transition below 200 K as shown in Fig. 4.10. However, no impurity peaks are observed in the XRD pattern of sample LMO6B (annealed at 1473 K) which show no well-defined magnetic transition in the measured temperature range.

When the compounds are synthesized by the low-temperature methods, the reflections in the XRD patterns are slightly broader due the smaller particle sizes (21 nm, 40 nm and 28 nm for LMO4A, LMO5A, and LMO6A, respectively) and it will be difficult to observe small amount of impurity phases in these powder XRD patterns, unless due care is given. The presence of small amounts of impurity phases may not be observed in the powder XRD pattern because of line broadening due to the

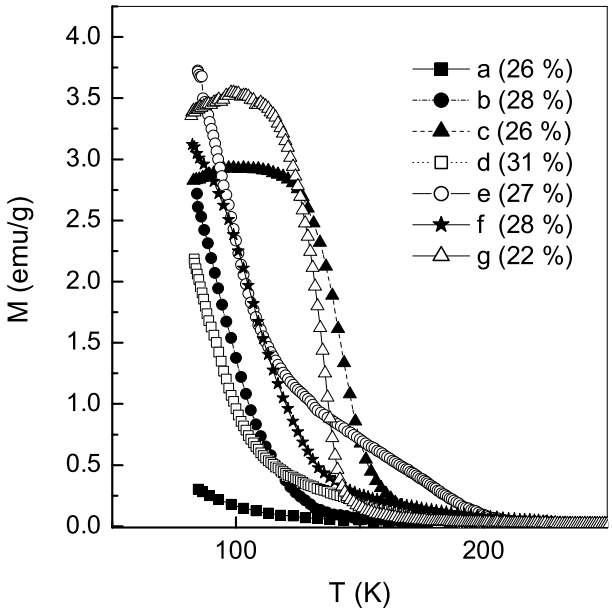

Figure 4.11: Comparison of the temperature variation of the magnetization (H = 50 Oe) of the $LaMnO_{3+\delta}$ samples, heated at 1473 K. The numbers indicate Mn^{4+} concentrations.

smaller particle size of the impurity phase or if the XRD patterns are recorded after the conversion of unreacted La_2O_3 to less crystalline $La(OH)_3$. This is likely to be the reason why impurity phases are not generally detected in low-temperature synthesized $LaMnO_{3+\delta}$ samples showing higher magnetic transition temperatures. The temperature variation of magnetization of the different $LaMnO_{3+\delta}$ samples, heated at 1473 K, is compared in Fig. 4.11 and none of these samples show identical magnetic characteristics. It is interesting to note that the final compound obtained in the two series synthesized from MnO_2 (LMO1B and 2-LMO1F), have different magnetic characteristics. A clear magnetic transition for 2-LMO1F, with a higher value of magnetization, is observed when compared to that of LMO1B. Similarly, though the Mn^{4+} content is identical for LMO1B and LMO3B, no magnetic transition is observed

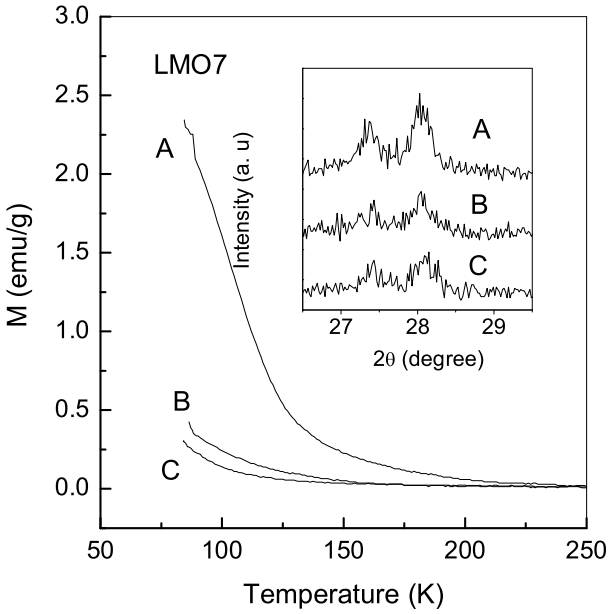

Figure 4.12: Temperature variation of the magnetization (H = 50 Oe) of the sample LMO7 heated at (A) 1273 K, (B) 1473 K, (C) 1573 K. Inset: the powder XRD patterns showing the impurity phase due to $La(OH)_3$ in the samples A, B and C.

for the former whereas a clear magnetic transition below 160 K is observed for the latter. These observations indicate the fact that it is not possible to reproduce the results on $LaMnO_{3+\delta}$ and this may be attributed to the formation of $La_{1-x}MnO_{3+\delta}$ with different small x values in the final products. Higher Curie temperatures are observed for $La_{1-x}MnO_{3+\delta}$, even for small values of x [Kim01].

In the La-Mn-O perovskite system, the different compositions, $LaMnO_{3+\delta}$ and $La_{1-x}MnO_{3+\delta}$ are generally prepared by the same methods and under identical conditions, by taking the starting components in the appropriate stoichiometric ratio. This implies that La and Mn oxides can react initially to form any composition in $La_{1-x}MnO_{3+\delta}$ even if the components are taken in the 1:1 ratio and the present results

indicate that it is easy to obtain $La_{1-x}MnO_{3+\delta}$ than $LaMnO_{3+\delta}$. This also implies that there is no control over the formation of $LaMnO_{3+\delta}$, and $La_{1-x}MnO_{3+\delta}$ with any value of x can form initially. The final small value of x is determined by this reaction and therefore cannot be reproduced. Hence the magnetic characteristics will be different for different samples even if they are synthesized under identical conditions.

Since the $LaMnO_{3+\delta}$ compositions synthesized from a 1:1 mixture of La and Mn compounds give rise to $La_{1-x}MnO_3$, another composition was synthesized by taking excess of La_2O_3. The magnetic properties of the composition which was prepared from La_2O_3 and MnO_2 by allowing La:Mn ratio of 1.1:1 and heated at various temperatures ranging from 1273 K to 1573 K with several intermediate grindings is studied (this is denoted by the sample code LMO7). This excess amount of lanthanum oxide is sufficient to show the presence of impurity phase of $La(OH)_3$ in the XRD patterns of the final compositions.

The ZFC magnetization curves of LMO7 are shown in Fig. 4.12 and the XRD patterns in a small region are shown in the inset of Fig. 4.12. There is no observation of ferromagnetic features in the measured temperature range for the samples LMO7B and LMO7C, which are annealed for 24h each at 1473 K and 1573 K respectively. However, LMO7A shows a fairly large value of magnetization at the lowest temperature measured showing the presence of ferromagnetic components. In the XRD pattern, the intensity of the peak corresponding to $La(OH)_3$ is maximum for LMO7A and is found to decrease as the samples are annealed at higher temperatures further indicating the incomplete formation of the final composition when annealed at 1273 K for 48h. Thus, the ferromagnetic nature is observed whenever there is an incomplete reaction as evidenced from various XRD and magnetic measurements.

A comparison of the temperature dependence of the ZFC magnetization of the $LaMnO_{3+\delta}$ samples prepared by ceramic method with various starting materials and some compositions with various values of x in $La_{1-x}MnO_{3+\delta}$ prepared by the ceramic

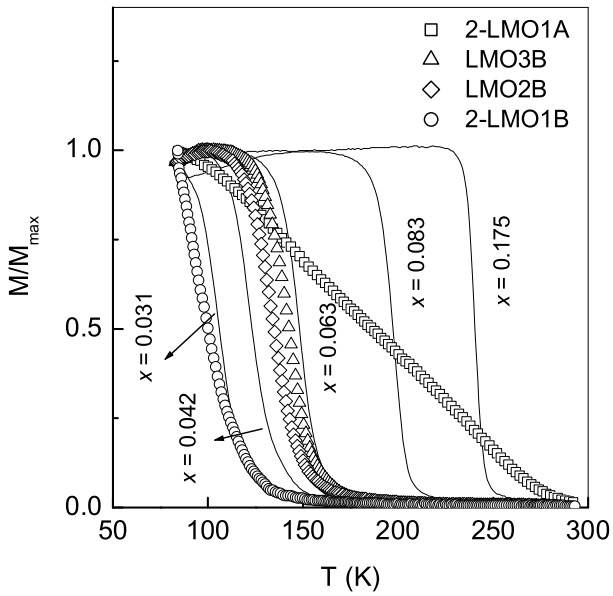

Figure 4.13: Comparison of the temperature variation of the magnetization (H = 50 Oe) of various $La_{1-x}MnO_{3\pm\delta}$ and $LaMnO_{3+\delta}$ samples. The numbers indicate the values of x in $La_{1-x}MnO_{3\pm\delta}$.

method from La_2O_3 and MnO_2 is shown in Fig. 4.13. The dependence of T_c on the processing conditions of $LaMnO_{3+\delta}$ is evident from Fig. 4.13. The sample 2-LMO1A shows an initial increase below 270 K and then the magnetization further increases almost linearly with decreasing temperature and there is no well defined ferromagnetic transition. This can be assumed to be due to the mixed phase behavior, in which, $La_{1-x}MnO_{3+\delta}$ compositions with almost all possible values of x are present. But this sample when annealed at 1473 K for 48h, shows a ferromagnetic transition temperature of $\approx$ 100 K. This corresponds to the T_c observed for the self-doped composition with $x = 0.031$. Also, for the samples LMO2B and LMO3B, a clear magnetic transition is observed around 150 K, corresponding to self-doped compositions with values of x between 0.063 and 0.042.

4.4 Conclusions

The present results give evidence for the fact that the ferromagnetism observed in oxygen excess $LaMnO_{3+\delta}$ is due to the formation of La-deficient compositions and the magnetic nature is largely dependent on the processing conditions of the samples. Our observations are in par with the results reported by various researchers that $LaMnO_{3+\delta}$ is $La_{1-x}Mn_{1-y}O_3$ where x may or may not equal to y. However, our observations suggest the formation of compositions with cationic vacancies with $x > y$, ie, the self-doped compositions, $La_{1-x}MnO_{3+\delta}$ during the synthesis of $LaMnO_3$. The origin of ferromagnetism in $LaMnO_{3+\delta}$ is, therefore, due to the formation of $La_{1-x}MnO_{3+\delta}$ compositions in the samples which are ferromagnetic due to the presence of Mn^{4+} ions. The processing condition is a major factor and depending on the reactants and the heating conditions, the self-doped compositions with various values of vacancy concentration may be formed. This explains the reason for the irreproducible magnetic properties of $LaMnO_{3+\delta}$ synthesized by the identical or different methods or conditions.

Chapter 5

Superspin Glass Behavior of $LaMnO_{3+\delta}$

Generally, a high T_c is expected for the compositions containing larger amounts of Mn^{4+} such as in $La_{0.625}Ca_{0.375}MnO_3$, among the calcium substituted lanthanum manganites [Tok00]. Conversely, a decrease in T_c with the increase in the amount of Mn^{4+} content is observed in $La_{1-x}MnO_{3\pm\delta}$, $LaMnO_{3+\delta}$ and some lightly substituted lanthanum calcium manganite compositions [Rit97, Tok00, Dez02]. Since these compounds tend to form compositions with excess oxygen non-stoichiometry ($+\delta$) under normal synthesis conditions, it can be assumed that the *δ-factor* plays an important role in determining the unusual magnetic properties of such compositions. The spin glass-like features of some oxygen nonstoichiometric compositions have been studied in this chapter.

5.1 Introduction

Oxygen non-stoichiometry in lanthanum manganite has been a subject of intense research over the years [Van94a, Van94b, Rao98, Tok00, Nak02a]. The uncontrollable oxygen stoichiometry in such compounds leads to interesting magnetic and charge transport properties which point out the complex electronic mechanisms involved in the system. The very sensitive nature to the oxygen stoichiometry induces certain

changes in the magnetic structure by changing the ratio of concentrations of magnetic manganese ions in trivalent to tetravalent states in the perovskite structure [Pav84, Rit97]. Oxygen non-stoichiometry in divalent ion doped lanthanum manganite composition, $La_{1-x}A_xMnO_{3+\delta}$, is normally observed when, $x < 0.1$. When x is higher than this value, the amount of Mn^{4+} ions becomes sufficient enough to minimize the structural distortion whereas in the lower doping concentration range, aid of excess oxygen helps to maintain a less strained crystal lattice by the same mechanism.

The excess oxygen affects the crystal structure to a considerable extent which in turn determines the magnetic properties of the material [Ver93, Van95]. But the accommodation of excess oxygen in the perovskite structure is difficult to be understood clearly, since no voids suitable for an interstitial oxygen anion are present in the close packed layers of LaO_3 [Mit02]. Thus, excess oxygen is accounted in terms of vacancies at cationic sites. In chapter 4, based on the magnetic properties as well as careful X-ray diffraction studies, the possible origin of ferromagnetism in $LaMnO_{3+\delta}$ has been concluded as due to the presence of self-doped compositions (unequal concentration of La and Mn ions) at very low doping concentrations. Also, Chapter 3 describes the magnetic properties of $La_{1-x}MnO_3$ and it has been suggested that vacancies are possible at Mn-site as well. The cation deficiencies at both the La and Mn sites along with the large amount of Mn^{4+} can have serious effects on the magnetic properties of $LaMnO_{3+\delta}$. In fact, spin glass (SG) nature is reported for $LaMnO_{3.15}$ though no antiferromagnetic contribution is detected from neutron diffraction studies.[Rit97] Based on a cation vacancy model, the effect of excess oxygen on the magnetic properties of $LaMnO_{3+\delta}$ is discussed in detail in this chapter.

5.2 Synthesis

Some of the $LaMnO_{3+\delta}$ samples discussed in the previous chapter are used for the detailed studies on the magnetic properties here. Since only selected samples are used, they have been given different code names and the details are given in Table 5.1. The values of δ as determined from the estimation of Mn^{4+} content from the iodometric titrations, where $\delta = 2$ x concentration of Mn^{4+}, are indicated in the table.

5.3 Results and Discussion

5.3.1 Formation of Superspin Clusters in $LaMnO_{3+\delta}$

The oxygen nonstoichiometry is known to control the structural features of the $LaMnO_{3+\delta}$ compositions [Pav84, Lai05]. From the Raman spectroscopic studies on certain $LaMnO_{3+\delta}$ samples, Laiho *et al.* have concluded that when $\delta = 0$, the structure is orthorhombic, when $\delta = 0.065$-0.112, the structure is cubic with small rhombohedral distortions and when $\delta = 0.125$-0.154, the structure becomes rhombohedral [Lai05]. It is described in chapter 4 that the ferromagnetism in $LaMnO_{3+\delta}$ is due to the formation of self-doped compositions with the general formula $La_{1-x}MnO_{3\pm\delta}$ or otherwise written as $La_{1-x}Mn_{1-y}O_3$, where x and y are generally small fractions which may be equal [Van94a, Top96, Top97b] or unequal [Tof74, Alo97a]. In Chapter 3, it is indicated that $La_{1-x}MnO_{3\pm\delta}$ with values of $1/8 < x < 1/14$ correspond to lanthanum deficient compositions with oxygen deficiency whereas compositions with $x < 1/14$ form manganese deficient compositions. Thus, a large amount of oxygen non-stoichiometry is known to affect both the cationic sites (La & Mn) arguably to different extents, and more on Mn-site when doping concentration is fairly low. Effect of oxygen non-stoichiometry on the magnetic properties is observed in Ca-substituted lanthanum manganite compositions, $La_{1-x}Ca_xMnO_3$, with values of $x < 0.2$ [Tok00].

Table 5.1: Details of the $LaMnO_{3+\delta}$ samples on which the current investigation is made

Sample code	Starting materials and method	Final Firing Temp. (K)/Duration	Mn^{4+} (±1%)	δ
A1	La_2O_3 & MnO_2	1273 K/ 48 h, 1473 K/ 48 h	26	0.13
A2		A1 heated at 1473 K/ 24 h	25	0.125
A3		A2 heated at 1573 K/ 24 h	23	0.115
B1*	La_2O_3 & MnO_2	1273 K/ 24 h, 1473 K/ 48 h, 1573 K/24 h	30*	0.15
C1	La_2O_3 & Mn_2O_3	1273 K/ 24 h, 1473 K/ 48 h, 1573 K/24 h	23	0.115
C2		C1 heated at 1573 K/ 24 h with excess La_2O_3	32	0.16
D1		1073 K, 12 h	36	0.18
D2	Citrate gel	D1 heated at 1273 K/ 12 h	33	0.165
D3		D2 heated at 1473 K/ 12h, 12 h 1573 K (Pellet)/ 24 h	23	0.115

∗ Sample prepared by taking La:Mn ratio of 1:1.2.

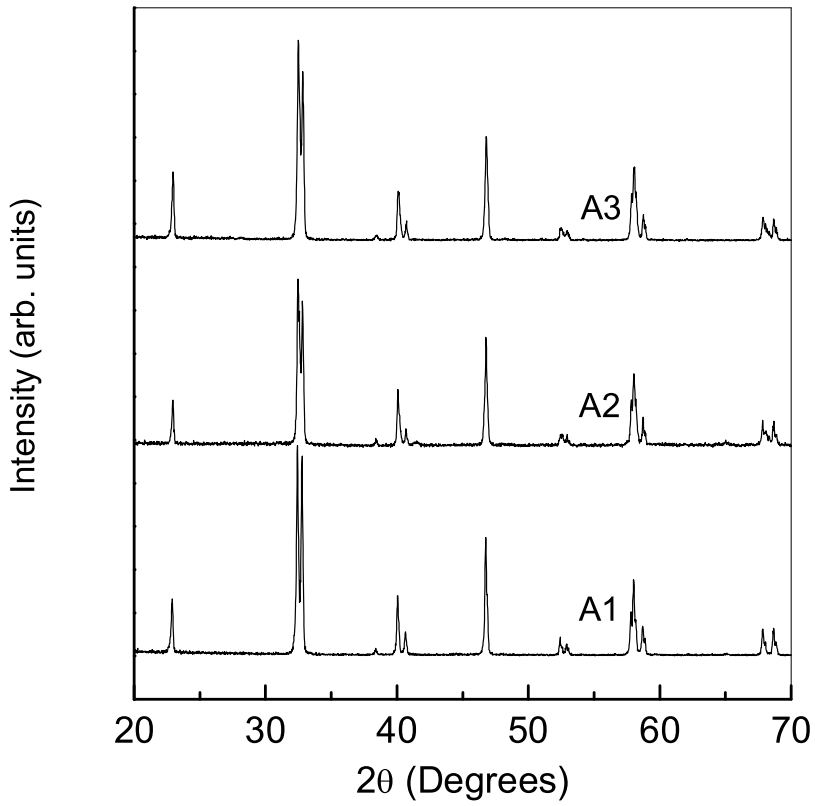

Figure 5.1: The powder XRD patterns of $LaMnO_{3+\delta}$ samples prepared by ceramic method with different values of δ, (A1 ($\delta = 0.13$), A2 ($\delta = 0.125$), A3 ($\delta = 0.115$)).

But, the Mn deficiency in such manganite system has not been considered in great deal or known to have effects on the physical properties of the manganites. Since manganese ions are responsible for the magnetic and transport properties of various manganite compositions, vacancies at the Mn-site in the manganites could be expected to have various effects on such properties.

In $LaMnO_{3+\delta}$ with different values of δ (Samples A1, A2 and A3), but all with rhombohedral structure with space group $R\bar{3}c$ (XRD patterns are shown in Fig. 5.1),

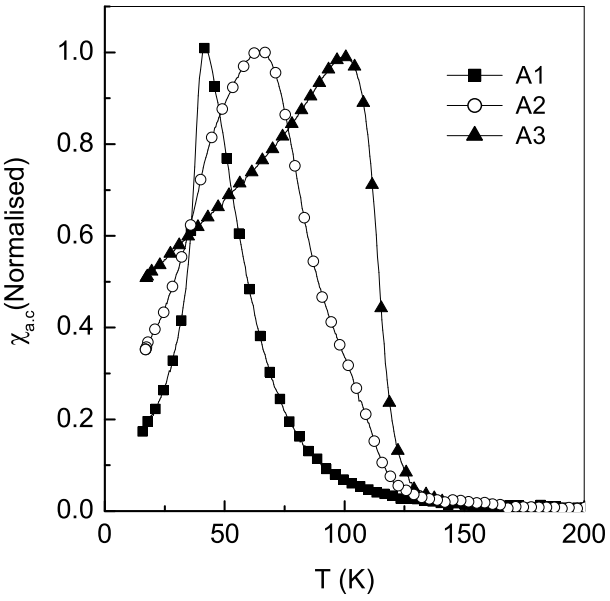

Figure 5.2: The *ac* susceptibility curves of $LaMnO_{3+\delta}$ samples, A1, A2, and A3 measured at 2 Oe and 210 Hz.

the ac susceptibility shows a well defined magnetic transition when the concentration of Mn^{4+} is below 25% (sample A3) and cusp-like nature when concentration of Mn^{4+} is above 25% (sample A1) as shown in Fig. 5.2. For a sample with 25% Mn^{4+} content, multiple magnetic transitions are observed indicating some kind of phase separation. The first magnetic transition for this sample is at the T_c of A3. In $LaMnO_{3.13}$ (sample A1), with 26% quadrivalent manganese ions, there is no sharp magnetic transition observed in the temperature dependent zero field cooled (ZFC) magnetization, but shows a cusp-like feature as shown in Fig. 5.3. Ritter *et al.* have observed certain short range ferromagnetically ordered phase but no antiferromagnetic type of ordered phase in their neutron diffraction studies on $LaMnO_{3+\delta}$, with $\delta = 0.15$ [Rit97].

This short range ordering is assumed to be due to the formation of tiny clusters

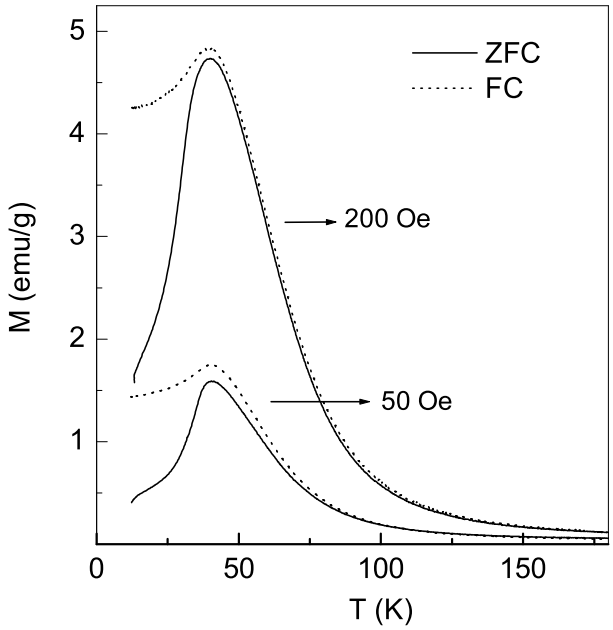

Figure 5.3: ZFC (solid lines) and FC (dotted lines) magnetization curves of sample A1 at two different fields, 50 Oe and 200 Oe.

with dimensions in the nanometer range which are isolated from one another in a non-magnetic matrix. Such compositions with high values of δ shows spin glass-like features which is thought to be produced as a result of competing interactions of FM and AFM types [Hau96, Rit97, Des98, Ghi99]. The ZFC and FC magnetization studies (as shown in Fig. 5.3) show a divergence which is generally considered to be a trademark property of spin glasses [Myd93]. But many superparamagnets, domain wall pinned magnets and other strongly anisotropic magnetic materials behave in a similar manner and a clear distinction of a spin glass phase is not possible from the divergence in the FC and ZFC magnetizations [Kum98a, Can01, Kum02, Han03, Sku03].

As described in Chapter 3, in the self-doped compositions of the general formula,

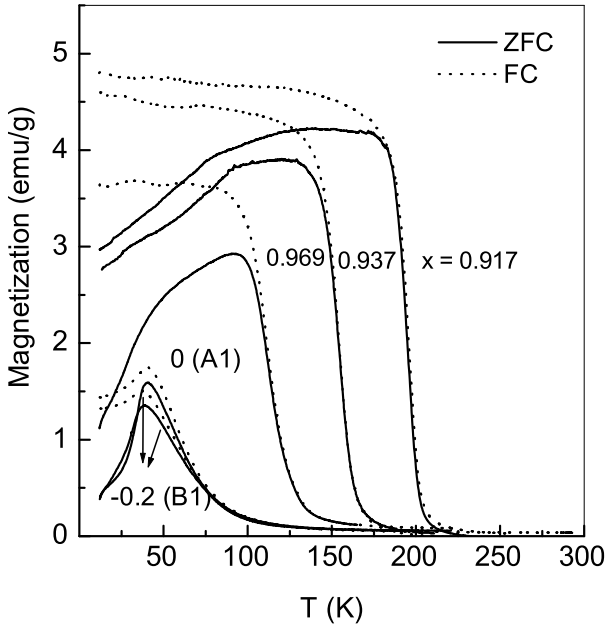

Figure 5.4: ZFC (solid lines) and FC (dotted lines) magnetization curves of self-doped compositions, $La_{1-x}MnO_3$; the numbers indicate the value of x in $La_{1-x}MnO_3$.

$La_{1-x}MnO_3$, there are definite probabilities for the formation of cation as well as anion deficient compositions due to the oxygen non-stoichiometry. It was found that when the value of x is small, the La/Mn ratio reaches unity and increases further on reducing the self-doping concentration. When La/Mn ratio decreases, compositions with La-deficiency are formed which introduces ferromagnetism in the non-stoichiometric lanthanum manganites. Also, as discussed in Chapter 4, $LaMnO_{3+\delta}$ is $La_{1-x}MnO_{3+\delta}$ with small values of x and large values of δ which are likely to be Mn-deficient compositions. The ZFC and FC magnetization curves of various self-doped compositions are compared with that of the $x = 0$ composition in Fig. 5.4. As the value of x is decreased, the broadness of the M-T curve is increased which is attributed to the formation of ferromagnetic clusters. The reason for the drop in the magnetization

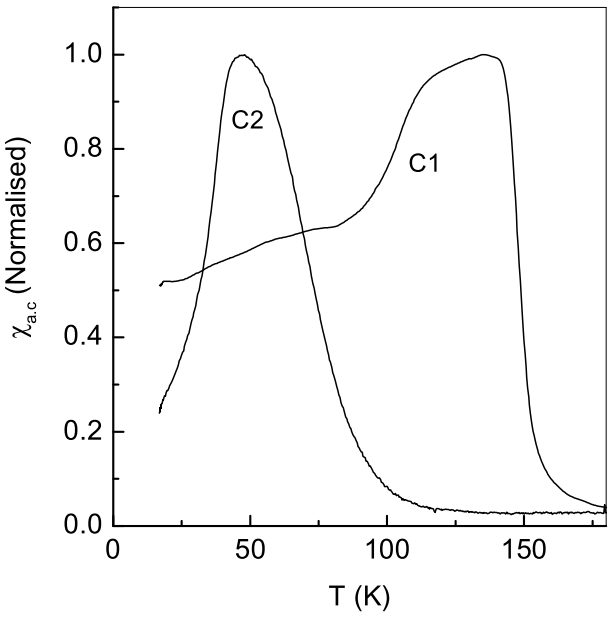

Figure 5.5: Temperature dependence of the ac susceptibilities of samples C1 and C2 (C1 heated with excess La_2O_3).

below T_c is addressed in detail in Chapter 3 and is attributed to domain wall pinning effect. The nature of the M-T curve for the composition when $x = 0$, completely changes and a cusp is ensued which is often identified as a spin-glass behavior. It is more likely to be an extreme case of a rather general trend as observed in the whole range of $La_{1-x}MnO_3$ compositions. Thus, when $\delta = 0.13$, as for the sample A1, a corresponding deficiency at Mn-site would have formed which is above the percolation limit for a perfect long range ordering. For the sample prepared with x = -0.2 (sample B1), excess La_2O_3 is observed as an impurity phase (as expected) in the the powder XRD patterns along with the reflections from a rhombohedral perovskite phase. A cusp has been observed in the ZFC magnetization curve of this sample as in the case of the sample A1, as shown in Fig. 5.4. Similarly when excess La is introduced in

a sample showing a well defined ferromagnetic transition (sample C1), a cusp-like feature is observed in the M-T curve for the resulting composition (sample C2). This further confirms the role of La/Mn ratio in determining the magnetic properties. The parent compound shows a rhombohedral perovskite structure and a well defined Curie temperature (T_c = 150 K) as shown in the *ac* susceptibility curves in Fig. 5.5. This behavior is quite similar to that of $La_{0.94}MnO_3$ as explained in Chapter 3. This composition is heated after mixing with La_2O_3 such that the resulting composition (sample C2) would contain a maximum La/Mn ratio of 1.1. The *ac* susceptibility curve of the modified sample now corresponds to a cusp-like behavior with the maximum susceptibility at around 45 K. This is in accordance with the observations made for the samples A1 and B1.

Based on the values of δ obtained from the Mn^{4+} concentrations, a large amount of cation vacancy should be observed in $LaMnO_{3+\delta}$ since there are no interstitial sites available for oxygen anion. If the cation vacancy is formed at the La-site alone, as in the case of $LaTiO_{3+\delta}$ [Mac94], presence of a second phase should have been observed in the phase purity analysis using powder XRD studies. Also, large amount of vacancies at the La-site would have resulted in well-defined, high ferromagnetic transition temperatures as observed in the case of the self-doped lanthanum manganite compositions, $La_{1-x}MnO_3$, $x \leq 0.125$. Conversely, no well defined ferromagnetic transition temperature is observed for the samples with very high values of δ $LaMnO_{3+\delta}$. This implies that the cation vacancies may be distributed among the La sites as well as the Mn sites giving rise to various possible compositions for different values of δ. An immediate inference should be the abrupt breakage of long-range ordering of spins (magnetic exchange) at the Mn site vacancies. Thus, the extent of exchange in $LaMnO_{3+\delta}$ is largely determined by the distribution of Mn vacancies induced by the excess oxygen present. $LaMnO_{3+\delta}$ is generally regarded as $La_{1-x}Mn_{1-x}O_3$, i.e, with equal amounts of La-site and Mn-site vacancies [Van94a, Top97b, Nak02a]. Other

models include unequal number of vacancies at the cationic sites which could be represented as $La_{1-x}Mn_{1-y}O_3$ - the end members being $La_{1-x}MnO_3$ and $LaMn_{1-y}O_3$ [Tof74, Alo97a, Ghi99]. In the latter model, three cases may be envisaged. Firstly, when $x > y$ which would result in lanthanum deficient compositions with La/Mn $<$ 1, Secondly, when $y > x$ which would result in lanthanum deficient compositions with values of La/Mn > 1, and finally when $x = y$ (La/Mn $= 1$), which is the generally accepted model with equal number of cationic vacancies to account the excess oxygen stoichiometry that is usually observed in perovskite type lanthanum manganites. But it may be seen from Chapter 3 on self-doped compositions that La/Mn ratio becomes more than unity when the doping concentration becomes less than 1/14. Also, non-stoichiometric lanthanum manganite compositions are reported to have La/Mn ratio greater than one [Aru96, Alo97a, Alo97b, Top97a]. Thus, there is a certain possibility that the value of y becomes greater than x resulting in the breakage of long-range magnetic order in the system. This abrupt breakage results in the formation of ferromagnetic clusters and if the clusters are very small in size, they may behave as single domain clusters and would show single domain behavior similar to the magnetic nanoparticles. The short range magnetic exchange responsible may be the double exchange between Mn^{3+} and Mn^{4+} ions as observed in other manganite compositions. Such double exchange clusters may be randomly distributed in the perovskite lattice. As δ decreases, the vacancies at Mn-site decreases and the magnetic order is less disturbed. Then the single domain clusters grow in size resulting in the increase of the cusp temperature (can be identified as the blocking temperature) which finally forms multidomain structure with well defined ferromagnetic character once the long range order becomes possible. Thus, if the oxygen non-stoichiometry, δ, is the factor which controls the magnetic structure of the compositions - either in terms of the amount of Mn^{4+} or La/Mn ratio - a decrease in δ or Mn^{4+} content would result in lowering of La/Mn ratio by reducing the number of vacancies at the

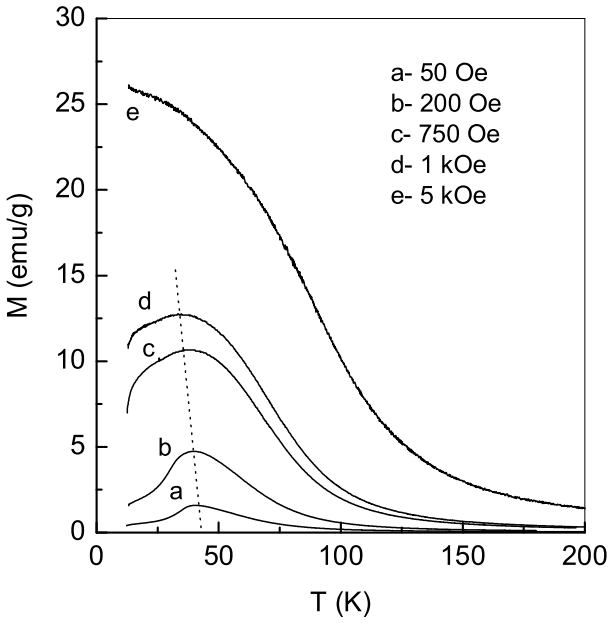

Figure 5.6: Field-dependence of the cusp (moves to lower temperatures as field strength is increased) of ZFC magnetization of the sample A1. The dotted line is a guide to eye.

Mn-site. As a result, long range order can be expected to be set in even though the amount of Mn^{4+} is decreased. The observed properties are found to be matching with the above arguments. The temperature corresponding to the cusp observed in the M_{ZFC}-T curve is identified with T_B, the equivalent superparamagnetic blocking temperature. Sample A1 shows a T_B of $\sim$40 K when measured at a field strength of 50 Oe, above which the thermal energy randomizes the individual cluster spin moments. Fig. 5.6 shows the M_{ZFC}-T curves of the sample A1 measured at different field strengths. The cusp remains at field strengths of 50, 200,750 and 1000 Oe, but vanishes when measured at a field strength of 5000 Oe. A characteristic feature of the superparamagnets and spin glasses is the field dependence of the cusp as well as the

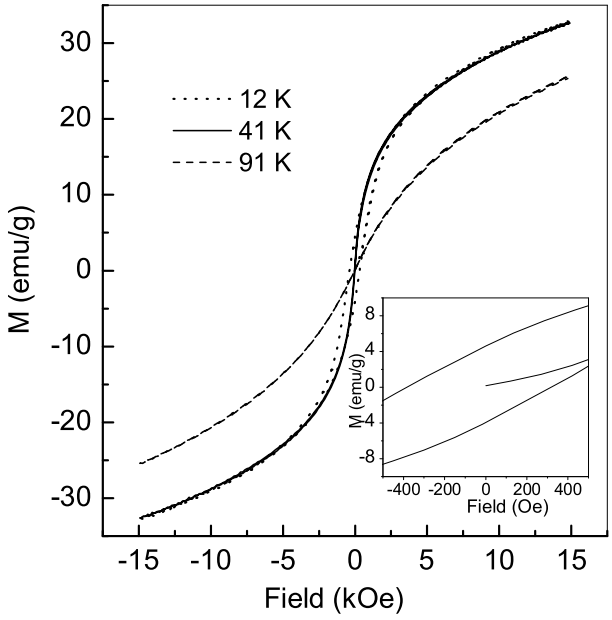

Figure 5.7: The M-H curves recorded at various temperatures for the sample A1. A portion of the hysteresis loop at 12 K is shown in the inset.

cusp temperature. At higher field strengths, the parallel alignment of single domain moments to the applied field become spontaneous leading to high magnetization values at the lowest temperature itself. Here, a shift of T_B towards low temperatures could be observed for the sample A1 as the field strength is increased from 50 to 5 kOe as shown in Fig. 5.6.

The M-H curves (field dependence of magnetization) of the sample A1 measured at different temperatures across the T_B are shown in Fig. 5.7. It can be seen that the loop opens up at temperatures below T_B and the coercivity of the sample is fairly large at the lowest temperature. But at temperatures very close to T_B $\sim$40 K, the loop closes up but with high magnetization values. Once the temperature is increased above T_B, typical superparamagnetic nature could be observed. For the M-H curve

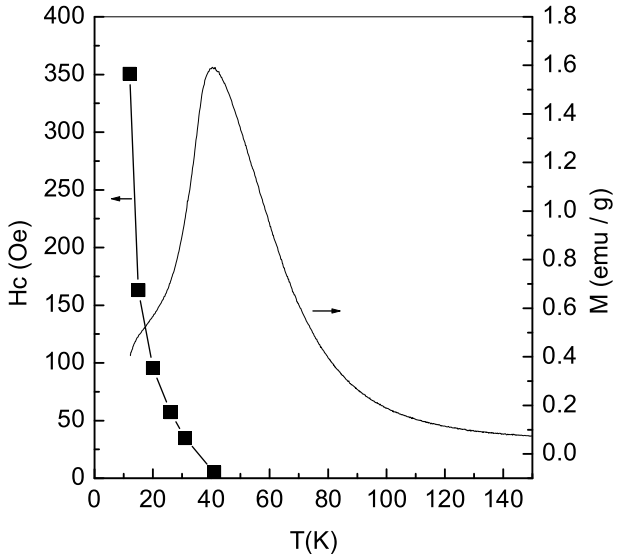

Figure 5.8: The variation of coercivity of the sample A1 with temperature. A sharp decrease of H_c is followed by a constant value (virtually zero) when T_B is reached.

measured at 91 K, shown in Fig. 5.7, there is no saturation of magnetization even at the maximum field of 15 kOe.

For the sample A1 with $\delta = 0.13$, the temperature dependence of the coercivity is shown in Fig. 5.8. The coercivity decreases abruptly when the temperature is raised, coming down to a value of around 160 Oe at 15 K from 350 Oe at 12 K. The coercivity is found to be decreased to zero as the temperature is increased further up to 40 K and beyond. This is a typical nature of superparamagnetic materials. The high values of coercivity observed at low temperatures can be explained as due to the rotation of total magnetization of the single domain magnetic clusters which is a difficult process when compared to the domain wall motion in multidomain structures. A similar behavior is observed for the sample B1, as shown in Fig. 5.9 where excess lanthanum was incorporated so as to make La/Mn $\geq$ 1.

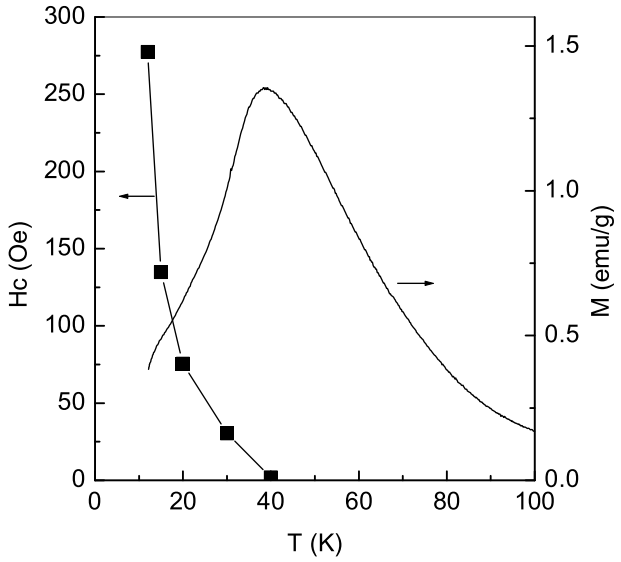

Figure 5.9: The variation of the coercivity with temperature for $La_{1-x}MnO_3$ with x = -0.1 (sample B1). Coercivity decreases abruptly to zero at T_B.

Similar behavior, however, is not observed in the case of self-doped lanthanum manganites that possess well defined ferromagnetic nature, as well as for the sample A3. The M-H behavior A3, a self-doped manganite, samples A1 and D1, measured at 12 K, are compared in Fig. 5.10.

The saturation magnetization and magnetic hysteresis of the sample with $x = 0$ and $Mn^{4+} = 23\%$ (sample A3) is similar to that of the self doped composition with x = 0.937 and $Mn^{4+} = 25\%$, whereas $LaMnO_{3+\delta}$ samples Mn^{4+} content $> 25\%$ do not attain saturation of magnetization even at 15 kOe and have high coercivity values. It is important to note that the magnetization at the largest field used in the present work, M(H = 15 kOe) is very low for the samples with high amount of Mn^{4+}.

All the above features are also observed in the samples prepared by a soft chemical route, i.e., citrate-gel method (samples D1, D2 and D3). The low-field *dc* magneti-

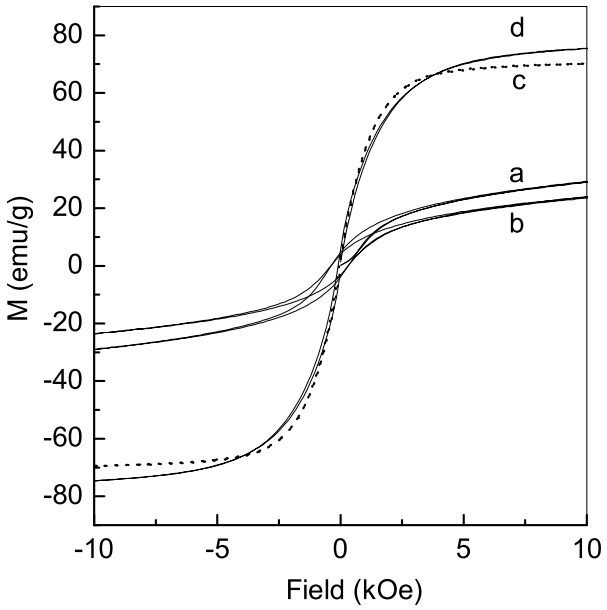

Figure 5.10: The M-H curves recorded for various nonstoichiometric lanthanum manganite compositions with a) $x = 0$, $Mn^{4+} = 26\%$ (sample A1), b) $x = 0$, $Mn^{4+} = 36\%$ (sample D1), c) $x = 0.937$, $Mn^{4+} = 25\%$, d) $x = 0$, $Mn^{4+} = 25\%$ (sample A3).

zation measurements done at a field of 50 Oe under ZFC and FC conditions for the samples D1, D2 and D3 are shown in Fig. 5.11. The XRD patterns of D1 and D2, shown in Fig. 5.12 could be indexed to the rhombohedral perovskite structure (the rhombohedral splitting of the most intense peak is not clearly evident for D1 because of the broad reflections due to the smaller particle size of the sample). The T_B for the sample D1 with $\delta = 0.18$ is $\sim$41 K and as the value of δ is decreased to 0.165, the magnetization of the sample is increased and T_B is also increased to $\sim$45 K (sample D2). For the sample heated at a higher temperature of 1573 K, δ is found to be decreased to 0.115 (sample D3) and a well defined ferromagnetic character with a sharp magnetic transition is observed. The Curie temperature of the sample D3 is

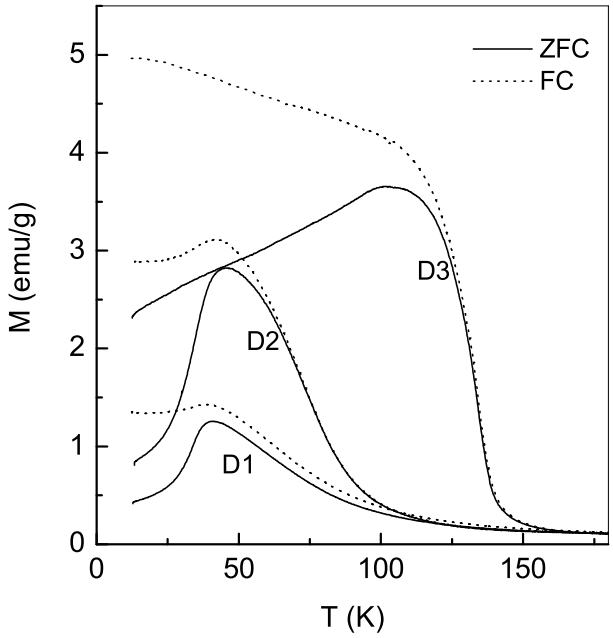

Figure 5.11: The ZFC and FC magnetization curves of the samples a. D1 with $\delta = 0.18$, D2 with $\delta = 0.165$ and D3 with $\delta = 0.11$

found to be ∼130 K, matching with the T_c of the self-doped compositions having low degree of doping. Also, as can be seen from the M-H behavior of the samples D1 and D3 (Fig. 5.13) measured at 12 K, there is no saturation of magnetization (M_s) for the sample D1 but has large coercivity whereas for sample D3 the magnetization saturates at higher fields and higher value of magnetization is observed. A low magnetization value of 27 emu/g even at 15 kOe for the sample D1 compared to 76 emu/g for the sample D3 also points out that the extent of ferromagnetic exchange is larger in D3 than that in D1, though an inverse conclusion would be expected from the amount of Mn^{4+} obtained.

Thus the studies on four different sets of the nonstoichiometric $LaMnO_{3+\delta}$ samples A, B, C, and D (see Table 1) indicate that when the Mn^{4+} concentration is

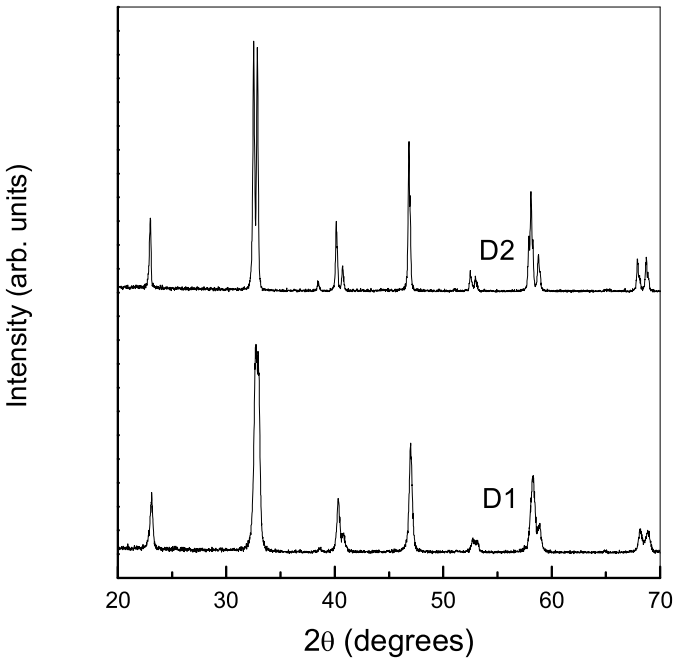

Figure 5.12: The powder XRD patterns of $LaMnO_{3+\delta}$ samples with different values of δ, prepared by citrate gel method; D1 with $\delta = 0.18$ and D2 with $\delta = 0.165$

below 25%, the samples show ferromagnetic character whereas for larger values, the observed characteristics are that of a spin glass or superparamagnet. These factors substantiate the conclusion that the long range order is disturbed in the $LaMnO_{3+\delta}$ compositions as the value of δ is increased beyond a certain extent. It can be, therefore, concluded that the cusp like magnetization behavior at low temperatures for $LaMnO_{3+\delta}$ samples with fairly large values of δ is due to the single domain clusters resulting in superparamgnetic-like behavior caused largely by the cationic vacancies. Based on the value of δ obtained for different $LaMnO_{3+\delta}$ samples, a cationic defect model comprising of both the types of vacancies could be considered. The increasing amount of δ produces greater number of vacancies of La and/or Mn ions to different

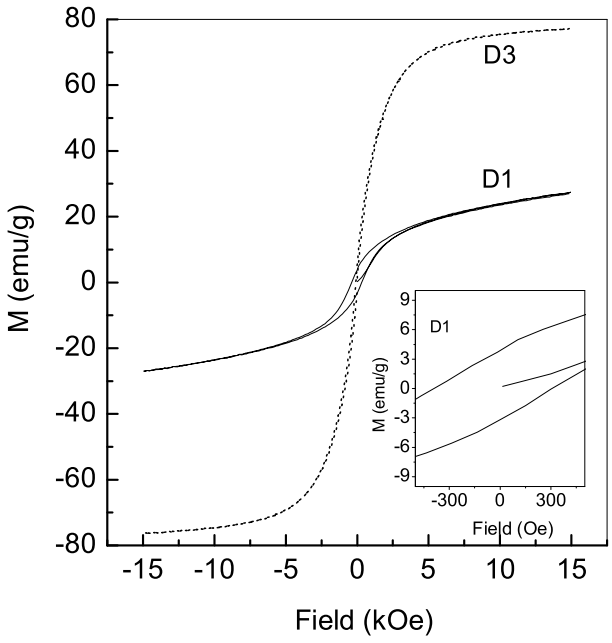

Figure 5.13: The M-H curves recorded for the samples D1 with $\delta = 0.18$ (solid line) and D3 with $\delta = 0.11$ (dotted line). For the sample D1, a large coercivity is observed and the enlarged hysteresis loop is shown in the inset.

extent. Such a model seems to be necessary to explain the present observations. It is important to consider the effects of Mn-site vacancies on the long range order and restrictions imposed on the domain structure while evaluating the magnetic properties of $LaMnO_{3+\delta}$. A general formula of $La_{1-x}Mn_{1-y}O_3$ is likely to explain the various magnetic features of $LaMnO_{3+\delta}$, with x number of La-site vacancies and y number of Mn-site vacancies. The total number of vacancies, i.e. $x + y$ is always equal to $2\delta/3$, with maximum limit of $2\delta/3$ and the lowest limit of zero for both La and Mn site vacancy concentrations. Thus, $LaMnO_{3.13}$, with $\delta = 0.13$, can be represented in many forms with a total of around 9% of vacancy concentration. An exact calculation of La and Mn site vacancies from the value of δ is not possible. Thus, contrary to

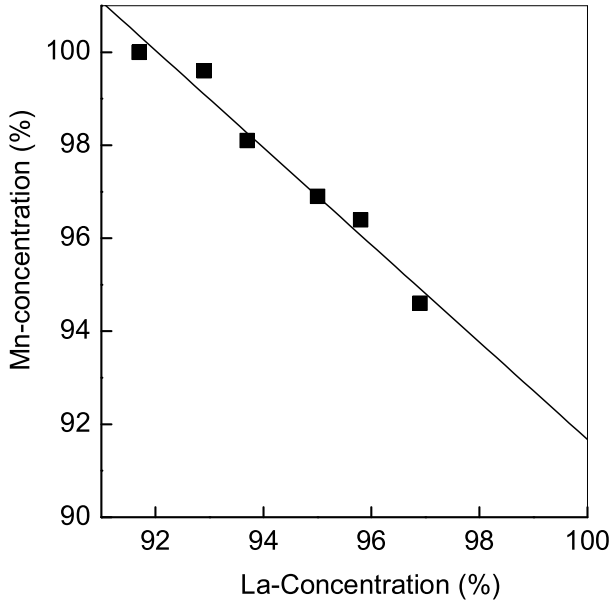

Figure 5.14: A compositional correlation diagram of $La_{1-x}MnO_{3\pm\delta}$ for $0 < x < 0.071$ (data from Table 3.1)

the previous reports, a maximum of $2\delta/3$ number of Mn-vacancies is possible in the unit cell which would have significant effects on controlling the magnetic exchange interactions and determining the size of the magnetic clusters. The variation in the magnetic properties with δ, can be easily explained by this model. It also explains the reason why the magnetic properties of $LaMnO_{3+\delta}$ are not reproducible, and why the properties in different technological regime differs from one another.

Based on the observations on the La and Mn vacancies in the self-doped lanthanum manganite $La_{1-x}MnO_3$ (differing amounts of La and Mn vacancies depending on the Mn^{4+} concentration) as shown in Table 3.1, a compositional correlation diagram drawn considering the concentration of both the types of cations in self-doped compositions is shown in Fig. 5.14. A linear behavior is observed where the

Mn stoichiometry reaches a very low value when the La stoichiometry reaches 100%. The extrapolated curve shows that when the value of La concentration approaches 100 %, Mn concentration is decreased almost to 92%. This is in accordance with the statement that, high degree of vacancies (∼8%) at the Mn-site is possible in lanthanum manganite with large excess of oxygen non-stoichiometry. The unexpectedly high values of Mn^{4+} obtained for lanthanum manganite, $LaMnO_{3+\delta}$ have at least two consequences; first one, obviously is the cationic deficiency created in the structure, and second one is regarding the distribution of cations. The latter one becomes important to be considered since the inhomogeneous cation distribution often has the tendency to cause phase separation in the system which may affect the long range magnetic order. Indication for such a phase separation is observed in the case of sample A2 with 25% of Mn^{4+} content and this sample shows two magnetic transitions. The scenario of such a phase separation in oxides has been gained tremendous interest and importance recently [Mor99, Ueh99, Rao03], and it is worth considering when explaining the formation of magnetic clusters and their isolation in the crystal lattice. The scenario of phase separation has much more implications on the types of magnetic clusters involved in the system. It is not essential that the compositions contain clusters with a single chemical formula. Corresponding to the same blocking temperature, there may be various entities with different values of x and y present in the form of magnetic clusters with nano-dimensions, isolated from each other.

Superparamagnetic behavior has been observed in polycrystalline Li-doped NiO from the low-field susceptibility measurements when there is more than 70% of the ordered phase is present [Baj00]. But the phase responsible for such a behavior is not well defined because of the inherent complexity associated with the polycrystalline materials. Formation of finite antiferromagnetic clusters have been reported by Nair *et al.* in $Pr_{0.5}Ca_{0.5}Mn_{0.975}Al_{.025}O_3$ composition [Nai04]. Al substitution in the charge ordered composition, $Pr_{0.5}Ca_{0.5}MnO_3$ introduces random impurities in the Mn-O-

Mn lattice thus reducing the range of charge ordered interactions and ultimately forming weakened charge ordered clusters. These mesoscopic clusters are believed to be thermally blocked and the magnetic properties are history dependent. In Cd doped $ZnCr_2O_4$, when the Cd doping exceeds 3%, the Neel ordering of the sample is destroyed and frozen phase of spin-correlated nanoclusters are formed [Rat02]. It is also observed that the local structure of the thermally blocked state closely resembles that of the cooperative paramagnetic phase. It is believed that in $Zn_{1-x}Cd_xCr_2O_4$, the exchange interaction is restricted to a short range by the lattice strain developed in the crystal when Zn^{2+} is replaced by the 1.3 times bigger ion Cd^{2+}. It has been observed that as the percentage of Cd doping is increased, a cusp observed in the magnetization Vs. temperature curve is shifted to low temperatures implying the weakening of long range magnetic interaction. A recent study on Ru-deficient strontium ruthenates show a decrease in T_c as the self-doping at Ru site is increased in $SrRu_{1-v}O_3$, where $0 \leq v \leq 0.12$ [Mar05]. This might be due to the similar reasons as in the case of $La_{1-x}Mn_{1-y}O_3$ with $y > x$. Thus the long range magnetic order could be affected by various factors such as impurity atoms, intrinsic chemical inhomogeneity or by the presence of impurity phases.

5.3.2 Interaction of Magnetic Nanoclusters in $LaMnO_{3+\delta}$

It is known that fine magnetic nanoparticles would interact with each other when they are densely packed, the strength of these interactions depends on various other factors such as size and type of the particle, their density in the matrix, distance between the particles etc. Also, the interaction may be of various kinds such as dipolar interaction between the magnetic particles, super exchange interactions if the particles are embedded in a matrix depending on the bonding at the matrix-particle interface, antisymmetric exchange types of Dzyaloshinski-Moriya (DM-exchange) type, or it may be RKKY type of exchange which becomes important if the matrix which we

consider is metallic. Such interactions between the fine magnetic particles lead them to show a collective behavior rather than typical superparamagnetism [Luo91, Dju97, Dor97, Fio99, Hel00, Pod02]. An immediate consequence of such strongly interacting magnetic particle systems is the formation of a spin-glass like magnetic state, which is commonly known as superspin glass nature. Thus, the strong dipolar interactions are thought to be largely responsible for such superspin glass behavior whereas weak interactions between the magnetic nanoparticles results in superparamagnetism. The collective dynamics in such a superspin glass system is evidenced by the magnetic relaxation and magnetic aging studies as reported in the literature [Jon95, Dor97, Jon04].

The low temperature properties of magnetic nanoparticles reveal the superspin glass type of behavior formed due to the interaction between the individual single domain particles called the superspins [Dor97, Sas05]. Recent reports reveal that the aging and memory effects in superspin structures are the reflections of the interacting behavior of such nanoparicles. The Field cooled (FC) and Zero field cooled (ZFC) protocols have been widely used in aging experiments to evaluate the interacting nature of these nanoparticles [Sun03, Jon04, Par05, Sas05, Tso05, Zhe05]. The glassy state dynamics of such tiny magnetic particle system is interesting and have been widely studied both experimentally and theoretically [Dor97, Fio99, Jon04]. However, it is still remaining a complex and vaguely understood area in the field of mesoscopic physics. Another important aspect of mesoscopic magnetism is the interaction behavior of nanoclusters. It is known that several lanthanum manganite compositions form nanosized magnetic clusters by effective tuning of the their structural features such as Mn-O-Mn bond angle, Mn- vacancies, and the presence of a non-magnetic ion in the magnetic Mn-sublattice [Bla97, Det97, Rit97]. In the present work, the similarity between the interacting behavior of a magnetic nanoparticle system and a phase separated nanocluster system of $LaMnO_{3.13}$ has been studied. The magnetic

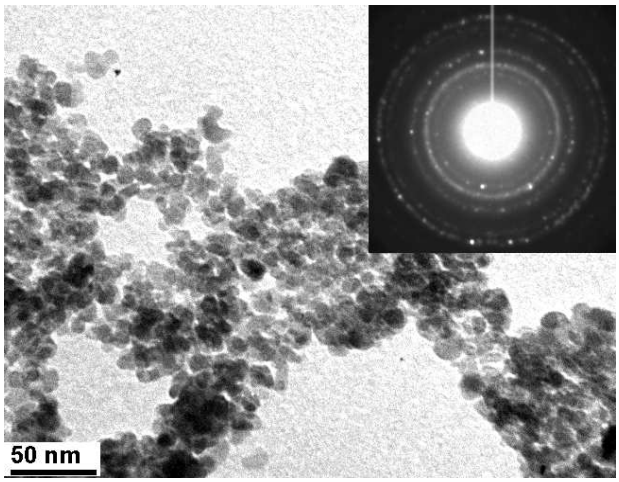

Figure 5.15: TEM image of NZF, particle size can be seen to be approximately 8 nm. The SAD pattern is shown in the inset.

properties of a dense nanoparticle system of nickel-zinc ferrite $Ni_{0.5}Zn_{0.5}Fe_2O_4$ (NZF) and the nonstoichiometric lanthanum manganite (LMO) composition, $LaMnO_{3.13}$ has been compared. A direct comparison reveal the common origin of spin glass-type of behavior in magnetic nanoparticle systems and lanthanum manganites with a large excess of oxygen non-stoichiometry. The NiZn ferrtie nanoparticles were synthesized by a soft chemical route invloving glycine and citrate as fuels and the synthesis method is reported elsewhere [Ver05]. A transmission electron microscopic (TEM) image of the nanoparticles was obtained using JEOL 1200 EX after dispersing the particles in amyl acetate on a carbon coated TEM copper grid. The NZF particles were investigated for their morphology, particle size and phase purity by electron microscopic studies. Fig. 5.15 shows the TEM picture and electron diffraction patterns of the sample. The particles are spherical and agglomerated into chain-like clusters. The particle size distribution obtained from TEM micrograph is found to be very narrow.

The mean particle size is obtained as ∼8 nm and it is similar to that obtained from the X-ray diffraction pattern [Ver05]. The selected area diffraction pattern (SAD) as shown as the inset of Fig. 5.15, is of diffused nature indicating nanocrystalline nature of the particles. The cubic lattice parameter obtained from SAD pattern is 8.40 Åwhich corresponds to that of a spinel phase agreeing well with the results obtained from powder XRD patterns.

The single domain behavior in $LaMnO_{3+\delta}$, with sufficiently high values of δ, has been discussed in the preceding section. Short range magnetic ordering is observed in $LaMnO_{3.15}$ from the neutron diffraction studies and the typical values of magnetic coherence length observed at the freezing temperature was found to be 18 Å [Rit97]. Such small magnetic clusters might behave as magnetic nanoparticles embedded in a matrix. The type and strength of the interactions between such small clusters depend on various parameters such as size and shape of the clusters, distance between the adjacent nanoclusters, presence of exchange interactions such as superexchange and DM types, and dipolar interactions.

Assuming that the magnetic clusters are similar to magnetic fine particles, and as the M-H behavior of LMO is similar to that of superparamagnetic particles [Che98], we have attempted to calculate the size of the the magnetic particles from the M versus H curves measured at a temperature above T_B where there is no magnetic hysteresis. For single domain particles, the magnetization is given by the Langevin function [Cul72],

$$M = M_s \left[\coth(\frac{mH}{kT}) - \frac{kT}{mH} \right]$$

where at temperature T, M is the magnetization at a given field H, M_s is the saturation magnetization, and m is the magnetic moment of a particle. M_s can be calculated by the extrapolation of M vs 1/H curves to the limit $1/H \rightarrow 0$. If there is a wide distribution of the size of the particles, the magnetization at lower fields is mainly

decided by the larger particles and by smaller particles at larger fields. The Langevin function can be reduced to $M = M_s(mH/3kT)$ in the limit $H \rightarrow 0$ and to $M = M_s(1-kT/mH)$ in the limit $H \rightarrow \infty$. Considering $M_s = Nm$ where N is the number of particles per unit volume, m can be calculated which in turn gives the estimate of individual particle size. This method is followed to calculate the size of the NZF magnetic nanoparticles and LMO nanoclusters. A distribution of particles with sizes 6-8 nm was observed in the case of NZF nanoparticles which is in agreement with the particle size obtained from the TEM analysis. Similarly, following the same method for the LMO composition, the magnetic cluster size obtained ranges from 2.5 to 3.5 nm. The SANS studies of Ritter *et al.* [Rit97] suggests the existence of small magnetic clusters in $LaMnO_{3.15}$ at low temperatures, of size typically around 2 nm.

The temperature dependence of the ZFC and FC magnetizations of the NZF nanoparticles and the lanthanum manganite composition are compared in Fig. 5.16. Identical cooling and heating rate of 2 $Kmin^{-1}$ were maintained for the FC and ZFC magnetization experiments.

A divergence between the FC and ZFC magnetizations below a cusp is observed in both cases and such a behavior is commonly exhibited by superparamagnetic and spin glass materials which are then identified as blocking temperature, T_B and freezing temperature, T_g respectively [Myd93, Ron99, Hel00]. It is reported that as the density of packing is decreased, the interactions between the particles become weaker and result in a lowering of T_B of the magnetic nanoparticles system [Dor97, Par05]. Also, there is an important feature in the divergence of FC magnetization (FCM) and ZFC magnetization (ZFCM) that the FCM matches with the ZFCM almost down to the T_B, below which either it keeps a constant value, slightly decreases or increases further depending on whether the interaction between magnetic nanoparticles is strong or weak [Sas05]. A similar feature is observed for LMO, where, the FC magnetization is found to be deviated below the cusp temperature (we use T_B to denote it) observed

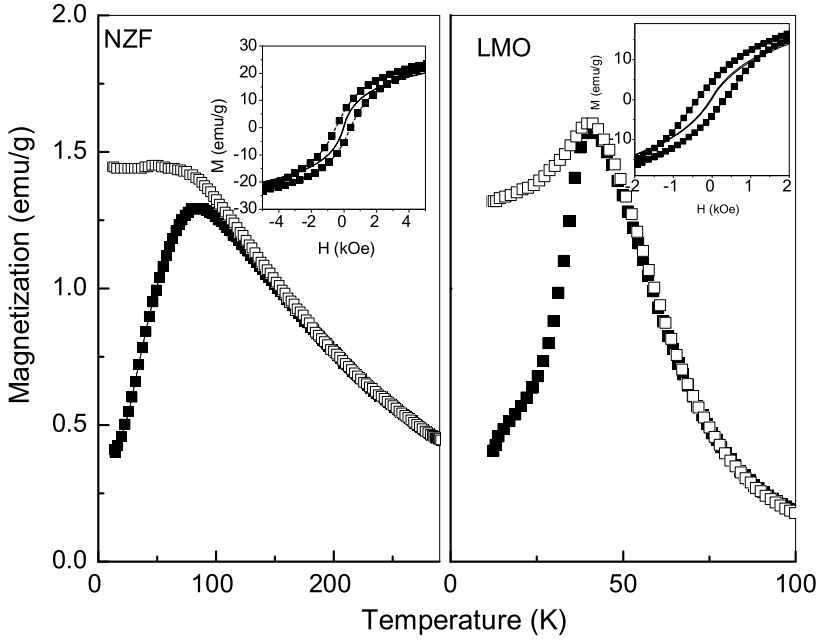

Figure 5.16: ZFC (filled symbols) and FC (open symbols) magnetizations of NZF and LMO composition. The cusp temperature is identified as T_B, which is 78 K for NZF and 41 K for LMO. Inset shows the M-H curves measured for NZF at 12 K (filled squares) and 100 K (solid line) and LMO at 12 K (filled squares) and 60 K (solid line)

in the ZFCM. The M-H curves measured at two temperatures, one above and another below T_B is shown in the inset of Fig. 5.16.

The M-H measurement shows a large coercivity at 12 K and when the temperature is raised above T_B, the loops are disappeared for both the NZF and LMO samples. The ZFC magnetization curves measured at various applied field strengths (H_{app}) for both the compositions show the dependence of T_B or T_g on H_{app}. As H_{app} is increased, the cusp was found to be shifted to lower temperatures. The dependence of the cusp temperature on H_{app} for both the compositions can be observed in Fig. 5.17. The M-H

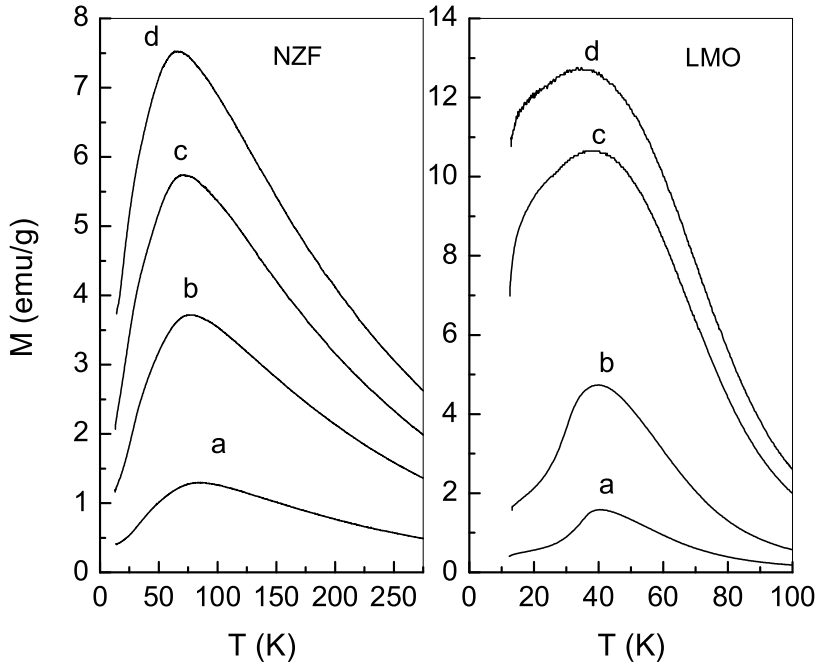

Figure 5.17: Field dependence of ZFC Magnetization of NZF measured at (a)50 Oe (b)200 Oe (c)350 Oe (d)500 Oe and that of LMO measured at (a)50 Oe (b)200 Oe (c)750 Oe (d)1000 Oe.

behavior of these two systems are also found to be identical, both show no magnetic hysteresis above the cusp temperature, but as the temperature is further decreased, the values of coercivity was found to be increased at low temperatures as shown in Fig. 5.18. This is a typical behavior shown by the magnetic nanoparticles. A common observation both in conventional spin glasses and interacting magnetic nanoparticles is the aging and memory effects they exhibit when cooled at various conditions with a particular waiting time given at a particular temperature spanning the temperature region below the cusp observed in normal ZFCM [Vin95, Dup01, Mat01b, Zot03, Ber04, Sas05]. In a typical experiment that follow an FC protocol, the system is

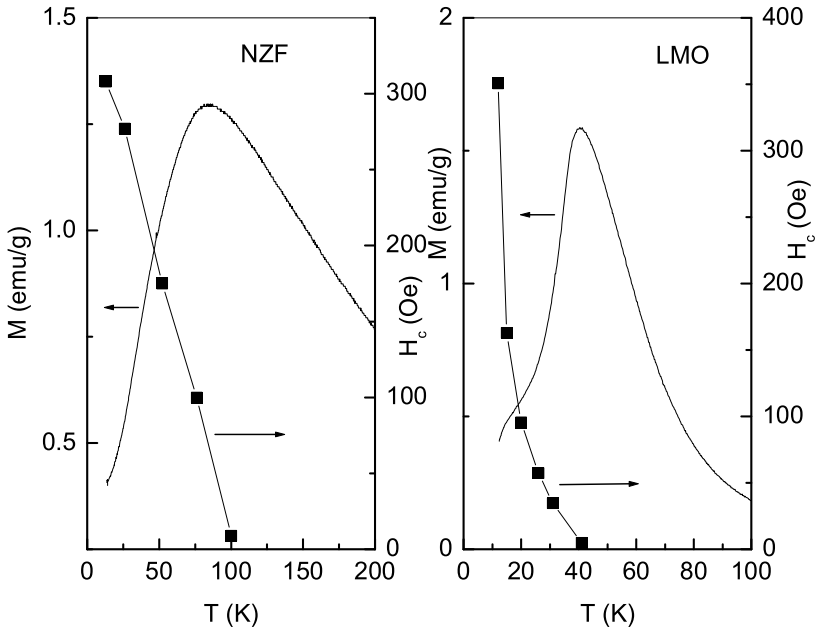

Figure 5.18: Comparison of the temperature dependence of the coercivity, H_c, and ZFC magnetization for NZF and LMO. H_c can be seen to decrease as the temperature approaches T_B and above which it becomes zero.

cooled in the presence of an external field (which is sufficiently small) and intermittent stops have been made at fixed temperatures (T_i) with the field switched off for some time and again switched on while cooling further [Myd93, Jon98a]. Once the system has reached the lowest temperature, the magnetization is measured and signatures of sharp memory effect will be observed in the case of typical spin glasses or interacting magnetic nanoparticles at temperatures where the system is allowed for a waiting time (t_w). The phenomenon of rejuvenation is often observed in the magnetization curves immediately after the aging process, once the sample is disturbed from the relaxed state at T_i and further cooled down in presence of an applied field, depending on the interaction behavior of superspins. A double memory experiment (DME) was

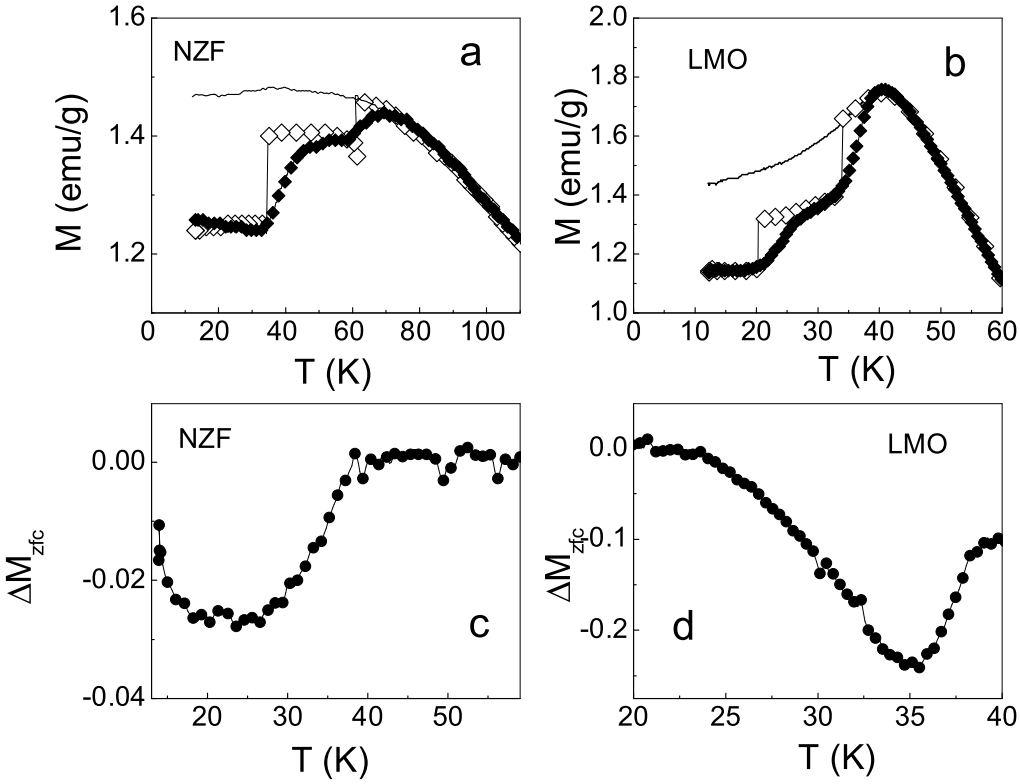

Figure 5.19: FC aging experiment (a) and (b) for NZF and LMO respectively. In both (a) and (b), the open symbols represent the magnetization curve measured during cooling with two halts (aging) and the filled symbols indicate the magnetization curve measured in the reverse thermal cycle (memory is observed) ZFC aging for both the samples. From (a), two halts (t_w = 2h) were made at T_1 = 62 K and T_2 = 34 K and from (b), halts (t_w = 2h) were made at T_1 = 34 K and T_2 = 20 K. The curves (c) and (d) represent the difference between ZFCM and ZFCM after aging for NZF and LMO respectively. The dips observed correspond to the temperature (T_i) at which the halt is made during cooling. For NZF, T_i = 25 K and for LMO, T_i = 35 K

performed for the NZF nanoparticle system where the temperature dependence of magnetization was measured during cooling under a field of 50 Oe. During cooling, the field was switched off at two temperatures (H = 0 Oe) T_1 and T_2 for a waiting time, t_w = 2 h as indicated in Fig. 5.19(a). The M-T measurement was repeated in the heating mode after cooling the sample down to 12 K. A constant heating and/or cooling rate of 2 $Kmin^{-1}$ was maintained in all the M-T measurements and the M-T curves measured on heating cycle is also shown in Fig. 5.19(a). The memory experiment on NZF nanoparticles with two halts, shows the aging, very weak rejuvenation and sharp memory effects as depicted in the Fig. 5.19(a). This has been shown as evidence for the presence of strong interactions between the individual nanosized particles or superspins. The reason for such memory effects is thought to be due to the formation and existence of metastable states (droplets) formed as a result of aging for a fixed timescale at a given temperature below T_B as proposed for the conventional spin glasses [Fis88a, Fis88b, Myd93, Jon00]. A similar experiment carried out for the LMO composition showed results identical to those of the nanosized NZF as shown in Fig. 5.19(b). Here it should be specially mentioned that there is no rejuvenation effects suggesting the existence of very strong interactions between the individual superspin clusters.

The rejuvenation characteristics alone are used to identify the interacting and non-interacting nature of superspins. A weak rejuvenation or absence of rejuvenation explicitly defines the superspin glass behavior in magnetic nanoparticles. For the NZF nanoparticle systems, we observe a weak rejuvenation after the first aging at T_1, but magnetization after aging at T_2 was found to be absolutely flat indicating the absence of rejuvenation. A reasonable explanation for the weak rejuvenation observed in the temperature region ΔT ($\Delta T = T_1$-T_2) lies in the strong interparticle interaction or the larger flip time required for the superspins when compared to those of atomic spin glasses and may be longer than the experimental time window.

Below T_2, the rejuvenation is absent either due to weak temperature chaos and/or cumulative aging processes and cannot be solely explained by the thermally activated dynamics of individual particles [Bou01]. Thus there is a strong interactive effect between the superspins themselves which result in a collective superspin dynamics. This explanation is in par with the memory effects observed at T_1 and T_2. Corresponding to the absence of rejuvenation below T_2, on the reverse thermal cycle, a strong memory effect is observed just above T_2. On the other hand, corresponding to a weak rejuvenation observed in the temperature window ΔT, the memory effect above T_1 is observed to be comparatively weak. This is indicative of the formation of metastable states (droplets) with varying length scales when aged at various conditions of field and temperature. A simple view of growing domains or droplets of interacting superspins as aging progresses, suggests the possibility of the formation and coexistence of more than one type of metastable states which are nucleated at different centers. These droplets may be frozen or locked on further cooling under a field or zero field depending on whether the field applied and/or thermal energy available is sufficiently large to collapse the metastable state. Consequently, rejuvenation will be observed in varying magnitudes depending on the thermal energy, field strength and the experimental time window.

However, it is generally accepted that FC memory experiments cannot confirm the spin glass-type or interacting superspin-type properties of the material [Mat01b, Sas04]. For this, we have performed aging and memory experiments which follow a ZFC protocol as suggested in previous reports [Mat01b, Sas04]. Figure. 5.19(c) and (d) show the difference between typical ZFCM and ZFCM with one halt aging process for NZF and LMO samples respectively. The dip in the magnetization shows the memory effect. This confirms the strongly interacting behavior of the superspins which results in the superspin glass-type of behavior. The M-H curves of the NZF nanoparticles and LMO composition measured at 12 K are compared in Fig. 5.20.

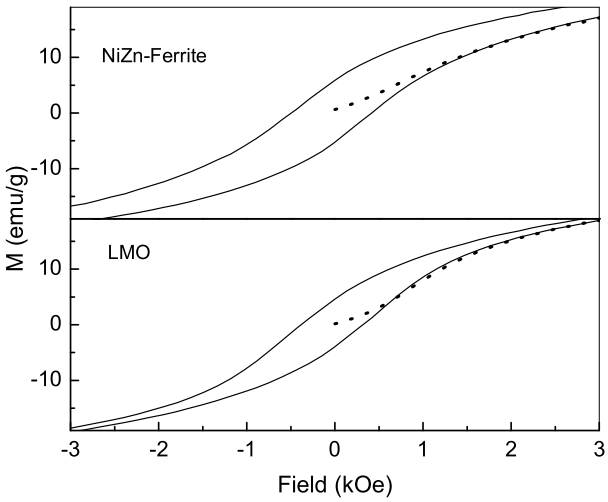

Figure 5.20: The M-H curves measured at 12 K for NZF and LMO. The virgin curves are shown as dotted lines.

It can be seen that the initial magnetization curve lies outside the loop for both these composition at temperatures, $T < T_B$ similar to those observed with highly anisotropic materials and spin glass compositions [Sen84, Joy00a]. The virgin curve of a ferromagnetic material generally reflects the properties related to the domain wall motion. But, the fact that the nanoparticles and nanoclusters behave in a similar way, suggests the unusual nature of the initial magnetization curves as indicative of the strong interaction present at the mesoscopic scale as observed in Fe_2O_3 nanoparticles [Zys01].

The low field M-H behavior of both the samples are shown in Fig. 5.21. The measurements were carried out initially by cooling the sample to a fixed temperature at zero field. A moderately fast field sweep rate (83 Oe s^{-1}) was maintained during the measurement. A distinctly S-shaped M-H curve is observed for both the samples when measured at the lowest temperature as shown in Fig. 5.21. As the temperature

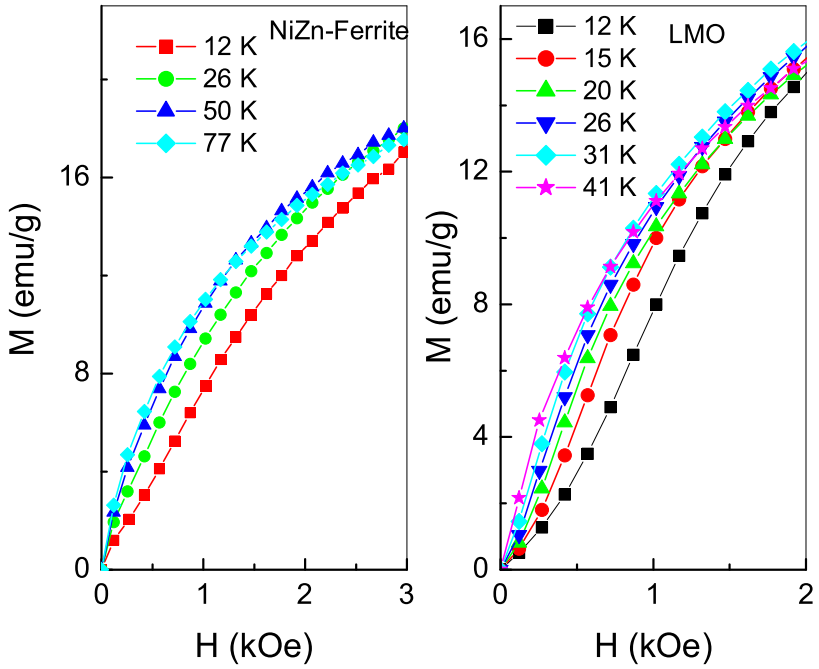

Figure 5.21: Nature of the initial magnetization curves measured at various temperatures below T_B for NZF and LMO.

is increased, the shape of the M-H curve is also found to be changed, gradually deviating from the S-shaped to a normal nature. Such a behavior is observed for certain spin glass-type of compounds [Kni77, Car03]. Thus, the magnetic properties of the two systems - NZF nanoparticles and LMO nanoclusters - consisting of mesoscopic magnetic entities are similar and the properties can be explained in terms of the interacting nature of the superspins resulting in the superspin glass behavior.

5.4 Conclusions

The magnetic properties of $LaMnO_{3+\delta}$ has been found to be dependent on the value of δ which decides the total Mn^{4+} content as well as the vacancies at cationic sites. It has been observed that the magnetic behavior of $LaMnO_{3+\delta}$ with large values of δ is more or less the same as observed in fine magnetic particles or single domain particles which show superparamagnetism above T_B and opens up the hysteresis loop below T_B. Further experiments reveal that the single domain limit is achieved when the value of δ in $LaMnO_{3+\delta}$ is fairly large. Since there are no interstitials available for oxygen anions in the perovskite type structure, cationic vacancies must be formed and a model with vacancies at La and Mn- sites to different extents can explain the present results. The magnetic properties of $LaMnO_{3+\delta}$, are explained using this model, which can be represented as $La_{1-x}Mn_{1-y}O_3$ with the possibilities of $x = y$, $x > y$ and $x < y$. When the value of δ is large, it can be approximated that the ratio of La/Mn becomes greater than 1, which implies a large concentration of Mn-site vacancies and this would result in abrupt breakage of magnetic exchange at Mn vacancy sites. A large concentration of Mn-site vacancies, thus helps creating tiny magnetic clusters, thereby destroying the long range magnetic order. A quantitative treatment becomes difficult since both x and y may not assume a fixed value as δ cannot be controlled during the synthesis. More careful studies have to be done on this system to have a knowledge of the exact concentration of various types of vacancies in $La_{1-x}Mn_{1-y}O_3$.

A long standing issue on the magnetic properties of $LaMnO_{3+\delta}$ which was thought to be due to spin-glass nature, caused by the FM-AFM competing interactions, have been thoroughly analyzed and it is proposed that the low-temperature cusp-like nature observed in the low-field ZFCM-T measurement is due to the presence of interacting single domain clusters. The correlation between the superspins is found to

be similar to that observed in the conventional atomic spin glasses. It is understood that magnetic nanoparticles and nanoclusters show this type of behavior due to the superspin disorder, which is thought to be largely controlled by the dipolar and/or exchange interactions between the superspins. However, these magnetic entities with mesoscopic dimensions behave in an identical fashion. Thus, the present work shows that the mesoscopic cluster interactions can explain the origin of spin glass-type behavior in lanthanum manganites as in the case of dense magnetic nanoparticles.

Chapter 6

Magnetic Behavior of Rare-earth ion Substituted $La_{0.67}Ca_{0.33}MnO_3$

In divalent ion substituted rare earth manganites, $R_{1-x}A_xMnO_3$, different choices of R (trivalent) and A (divalent) ions have different ionic sizes and hence produce different internal stresses acting on the Mn-O bonds. If the bond is compressed, buckling of the MnO_6 octahedra results and the effective Mn-O-Mn double exchange is very sensitive to this buckling. The strength of the double exchange is maximum when the Mn-O-Mn bond angle is 180°. Trivalent lanthanide ions are smaller than La^{3+} ion due to the lanthanide contraction. Consequently, substitution of La by R in $La_{1-x}Ca_xMnO_3$ would result in appreciable reduction of the Mn-O-Mn bond angle and will be expected to affect the magnetic properties significantly. The magnetic properties of such manganite systems have been studied in detail and explained in this chapter.

6.1 Introduction

The interest in the study of the substituted perovskite-type manganites, $La_{1-x}A_xMnO_3$, is to understand the different aspects of the complex magnetic behaviour exhibited by these compounds [Rao98, Tok00, Dag03]. Highest Curie temperature in the series when A = Ca, Sr, Ba, etc., is obtained for $x \approx 1/3$ and hence there are many

studies reported for the composition $La_{2/3}A_{1/3}MnO_3$ and $La_{0.7}A_{0.3}MnO_3$. Jin *et al.* [Jin95] observed an order of magnitude increase in the magnetoresistance in $La_{0.60}Y_{0.07}Ca_{0.33}MnO_3$, where La^{3+} in $La_{2/3}Ca_{1/3}MnO_3$ is partially replaced by Y^{3+}, and this is associated with a decrease in the Curie temperature from 230 to 140 K on substitution. Many interesting new magnetic behaviors are observed when La^{3+} is substituted by other trivalent rare-earth ions in $La_{2/3}Ca_{1/3}MnO_3$ and $La_{0.7}Ca_{0.3}MnO_3$ [Hwa95, Mai96, Bla96, Det96, Ter98, Nie99], though there are no changes in the Mn^3/Mn^{4+} ratio after substitution. The changes in the Mn-O-Mn bond angle, from structural distortions, are very crucial in determining the strength of the double exchange interactions in the substituted manganites. For the perovskite oxide of the general formula ABO_3, the tolerance factor is a measure of the degree of distortion of the structure of a given compound from the ideal cubic perovskite structure for which $t = 1$ [Goo70]. The B-O-B bond angle is very sensitive to the size of the A cation, r_A, and therefore, to the tolerance factor, and decreases from 180° with decreasing t. In the substituted manganites, when La^{3+}, ion is replaced by other smaller rare earth ions, the Mn-O-Mn bond angle is decreased considerably due to the distortion of the perovskite structure. Hwang *et al.* [Hwa95] found a direct correlation between the Curie temperature and the average ionic radius of the La-site ions where the Curie temperature decreases with decreasing average ionic radius, for fixed Mn^3/Mn^{4+} ratio in $La_{0.7-x}R_xCa_{0.3}MnO_3$ (R = Pr, Y), indicating the role of lattice effects in determining the ferromagnetic properties. From the phase diagram of Curie temperature versus tolerance factor, it was observed that the compositions are ferromagnetic and metallic for $t \geq 0.91$. Later on, from many such substitutional studies, it was found that this is a universal phase diagram, applicable for R other than Pr and Y, such as Tb and Dy [Det96, Rao98, Ter98].

6.2 Synthesis

Polycrystalline samples of $La_{0.67}Ca_{0.33}MnO_3$ and $La_{0.6}R_{0.07}Ca_{0.33}MnO_3$ (R = Pr, Sm, Gd, Tb, Dy, Er) were synthesized by the ceramic method from the corresponding oxides (La_2O_3, Pr_6O_{11}, Sm_2O_3, Gd_2O_3, Tb_4O_7, Dy_2O_3, Er_2O_3, $CaCO_3$ and MnO_2) taken in the required stoichiometric ratio. After an initial heating of the mixture of the oxides at 1273 K for 12 h, the powder samples were further heated in air twice at 1273 K for 12 h each, twice at 1373 K for 12 h each, at 1473 K for 24 h, twice at 1573 K for 24 h each, with intermediate grindings, and finally pressed pellets were heated at 1623 K for 24 h.

The Tb-substituted samples with the general formula $La_{0.67-x}Tb_xCa_{0.33}MnO_3$ (represented as LTC), have been synthesized by the conventional solid state route from the La_2O_3, Tb_4O_7, $CaCO_3$ and MnO_2 by mixing these oxides in the required stoichiometry for x = 0, 0.03, 0.07, 0.10, 0.11, 0.12, 0.125, 0.13, 0.15, 0.20, and 0.25. The well-mixed samples were then heated at 1273 K, 1473K, 1573 K, for 48 h each, then at 1623 K for 24 h with intermediate grindings at every 24 h steps to ensure the sample homogeneity and pelletized, which is finally sintered at 1673 K for 24 h.

6.3 Magnetic Properties of $La_{0.60}R_{0.07}Ca_{0.33}MnO_3$, R = Rare Earth Ion

In general, it has been observed that the Curie temperature varies linearly as a function of tolerance factor for $0.907 \leq t \leq 0.92$ [Hwa95]. Studies on $La_{0.67-x}Tb_xCa_{0.33}MnO_3$ by Blasco *et al.* [Bla96] showed that compositions with $t < 0.907$ are spin glass insulators and Terai *et al.* [Ter98] showed that a re-entrant spin glass state is possible in $La_{0.7-x}Dy_xCa_{0.3}MnO_3$ for a value of t between 0.907 and 0.913. In the case of $La_{0.67-x}Tb_xCa_{0.33}MnO_3$, Blasco *et al.* [Bla96] and Nie *et al.* [Nie99] found a small decrease in the *ac* susceptibility below ∼30 K as soon as a small amount of La is re-

placed by Tb (x as small as 0.027) and this behavior is observed till $x = 0.13$, above which the compounds show spin glass behavior. Similarly, Terai *et al.* [Ter98] found a small decrease in the zero field cooled (ZFC) susceptibility of $La_{0.6}Dy_{0.1}Ca_{0.3}MnO_3$, below ∼20 K. It is not known whether the decrease in the *ac* or ZFC susceptibility of the ferromagnetic compositions in the Tb- and Dy-substituted compounds has any contributions from Tb^{3+} and Dy^{3+} or not. The notable factor here is the lower temperature at which the drop in the susceptibility is observed for the Dy-substituted compound and the ionic size of Dy^{3+} is smaller than that of Tb^{3+}. Based on this argument, such anomalies are expected at higher temperatures as the rare-earth ionic size is increased. Therefore, the magnetic properties of $La_{0.60}R_{0.07}Ca_{0.33}MnO_3$ (R = Pr, Sm, Gd, Tb, Dy, Er) has been studied with a fixed concentration of the rare-earth ion, to probe whether there is any ionic size related contribution and if not, to understand the roles of Tb^{3+} and Dy^{3+} ions in determining such behavior. The degree of substitution (as $x = 0.07$) is selected in such a way that the tolerance factor is within $0.91 \leq t \leq 0.92$, so that the compounds are expected to be ferromagnetic according to the proposed universal phase diagram.

6.3.1 Results and Discussion

Figure. 6.1 shows the powder X-ray diffraction patterns of some $La_{0.6}R_{0.07}Ca_{0.33}MnO_3$ compositions. All compositions show the formation of an orthorhombic perovskite phase with the lattice parameters slightly decreasing for smaller rare-earth ion incorporated compositions. Few very weak reflections, other than those from the orthorhombic perovskite phase are observed for the Er-substituted compound (marked in the figure by *) and these reflections are identified as due to the hexagonal perovskite phase. It is known that the hexagonal perovskite phases are formed in smaller amounts in the case of the heavier rare earth manganites, $RMnO_3$, and this is unavoidable [Alo00].

Figure. 6.2 shows the temperature variation of the *ac* magnetic susceptibility of different compositions in $La_{0.6}R_{0.07}Ca_{0.33}MnO_3$, including that of the unsubstituted compound (R = La), measured in the temperature range 15–300 K. Sharp ferromagnetic transitions are observed for all compositions and the ferromagnetic transition temperature decreases continuously with changing R from Pr to Er. For Pr, Sm and Gd substituted compounds, the *ac* susceptibility decreases continuously with decreasing temperature after reaching a maximum below the Curie temperature. On the other hand, a sudden decrease in the susceptibility is observed for the Tb-substituted compound, below ∼30 K. The shape and features of the *ac* susceptibility curve of the Tb-substituted composition is similar to that reported by Blasco *et al.*[Bla97]. [Bla96] and Nie *et al.* [Nie99] for compositions in the range $0.03 \leq x \leq 0.13$ in $La_{0.67-x}Tb_xCa_{0.33}MnO_3$. A similar small decrease in the susceptibility is observed for the Dy-substituted composition also, below ∼19 K, as shown in the inset of Fig. 6.2. A sharp peak below T_c is observed for the Er-substituted compound and the susceptibility rises below 75 K after going through a minimum in the susceptibility. The powder XRD data of the Er compound showed the formation of a hexagonal phase as impurity and this could be the possible origin of the low-temperature increase in the susceptibility.

The field cooled (FC) and zero field cooled (ZFC) magnetization curves of the unsubstituted compound as well as the rare-earth substituted compositions are shown in Fig 6.3. The irreversibility between the FC and ZFC magnetizations, below T_c, is observed in all cases, as this is a common feature observed in the magnetically ordered systems, because of magnetocrystalline anisotropy [Kum99, Joy00b, Joy00c]. The difference between FC and ZFC magnetizations is more if the applied field is relatively smaller when compared to the coercive fields at different temperatures, below T_c. In general, the ZFC magnetization curve measured at low magnetic fields show the characteristics observed in the *ac* susceptibility curves. Compared to the

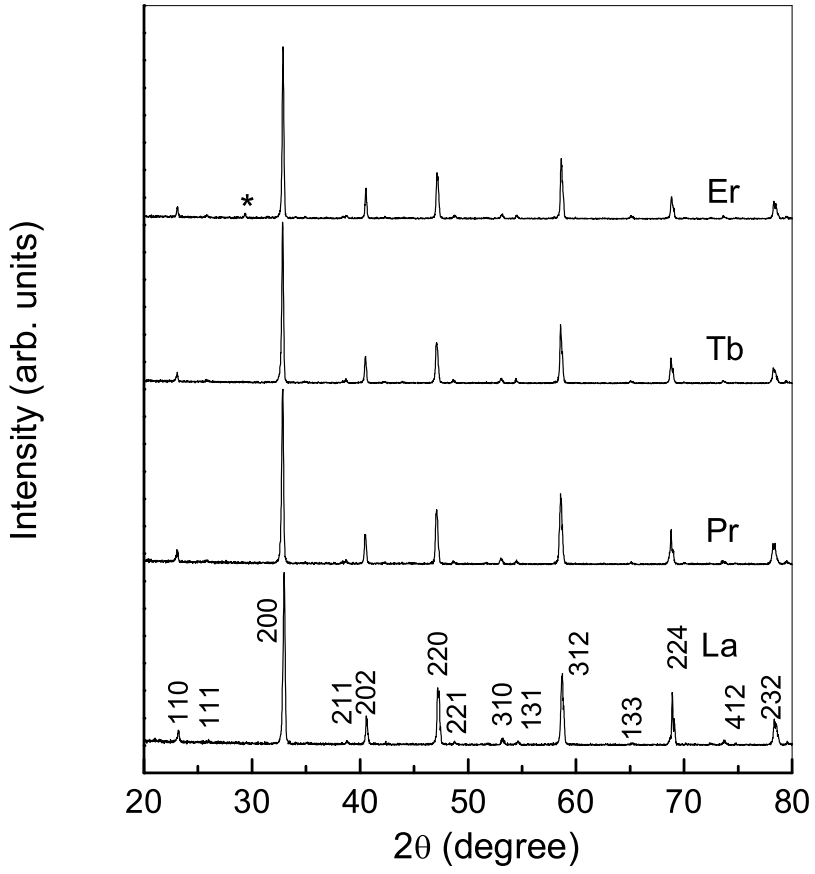

Figure 6.1: Powder XRD patterns of some compositions in $La_{0.6}R_{0.07}Ca_{0.33}MnO_3$, including that of the unsubstituted compound. * impurity due to hexagonal perovskite structure

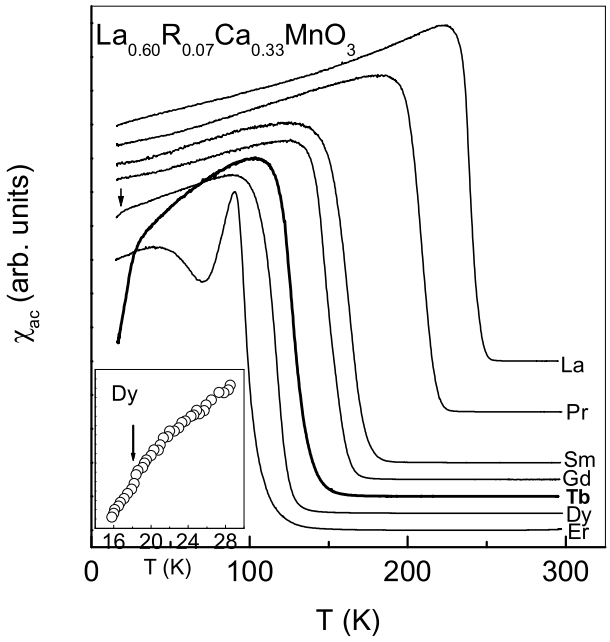

Figure 6.2: Temperature variation of the *ac* susceptibility of different compositions in $La_{0.6}R_{0.07}Ca_{0.33}MnO_3$, measured using a magnetic field of 2 Oe and at a frequency of 210 Hz. The curves are shifted along the y-axis for clarity.

ZFC magnetization curves of all other compositions, the Tb-substituted compound shows a small decrease in the magnetization below ∼30 K, as observed in the *ac* susceptibility measurements. For the Dy-substituted compound, a small decrease in the ZFC magnetization, below 20 K, is observed when measured using a small magnetic field of 10 Oe, as shown in the inset of Fig. 6.3.

Variation of the Curie temperature as a function of the tolerance factor as well as the average ionic size of the La-site ions in $La_{0.6}R_{0.07}Ca_{0.33}MnO_3$ is shown in Fig. 6.4. In the calculation of the tolerance factor, the coordination dependent ionic radius is used [Sha76]. The B-site ions are octahedrally coordinated in the perovskite structure and for the A-site ions, nine-fold coordination is generally used [Hwa95].

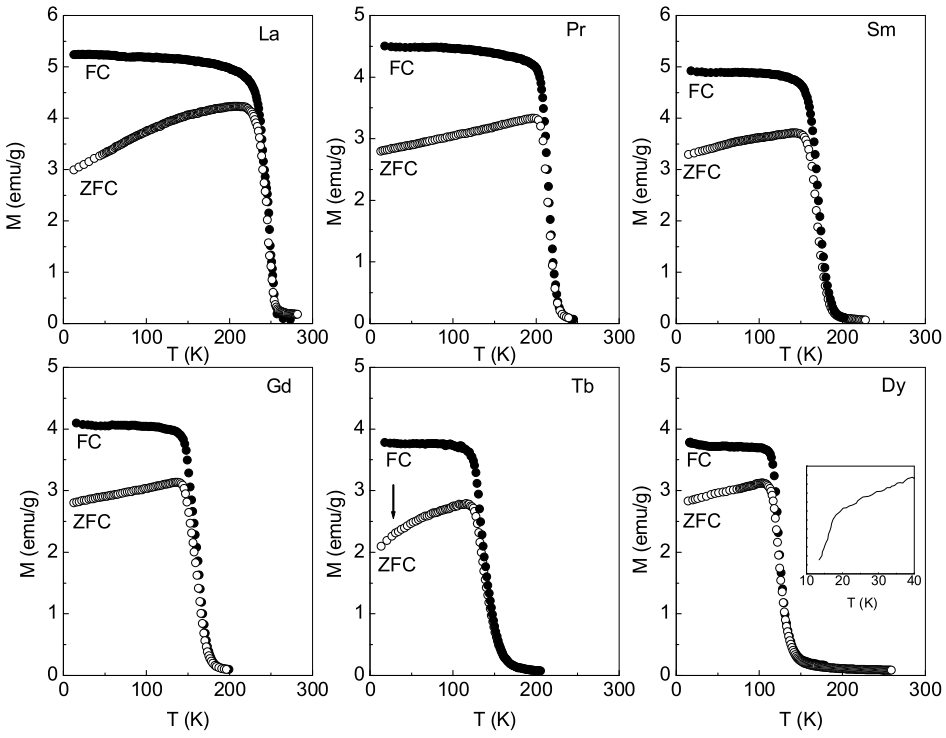

Figure 6.3: Zero field cooled and field cooled magnetization curves of different compositions in $La_{0.6}R_{0.07}Ca_{0.33}MnO_3$. Inset: ZFC magnetization of the Dy compound in a field of 10 Oe.

The Curie temperature decreases linearly with decreasing ionic radius of the rare-earth ion, indicating that the decrease in the Curie temperature is associated with the structural changes, mainly because of the decreasing Mn-O-Mn angle, which affects the strength of the magnetic exchange interactions [Rao98]. The Mn-O-Mn angle in rare-earth manganites is known to decrease with decreasing ionic size of the rare-earth ion in $RMnO_3$ [Alo00], due to the increased structural distortions and similar behavior is observed for varying the Tb^{3+} concentration in $La_{0.67-x}Tb_xCa_{0.33}MnO_3$ [Bla96]. As observed for different compositions in the $La_{0.67-x}Tb_xCa_{0.33}MnO_3$ series

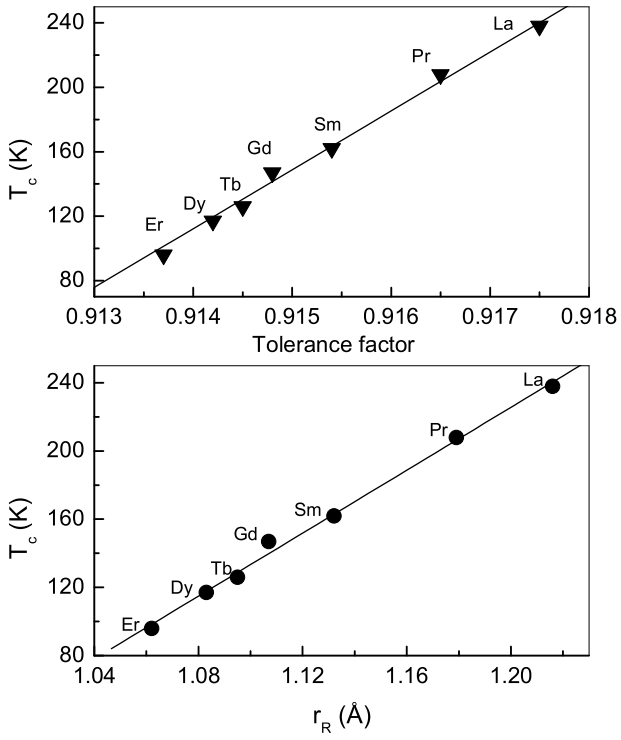

Figure 6.4: Variation of Curie temperature as a function of tolerance factor and average La-site ionic radius for $La_{0.6}R_{0.07}Ca_{0.33}MnO_3$. The solid line is least-squares fit to the data.

[Bla96], a linear variation of the Curie temperature with tolerance factor is observed in the region $0.913 \leq t \leq 0.918$ for the present system also, with different rare-earth ions, indicating the application of the universal phase diagram for fixed composition with different rare-earth ions.

A sudden decrease in the *ac* susceptibility at low temperatures, below the ferromagnetic ordering temperature, similar to that observed for the Tb compound, has been observed for different compositions in $La_{1-x}Ca_xMnO_3$ [Tok00] and $La_{1-x}MnO_3$ as discussed in chapter 3. In the latter cases, it was found that the temperature at

which a decrease in the susceptibility is observed varies with the degree of substitution, and the phenomenon could be explained in terms of domain wall pinning effects. On the other hand, the anomaly is observed at the same temperature for different Tb substituted compositions in $La_{0.67-x}Tb_xCa_{0.33}MnO_3$, as reported by Blasco *et al.* [Bla96] and Nie *et al.* [Nie99]. However, similar anomalies are not observed in the susceptibility curves of other rare-earth substituted compositions, except for R = Tb and Dy.

Recently, Goto *et al.* [Got04] reported a incommensurate-commensurate phase transition, below the Neel temperature, for $TbMnO_3$ and $DyMnO_3$ and this kind of transition is observed only for the Tb and Dy compounds in $RMnO_3$. This transition is accompanied by a ferroelectric transition, associated with a lattice modulation [Kim03]. A large change in the dielectric constant and magnetic field controlled polarization effects are reported at a temperature close to ∼30 K for $TbMnO_3$ and this temperature is lower than the antiferromagnetic ordering temperature (∼41 K) of the Mn sublattice in $TbMnO_3$ [Kim03, Got04]. This temperature is related to the incommensurate-commensurate transition, identified as a lock-in temperature, where the magnetic modulation vector is locked. Neutron diffraction studies also agree with this picture, where it has been identified that the locking of the wave vector amplifies the Mn moment [Kaj04]. Similarly, for $DyMnO_3$, a large change in the dielectric constant and electric polarization is observed below ∼20 K and the features are magnetic field dependent. Unexpectedly, the temperature below which the anomaly is observed in the *ac* susceptibility curve of $La_{0.60}Tb_{0.07}Ca_{0.33}MnO_3$ and $La_{0.60}Dy_{0.07}Ca_{0.33}MnO_3$ is at the same temperature where the lock-in behaviour is observed in $TbMnO_3$ and $DyMnO_3$, respectively. The fact that the temperature at which this anomaly is observed in the *ac* susceptibility is almost independent of the concentration of Tb [Bla96, Nie99] implies that similar reasons as observed in $TbMnO_3$ could be possible when La is partially substituted by Tb in $La_{0.67-x}Tb_xCa_{0.33}MnO_3$.

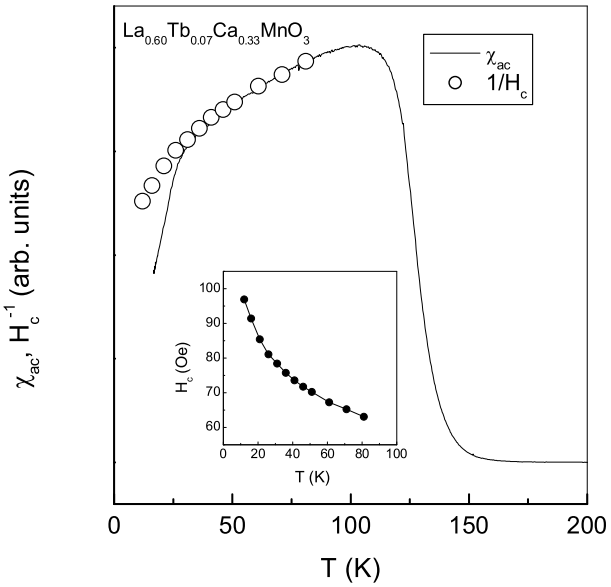

Figure 6.5: Comparison of the temperature variation of the normalized ac susceptibility and the inverse of the coercivity of $La_{0.60}Tb_{0.07}Ca_{0.33}MnO_3$. Inset: variation of coercivity as a function of temperature.

However, as the anomaly is observed in the ZFC magnetization curve of the compositions of $La_{0.60}Tb_{0.07}Ca_{0.33}MnO_3$, as a decrease in the magnetization below 30 K and since it is not observed in the FC magnetization, it is possible that the origin of the anomaly is associated with the magnetic domain structure. Such effects are commonly observed in domain wall pinned magnets [Ste02]. A small sharp increase in the coercivity has been observed for $La_{0.9}Ca_{0.1}MnO_3$ [Joy00c] at the temperature where an anomalous decrease in the *ac* susceptibility is observed. Fig. 6.5 shows that the coercivity of $La_{0.60}Tb_{0.07}Ca_{0.33}MnO_3$ decreases linearly down to 30 K and there is a drastic increase in the coercivity below 30 K where the anomalous drop in the susceptibility is observed. As shown in Fig. 6.5, there is a direct correlation between the changes in the susceptibility and the inverse of the coercivity with temperature.

As evidenced from the above studies and based on the arguments as in Chapter 3, the domain wall pinning effects may be regarded as responsible for the anomalous drop in the susceptibility, in the ferromagnetic region, at low temperatures.

6.3.2 Conclusions

The present study on $La_{0.60}R_{0.07}Ca_{0.33}MnO_3$, with fixed R ion concentration and Mn^{3+}/Mn^{4+} ratio shows that the universal phase diagram of Curie temperature versus tolerance factor is applicable for all the rare-earth ion substituted manganites. A small anomaly in the *ac* susceptibility and zero field cooled magnetization curves, below the Curie temperature, is observed only for the Tb- and Dy-substituted compositions. This is most likely to be due the contributions from similar local lattice distortions at Tb or Dy site at low temperatures as observed only in the case of $TbMnO_3$ and $DyMnO_3$ in the $RMnO_3$ series.

6.4 Evolution of Spin Glass State in $La_{0.67-x}Tb_xCa_{0.33}MnO_3$

The substitution of La by low concentrations of Tb ions in $La_{0.67}Ca_{0.33}MnO_3$ causes a low temperature anomaly as discussed in the preceding section. When the concentration of Tb ions is increased, a spin glass-type of behavior is observed [Bla96, Nie99]. The spin glass type of behavior is thought to be due to the competition between FM and AFM types of exchanges, or is more often explained as cluster glasses. Similarly yttrium (Y) substitution at La-site in $La_{0.7}Ca_{0.3}MnO_3$ results in the lowering of T_c (suppression of the long range FM order) and as the concentration of Y ions is increased further, cluster glass behavior was found to be gradually developed [Fre01]. The effect of Y substitution and confinement of FM clusters were studied for rather a short range of compositions and well defined cluster glass properties were observed for

the sample with 15% yttrium ions in the perovskite phase whereas well defined FM characteristics were observed when the concentration of Y ions is 10% or less. Nie *et al.* [Nie99] have also observed the formation of magnetic clusters and superparamagnetism in Tb-substituted lanthanum manganites with large values of Tb concentration of the order of 20%. The confinement of such clusters must be largely dependent on the distribution of Tb ions and the Mn-O-Mn bond angle at Tb locality. In order to explore such a possibility of confinement of magnetic clusters and to determine the critical concentration of Tb ions resulting in the formation of such clusters, a series of compositions with very close values of x in $La_{0.67-x}Tb_xCa_{0.33}MnO_3$ has been studied, for the values of $0 \leq x \leq 0.25$.

6.4.1 Results and Discussion

The powder XRD patterns of the samples indicate single phase formation and could be indexed to an orthorhombic unit cell, with *Pbnm* space group. The XRD patterns of some Tb-substituted compositions are shown in Fig. 6.6. It is observed that the unit cell parameters vary with the concentration of Tb-ions similar to the report of Blasco *et al.* [Bla96].

The *ac* susceptibility curves of the representative samples are shown in Fig. 6.7. Here, it can be seen that as the concentration of Tb in the composition increases, the magnetic transition temperature decreases, and the M-T curve shows a cusp-like nature when the concentration is increased beyond $x = 0.1$. Although well-defined T_c for the samples with low amounts of Tb is observed, there is a distinct anomalous feature in the susceptibility curve at low-temperatures; the origin of which is discussed in the preceding section. However, the cusp-like nature of the *ac* susceptibility and its shift to lower temperatures as the value of x in $La_{0.67-x}Tb_xCa_{0.33}MnO_3$ is increased is interesting.

Recent studies on Ga-substituted compositions, $La_{0.67}Ca_{0.33}Mn_{1-x}Ga_xO_3$ suggest

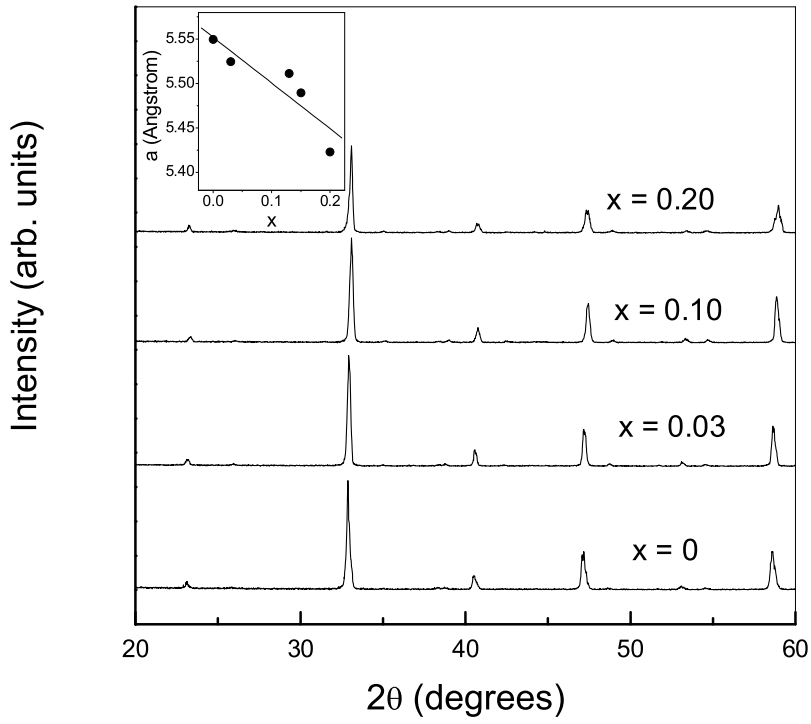

Figure 6.6: XRD patterns of representative $La_{0.67-x}Tb_xCa_{0.33}MnO_3$ compositions. Inset shows variation of orthorhombic unit cell parameter, a with value of x

the possible existence of the quantum critical point (QCP) as predicted by the theoretical calculations [Alo02, Det05]. The QCP is defined as a second order transition accompanied by the change of a non-thermal parameter. The QCP was expected by Alonso *et al.* [Alo02] for a value of 10-20% of Ga substitution. The substitution of a nonmagnetic ion like Ga at the Mn-sublattice of the perovskite-type oxide causes the localization of the electronic states suppressing the double exchange mechanism. Thus, it is possible that, such a QCP may exist in any manganite system, wherein the long range order or the double exchange mechanism is either disrupted or made considerably weak. One such possibility is through the reduction of Mn-O-Mn bond

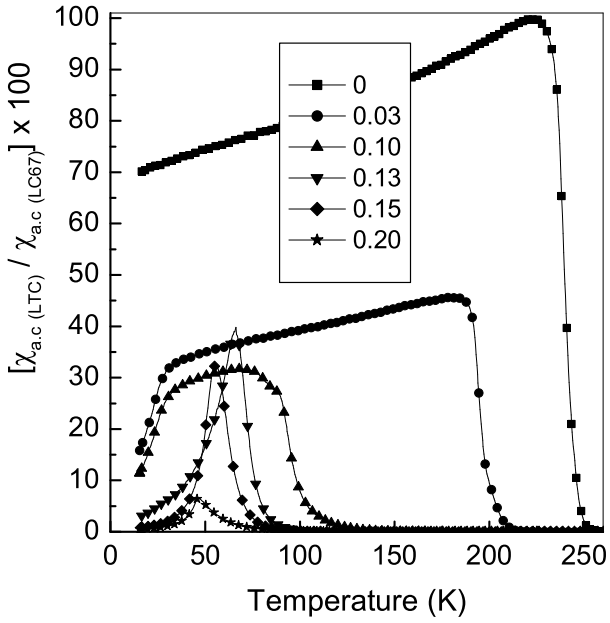

Figure 6.7: Temperature dependence of *ac* susceptibility of representative compositions $La_{0.67-x}Tb_xCa_{0.33}MnO_3$. The numbers indicate the value of x

angle, since the double exchange in manganites largely depends on this important parameter. Thus, by replacing La by other trivalent ions which have sufficiently low ionic radii and causes no structural instability, one should observe QCP for some concentration of the substituent. This may be viewed as breaking the long range ferromagnetic exchange by introducing either non-magnetic ions or tuning the Mn-O-Mn bond angle by introducing local structural defects. The substituent may be inhomogeneously distributed, which allows the long range magnetic order to coexist with the short range ordering, below a certain value of x in $La_{0.67}Ca_{0.33}Mn_{1-x}A_xO_3$ or $La_{0.67-x}R_xCa_{0.33}MnO_3$ (A = nonmagnetic ion and R = Rare earth ions with small size or Y ion). At a certain value of x, which enforces a homogeneous distribution of the substituent, structural ordering may cause the breakage of long range order to form

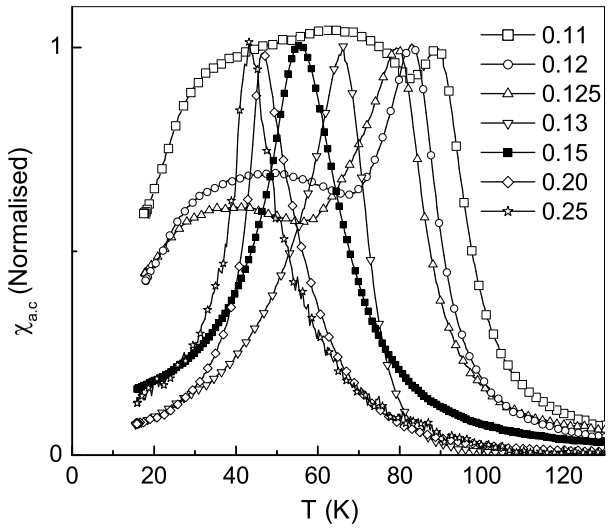

Figure 6.8: Temperature dependence of the *ac* susceptibility of the compositions in $La_{0.67-x}Tb_xCa_{0.33}MnO_3$, with values of x close to 1/8. The numbers indicate the values of x

tiny double exchange magnetic clusters. From various reports, it can be suggested that, such behavior is rather universal for substitution with various nonmagnetic ions at Mn-sublattice or smaller rare earth ions at La-site for the same Mn^{3+}/Mn^{4+} ratio and this critical concentration of substituent ions is always in between 10-20% [Bla97, Sun99, Liu00, Det05]. The 1/8 ordering of vacancies in $La_{1-x}MnO_3$ which causes the important limit of x in such compositions hints the possible importance of such a 1/8-ordered structure in determining the physical characteristics of manganites as discussed in chapter 3. Such a 1/8 ordering of the substituent ions may be seen in any manganite system when their concentration in the lattice is close to 1/8, and corresponding magnetic characteristics may be observed. Hence a close analysis has been made on the Tb-substituted compositions in detail and very closely near $x = 1/8$.

The *ac* susceptibility of the compositions with values of x close to 1/8, as a function of temperature, is shown in Fig. 6.8. For $x = 0.1$, a clear ferromagnetic transition is observed (see Fig. 6.7). It can be seen that for the sample with $x = 0.11$, there is a cusp like feature observed at a higher temperature which is succeeded by the normal flat curve, and finally a drop in susceptibility at around 28 K. This is a complex feature and is not commonly reported for the manganite compositions.

As the concentration of Tb ions is further increased, it can be seen that the cusp-like feature becomes more prominent, the flat region gradually vanishes, but the dip in susceptibility still corresponds to 28 K for the compositions $La_{0.67-x}Tb_xCa_{0.33}MnO_3$ with values of $x = 0.12$ and 0.125. A further increase of x ($x > 0.125$) results in a peculiar susceptibility behavior with a cusp like feature as observed in spin glass systems and superparamagnets. For the compositions with $x > 0.125$, there is a gradual shift of the cusp towards lower temperatures as the value of x is increased. Also, as is evident from Fig. 6.7, the relative susceptibility values also decrease with the increase in the Tb concentration. These observations point out to an important conclusion on the evolution of short range ordering due to decrease of the Mn-O-Mn bond angle and consequent formation of clusters as the concentration of Tb is increased. This clustering is likely to be due to the breaking or weakening of the double exchange at the Tb-sites caused by the local structural distortion which in turn is due to the smaller size of Tb ions and the cusp like feature originates from the formation of such clusters. Also, as the concentration of Tb ions is increased, the random distribution of these ions in the perovskite-type lattice results in short range ordered magnetic clusters with varying length scales. It is observed that the temperature corresponding to the cusp, identified as T_B henceforth, decreases with increasing values of x. This suggests the confinement of magnetic clusters to shorter and shorter length scales as the number of Tb centers are increased. The clusters of shorter length scales behave as single domains and hence may be called super-

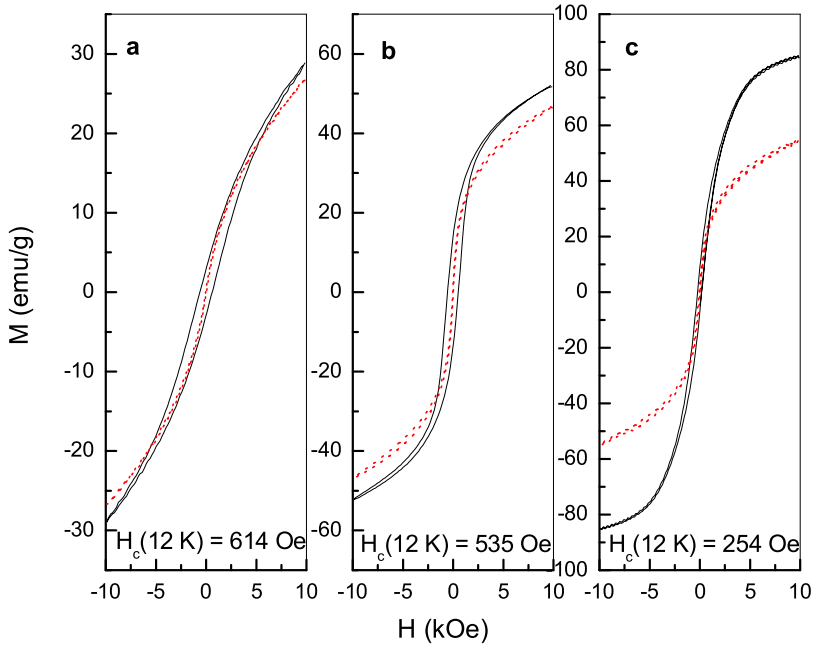

Figure 6.9: The M-H curves of $La_{0.67-x}Tb_xCa_{0.33}MnO_3$ (LTC) compositions for x = 0.25 (a), 0.15 (b), and 0.13 (c) The dotted curves represent the M-H curves obtained at 42 K, 54 K, and 66 K for the respective LTC compositions. Solid curves are obtained at 12 K. The values of the coercivity, H_c measured at 12 K are given in the figure.

spins (SP) individually. Thus, the clustering may be seen to start when $x = 0.11$, where a cusp is also observed along with the normal magnetic features. The small angle neutron diffraction studies in similar compositions also reveal the formation of magnetic clusters typically of nanometer scales [Wat01]. For further increase of x up to 0.125, the cusp shifts to lower temperatures, whereas the normal ferromagnetic plateau is gradually diminished. The shift of the cusp to lower temperatures is due to the decrease of the cluster size, and the overall features suggest the coexistence of FM and superspin (SP) clusters in these samples. As the length scales of these

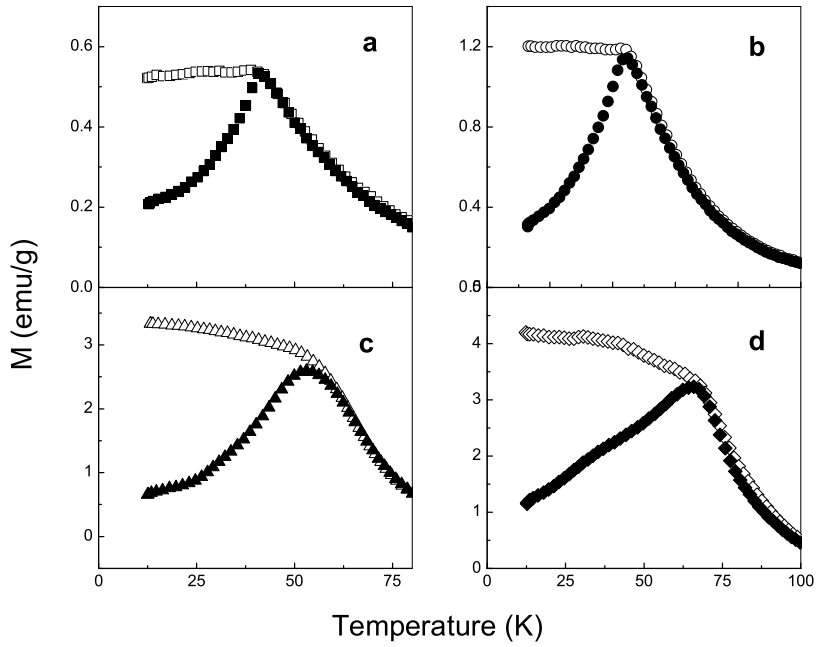

Figure 6.10: The ZFC and FC magnetization curves of $La_{0.67-x}Tb_xCa_{0.33}MnO_3$ compositions, with values of x = (a) 0.25, (b) 0.20, (c) 0.15, and (d) 0.13

clusters increase, the respective T_B also increases and eventually it appears above the Curie temperature T_c of the FM phases. Thus, the samples with $x = 0.11$, 0.12 and 0.125 show an unusual feature of coexistence of an FM phase and SP clusters. A detailed analysis of such a mixed phase system is difficult owing to its inherent complexity (overlapping FM and SP features). However, well defined susceptibility curves corresponding to those of SP clusters are available for the samples with $x > 0.125$. All these compositions show SP-like features in the *ac* susceptibility measurements. These compositions possess remarkably high values of coercivity at low temperatures well below T_B, and the coercivity was found to be increasing with increasing values of x as shown in the Fig. 6.9. Above T_B, all these samples show no hysteresis, and no

saturation of magnetization in the measured field range unlike those with low degree of substitution. These are typical features of superparamagnets. Besides, they show irreversible magnetic behavior when the samples are cooled under a field or zero field. As shown in Fig. 6.10, the cusp-like nature is evident for the temperature dependence of ZFC magnetization (ZFCM) for these samples and the FC magnetization (FCM) matches with that of ZFCM, above T_B and exhibits divergence below T_B. It can be seen that, below T_B, the FCM keeps a constant value for the samples with higher concentration of Tb ($x = 0.20$ and 0.25), whereas a gradually increasing FCM is observed for $x = 0.13$ and 0.15.

Thus, as the Tb concentration in the lattice is increased beyond a certain limit, the magnetic exchange weakens considerably. This results in the formation of tiny magnetic clusters. This clustering behavior is observed for the compositions with $x > 0.125$. The value of $x = 1/8$, possibly leads to an ordered arrangement of Tb in the manganite lattice and it may thus, be the critical concentration of Tb ions in such a manganite system above which superspin clustering phenomenon is observed.

6.4.2 Conclusions

Tb-substituted manganite compositions of the general formula $La_{0.67-x}Tb_xCa_{0.33}MnO_3$, where $0.25 \leq x \leq 0$ have been synthesized and all are found to be having orthorhombic crystal structure. There is a regular decrease in the values of unit cell parameters as evidenced from the XRD analysis. Introduction of Tb into the lattice of the parent $La_{0.67}Ca_{0.33}MnO_3$ composition creates local structural distortion at Tb locality which causes a reduction in the Mn-O-Mn bond angle which in turn weakens or destroys the long range double exchange thus weakening the ferromagnetism. This is evidenced by the decrease in T_c when Tb is progressively incorporated in the lattice. For low concentrations of Tb, i.e., when $x < 0.125$, a drop in the *ac* susceptibility at around 28 K is observed and is found to be independent of the value of x. This is found to be due

to domain wall pinning effects induced by a probable incommensurate-commensurate transition at Tb locality of the extended crystal lattice.

Ferromagnetic character is observed for the compositions with up to 12.5% of Tb ions, whereas a further increase of 0.5% results in magnetic cluster formation which behave like single domain particles. An increase of x beyond 0.125 results in further weakening of the magnetic order and magnetic clusters of shorter length scales are formed. This could be evidenced from the gradual decrease of the cusp temperature, T_B, when the concentration of the Tb ions approach the maximum value (here 25%). The irreversible behavior of ZFC and FC magnetization similar to that of magnetic nanoparticles suggests the superspin cluster formation beyond the critical value of $x = 0.125$. This points out the possibility of 1/8 ordering of Tb ions in the lattice and this limit could be called as superspin clustering limit in $La_{0.67-x}Tb_xCa_{0.33}MnO_3$. This behavior may be interpreted in terms of QCP also, as reported earlier for certain Ga-substituted manganites [Alo02, Det05]. However, a definite conclusion at this stage will be a premature one and more studies are required in order to explain various features of such nanoscale phase separation.

6.5 Studies on Superspin Clusters in $La_{0.67-x}Tb_xCa_{0.33}MnO_3$, $x = 0.13$, 0.15, and 0.25

A cusp like magnetic behaviour in the zero-field cooled magnetization (ZFCM) measurements and divergence of ZFCM and field cooled magnetization (FCM) below the cusp temperature are one of the characteristic properties of spin glasses [Myd93]. However, magnetic nanoparticle systems also show similar characteristics, known as superparamagnetic properties. Both systems show many similarities and hence it is very difficult to distinguish the spin glass and superparamagnetic systems from the FC/ZFC magnetization measurements alone [Dor92, Dor97]. Aging and memory ex-

periments can be used to distinguish the two systems. Fine magnetic particle systems can be of different type, depending on the strength of the interparticle interactions [Bat02]. It has been shown that when the interparticle interaction is negligible, the system is in the superparamagnetic (SPM) regime. However for dense nanoparticle systems, when strong interactions among the particles are present due to dipolar interactions and exchange interactions through the surface of the particles in contact, the systems may behave like spin glasses [Dor97]. The magnetic relaxation becomes slower when the degree of interaction increases [Lui02]. For the fine magnetic particles, each particle has a single spin called super spin (SP) and the interacting SPs exhibiting SG behaviour are termed as superspin glasses (SSG) [Dju97, Jon98a, Kle01, Sas05]. The SPM and SSG systems have been shown to be distinguishable by the nature of the FC magnetization curves, aging and relaxation effects. In the case of magnetic fine particles, the inter-particle interactions can be suppressed by dispersion in a non-magnetic matrix and the system can be driven from SSG to SPM [Dor97, Par05]. The low temperature magnetic features observed in certain Tb substituted manganite compositions as discussed in the preceeding section are similar to those of magnetic nanoparticles, owing to the formation of single domain clusters which can be regarded as superspins. The variation of the concentration of Tb in these compositions affects the magnetic features considerably, such as a well defined cusp and a decrease in the cusp temperature for larger concentrations of Tb. Thus, the studies on magnetic properties of compositions with $x = 0.13$, 0.15 and 0.25 in $La_{0.67-x}Tb_xCa_{0.33}MnO_3$ have been described in detail in this section.

6.5.1 Results and Discussion

The sample codes of LTC13, LTC15 and LTC25 have been used for identifying the samples with value of $x = 0.13$, 0.15, and 0.25, respectively henceforth in this section. The ZFCM and FCM curves of $La_{0.67-x}Tb_xCa_{0.33}MnO_3$ (LTC) for $x = 0.13$,

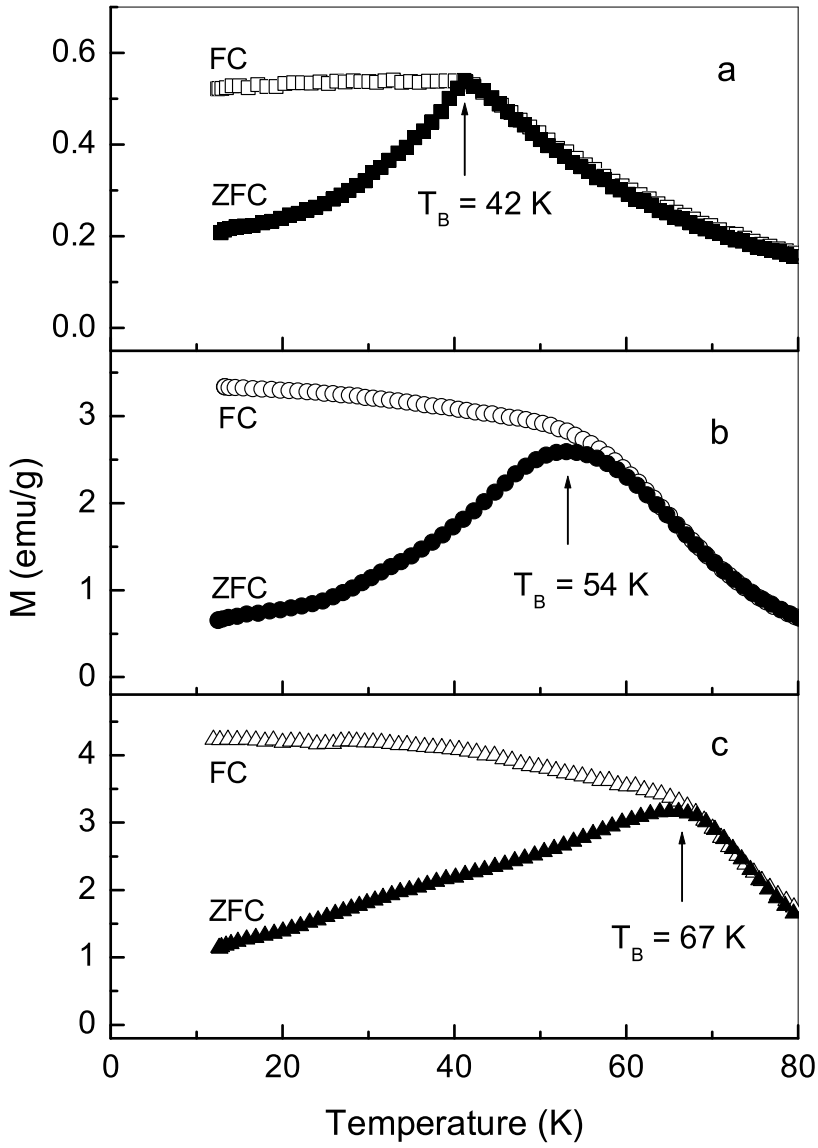

Figure 6.11: ZFC (filled symbols) and FC (open symbols) magnetization curves of $La_{0.67-x}Tb_xCa_{0.33}MnO_3$ for different Tb concentrations, measured at 50 Oe; (a) LTC25, (b)LTC15, and LTC13

0.15, and 0.25 are shown in Fig. 6.11. All the three compositions show a cusp in ZFCM and divergence between ZFCM and FCM below the cusp. Important features are the shift in the cusp to lower temperatures (identified as T_B hereafter) as the concentration of Tb is increased; from 67 K for LTC13 to 54 K for LTC15 and to 42 K for LTC25. The magnetization at low temperatures is decreased significantly with increasing Tb concentration. There are major differences in the nature of the FCM curves also as the temperature is decreased. FCM of LTC25 remains constant down to low temperatures below T_B whereas LTC15 and LTC13 show an increase in FCM below T_B. It is known that for SG systems the FC curve remains constant below T_B [Myd93]. FCM remains constant for interacting magnetic nanoparticles (SSG behaviour) whereas it increases continuously with decreasing temperature for non-interacting particles (SPM behaviour) [Sas05]. Generally, in the case of magnetic nanoparticles, the blocking temperature decreases with decreasing particle size and is expressed in terms of $K_{eff}V = 25k_BT_B$ where V is the volume of the particle and T_B is the blocking temperature [Cul72]. Based on the FCM behaviour below T_B and the shift in T_B, it can be assumed that in the case of $La_{0.67-x}Tb_xCa_{0.33}MnO_3$ the magnetic cluster size decreases with increasing concentration of Tb and the FM clusters are equivalent to interacting type of superspins resulting in SSG behaviour in LTC25 and non-interacting type leading to SPM behaviour in LTC15 and LTC13. These observations clearly indicate the role of Tb concentration in deciding the type of magnetic clusters and their interactions in these compositions. De Teresa *et al.* have observed magnetic cluster formation, which are typically having a size of 25 Å, for a similar composition with $x \sim = 0.17$, from the SANS studies [Det97]. From the support of this existing report on magnetic correlation lengths in $La_{0.67-x}Tb_xCa_{0.33}MnO_3$ [Det97], we can arrive at a conclusion that the large decrease of Mn-O-Mn bond angle in the vicinity of Tb helps in confining the magnetic exchange interactions within a shorter range to form SPs. The interactions between these SP clusters depend on

their size and distribution in the lattice.

Based on the assumption that the magnetic clusters in $La_{0.67-x}Tb_xCa_{0.33}MnO_3$ behave in a way similar to the fine magnetic particles, the size of the clusters can be calculated from the M versus H curves measured at a temperature above T_B where there is no magnetic hysteresis [Coe72] as described in section 5.3.2.

Following this procedure, the magnetic cluster sizes of LTC25, LTC15 and LTC13 were calculated from the M vs H curves measured at a temperature just above the respective T_Bs. In the low and high field limits, the cluster sizes were obtained as 29 Å and 25 Å for LTC25, 39 Å and 24 Å for LTC15, and 39 Å and 26 Å for LTC13, respectively. The lower limit of the magnetic cluster size is comparable, ∼25 Å, for all three compositions. It may be noted that the cluster size for LTC25 is comparable to the magnetic correlation length (18 Å) reported for $x = 0.22$ in $La_{0.67-x}Tb_xCa_{0.33}MnO_3$ [Det97], supporting the validity of the above assumptions. More over, the clusters are smaller with a narrow size distribution in LTC25 whereas larger and smaller clusters are present in LTC15 and LTC13.

SSG and SPM systems are known to exhibit aging and memory effects similar to SG systems under typical FC protocol [Jon98a, Sun03, Tso05, Zhe05] and general understanding is that a clear distinction between these two types of complex materials is not possible from such procedures. However, the present work suggests the possibility of identifying SSG and SPM types of behaviour in the magnetic cluster system. Results from typical double memory experiment (DME) are shown in Fig. 6.12 for the three compositions, measured following the FC protocol as described in section 2.4.2. During cooling, under a constant magnetic field of 50 Oe, the field was switched off (H = 0 Oe) at two temperatures T_1 and T_2 for a waiting time of $t_w = 3600$ s. The magnetization drops down during each waiting time (open symbols). The M-T measurement was repeated in the heating cycle after cooling to the lowest temperature, which clearly shows the memory effect (filled symbols). The same cooling or heating

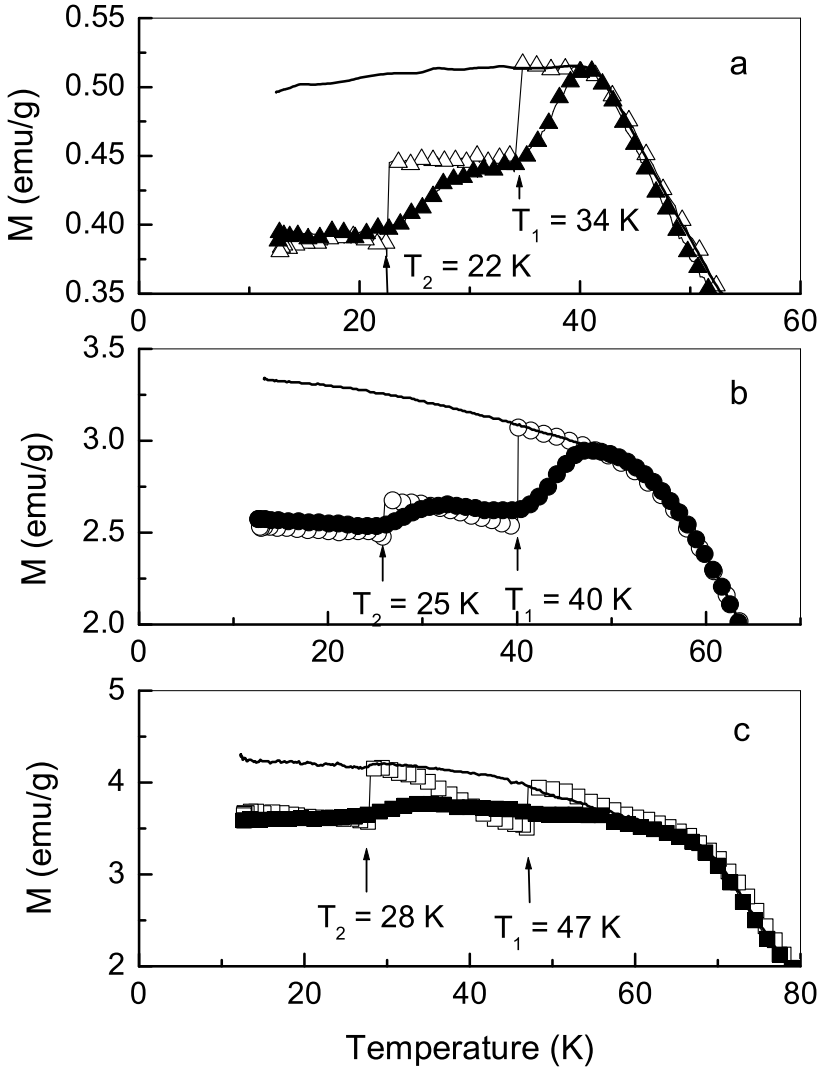

Figure 6.12: Aging effects in the FCM measurements during cooling (open symbols) and heating (filled symbols). The normal FCM curve without aging (solid line) for each composition is also shown for comparison; (a) LTC25, (b) LTC15, and (c) LTC13.

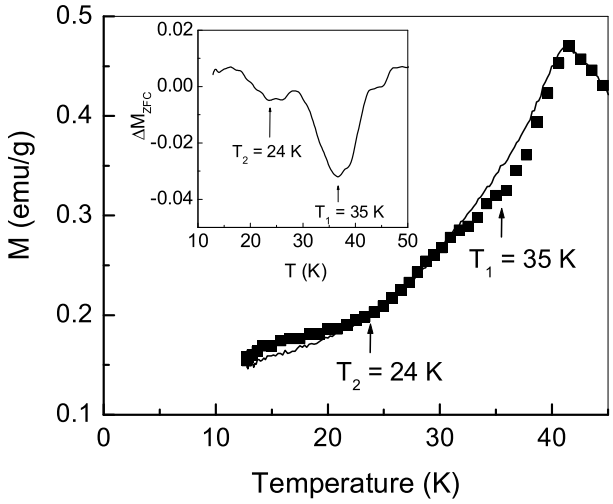

Figure 6.13: Aging effect in the ZFCM measurement of LTC25 with H = 0 Oe through out the cooling process. A waiting time of 3600 s was given at T_1 and T_2 during the ZFC process in one measurement (symbols) and continuously cooled without any aging in the second case (solid line). Inset: The difference between aged ZFCM(T) and normal ZFCM(T) (ΔM_{ZFC}(T).

rate (0.03 K s^{-1}) was maintained during the measurements [Jon98a, Zot03]. A clear aging effect is observed for LTC25 at two different temperatures, T_1 (34 K) and T_2 (22 K), below T_B (42 K). After an intermittent stop at T_1 for a waiting time of t_w = 3600 s and H = 0 while cooling, the magnetization remains constant till the next stop at T_2 and even below after aging at this temperature (Fig. 6.12(a)). That is, no rejuvenation effects are observed after aging. On the other hand, a similar DME for LTC15 exhibit weak rejuvenation effects after aging at T_1 = 40 K and T_2 = 25 K (T_B = 54 K) as shown in Fig. 6.12(b). Fig. 6.12(c) shows a strong rejuvenation below T_1 for LTC13 where the magnetization value progressively rises and touches the normal FCM curve as the temperature is decreased after the first aging. The rejuvenation effect at T_2 is weaker than that observed at T_1 ($T_2 < T_1$). This is likely to be due

to weak temperature (T)-chaos or cumulative aging effects which result in an apparent rejuvenation [Bou01]. Strongly interacting nanoparticle systems or SSGs do not show large rejuvenation effects [Jon05]. Hence, the present system consisting of small magnetic clusters can be thought of as interacting type (SSG) if the rejuvenation is weak or nil and noninteracting type (SPM) when sufficiently large rejuvenation is observed.

In order to confirm the SSG or SPM behaviour of the magnetic clusters, experiments on aging effects following the ZFC protocol are employed [Mat01b, Sah03, Zhe05]. The result of such a ZFC aging experiment for LTC25 is shown in Fig. 6.13. The difference between the aged and normal ZFCM curves, ΔM_{ZFC} (inset of Fig. 6.13), shows peaks at temperatures T_1 and T_2, where larger difference is observed at T_1. A comparison of ΔM_{ZFC} curves of all three compositions (Fig. 6.14) indicates that the system remembers the aged state at T_1 in LTC25 and LTC15 but not in LTC13. Aging effect in the ZFCM measurements is an evidence for interactions among the magnetic particles [Sas05]. This clearly points out the existence of strong interactions in the case of LTC25 and LTC15 and that the effect is more at a higher temperature T_1 than that at T_2 where $T_2 < T_1 < T_B$. On the other hand, larger aging effect is observed for LTC13 at a lower temperature T_2 than at T_1.

In terms of rejuvenation characteristics, it can be said that the interactions between smaller clusters lead to a stabler state. In the present case, the observed behaviour can be explained qualitatively using a droplet picture as suggested for SG systems [Jon00, Vin00]. An important factor which could be decisive in defining the interactive behaviour between the clusters during aging is likely to be the presence of strong and weak droplet pinning centers around Tb locality in the lattice. This model predicts the possibility of restricted growth of droplets having wide range of length scales at a fixed time scale and temperature, depending on the number and distribution of Tb ions in the lattice. This means that for a fixed time scale, instead

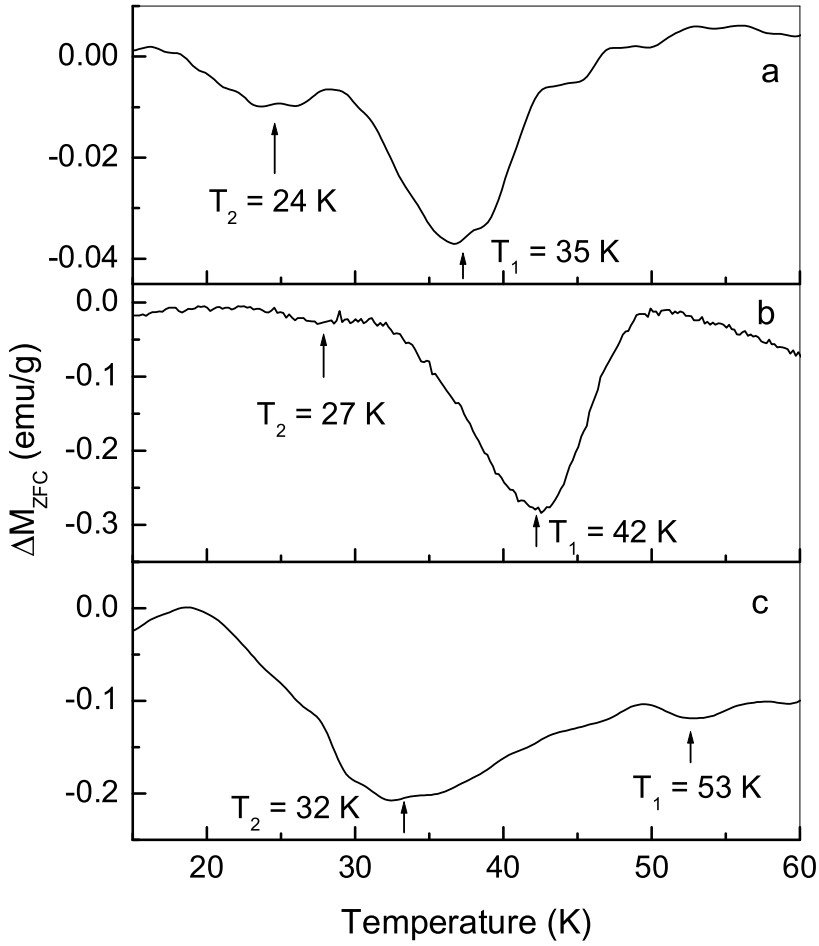

Figure 6.14: Comparison of the difference between aged ZFCM(T) and the normal ZFCM(T) (ΔM_{ZFC}) for three compositions; (a) LTC25, (b) LTC15, and (c) LTC13.

of defining the length scale as a function of temperature alone, a function representing the concentration and distribution of clusters is also important. It can be assumed that the droplets formed during aging at T_1 with larger length scales are blocked forming a metastable state, while those with smaller length scales relax down easily as temperature is further decreased till T_2. The rejuvenation depends on the stability of the blocked states.

In the case of FC aging of LTC25 at T_1, in which the concentration of pinning centers is more, the blocking of the droplets from reaching the new equilibrium when a finite field is applied, can assumed to be more effective during the negative temperature cycle. It is possible that the metastable states remain pinned due to very weak T-chaos [Bou01, Jon05]. The approximation of weak temperature chaos can be seen to be valid in the case of LTC15, where a weak rejuvenation effect is observed after aging (FC protocol) at T_1, though aging under ZFC protocol clearly suggested typical SSG behaviour. This apparent rejuvenation effect observed here can be attributed to the droplet size distribution which varies with the concentration of Tb ions. Since the Tb centers are less in this composition, the pinning may be weakened, and the state partially breaks up into individual clusters, once the field is applied below T_1. Hence there is a slight increase in magnetization till T_2. Aging at T_2 produces droplets with shorter but stabler length scales since the unpinning process is largely controlled by the thermal energy (also, a cumulative aging effect cannot be ruled out).

FCM aging studies in LTC13 (Fig. 6.12c) suggests that below T_1, the unpinning is complete with the field applied and the state formed at T_1 is unstable and will not be imprinted on the sample. A metastable state is formed when aged at T_2, below which the applied field is insufficient for the unpinning process and very weak rejuvenation is observed as in LTC15. For LTC13, a significant memory effect is observed at T_2 during heating corresponding to the weak rejuvenation whereas no memory effect is found at T_1 where strong rejuvenation is observed. Thus, in LTC13, we can assume

that there may be a distribution of clusters of different sizes, with more number of larger clusters. The results of the cluster size calculations is in direct support of this assumption. The larger clusters experience minimum inter-cluster interactions and smaller superspin clusters interact strongly resulting in SSG behaviour as in dense magnetic nanoparticle systems.

It is important to note from the FC aging results that, the memory effects are strong when samples are aged at T_1 in the case of LTC25 and LTC15, where no or weak rejuvenation is observed. On the other hand, no memory effect is observed when the rejuvenation is strong [Bou01]. This is in accordance with the droplet unpinning picture stated above. A similar behaviour is observed from the ZFC aging experiments also. The interacting cluster systems produce strong memory effects and the non-interacting clusters show no or weak memory effects in a typical ZFC aging process. This confirms the conclusion that as concentration of Tb in the composition decreases, interaction between the clusters gradually decreases and SSG state gradually results in SPM behaviour.

As the main contribution for the inter-cluster interactions, we can consider the anisotropy induced from dipolar interactions, as commonly observed in dense magnetic nanoparticles [Jon04]. Given a fixed time scale at a given temperature, the dipolar interactions between these clusters can result in the formation of metastable states (droplets). Another factor may be the anisotropic exchange interactions of the Dzyaloshinskii-Moriya (DM) type, which operate through the strongly distorted Mn-sublattice around Tb locality, as predicted in distorted lanthanum manganite [Sol96] and later on observed experimentally [Koi01]. DM exchange is known to produce large magnetic anisotropy in certain spin glass alloys [Fer80].

6.5.2 Conclusions

The characteristics of the magnetic clusters in some $La_{0.67-x}Tb_xCa_{0.33}MnO_3$ compositions are shown to be similar to that of the interacting and non-interacting behaviour of magnetic nanoparticle systems, depending on the concentration of Tb. A similar situation as in the case of magnetic fine particle systems can be envisaged at larger Tb concentrations, where the spin cluster confinement is due to the random distribution of Tb ions. This in turn controls the size of the clusters and result in the lowering of the Mn-O-Mn bond angle due to local structural distortion so that the exchange interaction becomes weak or impossible beyond the Tb centers.

The aging, rejuvenation, and memory effects are identified as reflections of interacting behaviour of small magnetic clusters in $La_{0.67-x}Tb_xCa_{0.33}MnO_3$. Different aging, memory, and rejuvenation effects are observed for these Tb substituted manganites, leading to superparamagnetic and superspin glass type characteristics. A change from SPM to SSG behaviour is possible when concentration of Tb is increased within the short range ordering limit.

Chapter 7

Double-peak Resistivity in Lanthanum Manganites

The perovskite-type substituted manganites are known to show metal-insulator (M-I) transition commensurate with the ferromagnetic-paramagnetic (FM-PM) transition. The double exchange mechanism explains the transport and magnetic characteristics of the manganites. But, the unexpectedly high values of resistance at the insulating region suggests the role of electron-lattice coupling in localizing the carrier (polaron formation). But anomalous double maxima in resistivity curves of some manganite compositions are observed. The presence of a second peak has been explained in terms of grain and grain boundary effects, phase separation etc. This chapter explains the origin of this double peak character observed in the resistivity curves of certain manganite compositions.

7.1 Introduction

The temperature dependence of resistivity of some hole-doped manganites show an unexpected second peak incommensurate with the FM-PM transition [Man97, Sun98, Abr99, Ver01, See04, Bel05]. Usually the second peak is observed at a lower temperature with respect to the first peak at the FM-PM transition temperature and it has a broad nature. Mandal *et al.* [Man97] have observed the double peak nature for Ce-

doped rare earth manganites. They have found that the shoulder-like feature grows into a peak, becomes more and more prominent with oxygen overdoping. They have also observed that the broad peak is not significantly affected by an external field, when compared to the commensurate M-I transition, and concluded that different origin may be possible for these features. The double peak resistivity nature is also found in a Gd-substituted lanthanum calcium manganites with oxygen nonstoichiometry and the origin of the double peak resistivity is attributed to the inhomogeneous oxygen content [Sun98]. The effect of grain and grain boundaries on the resistivity of $La_{0.7}Ca_{0.3}MnO_3$ has been studied by Vertruyen *et al.* [Ver01] and they have observed a shoulder-like feature in the resistivity below T_c of the material when the resistivity was measured across a single grain boundary, whereas within the grain a single M-I transition is observed. The role of grain boundary-like inhomogeneities have also been described by Belevtsev *et al.* [Bel05] for twinned crystals of $La_{0.67}Ca_{0.33}MnO_3$. The role of phase separation on the transport properties of Ru-substituted (at Mn sublattice) manganite compositions has been extensively studied by Raveau *et al.* [Rav00] and later by Seethalakshmi *et al.* [See04]. Raveau *et al.* [Rav00] suggests the possibility of competitive contribution from AFM-insulating regions and FM-metallic regions which causes two bumps in the resistivity curves. In a more comprehensive report, Seethalakshmi *et al.* [See04] describes the coexistence of two FM metallic phases causing the double peak resistivity behavior. The double peak character is also observed in certain composites which contain $La_{0.67}Ca_{0.33}MnO_3$ and Fe_3O_4 [Xia03]. It is suggested that, in these compositions, the magnetic domains related to the manganite phase and ferrite phase coexist at grain boundaries or surface layers which contribute to the double peak behavior of resistivity. A percolation model has been suggested by Tovtolytkin *et al.* [Tov99] for explaining the double peak character of the temperature dependence of resistance of manganites. Here, the coexistence of paramagnetic and ferromagnetic phases which have different types of conductivity,

over a wide range of temperature in the substituted manganites is considered to be responsible for the double peak character. Inter-grain tunneling mechanism has also been suggested in the case of fine particles of the substituted manganites as the origin of the double peak resistivity behavior [Zha97]. Thus, different origins for the double peak resistivity behavior in the manganites have been suggested. But, there are no systematic studies on this topic based on the variation of composition, reproducibility, processing conditions etc. Also, for the same material, this behavior is not always observed [Tok00, Rao98]. Thus, the various features of the double peak resistivity has been studied, taking the above factors into consideration. The origin of such a double peak resistivity in various hole-doped manganites is discussed in this chapter.

7.2 Synthesis

The conventional solid state reaction method has been used for the preparation of the samples as explained earlier. Three sets of different compositions have been prepared- (1) $La_{1-x}MnO_3$ where $0.031 \leq x \leq 0.125$ (LXMO - the same set of samples as described in chapter3), (2) $La_{0.67\pm y}Ca_{0.33}MnO_3$ and $La_{0.67}Ca_{0.33\pm y}MnO_3$ where y = 0 and 0.05 (LCYMO), and (3) $La_{1-x}Ca_xMnO_3$ (LCMO) where x varies between 0.395 and 0.365.

The resistivity of the samples were measured as a function of temperature by the four probe van der Pauw method as described in section 2.6. The *dc* and *ac* magnetic measurements were performed as explained in sections 2.4 and 2.5.

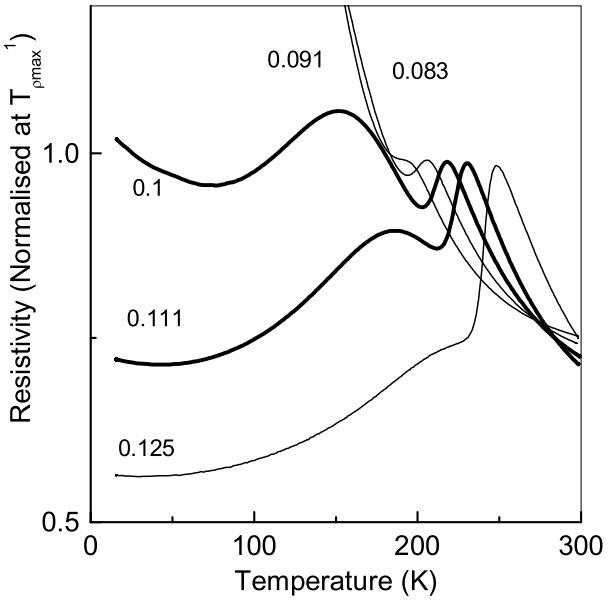

Figure 7.1: Temperature dependence of resistivity of $La_{1-x}MnO_3$ compositions. The arrows indicate the second peak observed for each compositions. The fractions indicate the values of x in $La_{1-x}MnO_3$

7.3 Results and Discussion

7.3.1 $La_{1-x}MnO_3$

The temperature dependence of the resistivity of the self doped compositions are shown in Fig. 7.1. All compositions show a metal-insulator transition (M-I) when the sample is cooled down from room temperature, commensurate with the respective ferromagnetic-paramagnetic (FM-PM) transition (as can be seen in Fig. 7.2). It can be seen that as the value of x in LXMO is decreased, a second maximum is observed in the resistivity curve. The temperature at which the first peak appeared during cooling the sample is designated as $T^1_{\rho_{max}}$. The *second peak* at $T^2_{\rho_{max}}$ is observed very close to the $T^1_{\rho_{max}}$ with a broad nature at a lower temperature. Also, the second peak

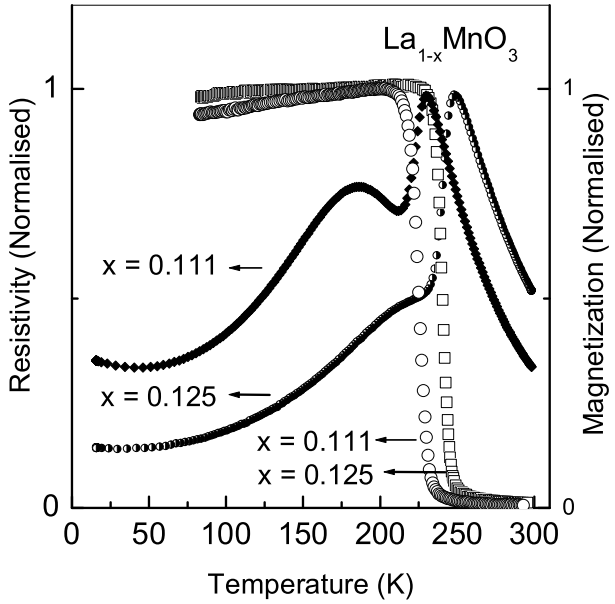

Figure 7.2: Temperature dependence of magnetization and resistivity of $La_{1-x}MnO_3$ compositions with $x = 0.125$ and $x = 0.111$.

at $T^2_{\rho_{max}}$ becomes more prominent as the value of x is decreased.

The temperature dependence of the ZFC magnetization and resistance of two LXMO samples with values of $x = 0.125$ and 0.111 are shown in Fig. 7.2. It is observed that the first peak at $T^1_{\rho_{max}}$ corresponds to the magnetic transition temperature, T_c, as observed in double exchange manganites. However, corresponding to $T^2_{\rho_{max}}$, there are no variations evident in the magnetization behavior for both the samples. The magnetization curves observed for the self-doped samples are sharp in nature for high values of x, but become broader as the value of x is decreased as explained in chapter 3. The broad nature of the magnetization curves are normally observed for the samples with high degree of compositional inhomogeneity. However, a conclusion based on the broadening of the magnetic transition in the M-T curves and concomitant

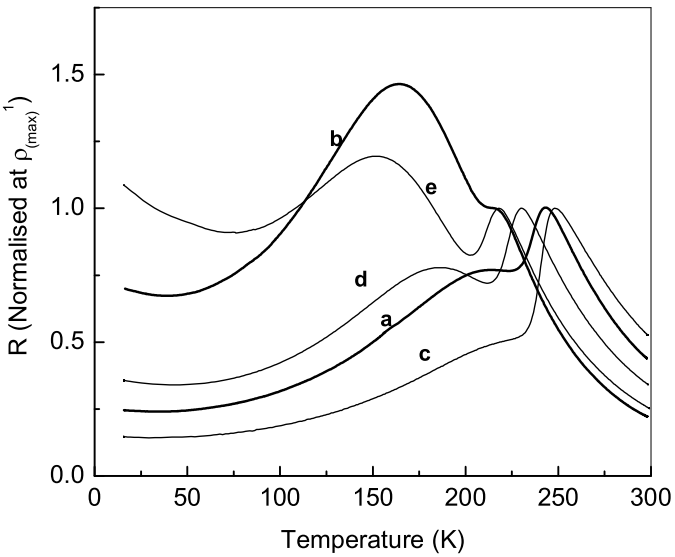

Figure 7.3: Temperature dependence of resistivity of $La_{1-x}MnO_3$ compositions processed at various temperature conditions. (a) $x = 0.125$ and (b)$x = 0.111$, powders were heated initially at 1273 K for 48 h, and pellets were sintered at 1573 K for 10 minutes. (c)$x = 0.125$, (d) 0.111, and (e) 0.10, were heated initially at 1273 K and then at 1473 K for 48 h each and pellets were sintered at 1473 K for 24 h.

enhancement of the double peak nature that the double peak resistivity is due to the compositional inhomogeneity will be a premature one. For this, a careful analysis of the resistivity behavior on the samples processing conditions has been done. Another set of samples with $x = 0.125$ and 0.111 were synthesized by ceramic method. The samples initially were fired at 1273 K for 48 h and then the pellets were sintered at 1573 K for 10 minutes. The samples were found to contain no phases other than the rhombohedral perovskite phase, from the XRD analysis, similar to that of the first batch of samples. The resistivity behavior of the second sets of samples are compared with that from the first batch sintered at 1473 K, in Fig. 7.3.

It can be seen that the double peak behavior is more prominent for the powder

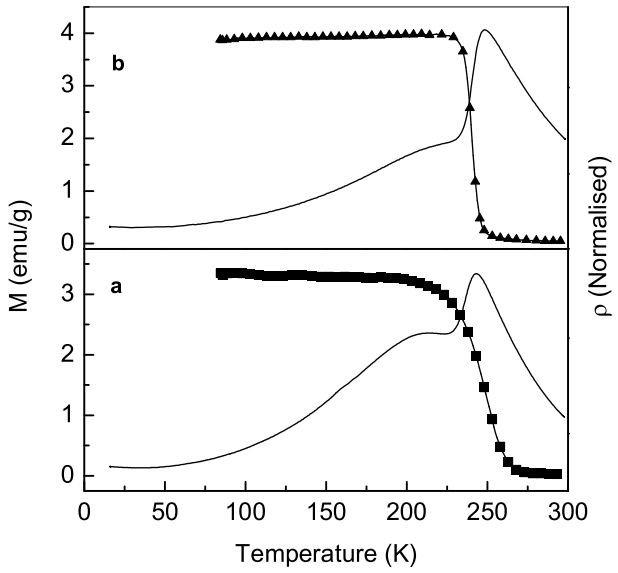

Figure 7.4: Temperature dependence of magnetization and resistivity of $La_{1-x}MnO_3$ compositions with $x = 0.125$ processed at (a) 1273 K, and pellet sintered at 1573 K for 10 minutes, (b) 1273 K and then at 1473 K for 48 h each and pellet was sintered at 1473 K for 24 h.

samples processed only at 1273 K when compared to that of the same processed at 1473 K. Correspondingly, a broad nature of the magnetic transition is also observed as shown in Fig. 7.4, which is known to be due to mixed phase behavior or compositional inhomogeneity, with possible values of $x = 0.125 \pm \Delta$, where Δ denotes very small values of x. However, the ferromagnetic transition temperature and the corresponding peak in the resistivity curve matches well and confirms the major phase as the one with $x = 0.125$. The sample with $x = 0.125$ in the second set showing the broad magnetic transition was then heated at 1473 K for 48 h, and a pellet was made and heated at 1473 K for 24 h. A sharp magnetic transition was observed after this thermal treatment of this sample and correspondingly, the magnitude of the *second peak* in the resistivity curve diminished. Similarly, for the sample with $x = 0.111$

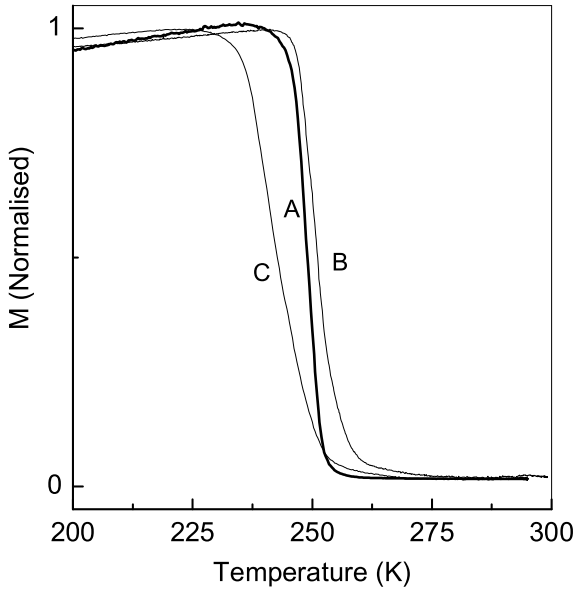

Figure 7.5: Temperature dependence of magnetization of $La_{0.67}Ca_{0.33}MnO_3$ compositions processed at various annealing conditions. A, B, and C corresponds to various heating conditions as given in the text.

and heated at 1273 K, there is a considerable variation of the $T^1_{\rho_{max}}$ when compared to that heated at 1473 K, as shown in Fig. 7.3. The peak at $T^1_{\rho_{max}}$, in the former corresponds to ∼225 K, which in turn corresponds to the $T^1_{\rho_{max}}$ of the sample with $x = 0.10$, processed at 1473 K. Thus, the processing conditions affect the nature of the resistivity and magnetization curves significantly. The probable reason for this processing dependence is the small scale phase separation, i.e., the formation of self-doped compositions with values of $x = x \pm \Delta$

For the well studied composition $La_{0.67}Ca_{0.33}MnO_3$, some reports show well defined single resistivity peak whereas there are also reports on the double peak resistivity behavior for this composition. Therefore, the processing condition dependence of the resistivity behavior is studied for the sample $La_{0.67}Ca_{0.33}MnO_3$ also , synthesized by

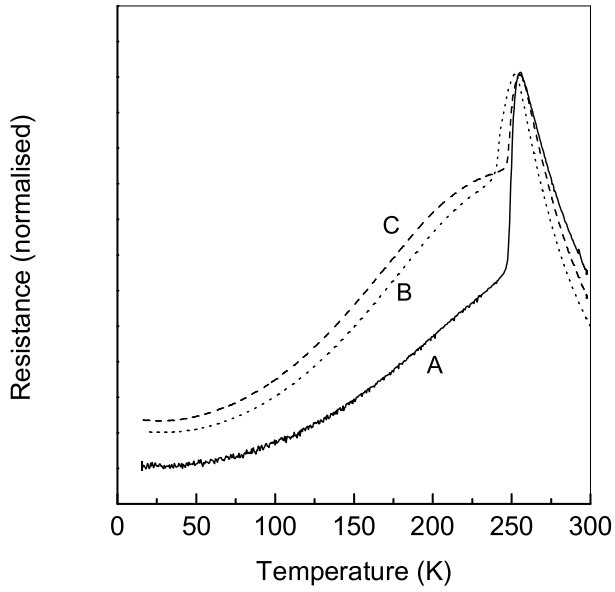

Figure 7.6: Temperature dependence of resistivity of $La_{0.67}Ca_{0.33}MnO_3$ compositions processed at various annealing conditions. A, B, and C corresponds to various heating conditions as given in the text.

he ceramic method. Three samples of the same composition have been synthesized by varying the heating conditions. The sample A was heated initially at 1273 K for 24 h, then at 1373 K for 24 h, 1473 K for 24 h, 1573 K at 48 h and finally sintered the pellet at 1623 K for 12 h. The sample B was heated at 1273 K, then at 1473 K and finally at 1573 K for 48 h each and finally the pellet is sintered at 1573 K. The sample C has been processed in a slightly different heating condition from that of sample A, and the powder sample was fired at 1673 K for 12 h before finally sintering the pellet at 1673 K for 12 h. Identical heating and cooling rates were maintained and the powder samples were ground well after each heating cycle in all the three cases. All the final samples were found to be single phase and with orthorhombic perovskite structure, from powder XRD analysis. All samples contain 33% ($\pm$1%) of Mn^{4+} ions,

as expected. The magnetization curves show magnetic transition corresponding to the resistivity peak at $T^1_{\rho_{max}}$, but a sharp transition is observed for the sample A, which become slightly broader in the case of B and much broader for the sample C as shown in Fig. 7.5. Concomitantly, the double peak nature is not observed for the sample A, but a broad shoulder peak is observed for samples B and C as shown in Fig. 7.6.

The distinct features observed in the electrical resistivity and magnetization curves point out that the processing conditions may affect the properties at least in two ways, the first being the phase separation or compositional inhomogeneity and the second is the microstructure changes such as grain and grain boundary modifications. It is also possible that the grain boundary modifications may be due to the small scale phase separation, where different phases are separated at the interior and near the grain boundaries [Bel05, Ver01]. These phases if formed, however cannot be identified from the techniques used in the present study due to the very minute changes in the compositions. However, this would be expected to affect the electronic transport to a large extent but not the bulk magnetic properties.

7.3.2 $La_{1-x}Ca_xMnO_3$ (LCMO) where $0.316 < x < 0.46$.

To verify whether the compositional dependence of the features in the electrical resistivity behavior of the self-doped $La_{1-x}MnO_3$ is a general behavior of the manganites or not, similar studies were made on the calcium substituted lanthanum manganite also. In order to see the changes in the resistivity behavior with Ca-concentration, a set of samples containing Ca in varying amounts in $La_{1-x}Ca_xMnO_3$ were prepared under identical conditions. A close analysis is made by selecting a narrow range of Ca-concentrations in $La_{1-x}Ca_xMnO_3$, with x = 0.316, 0.333, 0.35, 0.375, 0.4, 0.43, and 0.46. The estimated amount of Mn^{4+} in each composition was found to be matching with the expected values (within the error limit of ± 1), which suggests that the com-

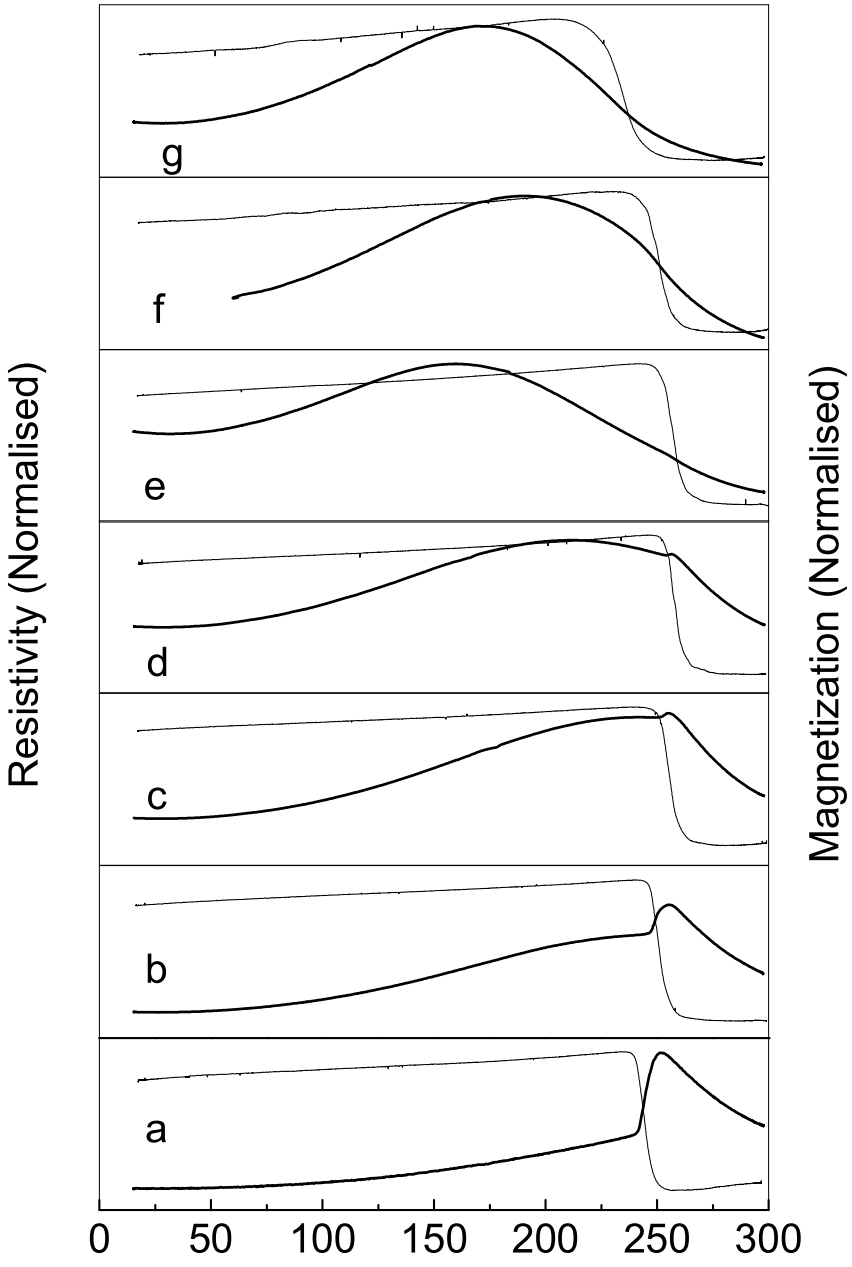

Figure 7.7: Temperature dependence of resistivity (normalized) and *ac* susceptibility (normalized) of $La_{1-x}Ca_xMnO_3$ compositions with x = (a) 0.316,(b) 0.333, (c) 0.35, (d) 0.375, (e) 0.4, (f) 0.43, and (g) 0.46

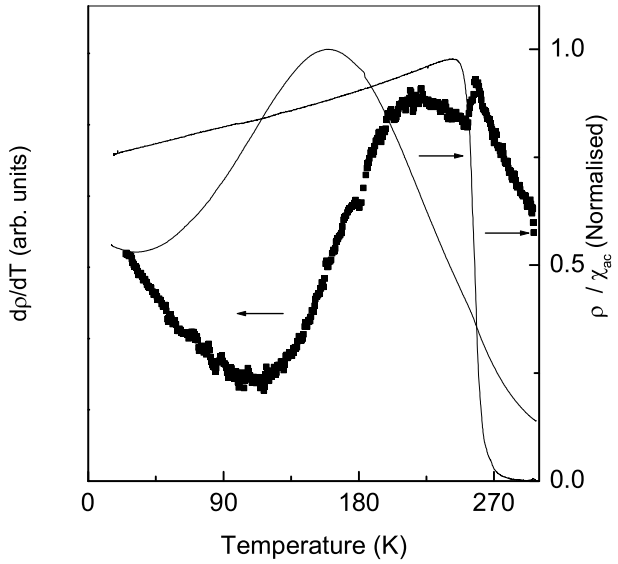

Figure 7.8: Derivative of the resistivity, $\frac{d\rho}{dT}$ and resistivity curves of $La_{1-x}Ca_xMnO_3$ composition with $x = 0.4$

positions contain no excess or deficient oxygen stoichiometry. The resistivity curves of all the compositions and the corresponding magnetization curves (as a function of temperature) are shown in Fig. 7.7. A clear M-I transition is observed for the sample with $x = 0.316$ at ∼250 K, and no anomalies in the resistivity curve is found below this temperature. But as the concentration of the Ca ions is increased to 0.333, a shoulder is appeared below the M-I transition at $T^1_{\rho max}$. The *second peak* observed at a lower temperature below the M-I transition is found to become prominent as the concentration of the Ca ions is increased further. The temperature corresponding to the maximum of resistivity visible from Fig. 7.7 is denoted as $T^2_{\rho max}$. As observed in the case of $La_{-1x}MnO_3$, no ferromagnetic transition is observed corresponding to the second resistivity peak for any of the compositions in $La_{1-x}Ca_xMnO_3$ and the magnitude of the second peak increases with increasing x. When $x = 0.375$, it can

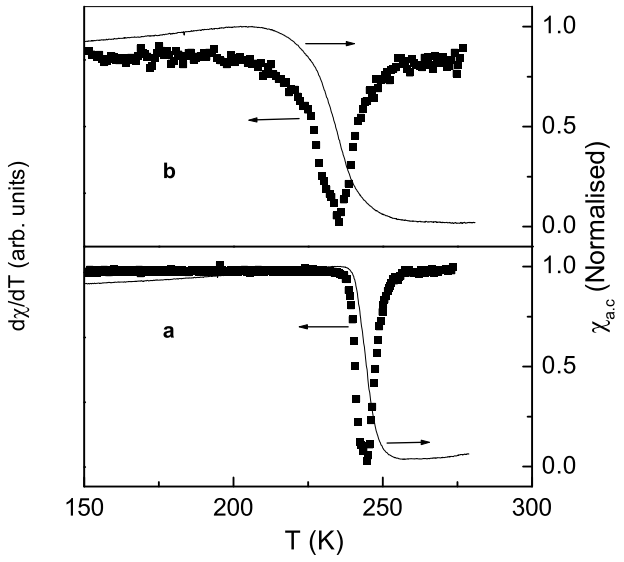

Figure 7.9: Derivative of the *ac* susceptibility, $\frac{d\chi}{dT}$ and *ac* susceptibility curves of $La_{1-x}Ca_xMnO_3$ compositions with x = (a) 0.316 and (b) 0.46

be seen that the peak resistivity observed at $T^2_{\rho max}$ is higher than that corresponding to $T^1_{\rho max}$. Further increase, however, results in the observation of only one peak as observed for the samples with $x = 0.4$, 0.43, and 0.46. But, it is evident from Fig. 7.7 that these peak positions do not match with the ferromagnetic transition temperatures. In fact, the maximum resistivity is observed at a much lower temperature than the T_c and the magnetic transitions of these compositions are unusually broad. Thus, the composition with $x = 0.4$, shows a broad maximum and no M-I transition corresponding to the ferromagnetic transition temperature. However, the derivative of the resistivity curve ($\frac{d\rho}{dT}$) of this composition shows two maxima, one of a sharp nature at the T_c and the other of broad nature as shown in Fig. 7.8. The sharp maximum owes to M-I transition corresponding to the ferromagnetic transition.

Broad M-I transitions which are not matching with the ferromagnetic transition

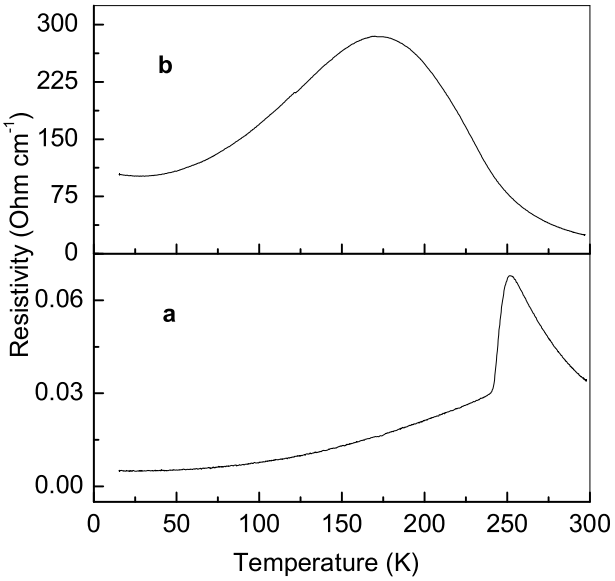

Figure 7.10: Resistivity curves of $La_{1-x}Ca_xMnO_3$ compositions with x = (a) 0.316 and (b) 0.46

temperatures are observed in several manganite compositions [Aru96]. Such an unusual behavior may be due to the overlapping contribution from the so called *second peak*. The origin of such a double peak character can be again speculated from the nature of the magnetization curves, where a broad magnetic transition is observed for the sample (x=0.46) with largest contribution of the *second peak*, whereas a sharp ferromagnetic transition is observed for the sample, which shows no double peak in the resistivity curve(x = 0.316). The broadness of the magnetic transitions in the *ac* susceptibility curves of these two samples are shown in Fig. 7.9 and can be easily identified from the derivative curves. The resistivity curves of the samples with x = 0.46 and x = 0.316 are shown in Fig. 7.10 for comparison. Though these end-compositions (in the present study) differ much in terms of their physical properties, the sharpness of the ferromagnetic transition does not vary considerably in the rest

of the compositions. This may be due to the closeness of the values of T_c of all these compositions which lie in the range 245-255 K. It is possible that as the amount of Ca increases, small scale phase separation is ensued which explains the broad magnetic transition and the concomitant observation of double peak resistivity.

7.3.3 $La_{0.67+y}Ca_{0.33}MnO_3$ and $La_{0.67}Ca_{0.33+y}MnO_3$ where $y = 0$ and ± 0.05 (LCYMO)

In order to study the role of cation deficiency or excess on the resistivity and magnetization behavior of lanthanum calcium manganites, two series of compositions, with the general formula $La_{0.67+y}Ca_{0.33}MnO_3$ and $La_{0.67}Ca_{0.33+y}MnO_3$ were studied for the values of y fixed as ± 0.05. The XRD patterns show the reflections due to orthorhombic unit cell with *pbnm* space group for all the compositions and no impurity peaks are observed for any of these samples as shown in Fig. 7.11. It is found that the amount of Mn^{4+} in the parent composition of the first series ($x = 0.33$) matches with the expected value. But, when a deficiency of La or Ca ions equivalent to 0.05 moles is introduced, the estimated amount of Mn^{4+} becomes 28% and 24% respectively, which are less than the expected values. This may be thought to be due to the formation of oxygen deficient compositions as found in the case of self-doped compositions (discussed in detail in Chapter 3).

However, an excess amount of La or Ca ions in the parent composition produces almost the expected amount of Mn^{4+} ions, i.e., 30% each (within the expected range, since a particular composition may not be defined). The *ac* susceptibility and resistivity curves measured for these samples are given in Fig. 7.12. It can be seen that the *second peak* is prominent in the resistivity curves when excess of La or Ca ions are introduced. From Fig. 7.12, it is also clear that, the ratio of the resistivity maximum at $T^2_{\rho max}$ and $T^1_{\rho max}$, i.e., $\rho_{max}(T_2)/\rho_{max}(T_1)$ is the highest when an excess amount of La is introduced. In the compositions with excess La or Ca is present,

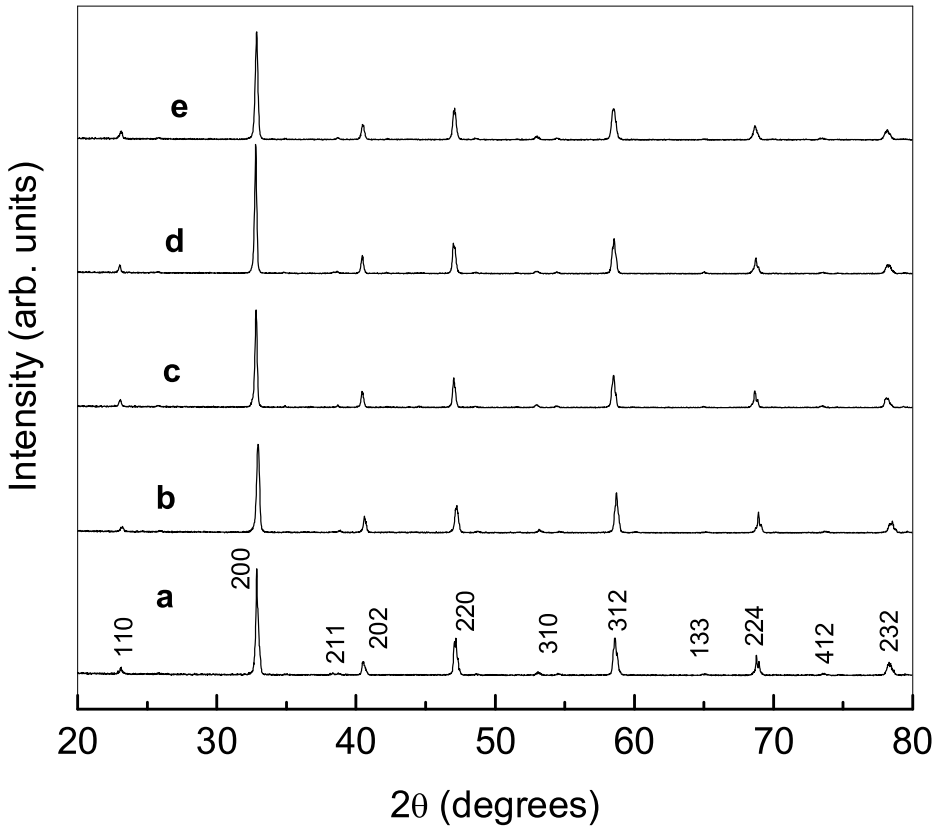

Figure 7.11: The powder XRD patterns of $La_{1-x+y}Ca_xMnO_3$, where $x = 0.33$ and y = (a) 0, (b) -0.05 (d) +0.05; and $La_{1-x}Ca_{x+y}MnO_3$ where $x = 0.33$ and $y =$ (c) -0.05 and (e) +0.05.

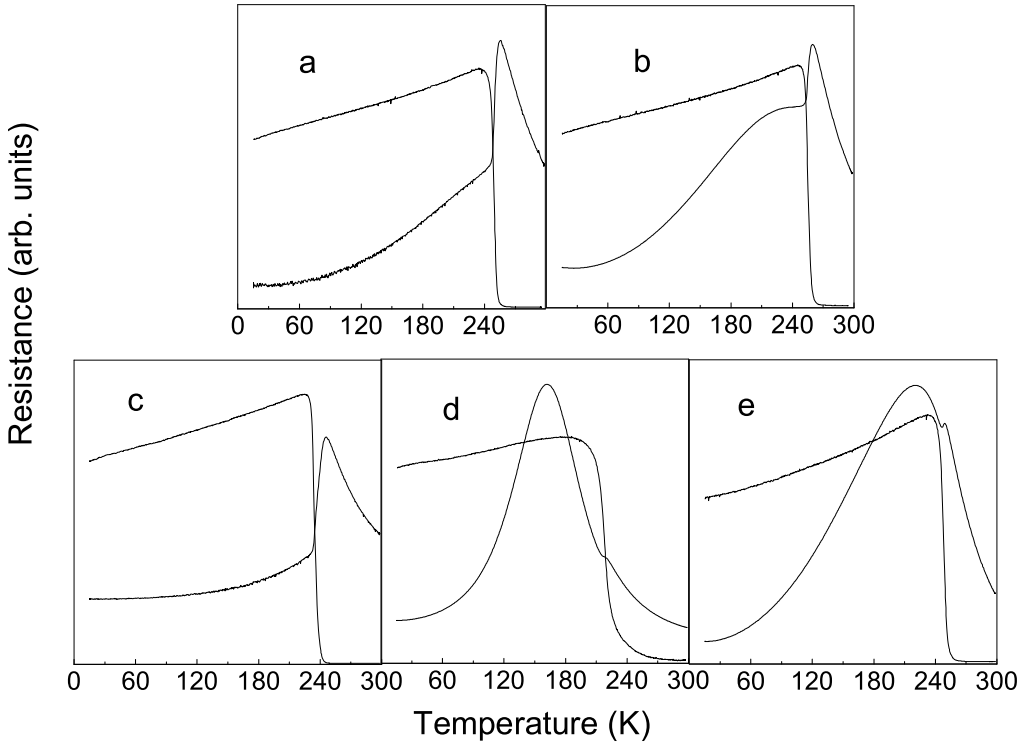

Figure 7.12: Resistivity and *ac* susceptibility curves of $La_{1-x+y}Ca_xMnO_3$, where x = 0.33 and y = (a) 0, (b) -0.05 (c) +0.05; and $La_{1-x}Ca_{x+y}MnO_3$ where $x = 0.33$ and y = (d) -0.05 and (e) +0.05.

an M-I transition is observed at T_c corresponding to the FM-PM transition and at a temperature lower than T_c, the *second peak* is observed. For this composition, the FM-PM transition is also found to be broad showing the typical nature of small scale phase separation. It is important here to note that, there is no correlation between the low-temperature magnetic anomaly observed in certain manganites as discussed in the chapter 3 for the self-doped lanthanum manganites and the current problem of double peak resistivity. The observation of both these anomalies in self-doped

compositions are rather accidental. However, such an apparent correlation is found to be invalid from the current studies on a number of compositions. Also, an unusual shift of M-I transition to a lower temperature than expected as observed in the case of $La_{0.54}Ca_{0.46}MnO_3$ can be attributed to the significant contribution from the *second peak*, which in fact hides the M-I transition that is usually observed at ferromagnetic transition temperature.

The phase separation scenario explains the double peak resistivity nature of lanthanum manganites by considering two important factors- firstly, the individual contribution of various phases present with compositions very much close to that of the major one that leads to a well defined FM-PM transition and concomitant M-I transition [Sun98, See04] and secondly the grain and grain boundary modifications [Ver01, Hua02, Bel05, Par04]. The fact that the second peak undergoes a magnetoresistive effect (at large field strengths), though sparingly, points out the role of different phases present in the sample as reported by Belevtsev *et al.* [See04, Bel05]. The separated phases existing in the sample may be of FM type alone or FM and AFM types, or FM and PM types [Tov99, Pog99, Rav00, Pra01]. The broadness of ferromagnetic transition also suggests the small scale phase separation. An equally possible mechanism which would result in the same type of double peak characteristics is the phase separation at grain boundaries [Ver01, Bel05]. It has been shown that the grain boundary regions have a smaller T_c than the interior of the grain and as a result, when the interior of the grain becomes FM and metallic, the grain boundary region remains PM and insulating [Bel05]. This offers a greater resistance for electronic conduction at the grain boundary regions. However, as cooling proceeds, the phases present at grain boundary regions become ferromagnetic and metallic, as a result the conductivity increases, ultimately resulting in the formation of a *second peak* in the resistivity curve below the T_c of the major phase (core of the grain). This explanation is in par with the results obtained with the self-doped compositions and

other La-Ca-Mn-O compositions.

Another possible factor to be considered is the intergrain connectivity [Bib03, Xia03, Xu05]. Had the weak inter-grain connectivity been the cause of *second peak* in resistivity curves, there should not be an appreciable effect of magnetic field. Hence no peak in the magnetoresistance curve would have been observed. But the results obtained by various groups show a second maximum observed in the magnetoresistive behavior below the M-I transition temperature. This suggests that the *second peak* is a feature completely originated from the sample properties. Similarly, grain boundaries offer a natural place for domain boundaries in ferromagnets. Thus, domain wall scattering at grain boundaries may cause such a double peak resistivity nature and correspondingly two peaks in the magnetoresistance [Ryb05]. However, in this case, a corresponding broadening of the magnetic transition is not expected. The possibility of formation of insulating tunnel barriers as envelopes for the FM-metallic phase also cannot be discarded [Bib03]. Such insulating tunnel barriers may be located at the surface of the grains. Thus, from various experimental observations made from the studies on magnetic and electronic transport characteristics, it has been identified that the probable cause for the double peak resistivity in certain lanthanum manganites is small scale phase separation.

7.4 Conclusions

A second M-I transition is observed at a lower temperature when compared to the M-I transition associated with the FM-PM transition for various manganite compositions. This double peak resistivity behavior and the dependence of double peak character on the processing conditions are also studied. By a comparison of double peak character with the magnetic properties of the compositions, it has been concluded that, the origin of the double peak resistivity behavior is small scale phase separation, a

scenario which is an inherent feature of these mixed oxides. It is found that when the concentration of Ca ions in $La_{1-x}Ca_xMnO_3$ increases from 0.316 to 0.46, the second peak becomes gradually prominent and finally results in a broad resistivity peak which does not correspond to the FM-PM transition. This is, in fact, due to the very large contribution of the *second peak* which effectively hides the M-I transition at the ferromagnetic transition temperature.

Bibliography

[Abi05] Abiko, S., Niidera, S., and Matsubara, F., *Phys. Rev. Lett.* **94** 227202 [2005]

[Abr99] Abramov, V. S., Pashchenko, V. P., Khartsev, S. I., and Cherenkov, O. P., *Func. Mater.* **6** 64 [1999]

[Alo97a] Alonso, J. A., Martinez-Lope, M. J., Casais, M. T., MacManus-Driscoll, J. L., De Silva, P. S. I. P. N., Cohen, L. F., and Fernandez-Diaz, M. T., *J. Mater. Chem.* **7** 2139 [1997]

[Alo97b] Alonso, J. A., Martizez-Lope, M. J., Casais, M. T., and Munoz, A., *Solid State Commun.* **102** 7 [1997]

[Alo00] Alonso, J. A., Martinez-Lope, M. J., Casais, M. T., and Fernandez-Diaz, M. T., *Inorg. Chem.* **39** 917 [2000]

[Alo02] Alonso, J. L., Fernandez, L. A., Guinea, F., Laliena, V., and Martin-Mayor, V., *Phys. Rev. B* **66** 104430 [2002]

[Alo03] Alonso, J. M., Arroyo, A., Gonzalez-Calbet, J. M., Hernando, A., Rojo, J. M., and Vallet-Regi, M., *Chem. Mater.* **15** 2864 [2003]

[And55] Anderson, P. W. and Hasegawa, H., *Phys. Rev.* **100** 675 [1955]

[Aru96] Arulraj, A., Mahesh, R., Subbanna, G. N., Mahendiran, R., Raychaudhuri, A. K., and Rao, C. N. R., *J. Solid State Chem.* **127** 87 [1996]

[Baj00] Bajpai, A., and Banerjee, A., *Phys. Rev. B* **62** 8996 [2000]

[Bar98] Barnabe, A., Millange, F., Maignan, A., Hervieu, M., Raveau, B., Van Tendeloo, G., and Laffez, P., *Chem. Mater.* **10** 252 [1998]

[Bat02] Battle, X., and Labarta, A., *J. Phys. D: Appl. Phys.* **35** R15 [2002]

[Bel04] Belevtsev, B. I., *Fiz. Niz. Temp.* **30** 563 [2004]

[Bel05] Belevtsev, B. I., Naugle, D. G., Rathnayaka, K. D. D., Parasiris, A., and Fink-Finowicki, J., *Physica B* **355** 341 [2005]

[Ben90] Bencini, A. and Gatteschi, D., *EPR of Exchange Coupled Systems* Springer-Verlag, Heidelberg [1990]

[Ber04] Bert, F., Dupuis, V., Vincent, E., Hammann, J., and Bouchaud, J.-P., *Phys. Rev. Lett.* **92** 167203 [2004]

[Bez02] Beznosov, A. V., Belevtsev, B. I., Fertman, E. L., Desnenko, V. A., Nangle, D. G., Rathnayaka, K. D. D., and Parasiris, A., *Fiz. Niz. Temp.* **28** 774 [2002]

[Bib03] Bibes, M., Balcells, Ll., Fontcuberta, J., Wojcik, M., Nadolski, S., and Jedryka, E., *Appl. Phys. Lett.* **82** 928 [2003]

[Bla96] Blasco, J., Garcia, J., De Teresa, J. M., Ibarra, M. R., Algarabel, P. A., Marquina, C., *J. Phys.: Condens. Matter.* **8** 7427 [1996]

[Bla97] Blasco, J., Garcia, J., De Teresa, J. M., Ibarra, M. R., Algarabel, P. A., Marquina, C., and Ritter, C., *Phys. Rev. B* **55** 8905 [1997]

[Bla02] Blasco, J., Garcia, J., Sanchcz, M. C., Campo, J., Subias, G., and Perez-Cacho, J., *Eur. Phys. J. B* **30** 469 [2002]

[Bos04] Bosak, A., Dubourdieu, C., Audier, M., Senateur, J. P., and Pierre, J., *J., Appl. Phys. A* **79** 1979 [2004]

[Bou01] Bouchaud, J.-P., Dupuis, V., Hammann, J., and Vincent, E., *Phys. Rev. B* **65** 024439 [2001]

[Bra03] Bracchi, A., Samwer, K., Schneider, S., and Loffler, J. F., *Appl. Phys. Lett.* **82** 721 [2003]

[Bus03] Buschow, K. H. J. and De Boer, F. R., *Physics of Magnetism and Magnetite Materials* Kluwer Academic/Plenum Publishers, Newyork [2003]

[Can71] Cannella, V., Mydosh, J. A., and Budnick, J. I., *J. Appl. Phys.* **42** 1689 [1971]

[Can01] Cannas, C., Concas, G., Gatteschi, D., Falqui, A., Musinu, A., Piccaluga, G., Sagregorio, C., and Spano, G., *Phys. Chem. Chem. Phys.* **3** 832 [2001]

[Car03] Cardoso, C. A., Araujo-Moreira, F. M., Awana, V. P. S., Takayama-Muromachi, E., de Lima, O. F., Yamauchi, H., and Karppinen, M., *Phys. Rev. B* **67** 020407 [2003]

[Cas99] Castro, M., Burriel, R., and Cheong, S. W., *J. Magn. Magn. Mater.* **196-197** 512 [1999]

[Cau98] Causa, M. T., Tovar, M., Caneiro, A., Prado, F., Ibanez, G., Ramos, C. A., Butera, B., Alascio, B., Obradors, X., Pinol, S., Rivadulla, F., Vazquez-Vazquez, V., Lopez-Quintela, M. A., Rivas, J., Tokura, Y., and Oseroff, S. B., *Phys. Rev. B* **58** 3233 [1998]

[Cha04] Chang, H., Guo, Y., Liang, J., and Rao, G., *J. Magn. Magn. Mater.* **278** 306 [2004]

[Che00] Chen, G. J., Chang, Y. H., and Hsu, H. W., *J. Magn. Magn. Mater.* **219** 317 [2000]

[Che98] Chen, Q. and Zhang,Z. J., *Appl. Phys. Lett.* **73** 3156 [1998]

[Chi90] Chick, L. A., Pederson, L. R., Moupin, G. D., Bates, D. L., Thomas, L. E., and Exarhos, G. J., *Mater. Lett.* **10** 6 [1990]

[Coe99] Coey, J. M. D., Viret, M., and von Molnar, S., *Adv. Phys.* **48** 167 [1999] and references therein

[Coe72] Coey, J. M. D., and Khalafalla, D., *Phys. Stat. Sol. (a)* **11** 229 [1972]

[Cor04] Cordero, F., Cracium, F., Franco, A., Piazza, D., and Galassi, C., *Phys. Rev. Lett.* **93** 097601 [2004]

[Cul56] Cullity, B. D., *Elements of X-ray Diffraction* Addison-Wesley Publishing Company, Inc. Massachustts [1956]

[Cul72] Cullity, B. D., *Introduction to Magnetic Materials* Reading: Addison-Wesley Publishing Company, Inc. Massachusetts [1972]

[Cus01] Cussen, E. J., Rosseinsky, M. J., Battle, P. D., Burley, J. C., Spring, L. E., Vente, J. F., Blundell, S. J., Coldea, A. I., and Singleton, J., *J. Am. Chem. Soc.* **123**, 1111 [2001]

[Dag03] Dagotto, E., (Ed.) *Nanoscale Phase Transition and Colossal Magneto-Resistance* Springer Verlag, Berlin [2003]

[Deb99] de Brion, S., Ciorcas, F., Chouteau, G., Lejay, P., Radaelli, P., and Chaillout, C., *Phys. Rev. B* **59** 1304 [1999]

[Deg60] de Gennes, P.-G., *Phys. Rev.* **118** 141 [1960]

[Dem98] Dempsey, N. M., Ghidini, M., Nozieres, J. P., Smith, P. A. I., Gervais, B., and Coey, J. M. D., *Phys. Rev. Lett.* **81** 5652 [1998]

[Des98] de Silva, P. S. I. P. N., Ricahrds, F. M., Cohen, L. F., Alonso, J. A., Martizez-Lope, M. J., Casais, M. T., Thomas, K. A., and MacManus-Driscoll, J. L., *J. Appl. Phys.* **83** 394 [1998]

[Det96] De Teresa, J. M., Ibarra, M. R., Garcia, J., Blasco, J., Ritter, C., Algarabel, P. A., Marquina, C., and del Moral, A., *Phys. Rev. Lett.* **76** 3392 [1996]

[Det97] De Teresa, J. M., Ritter, C., Ibarra, M. R., Algarabel, P. A., Garcia-Munoz, J. L., Blasco, J., Garcia, J., and Marquina, C., *Phys. Rev. B* **56** 3317 [1997]

[Det05] De Teresa, J. M., Algarabel, P. A., Ritter, C., Blasco, J., Ibarra, M. R., Morellon, L., Espeso, J. I., and Gomez-Sal, J. C., *Phys. Rev. Lett* **94** 207205 [2005]

[Dez02] Dezanneau, G., Sin, A., Roussel, H., Vincent, H., and Audier, M., *Solid State Commun.* **121** 133 [2002]

[Dez04] Dezanneau, G., Auider, M., Vincent, H., Meneghini, C., and Djurado, E., *Phys. Rev. B* **69** 014412 [2004]

[Dha04] Dhahri, R., and Halouni, F., *J. Alloys Compds.* **381** 21 [2004]

[Dha05] Dhahri, Ja., Zemni, S., Cherif, K., Dhahri, J., Oumezzine, M., Ghedira, M., and Vincent, H., *J. Alloys Compds.* **394** 51 [2005]

[Dho99] Dho, J., Kim, H., Lee, S., Kim, K. H., Lee, H. J., Jung, L. H., and Noh, T. W., *Phys. Rev. B* **59** 492 [1999]

[Dho02] Dho, J., Kim, W. S., and Hur, N. H., *Phys. Rev. Lett.* **89** 027202 [2002]

[Dju97] Djurberg, C., Svedlindh, P., Nordblad, P., Hansen, M. F., Bodker, F., and Morup, S., *Phys. Rev. Lett.* **79** 5154 [1997]

[Dor88] Dormann, J. L., Bessais, L., and Fiorani, D., *J. Phys. C: Solid State Phys.* **21** 2015 [1988]

[Dor92] Dormann, J. L. and Fiorani, D., (Eds.) *Magnetic Properties of Fine Particles*, North-Holland, Amsterdam [1992]

[Dor97] Dormann, J. L., Fiorani, D., and Tronc, E., *Adv. Chem. Phys.* **98** 283 [1997]

[Dup01] Dupuis, V., Vincent, E., Bouchaud, J.-P., Hammann, J., Ito, A., and Katori, H. A., *Phys. Rev. B* **64** 174204 [2001]

[Dut03] du Tremolet de Lacheisserie, E., Gignoux, D., Schlenker, M., (Eds.) *Magnetism Fundamentals*, Kluwer Academic Publishers [2003]

[Ele71] Elemans, J. B. A. A., Van Laar, B., Van Der Veen, K. R., and Loopstra, B. O., *J. Solid State Chem.* **3** 238 [1971]

[Fer80] Fert, A., and Levy, P. M., *Phys. Rev. Lett.* **44** 1538 [1980]

[Fer97] Ferris, V., Goglio, G., Brohan, L., Joubert, O., Molinie, P., Ganne, M., and Dordor, P., *Mater. Res. Bull.* **32** 763 [1997]

[Fio99] Fiorani, D., Dormann, J. L., Cherkaoui, R., Tronc, E., Lucari, F., D'Orazio, F., Spinu, L., Nogues, M., Garcia, A., and Testa, A. M., *J. Magn. Magn. Mater.* **196-197** 143 [1999]

[Fis88a] Fisher, D. S. and Huse, D. A., *Phys. Rev. B* **38** 373 [1988]

[Fis88b] Fisher, D. S. and Huse, D. A., *Phys. Rev. B* **38** 386 [1988]

[Fon59] Foner, S., *Rev. Sci. Inst.* **30** 548 [1959]

[Fre01] Freitas, R. S., and Ghivelder, L., *Phys. Rev. B* **64** 144404 [2001]

[Fre02] Freitas, R. S., Ghivelder. L., Levy, P., and Parisi, F., *Phys. Rev. B* **65** 104403 [2002]

[Gec01] Geck, J., Buchner, B., Hucker, M., Klingeler, R., and Gross, R., *Phys. Rev. B* **64** 144430 [2001]

[Ghi99] Ghivelder, L., Castillo, I. A., Gusmao, M. A., Alonso, J. A., and Cohen, L. F., *Phys. Rev. B* **60** 12184 [1999]

[Gol26] Goldschimdt, V. M., *Akad. Oslo. J. Natur.* **2** 7 [1926]

[Goo55] Goodenough, J. B., *Phys. Rev.* **100** 564 [1955]

[Goo61] Goodenough, J. B., Wold, A., Arnott, R. J., and Menyuk. N., *Phys. Rev.* **124**, 373 [1961]

[Goo63] Goodenough, J. B., *Magetism and the Chemical Bond* Interscience Publishers, New York [1963]

[Goo70] Goodenough, and J. B., Longo, J. M., *Magnetic and Other Properties of Oxides and Related Compounds* Hellwege, K. -H., Hellwege, A. M., (Eds.), Landolt-Börnstein New Series, Springer-Verlag, Berlin, **III**/4a 126 [1970]

[Goo98] Goodenough, J. B., *Annu. Rev. Mater. Sci.* **28** 1 [1998]

[Gor04] Gorkov, L. P. and Kresin, V. Z., *Phys. Rep.* **400** 149 [2004]

[Got04] Goto, T., Kimura, T., Lawes, G., Ramirez, A. P., and Tokura, Y., *Phys. Rev. Lett.* **92** 257201 [2004]

[Gup95] Gupta, A., McGuire, T. R., Duncombe, P. R., Rupp, M., Sun, J. Z., Gallagher, W. J., and Xiao, G., *Appl. Phys. Lett.* **67** 3494 [1995]

[Han03] Hanh, N., Quy, O. K., Thuy, N. P., Tung, L. D., and Spinu, L., *Physica B* **327** 382 [2003]

[Has04] Hasanain, S. K., Shah, W. H., Mumtaz, A., Nadeem, M., and Akhtar, M. J., *J. Magn. Magn. Mater.* **271** 79 [2004]

[Hau96] Hauback, B. C., Fjellvag, H., and Sakai, N., *J. Solid State Chem.* **124** 43 [1996]

[Hel00] Hellman, F., Queen, D. R., Potok, R. M., and Zink, B. L., *Phys. Rev. Lett.* **84** 5411 [2000]

[Hon04] Hong, C. S., Hur, N. H., and Choi, Y. N., *Solid State Commun.* **131** 779 [2004]

[Hua85] Huang, Y. C., *J. Magn. Magn. Mater.* **51** 1 [1985]

[Hua02] Huang,Y.-H., Yan, C.-H., Luo, F., Song, W., Wang, Z.-M., .and Liao, C.-S.,*Appl Phys Lett* **81** 76 [2002]

[Hwa95] Hwang, H.Y., Cheong, S.-W., Radaelli, P. G., Marezio, M., and Batlogg, B., *Phys. Rev. Lett.* **75** 914 [1995]

[Iva00] Ivanshin, V. A., Deisenhofer, J., Krug Von Nidda, H.-A., Loidl, A., Mukhin, A. A., Balbashov, A. M., and Eremin, M. V., *Phys. Rev. B* **61** 6213 [2000]

[Jef97] Jeffery, G. H., Bassett, J., Mendham, J., and Denney, R. C., *Vogel's Textbook of Quantitative Analysis* Fifth Edition Addision Wesley Longman Limited, Edinburgh [1997]

[Jim97] Jimenez, M., Martinez, J. L., Herrero, E., Alonso, J., Prieto, C., de Andres, A., Vallet-Regi, M., Gonzalez-Calbet, J., and Fernandez-Diaz, M. T., *Physica B* **234-236** 708 [1997]

[Jin94] Jin, S., Tiefel, T. H., McCormack, M., Fastnacht, R. A., Ramesh, R., and Chen, L. H., *Science* **264** 413 [1994]

[Jin95] Jin, S., O'Brian, H. M., Tiefel, T. H., McCormack, M., and Rhodes, W. W.,*Appl. Phys. Lett.* **66** 382 [1995]

[Jon50] Jonker, G. H., and van Santen, J. H., *Physica* **16** 337 [1950]

[Jon95] Jonsson, T., Mattson, J., Djurberg, C., Khan, F. A., Nordblad, P., and Svedlindh, P., *Phys. Rev. Lett.* **75** 4138 [1995]

[Jon98a] Jonason, K., Vincent, E., Hammann, J., Bouchaud, J. P., and Nordblad, P., *Phys. Rev. Lett.* **81** 3243 [1998]

[Jon98b] Jonsson, T., Svedlindh, P., and Hansen, M. F., *Phys. Rev. Lett.* **81** 3976 [1998]

[Jon00] Jonason, K., Nordblad, P., Vincent, E., Hammann, J., and Bouchaud, J. P., *Eur. Phys. J. B* **13** 99 [2000]

[Jon04] Jonsson, P. E., *Adv. Chem. Phys.* **128** 191 [2004]

[Jon05] Jonsson, P. E., Yoshino, H., Mamiya, H., and Takayama, H., *Phys. Rev. B* **71** 104404 [2005]

[Joy98] Joy, P. A., Kumar, P. S. A., and Date, S. K., *J. Phys: Condens. Matter.* **10** 11049 [1998]

[Joy00a] Joy, P. A. and Date, S. K., *J. Magn. Magn. Mater.* **210** 31 [2000]

[Joy00b] Joy, P. A. and Date, S. K., *J. Magn. Magn. Mater.* **218** 229 [2000]

[Joy00c] Joy, P. A. and Date, S. K., *J. Magn. Magn. Mater.* **220** 106 [2000]

[Kaj04] Kajimoto, R., Yoshizawa, H., Shintani, H., Kimura, T., and Tokura, Y., *Phys. Rev. B* **70** 012401 [2004]

[Kar80] Karavay, A. P., *Krist. Tech.* **15** 11 [1980]

[Kaw96] Kawano, H., Kajimoto, R., Kubota, M., and Yoshizawa, H., *Phys. Rev. B* **53** 2202 [1996]

[Kim01] Kim, S. J., Kim, C. S., Park, S.-I., and Lee, B. W., *J. Appl. Phys.* **89** 7416 [2001]

[Kim03] Kimura, T., Goto, T., Shintani, H., Ishizaka, K., Arima, T., and Tokura, Y., *Nature* **426** 55 [2003]

[Kni77] Knitter, R. W., Kouvel, J. S., and Claus, H., *J. Magn. Magn. Mater.* **5** 356 [1977]

[Kit02] Kityk, A. V., Rheinstadter, M. C., Knorr, K., and Rieger, H., *Phys. Rev. B* **65** 144415 [2002]

[Kle01] Kleemann, W., Petracic, O., Binek, Ch., Kakazei, G. N., Pogorelov, Yu. G., Sousa, J. B., Cardoso, S., and Freitas, P. P., *Phys. Rev. B* **63** 134423 [2001]

[Klu54] Klug, H. P. and Alexander, L. E., *X-ray Diffraction Procedures* John Wiley& Sons, Newyork [1954]

[Kod99] Kodama, R. H., *J. Magn. Magn. Mater.* **200** 359 [1999]

[Koi01] Koide, T., Miyauchi, H., Okamoto, J., Shidara, T., Sekine, T., Saitoh, T., Fujimori, A., Fukutani, H., Takano, M., and Takeda, Y., *Phys. Rev. Lett.* **87** 246404 [2001]

[Kum98a] Kumar, P. S. A., Joy, P. A., and Date, S. K., *J. Phys.: Condens. Matter.* **10** L487 [1998]

[Kum98b] Kumar, P. S. A., Joy, P. A., and Date, S. K., *J. Mater. Chem.* **8** 1219 [1998]

[Kum99] Kumar, P. S. A., Joy, P. A., and Date, S. K., *J. Phys.: Condens. Matter.* **10** L487 [1999]

[Kum02] Kumar, D., Pennycook, S. J., Lupini, A., Duscher, G., Tiwari, A., and Narayan, J., *Appl. Phys. Lett.* **81** 4204 [2002]

[Lai03] Laiho, R., Lisunov, K. G., Lahderanta, E., Petrenko, P. A., Salminen, J., Stamov, V. N., Stepanov, Yu. P., and Zakhvalinskii, V. S., *J. Phys. Chem. Solids* **64** 2313 [2003]

[Lai05] Laiho, R., Lisunov, K. G., Lahderanta, E., Stamov, V. S., Zakhvalinskii, V. S., Colomban, Ph., Petrenko, P. A., and Stepanov, Yu. P., *J. Phys. Condens.Matter.* **17** 105 [2005]

[Lic96] Licci, F., Turilli, G., and Ferro, P., *J. Magn. Magn. Mater.* **164** L268 [1996]

[Liu99] Liu, J. F., Zhang, Y., and Hadjipanayis, G. C., *J. Magn. Magn. Mater.* **202** 69 [1999]

[Liu00] Liu, X., Xu, X., and Zhang, Y., *Phys. Rev. B* **62** 15112 [2000]

[Lob00] Lobanov, M. V., Balagurov, A. M., Pomjakushin, V. Ju., Fischer, P., Gutmann, M., Abakumov, A. M., D'yachenko, O. G., Antipov, E. V., Lebedev, O. I., and Van Tendeloo, G., *Phys. Rev. B* **61** 8941 [2000]

[Los01] Loshkareva, N. N., Solin, N. I., Sukhorukov, Y. P., Lobachevskaya, N. I., and Panfilova, E. V., *Physica B* **293** 390 [2001]

[Lui02] Luis, F., Petroff, F., Torres, J. M., Garcia , L. M., Bartolome, J., Carrey, J., and Vaures, A., *Phys. Rev. Lett.* **88** 217205 [2002]

[Luo91] Luo, W., Nagel, S. R., Rosenbaum, T. F., and Rosenweig, R. E., *Phys. Rev. Lett.* **67** 2721 [1991]

[Mac94] MacEachern, M. J., Dabkowska, H., Garrett, J. D., Amow, G., Gong, W., Liu, G., and Greedan, J. E., *Chem. Mater.* **6** 2092 [1994]

[Mah96] Mahendiran, R., Tieary, S. K., Raychaudhri, A. K., Ramakrishnan, T. V., Mahesh, R., Rangavittal, N., and Rao, C. N. R., *Phys. Rev. B* **53** 3348 [1996]

[Mai96] Maignan, A., Simon, C., Caignaert, V., and Raveau, B., *J. Appl. Phys.* **79** 7891 [1996]

[Mai97] Maignan, A., Michel, C., Hervieu, M., and Raveau, B., *Solid State Commun.* **101** 277 [1997]

[Mal79] Maletta, H., and Felsch, W., *Phys. Rev. B* **20** 1245 [1979]

[Mal05] Malavasi, L., Ritter, C., Mozzati, M. C., Tealdi, C., Saiful Islam, M., Azzoni, C. B., and Flor, G., *J. Solid State Chem.* **178** 2042 [2005]

[Man97] Mandal, P. and Das, S., *Phys. Rev. B* **56** 15073 [1997]

[Mar02] Markovich, V., Rozenberg, E., Shames, A. I., Gorodetsky, G., Fita, I., Suzuki, K., Puzniak, R., Shulyatev, D. A., and Mukovskii, M. Ya., *Phys. Rev. B* **65** 144402 [2002]

[Mar03] Markovich, V., Fita, I., Shames, A. I., Puzniak, R., Rozenberg, E., Yuzhelevski, Y., Mogilyansky, D., Wisniewski, A., Mukovskii, M. Ya., and Gorodetsky, G., *J. Phys. Condens. Matter.* **15** 3985 [2003]

[Mar05] Marco, M. D., Coffey, D., Heary, R., Dabrowski, B., Klamut, P., Maxwell, M., Toorongian, S., and Haka, M., *Phys. Rev. B* **71** 104403 [2005]

[Mat70] Matsumoto, G., *J. Phys. Soc. Japan* **29** 606 [1970]

[Mat99] Mathur, N. D., Littlewood, P. B., Todd, N. K., Isaac, S. P., Teo, B.-S., Kang, D.-J., Tarte, E. J., Barber, Z. H., Evetts, J. E., and Blamire, M. G., *J. Appl. Phys.* **86** 6287 [1999]

[Mat01a] Mathieu, R., Nordblad, P., Nam, D. N. H., Phuc, N. X., and Khiem, N. V., *Phys. Rev. B* **63** 174405 [2001]

[Mat01b] Mathieu, R., Jonsson, P. E., Nordblad, P., Katori, H. A., and Ito, A., *Phys. Rev. B* **65** 012411 [2001]

[Mcc98] McCarroll, W. H., Ramanuchary, K. V., Greenblatt, M., and Cosandey, F., *J. Solid State Chem.* **136** 322 [1998]

[Mil98] Millis, A. J., *Nature* **392** 147 [1998]

[Mit96] Mitchell, J. F., Argyriou, D. N., Potter, C. D., Hinks, D. G., Jorgensen, J. D., and Bader, S. D., *Phys. Rev. B* **54** 6172 [1996]

[Mit02] Mitchell, R. H., *Perovskites: Modern and Ancient* Almaz Press Inc., Canada [2002]

[Mor60] Moriya, T., Phys. Rev. **120** 91 [1960]

[Mor99] Moreo, A., Yunoki, S., and Dagotto, E., *Science* **283** 2034 [1999]

[Mot90] Mott, N. F., *Metal-Insulator Transitions* Taylor and Francis, London [1990]

[Mun04] Munoz, A., Alonso, J. A., Martinez-Lope, M. J., and Martinez, J. L., *Chem. Mater.* **16** 4087 [2004]

[Myd93] Mydosh, J. A., *Spin Glasses: An Experimental Introduction* Taylor & Francis, London [1993]

[Nai04] Nair, S., and Banerjee, A., *Phys. Rev. Lett.* **93** 117204 [2004]

[Nak02a] Nakamura, K., and Ogawa, K., *J. Solid State Chem.* **163** 65 [2002]

[Nak02b] Nakamura, K., and Ogawa, K., *J. Appl. Phys.* **92** 6684 [2002]

[Nak03] Nakamura, K., *J. Solid State Chem.* **173** 299 [2003]

[Nie99] Nie, J. C., Wang, J. H., and Zhao, B. R., *J. Magn. Magn. Mater.* **192** L379 [1999]

[Noj99] Nojiri, H., Kaneko, K., Motokawa, M., Hirota, K., Endoh, Y., and Takahashi, K., *Phys. Rev. B* **60** 4142 [1999]

[Oha00] O′Handley, R. C., *Modern Magnetic Materials* Wiley-Interscience Publication, New York [2000]

[Ose96] Oseroff, S.B., Torikachvili, M., Singley, J., Ali, S., Cheong, S.-W., and Schultz, S.,*Phys. Rev. B* **53** 6521 [1996]

[Par01] Parisi, F., Levy, P., Ghivelder. L., Polla, G., and Vega, D., *Phys. Rev. B* **63** 144419 [2001]

[Par04] Park, J. S., Kim, C. O., Lee, Y. P., Lee, Y. S., Shin, H. J., Han, H., and Lee, B. W., *J.Appl. Phys.* **96** 2033 [2004]

[Par05] Parker, D., Ladieu, F., Vincent, E., Meriguet, G., Dubois, E., Dupuis, V., and Perzynski, R., *J. Appl. Phys.* **97** 10A502 [2005]

[Pap04] Papastaikoudis, C., and Syskakis, E., *J. Magn. Magn. Mater.* **272-276** 444 [2004]

[Pav84] Pavlov, V. I., Bogush, A. K., and Balyko, L. V., *Crys. Res. Tech.* **19** 237 [1984]

[Pha03] Phan, M.- H., Yu, S. C., and Hur, N. H., *J. Magn. Magn. Mater.* **262** 407 [2003]

[Pig97] Pignard, S., Vincent, H., Senateur, J. P., Pierre, J., and Abrutis, A., *J. Appl. Phys.* **82** [1997]

[Pod02] Poddar, P., Telem-Shafir, T., Fried, T., and Markovich, G., *Phys. Rev. B* **66** 060403 [2002]

[Pog99] Pogorilyi, A. N., Belous, N. A., Tovstolytkin, A. I., Belous, A. G., and Yanchevski, O. Z., *Low Temp. Phys.* **25** 74 [1999]

[Pra99] Prado, F., Sanchez, R. D., Caneiro, A., Causa, M. T., and Tovar, M., *J. Solid State Chem.* **146** 418 [1999]

[Pra01] Pradhan, A. K., Roul, B. K., Feng, Y., Wu, Y., Mohanty, S., Sahu, D. R., and Dutta, P., *Appl. Phys. Lett.* **78** 1598 [2001]

[Qia02] Qian, Q., Tyson, T. A., Dubourdieu, C., Bossak, A., Senateur, J. P., Deleon, M., Bai, J., and Bonfait, G., *Appl. Phys. Lett.* **80** 2663 [2002]

[Ran96] Ranno, L., Viret, M., Mari, A., Thomas, R. M., and Coey, J. M. D., *J. Phys. Condens. Matter.* **8** L33 [1996]

[Rao94] Rao, C. N. R., *Chemical Approaches to the synthesis of Inorganic Materials*, Wiley Eastern Ltd., New Delhi, [1994]

[Rao98] Rao, C. N. R., and Raveau, B., (Eds.) *Colossal Magnetoresistance, Charge Ordering and Related Properties of Manganese Oxides* World Scientific, Singapore [1998]

[Rao03] Rao, C. N. R., Vanitha, P. V., and Cheetham, A. K., *Chem. Eur. J.* **9** 829 [2003]

[Rat02] Ratcliff II, W., Lee, S.-H., Broholm, C., Cheong, S.-W., and Huang, Q., *Phys. Rev. B* **65** 220406 [2002]

[Rav00] Raveau, B., Maignan, A., Martin, C., Mahendiran, R., and Hervieu, M., *J. Solid State Chem.* **151** 330 [2000]

[Ret97] Rettori, C., Rao, D., Singley, J., Kidwell, D., Oseroff, S. B., Causa, M. T., Neumeier, J. J., McClellan, K. J., Cheong, S.-W., and Schultz, S., *Phys. Rev. B* **55** 3083 [1997]

[Rit97] Ritter, C., Ibarra, M. R., De Teresa, J. M., Algarabel, P. A., Marquina, C., Blasco, J., Garcia, J., Oseroff, S., and Cheong, S.-W., *Phys. Rev. B* **56** 8902 [1997]

[Ron99] Rondinone, A. J., Samia, A. C. S., and Zhang, Z. J., *J. Phys. Chem. B* **103** 6876 [1999]

[Roy96] Roy, S. B., Pradhan, A. K., and Chaddah, P., *Physica B* **223-224** 198 [1996]

[Roy97] Roy, S. B., Pradhan, A. K., Chaddah, P., and Sampathkumaran, E. V., *J. Phys.: Condens. Matter.* **9** 2465 [1997]

[Ryb05] Rybchenko, S. I., Fujishiro, Y., Takagi, H., and Awano, M., *Phys. Rev. B* **72** 054424 [2005]

[Sah02] Sahoo, S., Petracic, O., Binek, Ch., Kleemann, W., Sousa, J. B., Cardoso, S., and Freitas, P. P., *Phys. Rev. B* **65** 134406 [2002]

[Sah03] Sahoo, S., Petracic, O., Kleemann, W., Nordblad, P., Cardoso, S., and Freitas, P. P., *Phys. Rev. B* **67** 214422 [2003]

[Sak96] Sakai, N. and Fjellvag, H., *Acta. Chem. Scand.* **50** 580 [1996]

[Sal01] Salamon, M. B. and Jaime, M., *Rev. Mod. Phys.* **73** 583 [2001]

[Sas04] Sasaki, M., Jonsson, P. E., Takayama, H., and Nordblad, P., *Phys. Rev. Lett.* **93** 139701 [2004]

[Sas05] Sasaki, M., Jonsson, P. E., Takayama, H., and Mamiya, H., *Phys. Rev. B* **71** 104405 [2005]

[Sat01] Sato, T., Ando, T., Ogawa, T., Morimoto, S., and Ito, A., *Phys. Rev. B* **64** 184432 [2001]

[See04] Seetha Lakshmi, L., Sridharan, V., Natarajan, D. V., Rawat, R., Chandra, S., Sankara Sastry, V., and Radhakrishnan, T. S., *J. Magn. Magn. Mater.* **279** 41 [2004]

[Sen84] Senoussi, S., *J. Physique* **45** 315 [1984]

[Sen98] Senis, R., Laukhin, V., Martinez, B., Fontcuberta, J., Obradors, X., Arsenov, A., and Mukovskii, Y. M., *Phys. Rev. B* **57** 14680 [1998]

[Sha76] Shannon, R. D., *Acta Crystallogr. Sect. A* **32** 751 [1976]

[She96] Shengelaya, A., Zhao, G., Keller, H., and Muller, K. A., *Phys. Rev. Lett.* **77** 5296 [1996]

[Shi02] Shibata, T., Bunker, B., Mitchell, J. F., and Schiffer, P., *Phys. Rev. Lett.* **88** 207205 [2002]

[Sin01] Singleton, J., *Band Theory and Electronis Properties of Solids*, Oxford University Press Inc., New York [2001]

[Sku99] Skumryev, V., Blythe, H. J., Cullen, J., and Coey, J. M. D., *J. Magn. Magn. Mater.* **196-197** 515 [1999]

[Sku03] Skumryev, V., Stoyanov, S., Zhang, Y., Hadjipanayis, G., Glvord, D., and Nogues, J., *Nature* **423** 850 [2003]

[Sol96] Solovyev, I., Hamada, N., and Terakura, K., *Phys. Rev. Lett.* **76** 4825 [1996]

[Sor81] Sorensen, O. T., Nowick, A. S., and Libowitz, G. G., (Eds.) *Non Stoichiometric Oxides*, Acadamic Press, San Diego [1981]

[Sun98] Sun, J. R., Rao, G. H., and Zhang, Y. Z.,*Appl. Phys. Lett.* **72** 3208 [1998]

[Sun99] Sun, Y., Xu, X., Zheng, L., and Zhang, Y., *Phys. Rev. B* **60** 12317 [1999]

[Sun00] Sun, Y., Xu, X., Tong, W., and Zhang, Y., *Appl. Phys. Lett.* **77** 2734 [2000]

[Sun03] Sun, Y., Salamon, M. B., Garnier, K., and Averback, R. S., *Phys. Rev. Lett.* **91** 167206 [2003]

[Ste02] Steren, L. B., Sirena, M., and Guimpel, J., *Phys. Rev. B* **65** 094431 [2002]

[Tag97] Taguchi, H., Matsu-ura, S.-i., Nagao, M., Choso, T., and Tabata, K., *J. Solid State Chem.* **129** 60 [1997]

[Tak91] Takeda, Y., Nakai, S., Kojima, T., Kanno, R., Imanishi, N., Shen, G. Q., Yamamoto, O., Mori, M., Asakawa, C., and Abe, T., *Mater. Res. Bull.* **26** 153 [1991]

[Tay95] Taylor, J. A. T., *Amer. Cer. Soc. Bull.* **74** 81 [1995]

[Ter98] Terai, T., Kakeshita, T., Fukuda, T., Saburi, T., Takamoto, N., Kindo, K., and Honda, M., *Phys. Rev. B* **58** 14908 [1998]

[Tiw97] Tiwari, A. and Rajeev, K. P., *J. Mater. Sci. Lett.* **16** 521 [1997]

[Tof74] Tofield, B. C. and Scott, W. R., *J. Solid State Chem.* **10** 183 [1974]

[Tok00] Tokura, Y., (Ed.) *Colossal Magnetoresistive Oxides* Gordon and Breach Science Publishers, Singapore [2000]

[Top96] Topfer, J., Doumerc, J.-P., and Grenier, J.-C., *J. Mater. Chem.* **6** 1511 [1996]

[Top97a] Topfer, J., and Goodenough, J. B., *Chem. Mater.* **9** 1467 [1997]

[Top97b] Topfer, J., and Goodenough, J. B., *J. Solid State Chem.* **130** 117 [1997]

[Tov99] Tovstolytkin, A. I., Pogorilyi, A. N., and Kovtun, S. M., *Low Temp. Phys.* **25** 962 [1999]

[Tro03] Troyanchuk, I. O., Khomchenko, V. A., Chobot, A. N., and Szymczak, H., *J. Phys.: Condens. Matter.* **15** 6005 [2003]

[Tro04] Troyanchuk, I. O., Khomchenko, V. A., Tovar, M., Szymezak, H., Barner, K., *Phys. Rev. B* **69** 054432 [2004]

[Tso05] Tsoi, G. M., Wenger, L. E., Senaratne, U., Tackette, R. J., Buc, E. C., Naik, R., Vaishnava, P. P., and Naik, V., *Phys. Rev. B* **72** 014445 [2005]

[Tsu01] Tsurkan, V., Hemberger, J., Klemm, M., Klimm, S., Loidl, A., Horn, S., and Tidecks, R., *J. Appl. Phys* **90** 4639 [2001]

[Ueh99] Uehara, M., Mori, S., Chen, C. H., and Cheong, S.-W., *Nature* **399** 560 [1999]

[Van58] van der Pauw, L. J., *Phillips Res. Rep.* **13** 1 [1958]

[Van82] van Duyneveldt, A. J., *J. Appl. Phys.* **53** 8006 [1982]

[Van94a] van Roosmalen, J. A. M., and Cordfunke, E. H. P., *J. Solid State Chem.* **110** 109 [1994]

[Van94b] van Roosmalen, J. A. M., Cordfunk, E. H. P., Helmholdt, R. B., and Zandbergen, H. W., *J. Solid State Chem.* **110** 100 [1994]

[Van95] van Roosmalen, J. A. M., van Vlaandeen, P., Cordfunke, E. H. P., Ijdo, W. L., and Ijdo, D. J. W., *J. Solid State Chem.* **114** 516 [1995]

[Van04] van Tandeloo, G., Lebedev, O. I., Hervieu, M., and Ravean, B., *Rep. Prog. Phys.* **67** 1315 [2004]

[Var05] Vargas, M. J., Nunes, W. C., Socolovsky, L. M., Knobel, M., and Zanchet, D., *Phys. Rev. B* **72** 184428 [2005]

[Veg05] Veglio, N., Bermejo, F. J., Gutierrez, J., Barandiaran, J. M., Pena, A., Gonzalez, M. A., Romano, P. P., and Mondelli, C., *Phys. Rev. B* **71** 212402 [2005]

[Ver93] Verelst, M., Rangavittal, N., Rao, C. N. R., and Rousset, A., *J. Solid State Chem.* **104** 74 [1993]

[Ver01] Vertruyen, B., Cloots, R., Rulmont, A., Dhalenne, G., Ausloos, M., and Vanderbemden, Ph., *J. Appl. Phys.* **90** 5692 [2001]

[Ver05] Verma, S., Pradhan, S. D., Pasricha, R., Sainkar, S. R., and Joy, P. A., *J. Am. Ceram. Soc* **88** 2597 [2005]

[Vin95] Vincent, E., Bouchaud, J. P., Hammann, J., and Lefloch, F., *Phil. Mag. B* **71** 489 [1995]

[Vin00] Vincent, E., Dupuis, V., Alba, M., Hammann, J., and Bouchaud, J. P., *Europhys. Lett.* **50** 674 [2000]

[Vin02] Vincent, H., Audier, M., Pignard, S., Dezanneau, G., and Senateur, J. P., *J. Solid State Chem.* **164** 177 [2002]

[Wat01] Watahiki, M., Metoki, N., Suzuki, J.-i., Oikawa, K.-i., Nie, J., Tachiki, M., and Yamada, Y., *J. Phys. Soc. Jpn.* **70** 1090 [2001]

[Wol55] Wollan, E. O., and Koehler, W. C., *Phys. Rev. B* **100** 545 [1955]

[Xia03] Xia, Z. C., Yuan, S. L., Feng, W., Zhang, L. J., Zhang, G. H., Tang, J., Cheng, L., Zheng, Q. H., Liu, L., Liu, S., and Tang, C. Q., *Solid State Commun.* **126** 567 [2003]

[Xu05] Xu, Q. Y., Wang, R. P., and Zhang, Z., *Phys. Rev. B* **71** 092401 [2005]

[Yam96] Yamada, Y., Hino, O., Nohdo, S., Kanano, R., Inami, T., and Katano, S., *Phys. Rev. Lett.* **77** 904 [1996]

[Yun98] Yunoki, S., Hu, J., Malvezzi, A. L., Moreno, A., Furukawa, N., and Dagotto, E., *Phys. Rev. Lett.* **80** 845 [1998]

[Yvo77] Yvon, K., Jeitschko, W., and Parthe, E., *J. Appl. Cryst.* **10** 73 [1977]

[Zen51] Zener, C., *Phys. Rev.* **82** 403 [1951]

[Zen93] Zeng, W. G. and Siu, G. G., *J. Phys.: Condens. Matter.* **5** 6461 [1993]

[Zha97] Zhang, N., Ding, W., Zhong, W., Xing, D., and Du, Y., Phys. Rev. B 56 8138 [1997]

[Zhe01] Zheng, L. Q. and Fang, Q. F., *Phys. Stat. Sol. (a)* **185** 267 [2001]

[Zhe05] Zheng, R. K., Gu, H., Xu, B., and Zhang, X. X., *Phys. Rev. B* **72** 014416 [2005]

[Zot03] Zotev, V. S., Rodriguez, G. F., Kenning, G. G., Orbach, R., Vincent, E., and Hammann, J., *Phys. Rev. B* **67** 184422 [2003]

[Zys01] Zysler, R. D., Fiorani, D., and Testa, A. M., *J. Magn. Magn. Mater.* **224** 5 [2001]

List of Publications

1. Sankar, C. R. and Joy, P. A., "Superspin glass behavior of a non-stoichiometric lanthanum manganite, $LaMnO_{3.13}$", *Phys. Rev. B* **72** 132407 [2005]

2. Bala, T., C. R. Sankar, Baidakove, M., Osipov, V., Enoki, T., Joy, P. A., Prasad, B. L. V., and Sastri, M, "Cobalt and Magnesium ferrite nanoparticles: Preparation using liquid foams as templates and their magnetic characteristics" *Langmuir* **21** 10638 [2005]

3. Sankar, C. R. and Joy, P. A., "Magnetic properties of the self-doped lanthanum manganites $La_{1-x}MnO_3$", *Phys. Rev. B* **72** 024405 [2005]

4. Sankar, C. R. and Joy, P. A., "Studies on the evolution of a low temperature anomaly in the *ac* susceptibility of ferromagnetic compositions in the $La_{1-x}MnO_3$ ($0 < x < 0.125$) series", *J. Magn. Magn. Mater.* **277** 209 [2004]

5. Joy, P. A., Sankar, C. R., and Date, S. K., "The limiting value of x in the ferromagnetic compositions $La_{1-x}MnO_3$", *J. Phys. Condens. Matter* **14** L663 [2002]

6. Joy, P. A., Sankar, C. R., and Date, S. K., "The origin of ferromagnetism in $LaMnO_{3+\delta}$", *J. Phys. Condens. Matter* **14** 4985 [2002]

7. Sankar, C. R. and Joy, P. A., "Interacting and noninteracting ferromagnetic clusters in $La_{0.67-x}Tb_xCa_{0.33}MnO_3$", *Communicated*

Awards

"Keerti Sangoram Endowment Award" by the National Chemical Laboratory Research Foundation, for the BEST RESEARCH SCHOLAR OF THE YEAR 2005, of National Chemical Laboratory, in Physical/Material Sciences.

Symposia and Conferences

1. Sankar, C. R., Joy, P. A., and Date, S. K., "Comparison of the structural and magnetic properties of $LaMnO_{3+\delta}$ and $La_{1-x}MnO_3$", Poster presentation, International Symposium on Recent Advances in Inorganic Materials, IIT Bombay, India, December [2002].

2. Sankar, C. R. and Joy, P. A., "Self-doped lanthanum manganites: A potential magnetoresistive material for future Applications", Oral Presentation, Materials for Electrical, Electronic and Magnetic Applications (MEEMA) Pune, India, November [2003]

3. Sankar, C. R. and Joy, P. A., "Magnetic anomalies of self-Doped lanthanum manganites", Poster presentation, 16th AGM of the Materials Research Society of India and Symposium on Materials for Automotive Industries, National Chemical Laboratory, Pune, India, February [2005].

4. Sankar, C. R., Joy, P. A., and Date, S. K., "Magnetic properties of self-doped lanthanum manganites", Poster Presentation, National Seminar on Electro and Magneto Ceramics Devices and Systems (NSEMCDS) at Akluj, India [2002]

Workshops

1. 'SERC School Methods in Materials Characterization' sponsored by the Department of Science and Technology held at Indira Gandhi Centre for Atomic Research, Kalpakkam, India, February [2004]